

**Transition metal-based nanocatalysts for (de)-
hydrogenation reactions**

Thesis Submitted to AcSIR
For the award of the
Degree of Doctor of Philosophy
in
Chemical Sciences



By

Garima Jaiswal

AcSIR No. 10CC13A26023

Under the guidance of

Dr. E. Balaraman

CSIR-National Chemical Laboratory

Pune-411008

July 2018



सीएसआईआर - राष्ट्रीय रासायनिक प्रयोगशाला

(वैज्ञानिक तथा औद्योगिक अनुसंधान परिषद)

डॉ. होमी भाभा मार्ग, पुणे - 411 008, भारत

CSIR - NATIONAL CHEMICAL LABORATORY

(Council of Scientific & Industrial Research)

Dr. Homi Bhabha Road, Pune - 411 008, India



Ph.D. Thesis Certificate

This is to certify that the work incorporated in this thesis entitled "*Transition metal-based nanocatalysts for (de)-hydrogenation reactions*" submitted by *Ms. Garima Jaiswal* (Registration Number AcSIR No. 10CC13A26023) to the Academy of Science and Innovation Research (AcSIR) in the fulfillment of the requirement for the award of the Degree of the Doctor of Philosophy, embodies original research work under my supervision at Catalysis Division and Organic Chemistry Division, CSIR-National Chemical Laboratory (CSIR-NCL), Pune, India. Such material obtained from other sources has been duly acknowledged in the thesis. Any text, illustration, table, etc used in the thesis from other source have been duly cited and acknowledged.

Garima Jaiswal
02/07/2018

Ms. Garima Jaiswal

(Research Student)

E. Balaraman
02/July/2018

Dr. E. Balaraman

(Research Supervisor)

वैज्ञानिक/Scientist
कार्बनिक रसायन प्रभाग
Division of Organic Chemistry
राष्ट्रीय रासायनिक प्रयोगशाला
NATIONAL CHEMICAL LABORATORY
पुणे / PUNE - 411 008

Communication Channels

NCL Level DID : 2590
NCL Board No. : +91-20-25902000
EPABX : +91-20-25893300
: +91-20-25893400



FAX

Director's Office : +91-20-25902601
COA's Office : +91-20-25902660
SPO's Office : +91-20-25902664

WEBSITE

www.ncl-india.org

DECLARATION

I hereby declare that the original research work embodied in this thesis entitled "*Transition metal-based nanocatalysts for (de)-hydrogenation reactions*" submitted for the degree of *Doctor of Philosophy in Chemical Sciences* to the Academy of Scientific and Innovative Research (AcSIR), New Delhi, is the outcome of experimental investigations carried out by me under the supervision of *Dr. Ekambaram Balaraman, Senior Scientist*, CSIR-National Chemical laboratory (CSIR-NCL), Pune. I affirm that the work incorporated is in original, and has not been submitted to any other academy, university or institute for the award of any degree or diploma.

Date: 02/07/2018

Place: Pune

Garima Jaiswal

Garima Jaiswal

Research Scholar

ACKNOWLEDGEMENT

The process of earning a doctorate and writing a dissertation is long and arduous and it is certainly not done singlehandedly. So, I am using this opportunity to express my gratitude to everyone who helped and supported me throughout the course of my research.

*Firstly, I would like to express my special appreciation and thanks to my research supervisor **Dr. Ekambaram Balaraman** and Co-supervisor Dr. Dinesh Jagadeesan for their valuable guidance and scholarly inputs. I have enjoyed the opportunity to watch and learn from my supervisor's knowledge and experience. His enthusiasm, encouragement and faith in me throughout have been extremely helpful. He is the one who moulded me into a good researcher. I am thankful to the god almighty for giving me such a wonderful and humble personality as my mentor. He has given me full freedom in my research and I could not imagine to have a better mentor than him.*

I wish to express my sincere thanks to the Doctoral Advisory Committee members, Dr. Chinnakonda S.Gopinath, Dr. Manjusha V. Shelke, Dr. A. T. Biju, and Dr. Utpal Das whose contribution in stimulating suggestions and encouragement helped me to coordinate my work.

I am grateful to Prof. A. K. Nangia, (Director, NCL), Dr. V. K. Pillai and Prof. S. Pal (Former Director, NCL), Dr. S. P. Chavan (Head, Organic chemistry Division), Dr. D. Srinivas, Dr. C. S. Gopinath (Head, Catalysis Division) for giving me this opportunity and providing all necessary infrastructure and facilities. I also acknowledge the financial support of UGC, New Delhi in terms of junior and senior research fellowships.

I extend my thanks to our collaborators Dr. Manoj B. Gawne for material characterization, and Dr. C.P. Vinod and Dr. C. S. Gopinath for XPS analysis. I would also like to thank Mrs. B. Santhakumari, for HRMS analysis, Dr. Rajamohanan and Dr. Sapna Ravindranathan for NMR facilities and Center for material characterization CSIR-NCL for providing material characterization facilities.

I express my sincere thanks to B. Gnanaprakasam, IISER-Pune for flow chemical reaction and DIAT-Pune (TEM analysis), IIT-Bombay (EPR analysis), IACS-Kolkata (STEM analysis), and JNCASR-Bangalore (HRTEM) for analytical support.

I also want to thank my Master's project mentor Prof. A.K. Ganguli from IIT Delhi for getting me interested in research and making me realize that I can take it further too.

A special thanks goes to My labmates Manoj, Siba, Vinod, Rana, Akash, Vinita, Subra, Saro and Shiv for their valuable advice and help in lab practices which I greatly acknowledge. A special

thanks goes to all my friends from CSIR-NCL, Yogita, Sharad, Vinod, Mahesh, Govind, Sumanta, Manoj, Sandeep, Sweccha, Ragini, Sandip Singh, Shazia, Dnyanesh from NCL and Pulak maity CBMRI for their help .

I owe a lot to my beloved parents who encouraged and helped me at every stage of my personal and academic life, and longed to see this achievement come true. My sincere thanks to my beloved family members Mr. Rajendra Prasad, Mrs. Savitri devi, Gaurav, Pratima, Praveen, Sonali, Nitesh, Neha, Shashank, Kashvi and Rayasnh for their endless support. I am very much indebted to my whole family who supported me in every possible way to see the completion of this research work.

Above all, I owe it all to Almighty God for granting me the wisdom, health and strength to undertake this research task and enabling me to its completion.

Garima Jaiswal

Dedicated to my parents

Abbreviations

ADC-acceptorless dehydrogenative coupling

BHT- 2,6-di-tert-butyl-4-methylphenol

GC - Gas Chromatography

DCE-1,2-dichloroethane

DCM- Dichloromethane

EPR- Electron Paramagnetic Resonance

EDX Energy-dispersive X-ray spectroscopy

FTY- Iron Time Yield

HRMS-High resolution mass spectrometry

HA-Hydrogen autotransfer

ICP - Inductively Coupled Plasma

JCPDS- Joint council for Powder Diffraction Studies

Methanol-Methanol

MB - Molecular Beam

PXRD – Powder X-ray Diffraction

RWGS – Reverse Water Gas Shift Reaction

SEM - Scanning Electron Microscopy

SPR- Surface Plasmon Resonance

TFE - Trifluoro Ethanol

TOS- Time on Stream

TEM - Transmission Electron Microscopy

TGA- Thermogravimetric Analysis

XPS - X-ray photoelectron spectroscopy

Table of contents

Abbreviations

Preface

Chapter 1: Dehydrogenation and related reactions

1.1: Introduction

1.2. Dehydrogenation reaction and applications in energy storage

1.2.1. Dehydrogenation of formic acid

1.2.2. Dehydrogenation of Methanol

1.2.3. Dehydrogenation of amine-borane adduct

1.2.4. Dehydrogenation of Alcohols

1.2.5. Dehydrogenative hydrogen transfer of alcohols (N-Alkylation of Amines)

1.2.6. Dehydrogenation of amines

1.2.7. Dehydrogenation of Alkanes

1.3. Current Status and Challenges

1.4. Heterogeneous Catalysis

1.4.1. Heterogenization of the homogeneous catalysts

1.4.2. Pathways for Heterogeneous catalysis

1.5. Analytical Methods

1.5.1. X-ray diffraction analysis

1.4.2. X-Ray Photoelectron Spectroscopy

1.4.3. Inductively coupled Plasma spectroscopy (ICP)

1.5.4. Scanning Electron Microscopy (SEM)

1.5.5. Raman Spectroscopy

1.5.6. Transmission Electron Microscopy (TEM)

1.5.7. Thermal Analyses

1.5.8. Gas Chromatography (GC)

1.5.9. Nuclear Magnetic Resonance Spectroscopy (NMR)

1.6. Scope and Objectives of the Thesis Work

1.7. References

Chapter 2: Iron nanocatalyst for the acceptorless dehydrogenation reactions

Part A: Dehydrogenation of N-Heterocycles and Alcohols

2A.1. Introduction

2A.2. Statement of the Problem

2A.3. Catalyst Synthesis and Characterization

2A.3.1. Synthesis of Fe-L1@EGO-900 catalyst

2A.3.2. Catalyst Characterization

2A.3.2.1. Powder X-ray diffraction (PXRD)

2A.3.2.2. Energy-Dispersive X-ray Spectroscopy (EDX)

2A.3.2.3. Scanning Electron Microscopy (SEM) analysis

2A.3.2.4. Transmission Electron Microscope (TEM) Analysis

2A.3.2.5. Electron Paramagnetic Resonance (EPR) Analysis

2A.3.2.6. X-ray Photoelectron Spectroscopy (XPS)

2A.3.2.7. Raman Spectra

2A.3.2.7. Thermogravimetric Analysis (TGA)

2A.6.8. Effect of different ligand

2A.6.9. Effect of pyrolysis temperature

2A.4. Result and Discussion

2A.4.1. Optimization Table

2A.4.2. Substrate scope of *N*-heterocycles

2A.4.3. Dehydrogenation of amines to imines with extraction of H₂

2A.4.3. Substrate scope of primary alcohols

2A.4.5. Substrate scope of secondary alcohols and diol

2A.4.6. Mechanistic Study

2A.4.6.1. Qualitative analysis of hydrogen gas formation

2A.4.6.2 Quantitative analysis of hydrogen gas by dual catalysis

2A.4.6.3. Hydrogen gas quantification: A volumetric quantitative analysis

2A.4.6.4. Reaction under presence of radical (O•-2) scavenger

2A.4.6.5. Hot filtration test

2A.4.6.6. Leaching test

2A.4.6.7. Recyclability of the catalyst

2A.4.7. Application

2A.4.7.1. Applications in synthesis of drug molecule

2A.4.7.2. Magnetic separation of catalyst

2A.5. Experimental section

2A.5.1. General procedure for the acceptorless dehydrogenation of *N*-heterocycles

2A.5.2. General procedure for the acceptorless dehydrogenation of amines to imines

2A.5.3. General procedure for the iron-catalyzed alcohol dehydrogenation

2A.6. Conclusion

2A.7. References

Part B: Synthesis of imine via Acceptorless Dehydrogenation

2B.1. Introduction

2B.2. Statement of the Problem

2B.3. Catalyst Synthesis and Characterization

2B.4. Result and Discussion

2B.4.1. Optimization table

2B.4.2. Substrate scope of alcohols and amine to imine

2B.4.3. Gram-scale synthesis

2B.4.4. Mechanistic Investigation

2B.4.4.1. Determination of hydrogen gas formation

2B.4.4.2. Reaction under presence of radical ($O\bullet-2$) scavenger

2B.4.4.3. Hot filtration test

2B.4.4.4. Reaction under homogeneous conditions

2B.4.4.5. Presence of Lewis acid sites

2B.4.4.6. Deuterium labeling studies

2B.4.4.7. Kinetic study

2B.4.3.8. Reusability and Heterogeneity

2B.5. Experimental section

2B.5.1. General procedure for the iron-catalyzed direct imine formation

2B.6. Conclusion

2B.7. References

Chapter 3: Cobalt nanocatalyst for the transfer hydrogenation of alkynes and dehydrogenation reactions

Part A: Reusable Robust Cobalt-Catalyst for Dehydrogenation of N-Heterocycles with the Liberation of H₂

3A.1. Introduction

3A.2. Statement of the Problem

3A.3 Catalyst Synthesis and Characterization

3A.3.1 Synthesis of Co-Phen@C

3A.3.2. Catalyst Characterization

3A.3.2.1. Powder X-ray Diffraction

3A.3.2.2. SEM and TEM images

3A.3.2.3. XPS analysis

3A.3.2.4. EDX analysis

3A.3.2.5. Raman analysis

3A.4. Result and Discussion

3A.4.1. Optimization Table

3A.4.2. Substrate scope of *N*-Heterocycles

3A.4.3. Mechanistic Investigation

3A.4.3.1. Determination of hydrogen gas formation

3A.4.3.2. Reaction under the presence of radical ($O\bullet-2$) scavenger

3A.4.3.3. Recyclability of the catalyst

3A.5. Experimental section

3A.5.1. General procedure for the acceptorless dehydrogenation of *N*-heterocycles

3A.6. Conclusion

3A.7. References

Part B: Cobalt-based nanocatalyst for selective transfer hydrogenation of alkynes

3B.1. Introduction

3B.2. Statement of the Problem

3A.3. Catalyst Synthesis and Characterization

3B.4. Result and Discussion

3B.4.1. Optimization table

3B.4.2. Substrate scope of alkynes

3B.4.3. Application of semihydrogenation

3B.4.4. Mechanistic Investigation

3B.4.4.1. Reaction Kinetics.

3B.4.5.2. Recyclability of the catalyst

3B.5. Experimental section

3B.5.1. General Procedure for *Z*-selective semi-hydrogenation of internal alkynes

3B.5.2. General Procedure for semi-hydrogenation of terminal alkynes

3B.6. Conclusion

3B.7. References

Chapter 4: Reusable Manganese nanocatalyst for chemo-selective hydrogenation of nitroarenes

4.1. Introduction

4.2. Statement of Problem

4.3. Catalyst Synthesis and Characterization

4.3.1. Synthesis of Mn-Phen@G catalyst

4.3.2. Characterization of Catalyst

4.3.2.1. Powder X-ray Diffraction

4.3.2.2. EDX

4.3.2.3. SEM, TEM and XPS analysis

4.4. Result and Discussion

4.4.1. Optimization table

4.4.2. Substrate scope of nitroarenes

4.4.3. Continuous flow chemistry:

4.4.4. Reaction under hydrogen pressure

4.4.5. Application for drug synthesis

4.4.6. Mechanistic study

4.4.6.1. EPR Study

4.5. Experimental Details

4.5.1. General procedure for transfer hydrogenation of nitrocompounds.

4.6. Conclusion

4.7. References

Chapter 5: Fe Based nanocatalyst for partial hydrogenation of CO₂ to CO

5.1. Introduction

5.2. Statement of problem

5.3. Catalyst Synthesis and Characterization

5.3.1. Catalyst Characterization

5.4. Result and Discussion

5.4.1. Catalytic performance of catalysts

5.5. Experimental section

5.5.1 Activity test

5.6 Conclusion

5.7. References

Appendix

Preface



Synopsis of the Thesis to be submitted to the Academy of Scientific and Innovative Research for Award of the Degree of Doctor of Philosophy in Chemistry

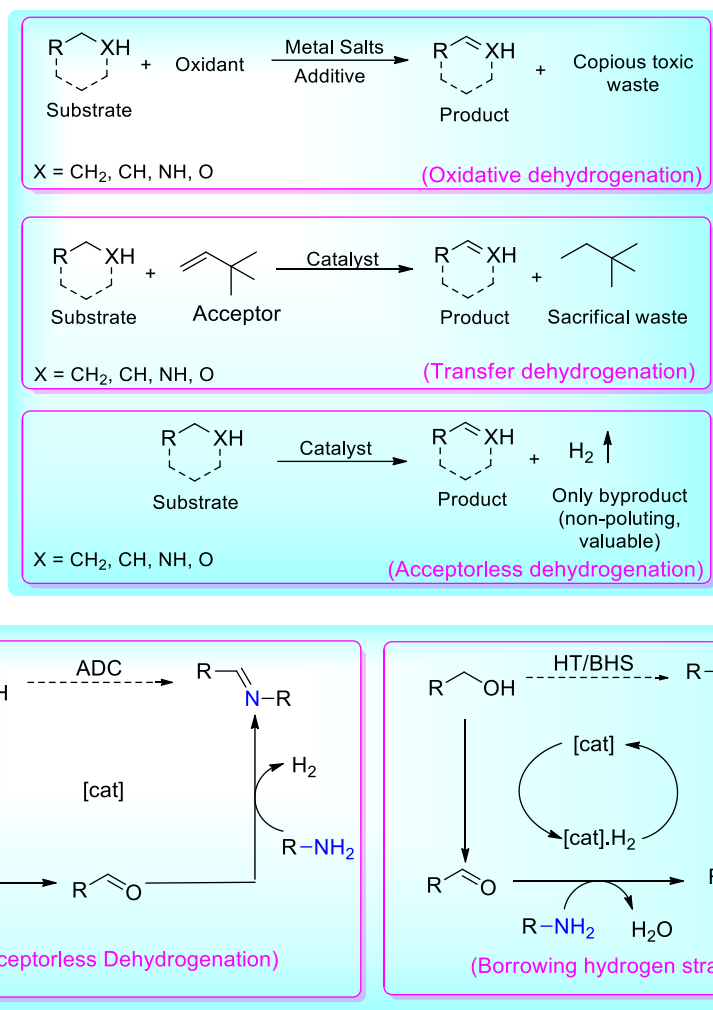
Name of the Candidate	Ms. GARIMA JAISWAL
Degree Enrolment No. & Date	Ph. D in Chemical Sciences (10CC13A26023); August 2013
Title of the Thesis	Transition metal-based nanocatalysts for (de)-hydrogenation reactions
Research Supervisor	Dr. E. Balaraman (CSIR-NCL, Pune)

This thesis describes design and development of new catalytic materials based on first - row transition metals (Mn, Fe, Co) and their applications in dehydrogenation and related reactions. I have divided my thesis into five chapters. The first chapter is introduction part which deals with the importance of dehydrogenation reactions and recent literature precedents. The second chapter is a working, where synthesis and characterization of iron based nanocatalyst and its application in acceptorless dehydrogenation (AD) of diverse alcohols, partially saturated *N*-heterocycles, and amines with the liberation of dihydrogen is described. This protocol is successfully applied to synthesis of diverse cyclic, acyclic imines and lactones under design condition. The third chapter is mainly focused on synthesis of cobalt nanoparticles with different supports and their catalytic activity in the dehydrogenation of *N*-heterocycles. The above catalytic system was further investigated for the chemoselective transfer hydrogenation of alkynes to *Z*-alkenes. The fourth chapter is focused on Mn-catalyzed chemoselective transfer hydrogenation of nitroarenes using ammonia-borane as a transfer hydrogenating source with mechanistic illustration. The final chapter of the thesis is mainly focused on partial and selective hydrogenation of CO₂ to CO (Reverse Water Gas Shift Reaction) catalyzed by iron-based nano catalyst. The details are presented below.

Chapter 1: Dehydrogenation and related reactions

Development of new and sustainable catalytic systems for fundamentally important synthetic transformations and energy storage applications is an important and an intellectually stimulating challenge. Conventionally dehydrogenation is well explored with aid of oxidants

or in the presence of organic acceptors, in which copious waste has been generated or organic molecules will be sacrificed (Scheme 1). Acceptorless dehydrogenation is an alternative and sustainable way of dehydrogenation process, as molecular hydrogen is the only side product. Catalytic dehydrogenation of feedstock chemicals, such as alcohols and amines to value-added products with the concomitant generation of dihydrogen is of much interest in the context of ‘hydrogen economy’ and is an effective appealing alternative to the classical oxidation reactions.



Scheme 1. Dehydrogenation related reactions

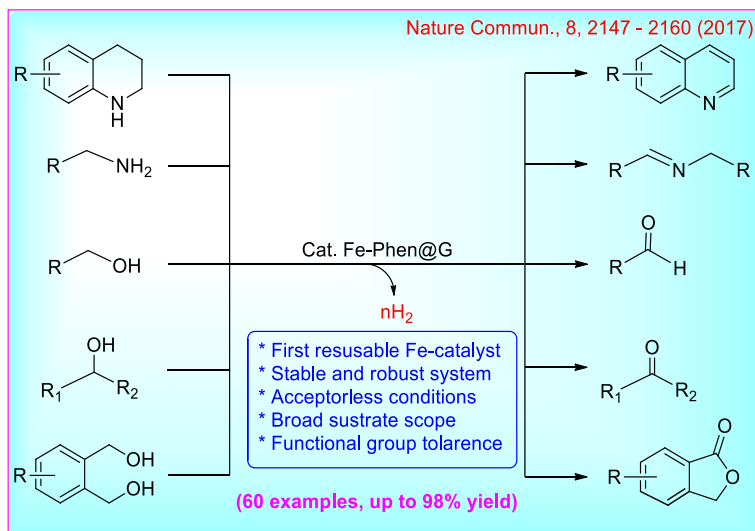
Similarly, hydrogen auto-transfer (HA) or borrowing hydrogen strategy (BHS) is one of the important organic transformations in synthetic chemistry, where hydrogen is borrowed from the starting materials and effectively being utilized for the catalytic hydrogenation (*in situ*) at the

final step of process (Scheme 1). Thus, the net result would be highly atom-, and step of economical with zero carbon footprint process. Borrowing hydrogen methodology can be used for the synthesis of wide range of C-C and C-N bonds by using alcohols as alkylating reagent.

Chapter 2: Iron nanocatalyst for the acceptorless dehydrogenation reactions

Despite a number of homogeneous catalysts based on noble metal being identified for the acceptorless dehydrogenation (AD), the use of high price and limited availability of precious metals and poor recovery of the catalyst have spurred interest in catalysis with more earth-abundant alternatives, especially iron. However, no report has described a reusable iron-based heterogeneous catalyst for oxidant-free and acceptorless dehydrogenation reactions prior to our report. In the present chapter, we have replaced expensive noble metal catalysts with an inexpensive, benign, and sustainable iron based nanocatalyst for the efficient acceptorless dehydrogenation (AD), and acceptorless dehydrogenative coupling (ADC) reactions. This working chapter has been further divided into two parts.

Part A:



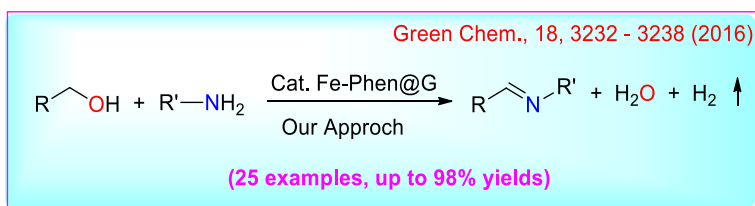
Scheme 2. Acceptorless dehydrogenation catalyzed by iron-based nanocatalyst.

Chapter 2A deals with the heterogenization of homogeneous metal complex ($Fe:N^x$). Heterogeneous catalyst was well-characterized using the state-of-the-art techniques and then the catalytic material was successfully applied for the dehydrogenation of feedstock chemicals, such

as alcohols, amines, and *N*-heterocycles to value-added products with the concomitant generation of dihydrogen (Scheme 2). The present catalytic approach possesses a dual role; acting as a catalyst as well as can be magnetically separable. The sustainable reuse of heterogeneous iron catalyst is also shown.

Part B

Chapter 2B deals with ADC of alcohols with amines to get imine using as synthesized heterogeneous Fe-catalyst. Imines are an exceptionally versatile functional group and are ubiquitous in pharmaceuticals, biological active heterocycles, and natural products. The reaction operates under mild reaction conditions with the liberation of dihydrogen and water as the byproducts. The developed ADC strategy is simple, efficient, exhibits wide functional group tolerances and can be scaled up.



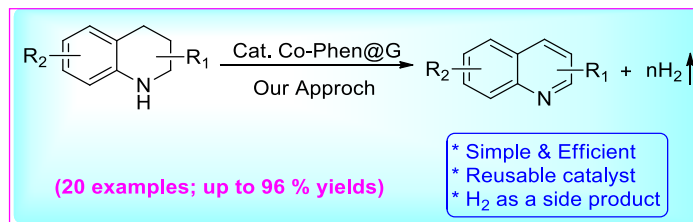
Scheme 3. Synthesis of imine *via an* acceptorless dehydrogenative coupling.

Chapter 3: Cobalt nanocatalyst for the transfer hydrogenation of alkynes and dehydrogenation reactions

The third chapter is mainly focused on cobalt nanoparticles deposited on different supports and their catalytic activity on AD and transfer hydrogenation reactions. This chapter is also divided into two parts.

Part A

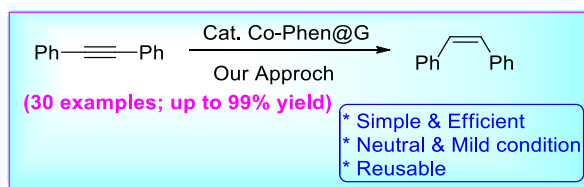
In continuation with our interest in the development of efficient heterogeneous catalyst containing sustainable transition metals, we have investigated cobalt based heterogeneous catalyst for the dehydrogenation of *N*-heterocyclic motif. Here, we report the first cobalt based heterogeneous catalytic system for challenging catalytic dehydrogenation reactions of *N*-heterocycles. The reaction is general and 20 examples with a yield up to 96% was achieved under optimized condition.



Scheme 4. Cobalt-catalyzed acceptorless dehydrogenative of *N*-heterocycles.

Part B

The catalytic hydrogenation of unsaturated compounds is a fundamental synthetic transformation, which has applications in the agrochemical, pharmaceutical, and commodity chemical industries. Thus, the stereoselective semi-hydrogenation of alkynes under mild conditions is a great challenge. The contiguous effort has been made for synthesis of olefins using homogeneous and heterogeneous catalysis using H₂ at the high pressure. The reduction of alkynes into stereoselective olefins and avoid the formation of over reduced alkane is very challenging. Ammonia-borane (AB) has the advantages of high hydrogen content (19.6 wt.%), low molecular weight and high stability in solutions. It can be safely transported without hydrogen loss, thus making it a highly promising alternative for chemical hydrogen storage material. Herein, we report an operationally simple, mild, and highly *cis*-selective hydrogenation of alkynes and terminal alkyne, applying a reusable cobalt heterogeneous catalyst deposited on graphene.

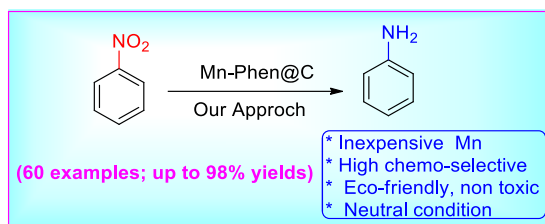


Scheme 5. Cobalt-catalyzed semihydrogenation of alkynes.

Chapter 4: Reusable Manganese nanocatalyst for chemo-selective hydrogenation of nitroarenes

Aromatic amines serve as industrially important intermediates and play a key role in agrochemicals, biorenewable chemicals, pharmaceuticals, and fine chemicals. The significant growth has been devoted to hydrogenation of nitroarenes to anilines by precious metal based catalysts and this protocol lacks in selectivity and functional group tolerance. The high pressure

H₂ gas is mainly used for the hydrogenation of polar or non-polar compounds and indeed possess safety and handling issues. Nowadays, transfer hydrogenation or auto-transfer hydrogenation had received much attention, in which the *in situ* generated hydrogen can be utilized for reduction process (Scheme 6). Novel manganese-based nanocatalyst has been investigated for chemoselective hydrogenation of nitroarenes using AB as transfer hydrogenating reagent. The strategy works under the very mild condition and neutral condition with high chemoselectivity. To the best our knowledge there is no report on dehydrogenation of AB and subsequent chemoelective hydrogenation of nitroarenes to anilines either under homogeneous and heterogeneous conditions.



Scheme 6. Manganese catalyzed chemo-selective hydrogenation of nitroarenes.

Chapter 5: Fe Based nanocatalyst for partial hydrogenation of CO₂ to CO

Fifth chapter is mainly focused on utilization of iron-based catalyst for partial selective hydrogenation of carbon dioxide to carbon monoxide (RWGS). One of the important strategies is to utilize CO₂ can be partial hydrogenation of CO₂ to produce CO₂-containing syngas (CO₂+SG). Syngas can be used as a feed in crucial energy technologies based on Fischer Tropsch synthesis, CAMERE process, and fuel cells. Selectivity is the issue as methane is one the side product in RWGS reaction. We have successfully used an iron-based heterogeneous catalyst for the selective, partial hydrogenation of CO₂ to CO (selectivity up to 98%).

Chapter 1

Dehydrogenation and related reactions

1.1: Introduction

Catalysis based on fundamentally important feedstocks that enable the access for the sustainable approach is an important tool in the advancement of the chemical production and energy storage applications. In this regard, global demand for energy does make a constant search for renewable feedstocks which can reduce the major dependency of depleting fossil fuel. Irreversible consumption of limited, non-renewable fossil fuel emits greenhouse gases, which cause harmful environmental damages related to global warming. Thus, increasing global demand for energy and environmental concern has set a challenge to establish alternative energy sources for manifold practical applications such as transportation, electricity and as a reagent for chemical synthesis. Nevertheless, there are some obstacles addressed for the deployment of renewable resources such as biomass, the wind, solar, and hydroelectric as almost unlimited energy sources. These renewable resources are only for the specific period which cannot be gained on demand. Thus, an efficient route for energy storage has to be established for a steady supply of energy on demand. Among many storage mediums, the hydrogen economy is an efficient and appealing alternative for the modern society. Hydrogen holds great potential as a secondary energy carrier and consumption of H₂ leads to water as an only benign byproduct. However, there are many unresolved problems associated with the hydrogen economy for practical applications. Mainly, the production of hydrogen is currently affected with fossil fuel. The storage and transport of low volumetric energy density of hydrogen are the second major challenging task for providing safe and clean fuel technology.¹

With this concern, few possibilities have been explored based on physical storage of hydrogen in which hydrogen is stored as diatomic molecular form such as high-pressure tanks, various carbon materials, zeolites, clathrate hydrates, and metal-organic frameworks. Most of these techniques are less energy efficient due to the large energy gap between storage and release process. In chemical hydrogen storage, hydrogen is stored as its chemical bond instead of molecular hydrogen. Usually, a suitable chemical compound, having a high hydrogen content is used, which can easily release hydrogen at ambient temperature *via* catalytic process or non-catalytic process. Examples of these molecules include alcohol, metal borohydrides, amine-borane adduct, formic acid, hydrous hydrazine, metal hydrides etc. Suitability of these molecules in practical applications mainly depends on the choice of dehydrogenation strategy. Most interestingly, the

recent development of molecular catalytic dehydrogenation strategy provides new opportunities for the utilization of organic compounds as a safe, storable, and transportable medium. In addition to that, the fundamental process of catalytic dehydrogenation chemistry also affects the production of hydrogen from renewable biomass derivatives making hydrogen economy as an environmentally benign and sustainable energy source. Furthermore, catalytic dehydrogenation of renewable chemical feedstock's with the liberation of molecular hydrogen opens a new avenue in contemporary science to enable the direct access of abundant organic substrates and it manifolds practical applications for the chemical production and energy storage.^{2,3}

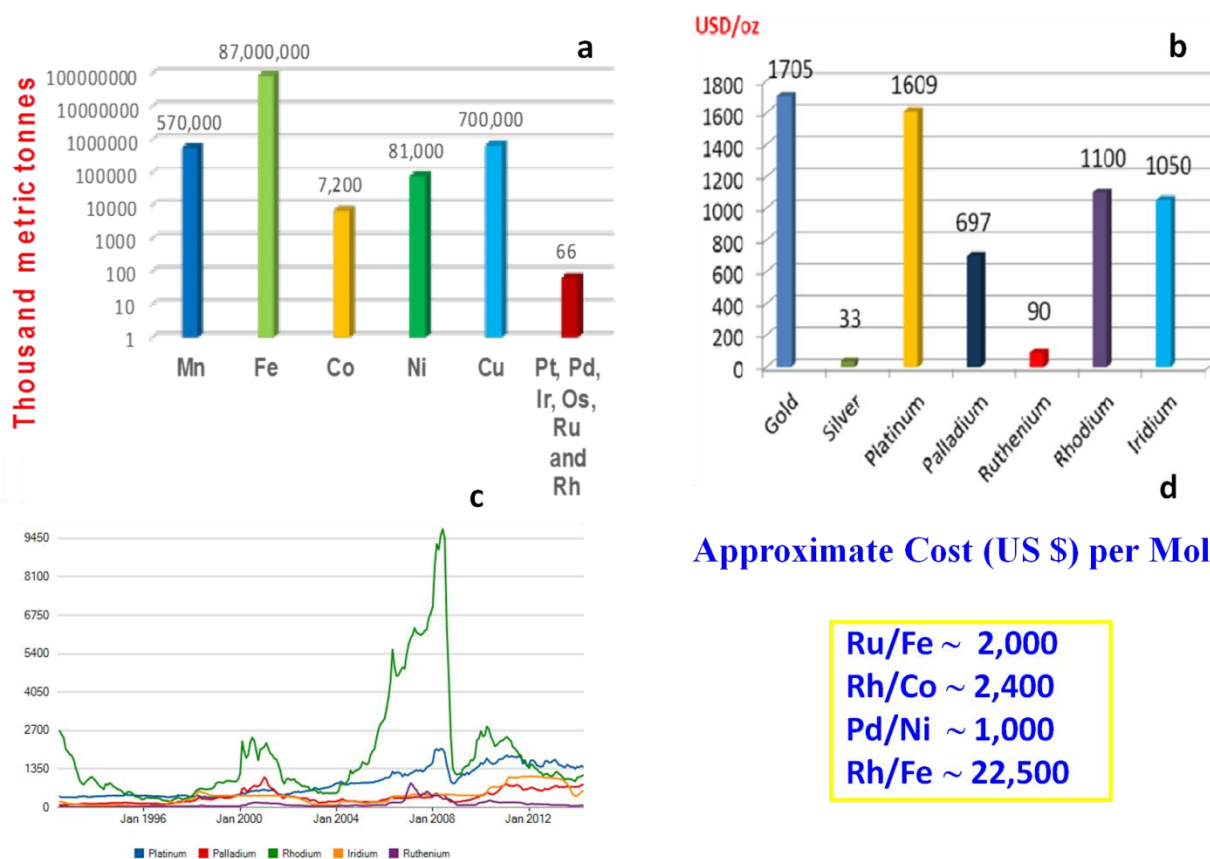


Figure 1.1. a) Known global reserves of metals; b) Price of precious metals; c) Price fluctuation of traditional transition-metal catalysts; d) Price comparison of base metals vs precious metals (Costs calculated in US dollars from Strem catalog using lowest cost metal powder with purity $\geq 99\%$).

Undeniably, the catalytic dehydrogenation has been deployed mostly by using precious noble metal catalysts such as Pd, Rh, Ru, and Ir to afford the eco-benign, and atom-economical strategy.^{4,5} Classically, they often follow $\pm 2e^-$ oxidation state change to facilitate the elementary bond forming and breaking event through oxidative addition and reductive elimination at the

metal center. This precious transition-metal catalyzed dehydrogenation process enabled the direct access to convert unreactive organic feedstocks into valuable intermediates and provided unprecedented chemical transformations. However, the limited availability of the precious metal salts and their high-price urge chemists and chemical. Industries to search for new sustainable systems to facilitate practical applications.

In recent times, catalysis based on relatively abundant and economical first-row transition metals (Fe, Co, Mn, and Ni) is becoming more fascinating and an appealing alternative to precious metal-based catalytic systems. However, the exploration of an efficient catalytic system based on first-row transition metals is extremely rare. This is mainly attributed due to the very narrow energy gap between the d-orbitals of first-row transition metals and their propensity to participate in one electron chemistry as opposed to the traditional two electron transformation, which is ubiquitous in the precious second- and third-row transition metals. Further, it's a challenge to work with paramagnetic materials that are kinetically labile in nature and underdeveloped mechanistic studies. In recent years, the above challenges have been overcome by designing metal catalysts with appropriate ligands to enable successful progress in the development of a new and sustainable system for energy storage and catalysis.

In this regard, earth-abundant, and inexpensive iron-catalysis has become more fascinating and a viable system for environmentally benign reactions. The economical, biorelevant, and ample supply of these salts, coupled with their lack of toxicity, makes them ideal candidates for both academic and industrial applications. In the recent past, there is an increasing interest in the use of cheaper and non-noble iron complexes in dehydrogenation strategy. Iron catalysts for chemical synthesis have been experienced renaissance due to not only its abundance in various biological systems; nevertheless, its reactivity and selectivity are presently comparable with the state-of-art of precious metal catalysts. Iron-catalyzed synthetic transformations have been proved to be efficient, and that became one of the hot topics in modern science.⁶⁻¹³

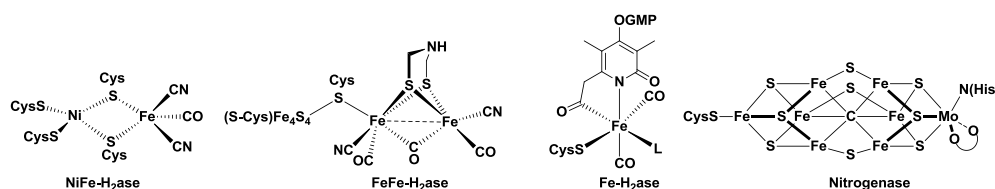
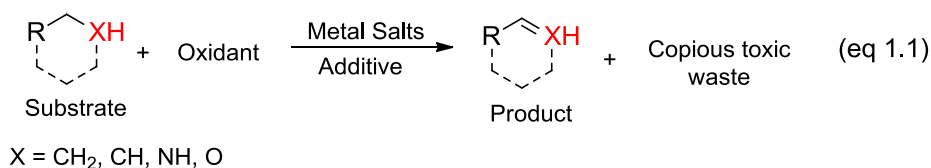


Figure 1.2. Active sites of hydrogenase and nitrogenase enzymes.

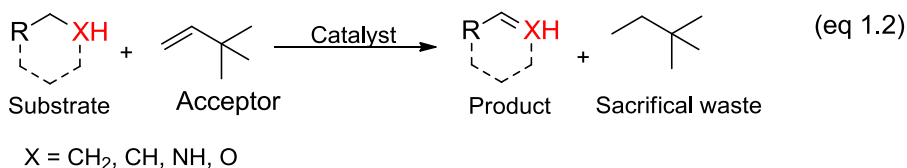
1.2. Dehydrogenation reaction and applications in energy storage

Removal of hydrogen atoms from adjacent atomic centers of an organic molecule is dehydrogenation reaction. It is a highly thermodynamically uphill process. Conventionally, oxidative dehydrogenation reaction has been performed using stoichiometric or excess amounts of oxidants such as DDQ, peroxides, iodates, chromium (IV) reagents and metal oxides, that produce a large excess of hazardous waste equivalent to the oxidants (eq 1.1).¹⁴⁻¹⁵ An alternative to these strong and toxic oxidants is to use pressurized oxygen air or oxygen which can cause explosion hazards. Catalytic dehydrogenation can also be performed in the presence of hydrogen acceptor such as sterically hindered alkene, ketones etc (eq 1.2). The overall process is redox neutral and does not involve net hydrogen evolution; however, it generates the stoichiometric amount of sacrificial organic waste.⁶⁻¹⁴ Catalytic dehydrogenation is one of the most fundamental processes in synthetic chemistry and chemical biology. Thus, it would be challenging to explore the catalytic performance of efficient robust catalysts for the removable of dihydrogen molecule.

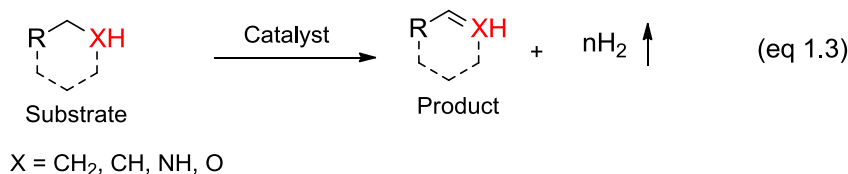
Oxidative dehydrogenation



Transfer dehydrogenation

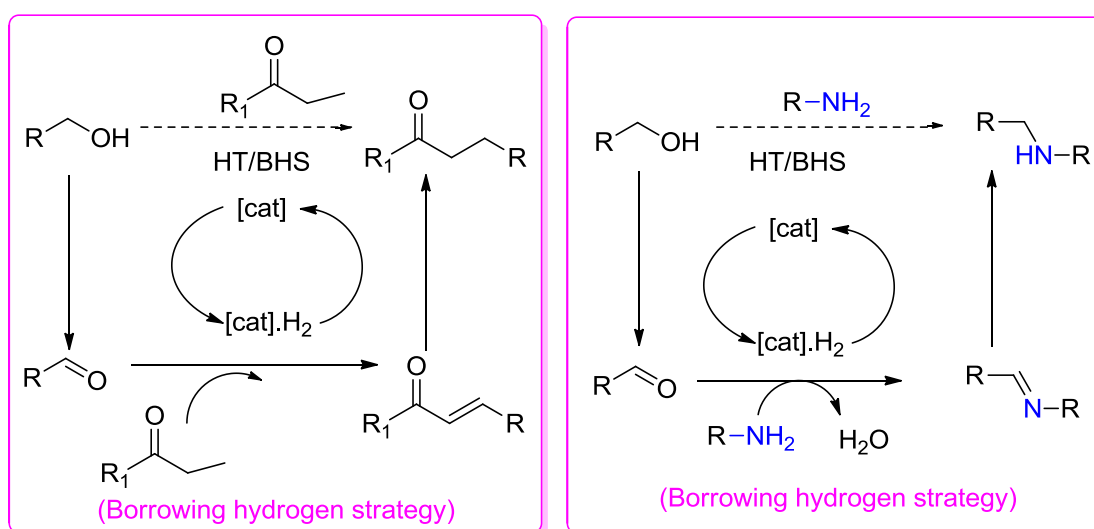


Acceptorless dehydrogenation



Scheme 1.1. Various methods of dehydrogenation reaction.

Acceptorless dehydrogenation (AD) and Hydrogen-Auto (HA) (or) Borrowing Hydrogen (BH) transfer reaction strategies have attracted considerable interest in recent times, in large part due to the excellent step-economy and high atom-efficiency, thus obviating the need of stoichiometric non-selective strong oxidants. Interestingly, the AD strategy plays a crucial role in the selective activation of adjacent hydrogen atoms in alcohols ($-\underline{\text{C}}\text{H}-\underline{\text{O}}\text{H}$) and amines ($-\underline{\text{C}}\text{H}-\underline{\text{N}}\text{H}$) without pre-functionalization and provides reactive intermediates for further synthetic transformations with the liberation of molecular hydrogen as the green byproduct (eq 1.3).



Scheme 1.2. Borrowing hydrogen strategy (formation of C-C and C-N bonds)

Reversible catalytic dehydrogenation of alcohols and amines is one of the emerging fields of molecular catalysis which can deliver a sustainable approach for the safe, storable and transportable energy storage systems (*hydrogen economy*). Besides, the catalytic acceptorless dehydrogenative coupling (ADC) reactions provide benign synthetic approaches for efficient organic transformations through tandem C-X bond (X = C, N, and O) forming reactions, with the liberation of H_2 and H_2O . The hydrogen-atom (HA) transfer reaction affords an elegant route to construct C-C and C-N coupling reactions, with the loss of water as the only sole by-product. This strategy consists of

1. Initial catalytic dehydrogenation of alcohols.
2. The reactive intermediate undergoing a chemical transformation with nucleophiles,

3. Hydrogenation of the intermediate with the initially removed dihydrogen.

Overall, the hydrogen-auto transfer reaction follows a net redox neutral catalytic cycle. Thus, catalytic AD and HA reactions of renewable chemical feedstocks with the liberation of molecular hydrogen/water open a new avenue in the contemporary organic synthesis and have manifold practical applications in sustainable energy.¹⁷

1.2.1. Dehydrogenation of formic acid

Formic acid (FA), containing 4.4% of hydrogen with a volumetric capacity of 53.4 g/L at standard temperature and pressure, is a low-toxic, renewable liquid and has recently attracted much attention as a reversible hydrogen storage material. In earlier studies, formic acid and its conjugate base, formate ion have been extensively used in the transition-metal catalyzed transfer hydrogenation reactions. Catalytic dehydrogenation of formic acid offers zero-carbon footprint hydrogen storage (Figure 1.3).^{3, 16-20}

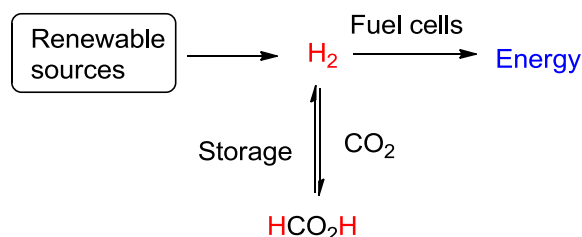
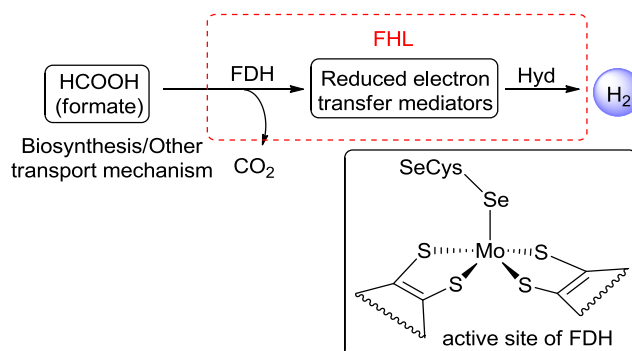


Figure 1.3. HCOOH/CO₂ involving hydrogen storage cycle.

Indeed, in the catalytic dehydrogenation of formic acid to gaseous H₂ and CO₂, the co-product CO₂ can be hydrogenated back to formic acid and thus, completes the hydrogen storage and delivery cycle, or it can be utilized directly as an abundant C₁-feedstock by mineral carbonation. Notably, dehydration of formic acid into water and CO is considered as an undesired side reaction and deactivates the Pt-catalyst of the fuel cell. In this regard, development of an efficient and sustainable catalytic system for the selective dehydrogenation of FA suppressing the undesired decarbonylation has received increasing attention.

In the biochemical process, a complex formate hydrogenlyase (FHL) consisting of two metalloenzymes namely formate dehydrogenase (FDH) and hydrogenase (Hyd), catalyzes the

processing of formate ion into molecular hydrogen and CO₂ as a key step in bio-hydrogen production (scheme 1.3).²⁰



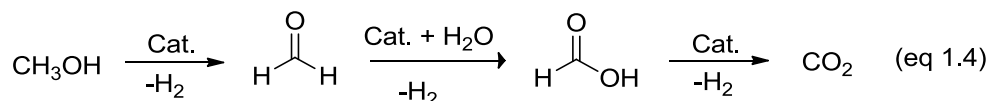
Scheme 1.3. various method of oxidative dehydrogenation reaction.

Formate dehydrogenase contains an active center of Mo atom coordinated with two ene-dithiolate ligands. An electronic and structural feature of above biocatalysts inspired for the designing of artificial catalytic systems. Extensive research and developments are still required to make this HCOOH/CO₂ catalytic cycle viable for hydrogen storage applications. Several obstacles have been explored in the search for suitable catalysts both under homogeneous and heterogeneous conditions for selective dehydrogenation of formic acid. However, the success on selective dehydrogenation of formic acid using an earth-abundant, inexpensive metal catalyst remains elusive and very challenging.

1.2.2. Dehydrogenation of methanol

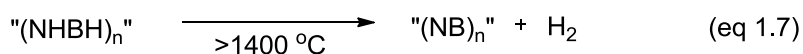
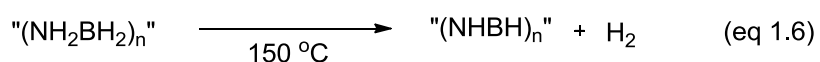
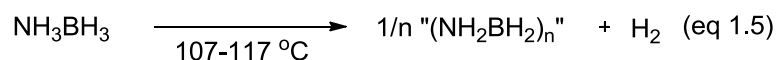
Methanol represents a promising target of a chemical energy carrier as it has a high gravimetric hydrogen content of 12.6 %. The combined advantages of methanol transportation under practical conditions and the efficiency of the proton exchange membrane fuel cell, reformed ethanol fuel cell (RMFC) has been developed where methanol reforming takes place according to the equation 1.4. Methanol steam reforming usually promoted by heterogeneous catalysts and requires very high temperature, which limits the overall efficiency of fuel cell (c.a 40%). In addition, catalyst produces a significant amount of CO and poisons the Pt-electrode of the fuel cell. In recent times, Ru- and Ir-based homogeneous catalytic system for complete dehydrogenation of methanol in an aqueous solution is reported, which operates at a significantly lower temperature (80 - 100 °C) and produces less CO.² However, limited availability and the

high cost of noble metal catalytic system strongly demands a new catalytic system based on abundant and inexpensive non-noble metal catalysts.



1.2.3. Dehydrogenation of amine-borane adduct

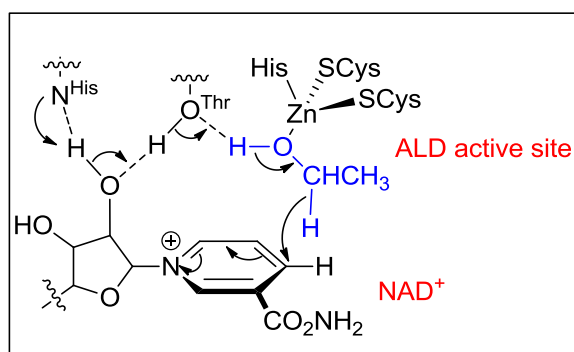
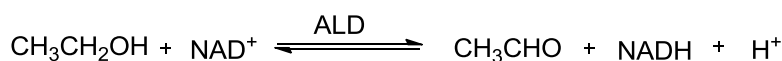
In recent times, ammonia-borane adduct ($\text{H}_3\text{N}:\text{BH}_3$, AB) has gained much attention due to its potential to be utilized as a chemical hydrogen storage material. It contains hydrogen content of 6.5, 13.1 and 19.6 % for the step-wise release of the first, second and third equivalent of H_2 respectively, which indeed, exceeds wt% of gasoline. Thermal dehydrogenation and acid-catalyzed hydrolysis of AB adduct are shown in equations 1.5-1.9. Due to high temperature and slow reaction rate of hydrogen release, the option to use AB for practical applications remains a challenge. In past decades, a few advancements on the dehydrogenation of AB adduct have been achieved at ambient temperature using precious-metal based catalytic systems. Although the high extent of hydrogen release thereby taking the advantage of the high gravimetric content of hydrogen in AB system has been achieved, the material that emerges from cheap and abundant metals are preferred for the large-scale hydrogen storage and transportation.²¹ Despite hydrogen storage applications, dehydrogenation of AB adduct affords valuable inorganic materials such as a B-N bonded oligomer and/or a polymer.



1.2.4. Dehydrogenation of Alcohols

Alcohols are the common feedstocks for chemical synthesis, albeit they are quite unreactive. Several synthetic transformations would be more efficient and more eco-friendly if there were

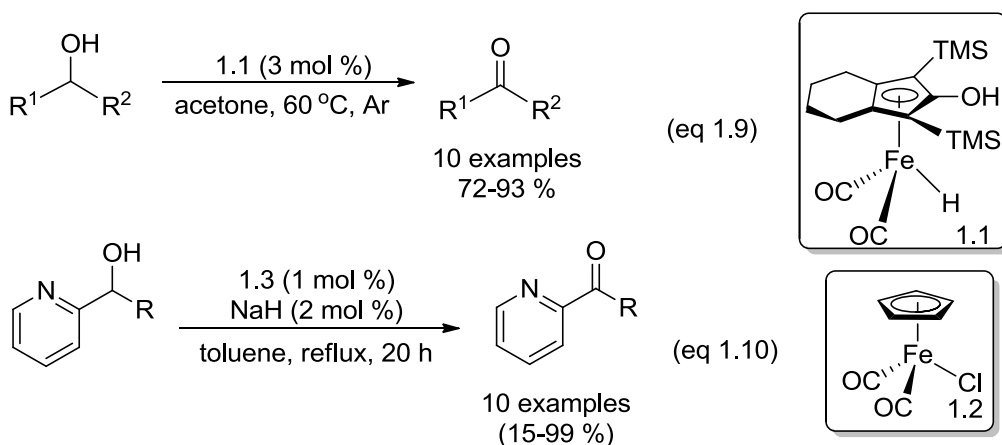
the advancements of making alcohols to be more reactive. An attractive and ideal approach for alcohol activation is being developed, which uses a catalyst to extract dihydrogen (a potential energy carrier) from adjacent atoms center of alcohol ($\underline{\text{CH-OH}}$ atoms). This process oxidizes the alcohol under *oxidant-free* conditions to form a highly reactive carbonyl compound. Traditionally, dehydrogenation of alcohols has been achieved with the aid of stoichiometric amount of sacrificial hydrogen acceptors. In nature, dehydrogenation of ethanol can be effected with the aid of metalloenzyme, alcohol dehydrogenase (ALD) associated with coenzyme nicotinamide adenine dinucleotide (NAD) leading to the reversible formation of acetaldehyde. In this biological system, ALD activates the proton transfer process whereas NAD receives hydride forming NADH and carbonyl compounds (Scheme 1.4).² This is the classic example of metal-ligand cooperative hydrogen transfer process that directs implications in the development of redox active ligand having catalytic systems. The acceptorless dehydrogenation (AD) strategy has made the renewable alcohols as versatile starting materials for an assortment of synthetic transformations.⁴ Based on these insights, iron-based catalytic systems are explored to make this simple and clean acceptorless-dehydrogenation into the much more valuable sustainable approach. Recently, it has been recognized that iron-based dehydrogenation process with the liberation of dihydrogen as the byproduct, competes with the state-of-art of precious metal-based catalytic systems.



Scheme 1.4. Dehydrogenation pathway of alcohol dehydrogenase (ALD).

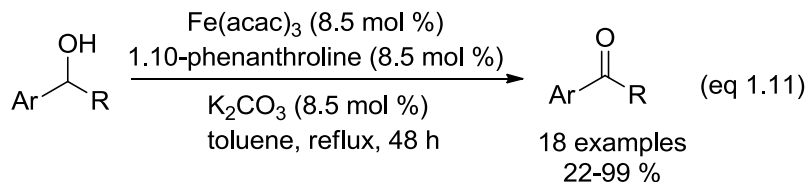
Casey *et al.* reported the well-defined iron complex (hydroxycyclopentadienyl)iron dicarbonyl hydride **1.1** as a catalyst for the efficient and chemoselective hydrogenation of

aldehydes and ketones.²² Iron complex **1.1** was initially synthesized by Knölker *et al.* and the three-dimensional structure was assigned using X-ray analysis.²³ Having the mechanistic insights of above hydrogenation, initial iron-based dehydrogenation of alcohols have been achieved in the presence of acetone that serves as both solvent and hydrogen acceptor.²⁴ Dehydrogenation reactions were proceeded under mild conditions with a wide functional group tolerance including easily interconvertible olefins and cyclopropyl motif. However, this reaction was limited to secondary alcohol derivatives and conjugated primary alcohols due to issues associated with the unfavorable equilibrium of reversible reaction (eq 1.9).

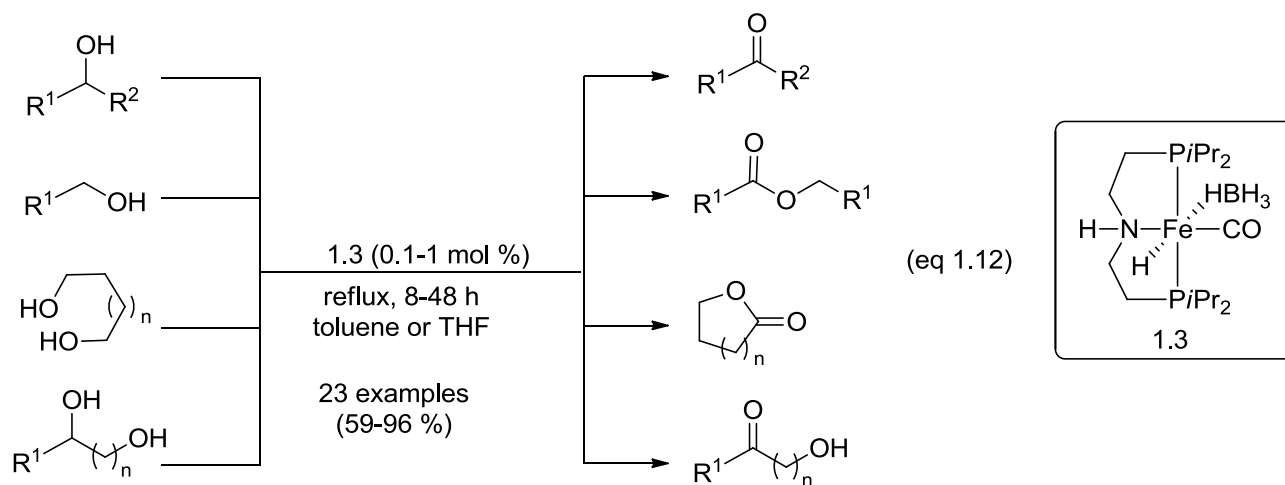


In 2014, iron-cyclopentadienyl complex **1.2** has been reported for the first oxidant-free and acceptorless dehydrogenation of 2-pyridylmethanol derivatives.²⁵ This complex was predominantly used to transform 2-pyridylmethanol derivatives into corresponding carbonyl compounds with a turnover number up to 67000. Mechanistic insights revealed that the success of this catalytic process is due to the crucial involvement of 2-pyridyl motif (substrate) in the catalytic cycle which limits the scope of this methodology to solely 2-pyridyl derivatives (eq 1.10).

Song *et al.* developed a simple iron catalytic system for selective dehydrogenation of secondary benzyl alcohol derivatives.²⁶ The active iron-complex was generated *in situ* by a mixing of Fe(III) acetylacetonate, 1,10-phenanthroline, and K_2CO_3 under ambient conditions. Notably, other secondary alcohols and primary alcohols were ineffective, and no dehydrogenation was observed. The kinetic isotope effect reveals that $C_{(\alpha \text{ position of alcohol})-H}$ cleavage is the rate-limiting step similar to other precious metal-based catalytic transformation (eq 1.11).

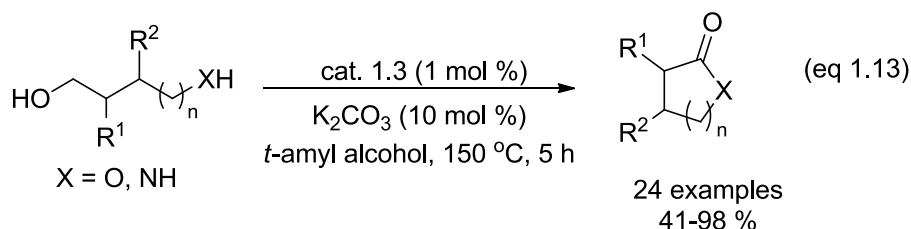


Jones and Schneider research teams have reported the well-defined iron-complex **1.3** chelated with aliphatic PNP pincer for the acceptorless dehydrogenation of alcohols based on metal-ligand cooperation mechanism.²⁷ This was the first iron-based homogeneous catalytic system explored for dehydrogenation of both primary and secondary alcohols with the extrusion of hydrogen gas. Secondary alcohols were successfully converted into corresponding ketones in good to excellent yields with a low catalytic loading (0.1 mol %, TON = 10³). Interestingly, primary alcohols were undergone dehydrogenative coupling presumably *via* Tishchenko reaction to result in the formation of esters. Similarly, diols were selectively converted into the corresponding lactones which are marked as biologically and synthetically significant building blocks. In the presence of both primary and secondary alcohols, chemoselectivity of dehydrogenation proceeded at secondary alcohols over primary alcohols under similar catalytic conditions, which were observed only a few noble-metal-based catalytic systems (eq 1.12).



The success of iron-pincer complex **1.3** in acceptorless-dehydrogenation was further explored by Beller and co-workers for the construction of heterocycles such as lactones and lactams via the dehydrogenative tandem process.²⁸ A broad range of 1,4-diol derivatives was converted into lactones with the liberation of molecular hydrogen. Similarly, under the same reaction

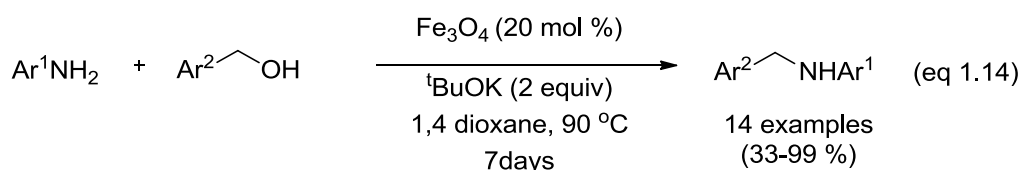
conditions, 1,5 and 1,6-diols were also utilized to yield the corresponding lactones. Interestingly, 1,5 and 1,6-amino alcohols were transformed into cyclic amides (lactams). Thus, this method provided the broad spectrum of heterocyclic compounds from easily accessible alcohol derivatives with high atom economy (eq 1.13).



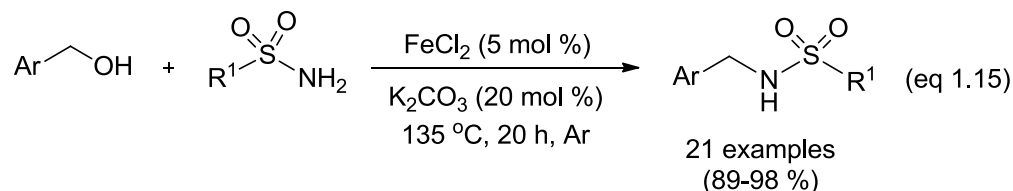
1.2.5. Dehydrogenative hydrogen transfer of alcohols (*N*-Alkylation of Amines)

Dehydrogenative hydrogen transfer, so-called borrowing hydrogen strategy consists of initial dehydrogenation of an alcohol into an aldehydic intermediate with extrusion of H₂, imine formation with the liberation of water and hydrogenation of imine by utilizing the hydrogen liberated in the first step, leading to a net redox-neutral reaction. Recently, noble-metal-based hydrogen transfer process has set as emerging trend in organic synthesis to achieve step- and atom-economical approach. In this aspect, the construction of C-N bond through *N*-alkylation of amine has evolved in terms of atom-economical and eco-benign route by utilizing renewable and easily accessible alcohol as alkylating reagent with the release of water as the only by-product.⁴ Precious-metal based hydrogen transfer *N*-alkylation process has made the significant progress on sustainable chemical synthesis ranging from fine chemicals to complex molecules. The mechanism for the transition-metal catalyzed *N*-alkylation process is shown in Scheme 1.2.

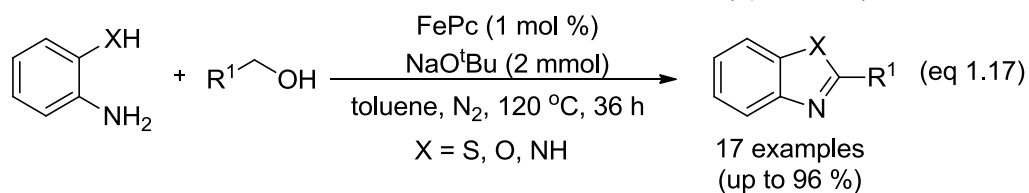
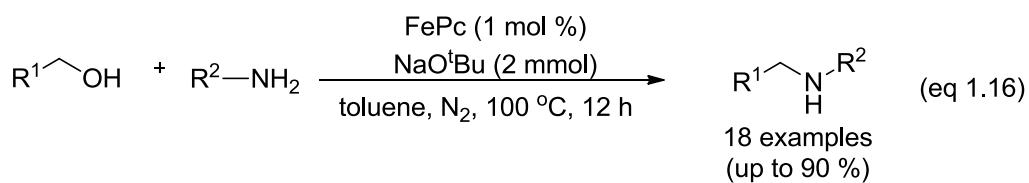
Yus and co-workers reported *N*-alkylation of amine by using alcohol as alkylating agents catalyzed by a commercially available magnetite as a stable and recyclable heterogeneous catalyst (eq 1.14). This catalyst was recycled and reused up to eight cycles without loss of its activity.²⁹



Similarly, environmentally-benign and the simple $\text{FeCl}_2/\text{K}_2\text{CO}_3$ catalytic system was reported for the N-alkylation of sulphonamide with benzyl alcohols *via* the hydrogen transfer process (eq 1.15).³⁰

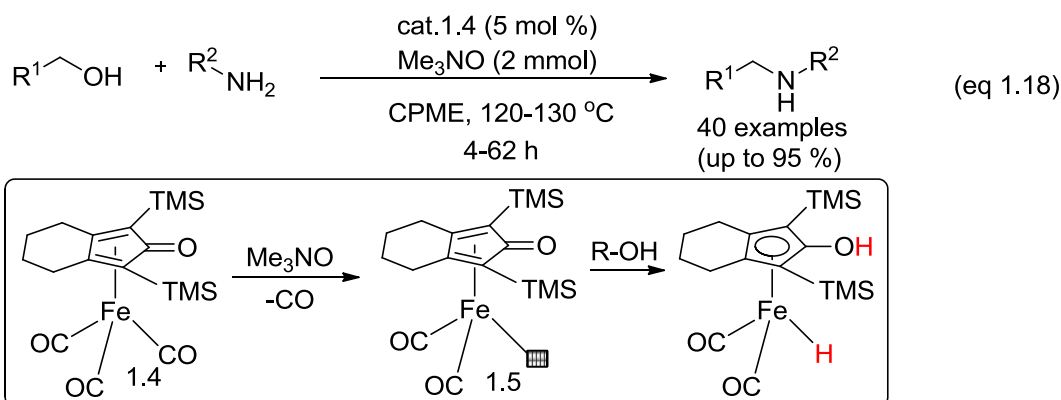


Significantly, hydrogen auto transfer strategy was successfully applied to the synthesis and functionalization of privileged heterocyclic scaffolds using iron phthalocyanine (FePc) as a cheap, eco-benign, and versatile catalyst.³¹ Amino-substituents on heterocyclic scaffolds such as amino benzothiazoles, aminopyridines, and aminopyrimidine were selectively functionalized with alcohols as an alkylating reagent in presence of iron phthalocyanine catalyst. The iron-phthalocyanine complex was also applied for the construction of heterocyclic frameworks by the dehydrogenative coupling of *ortho*-substituted anilines (-NH₂, -SH and -OH) to afford the benzimidazoles, benzothiazoles, and benzoxazoles. The coupling of benzyl alcohol derivatives with *ortho*-substituted anilines provided good to excellent (up to 99%) yields whereas aliphatic alcohols showed moderate reactivity (eq 1.16 and 1.17).

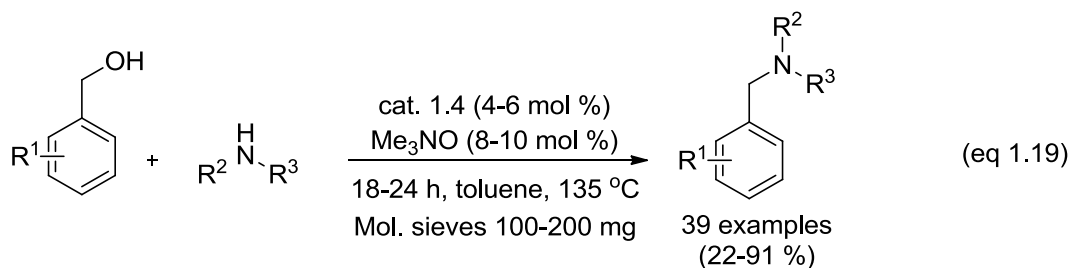


The general method for N-alkylation of amines such as aliphatic and aromatic amines by alcohols was reported by using a well-defined homogeneous iron catalyst **1.4** using a cooperative ligand.³² The non-innocent ligand, cyclopentadienone plays an important role in the catalytic cycle during dehydrogenation and hydrogenation process.³³⁻³⁶ The success of this catalyst is the suitability of both initial dehydrogenation of alcohol and the final

hydrogenation of imine at a sufficient rate through the metal-ligand cooperative mechanism. The catalytically active complex **1.5** was generated *in situ* from air and moisture stable complex **1.4** in the presence of oxidant Me₃NO. The effective mono-*N*-alkylation of anilines and benzyl amines were achieved in this methodology, and aniline possesses electron withdrawing groups such as ester, nitro, cyano were not successful in this process. The *N*-alkylation of amines with diols and diamine with diol was developed for the construction of various five- to seven-membered heterocyclic compounds through borrowing hydrogen strategy (eq 1.8).

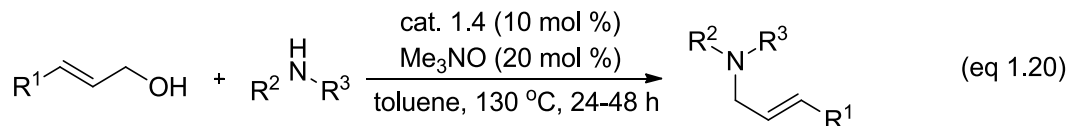


Similarly, the construction of benzylamines from readily available benzyl alcohols was reported using **1.4** as a catalyst providing a variety of substituted secondary and tertiary benzylamines in moderate to excellent yields (eq 1.19).³⁷ Indeed, substituted benzyl alcohols such as electron withdrawing and donating group and heterocyclic containing motif was successfully explored in this strategy.

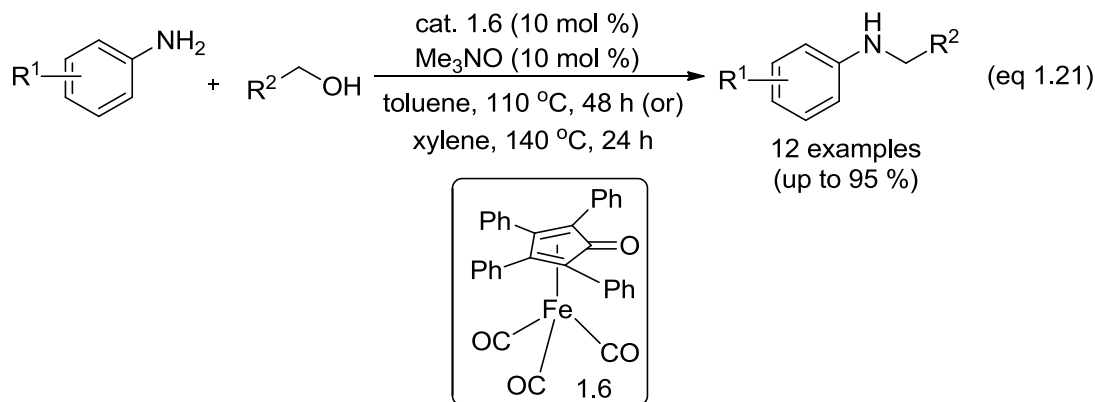


Moreover, the unprecedented synthetic transformation of renewable building block 2,5-furan-dimethanol to pharmaceutically relevant compounds was achieved using Fe-based hydrogen transfer as key transformation. Sundararaju and co-workers developed the regioselective transformation of allylic alcohols into allylic amines with the aid of complex

1.4 through borrowing hydrogen strategy competing for traditional π -allylic activation pathway (eq 1.20).³⁸

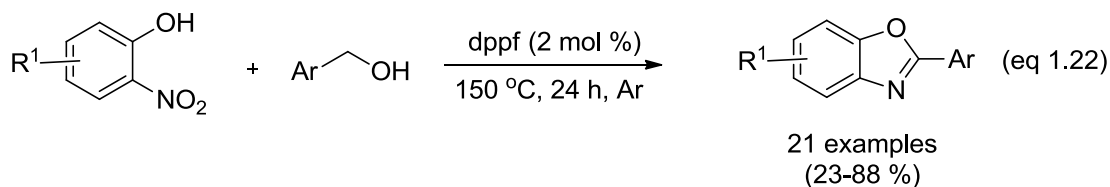


In addition to that, the significance of this strategy was applied to the direct synthesis of common drugs, cinnarizine, and naftifine from commercially available cinnamyl alcohol eliminating water as an only by-product. Wills and co-workers reported the iron-tetraphenylcyclopentadienone complex **1.6** for the selective *N*-alkylation of aniline derivatives.³⁹ In this reaction, an aniline possesses *ortho*/electron withdrawing substituents showed the lower yield of *N*-alkylation product whereas the electron-releasing substituents marked in good yields (eq 1.21). The catalytic activity and selectivity of a similar type of complexes **1.4** and **1.6** reveal that turning off an electronic and steric factor of the non-innocent ligand can be modified the catalytic properties of iron complex.

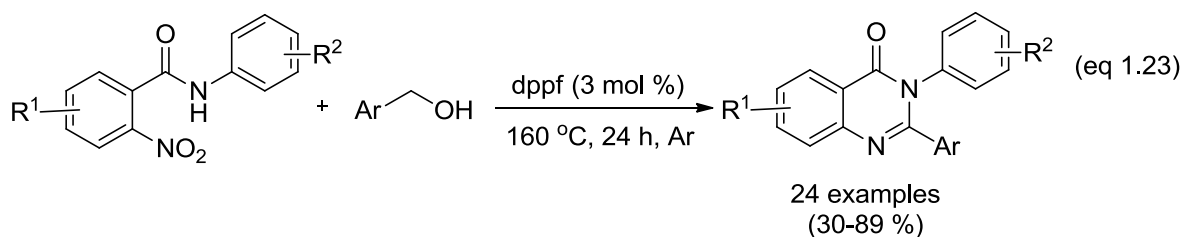


In the arena of catalytic hydrogen transfer process, significant progress has been made by the coupling of nitroarene with alcohol to result in *N*-alkylated amine in the absence of external reductant. This strategy utilizes nitroarene as an alternative source of the amino group whereas the alcohol act as both reducing reagent and substrate for carbon backbone in the absence of external oxidant or reductant thus avoiding the pre-functionalization of starting materials. In this process, Deng and co-workers reported the coupling reaction of *o*-nitrophenol and benzyl alcohol using 1,10-bis(diphenylphosphino)ferrocene (dppf) as a most efficient catalyst to afford 2-aryl benzoxazoles with the elimination of water as the byproduct.⁴⁰ The coupling reaction consists of the following series of reactions; initial

alcohol oxidation, nitro group reduction, condensation, and dehydrogenation in a single operation without any external additives. This greener methodology utilized alcohol as both reductant and coupling reagent enabling the broad range of substrate scope of various benzyl alcohols and *o*-nitrophenols (eq 1.22).



The complementary method for the construction of medicinally important 2,3-diarylquinazolinones was reported by the coupling reactions of stable 2-nitro-*N*-aryl benzamides with benzyl alcohol derivatives using dppf as an iron catalyst.⁴¹ Other primary and secondary alcohols did not proceed with this redox condensation reaction (eq 1.23).

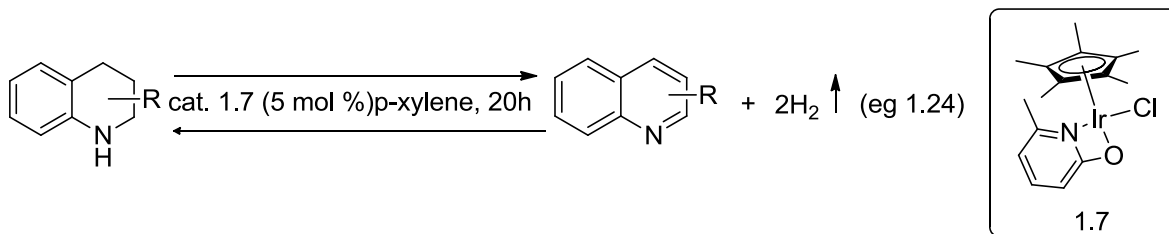


1.2.6. Dehydrogenation of amines

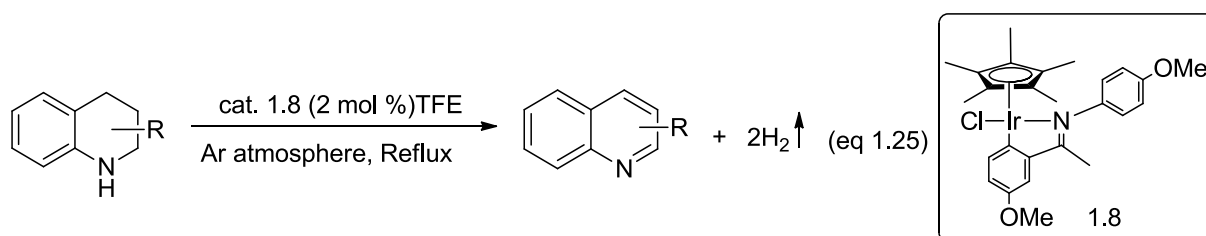
Imines are versatile intermediate in organic synthesis and the synthesis of wide range of value-added and biologically active compounds. Traditionally, they have been prepared by condensation of the amine with extremely reactive carbonyl compounds. Catalytic temporary oxidation of alcohol into aldehyde provides the alternative strategy for imine formation by catalytic coupling reaction of an aldehyde with amine employing expensive rare metals as a catalyst. Moreover, this approach requires high reaction temperature and challenges to control over the reduction of imine to the amine (borrowing hydrogen strategy).⁴² Recently, acceptorless dehydrogenation of amine to imine by precious metals gave the oxidant-free strategy with extrusion of dihydrogen as a by-product.⁴

In 2009, Fujita and co-worker has reported the first example of iridium-based pincer complex **1.7** for dehydrogenation-hydrogenation reactions of nitrogen heterocycles.⁴³ The dehydrogenation was carried in *p*-xylene under reflux for 20 h under argon and the hydrogenation was carried out with hydrogen balloon connected with glass eq. 1.24. Following

system shows the limitation of only a few examples of 1,2,3,4-tetrahydroquinolines were demonstrated. The reaction conditions were relatively harsh (refluxing p-xylene or in mesitylene)

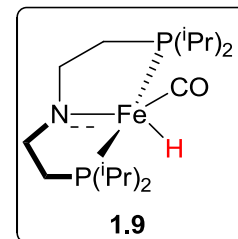
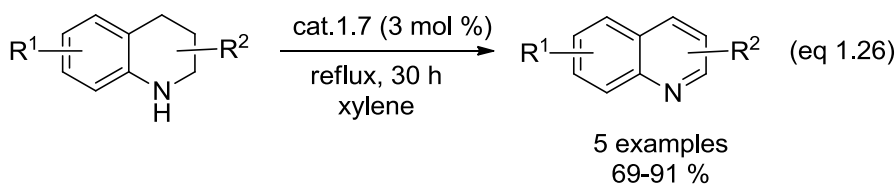


In the continuous effort for the development of a catalyst for acceptorless dehydrogenation (AD), Xio and co-workers reported the cyclometalated [Cp*IrIII]/imino complex **1.8** for the AD and excellent catalytic activity.⁴⁴ The dehydrogenation reaction takes place in TFE (trifluoro ethanol) under nitrogen atmosphere. The above catalytic system showed high activity and broad substrate scope to make it a promising alternative for industrial and laboratory applications.

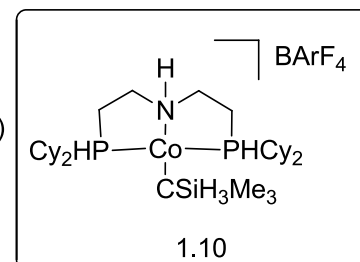
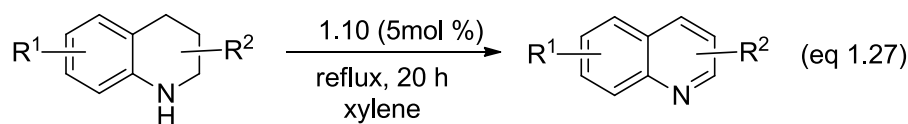


Despite the recent progress with these iridium-based catalysts, development of inexpensive, earth-abundant first-row transition metal catalysts for the dehydrogenation and hydrogenation of *N*-heterocycles is highly desirable. These insights are put to use for the development of more economical and environmental friendly catalytic systems for the conversion of an amine into imine.

In this context, Jones has developed iron-based catalyst **1.9** for dehydrogenation reaction operated at 140 °C in xylene (eq 1.26).⁴⁵ The efficiency and activity complex for amine dehydrogenation was initially studied with 1,2,3,4-tetrahydroquinoline to afford quinoline with extrusion of dihydrogen. Above methodology was underlined with many heterocyclic scaffolds such as 1,2,3,4-tetrahydroquinoline derivatives, 1,2,3,4-tetrahydroisoquinoline, 2-methylindoline, 2,6-dimethylpiperidine, 1,2,3,4-tetrahydroquinoxaline and 1,2,3,4-tetrahydroquinoxaline into corresponding *N*-heteroaromatic compounds and thus, enables a broad range of substrates scope.

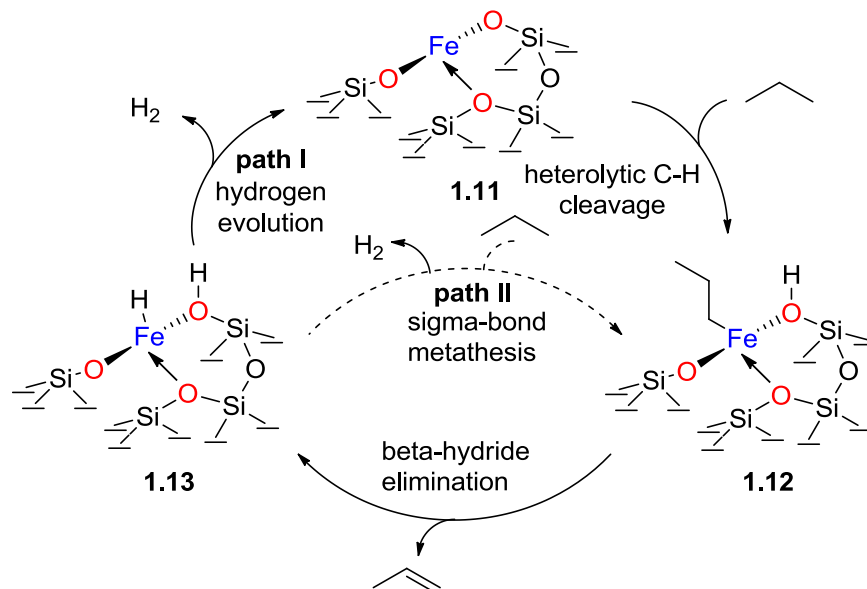


Jones and co-workers has further developed cobalt metal based pincer complex **1.10** for the dehydrogenation of *N*-heterocycles (eq 1.27).⁴⁶



1.2.7. Dehydrogenation of alkanes

Selective functionalization of abundant alkane substrates into value-added products is an attractive and challenging task in chemical science. Catalytic dehydrogenation of alkane feedstock has provided the important and valuable intermediate olefins or arenes that are widely used as a raw material in many industrial processes.⁴ Dehydrogenation of an alkane is industrially achieved by hydrocarbon cracking under harsh condition (high temperature, >500 °C) which limits their applicability in direct synthetic manipulations. For instance, thermodynamically favorable dehydrogenation of propane to propene requires the temperature of about 400 °C. However, the competing reaction of C-C bond cleavage of propane to afford methane and ethane is favorable at 200 °C.



Scheme 1.5. The mechanism for dehydrogenation of propane using isolated FeII on silica.

Both thermodynamic and kinetic attentions make this dehydrogenation protocol particularly more challenging. Yun and Lobo reported an iron-containing zeolite-framework for the catalytic dehydrogenation of propane.⁴⁷ The synthesized iron-silicates showed nearly 20 times higher dehydrogenation rates than cracking rates. The redox catalytic cycle reveals that the hydrocarbon conversion over the isolated iron site proceeds with the formation of radical propane cations since the protolytic mechanism unable to explain the observed difference in the activation energy and selectivity (Scheme 1.5). Similarly, Miller and Hock co-workers reported the synthesis of well-defined isolated Fe^{II} on silica for non oxidative found to be three coordinate Fe^{II} having Lewis-acidic nature. Mechanistically, two possible non-redox mechanisms for dehydrogenation were proposed involving heterolytic C-H cleavage as a common initial process (**1.11**→**1.12**). The resulting common intermediate iron-hydride species **1.12** could undergo two potential pathways: regeneration of three coordinated iron species with extrusion of hydrogen or direct sigma bond metathesis reaction of the Fe-H with propane (Scheme 1.5).

1.3. Current status and challenges

Over the past decade, molecularly-defined organometallic complexes with sophisticated and unstable ligands have led a significant development, which has brought a revolutionary trend in organic synthesis, as well as the industrial scale for the production of value-added chemicals. Mostly heterogeneous materials explored for electrocatalytic, magnetic activity, hydrogenation and oxidation reactions. As compared to homogeneous catalysts heterogeneous catalysts were structurally less understood. However, often more stable, robust, and easy to recover and can be reused. Conventional supports such as Al_2O_3 , and SiO_2 are having high surface area and are highly desirable as support for heterogeneous catalysts. In recent time, a carbon-based support has paid much attention in material science due to its conductive nature, microporous structure, excellent electrical, and high stability. In general, the activity of carbon supported catalysts is controlled by the size and the shape of the particles as well as their interaction with the support. By tailoring the particle size, shape and morphology of nanoparticles and controlling the metal–ligand ratio and metal interaction with support, the catalytic activity and selectivity towards the product can be tuned. In the present study, we are very much interested to develop heterogeneous catalysts based on first-row transition metal with an optimal and broad performance.

Therefore, modification of the support surface by changing the electron density in the support with the incorporation of a heteroatom such as N, B, P allows one to tune the selectivity and activity of such systems. In this perspective, metals supported on nitrogen-doped carbon materials are known to alter catalytic activity and selectivity of the catalyst. More specifically, the development of N-doped graphenes is of special interest because their redox behavior can be easily controlled. Following our interest in the development of first-row transition-metal based heterogeneous catalyst, in the present thesis, we have reported the synthesis of iron, cobalt and manganese metal based heterogeneous nanocatalyst supported on N-doped graphene and their efficient application for dehydrogenation and hydrogenation reactions. For the synthesis of active catalyst molecularly defined metal-complex were decomposed on different support. Above strategy has been accomplished as a result of advancement in the field of catalysis by modifying transition metal complexes with different ligand. Herein this thesis we have replaced expensive noble metal catalysts with an inexpensive, benign, and sustainable first-row transition metal

based nanoscale catalyst for the efficient acceptorless dehydrogenation and transfer hydrogenation reactions.

1.4. Heterogeneous Catalysis

Most of the dehydrogenation reaction given above is based on homogeneous catalyst. In the literature, there are only limited reports based on heterogeneous catalyst. There is a strong need in the scientific community for the development of a heterogeneous catalyst for the acceptorless dehydrogenation reactions. The heterogeneous word explains itself that when the physical state of the catalyst is in a different phase from that of reactants and products separated by a phase boundary, the type of catalysis is called as heterogeneous catalysis. Usually, the catalyst is in solid phase and products or reactants are generally in gas, vapor or liquid phases in heterogeneous catalysis. The easy recovery of the catalyst, recyclability for several times, and adaptability to either batch or continuous flow reactors are the salient features of this type of catalysis. The main disadvantages of these catalysts are harsh reaction conditions such as high temperature or pressure and lack of specificity in many catalytic systems. It is highly accomplished in industries for the production of organic chemicals, automobile industries, biomass conversion and petroleum products. Heterogeneous catalysts have generally a higher catalyst life, are stable to temperature and offer an easy catalyst-product separation.

A heterogeneous catalyst is normally insoluble in the reaction medium. This is the reason why only 20 % of the industrial catalytic reactions involve homogeneous catalysis whereas 80 % employing the classical heterogeneous catalysis involving supported metal catalysts. The catalyst may be pure, mixed with other catalysts or dispersed on an inert support e.g. metals and metal oxides. In present scenario chemists, scientists, researchers all around the world are having the challenges in the development of a new catalyst which is economical, highly active and selective under lower temperatures and pressures. Catalysis is predominantly known for its importance in making the process more efficient and increases its product selectivity. The use of heterogeneous catalysts has the inherent advantages over homogeneous catalysis affected by electrolytes since they eliminate the corrosive environment and can be removed from the reaction mixture by decantation and filtration. In spite of this heterogeneous catalysts suppress the side reaction, leading to the high purity of the product. The aim is combining the advantages (activity and

selectivity) of homogeneous catalysts with the facility of heterogeneous systems to recycle the catalyst.

In present era researcher and scientist has an intense interest in a new branch of science called as nanocatalysis. It is considered that nanoscience field was started by Michael Faraday, has coined the term ‘divided metal’ to colloidal Au. Nanoparticles obtained from the bulk metals has great potential for heterogeneous catalysts for several catalytic activities. Nanoparticles are of great scientific interest as they are a bridge between bulk materials and atomic or molecular structures. The smaller the catalyst particles, the greater would be the surface area per unit volume. Then, the more would be the number of active centers present on the material and the greater the efficiency with which it performs. Hence, catalytic materials, when present in nanoparticle form would have a tremendously larger surface area and a greater proportion of their constituent atoms at the surface, enabling them to achieve a correspondingly greater catalytic efficiency. Nanocatalysts may be able to show greater selectivity as compared to their bulk forms for e.g., nanogold shows remarkable selectivity in partial oxidation reactions, like that of propylene to propylene oxide, not shown by its bulk counterpart. Nanotechnology, therefore, has great potential to improve catalyst design for the chemical, petroleum, automotive, pharmaceutical, and food industries among others. As the size of particles changed from bulk scale to nanoscale size-dependent effects can be seen from non-scalable bulk material to the fraction of atoms on the surface and quantum size.

Since in the present thesis catalysis is mostly based on heterogeneous catalysis, so further discussions will be mainly on the aspects of heterogeneous catalysis. Nanocatalysis has clearly emerged as a domain at the interface between homogeneous and heterogeneous catalysis with the development of nanoscience, which offers unique solutions to answer the demanding conditions for catalyst improvement. Nanocatalysis combines the advantageous characteristics of both homogeneous and heterogeneous catalysts while reducing their respective drawbacks. Heterogenization of the homogeneous catalysts is a need for the industry to extract all the advantages of homogeneous and heterogeneous catalysis. Supported Nanoparticles have several the advantages such as easy handling, recovery, and recyclability.

1.4.1. Heterogenization of the homogeneous catalysts

Recognizing the limitations of the homogeneous catalyst led to the great activity to heterogenize homogeneous catalysts. There are several advantages for heterogenizing a homogeneous catalyst. The aim is to combine the advantages (activity and selectivity) of homogeneous catalysts with the facility of heterogeneous systems to recycle the catalyst. The advantages are given below,

1. Good host material for guest species (i.e. heterogenization of homogeneous species or metal complexes on the walls).
2. Very high surface area of the catalyst.

Overall the synthesis of the heterogeneous catalyst can be divided mainly into two categories:

1. The catalytically active phase of the catalyst is generated as a new solid phase by either precipitation or a decomposition reaction.
2. The active phase of the catalyst is introduced or fixed onto a preexisting support by modifying the surface of the solid support.

The precipitation method is one of the most commonly used synthetic procedures for the synthesis of both mono-metallic and multi-metallic oxide catalysts. Usually, it results in a new solid phase that is formed from a homogeneous liquid solution. Several parameters, such as temperature, the addition of complexing agents, solvents, and addition of bases or acids, play an important role in this method. Another modified method is co-precipitation, which is used for the synthesis of binary or multi-metallic oxide catalysts in which multi-component precipitates together. Active species can be also dispersed on the surface of the catalyst by wet impregnation and adsorption. The average size of the catalytic species depends on the concentration of the solution used for the precipitation. It has been observed that larger particles have been formed with high loadings as compared to small particles used to form with low loadings.

1.4.2. Pathways for Heterogeneous catalysis

Heterogeneous catalysis mainly takes place on the surface. The overall process can be divided into three stages:

1. Physisorption or chemisorption of reactant molecules on the surface of the catalyst.
2. Chemical reaction on the surface of the catalyst.

3. Desorption of products from the catalytic surface.

Optimum catalyst activity can be explained by Sabatier Principle.⁴⁸ According to the Sabatier principle for best catalytic activity the reactant molecule should bind with an intermediate strength, neither too strong nor too weak with the surface of the catalyst to activate the reactants and easy desorption of the products molecule from the surface. This leads to volcano type relationship between activity and bond strength as shown in Figure 1.4b.⁴⁸

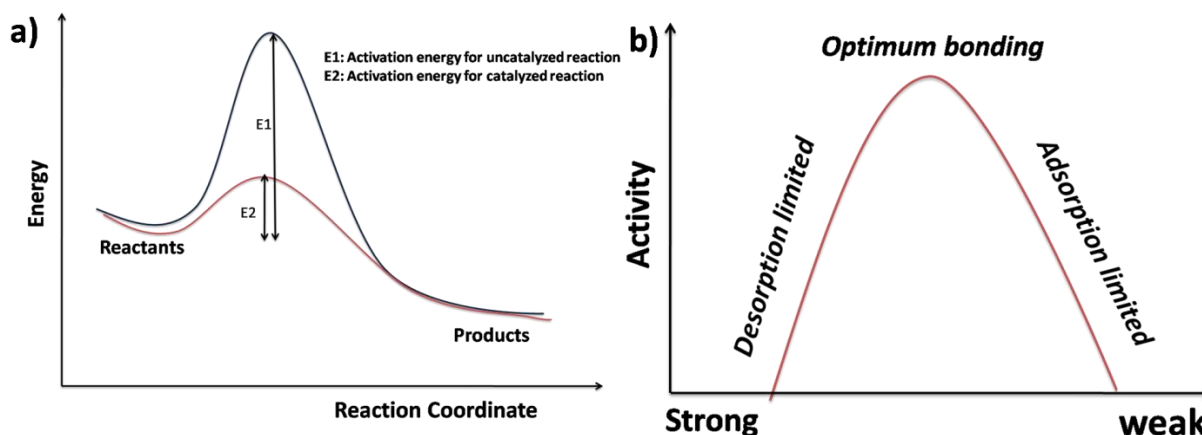


Figure 1.4. The energy profile diagram for a catalytic activation and representation of qualitative Sabatier principle.⁴⁸

1.5. Analytical Methods

Heterogeneous catalyst can be characterized by various analytical tools. The following section gives a brief introduction to these techniques and also the equipments used in this thesis for studying catalysis by these materials.

1.5.1. X-ray diffraction analysis

Powder X-ray diffraction technique, based on wide-angle elastic scattering of X-rays is one of the most important tool to identify the unknown compounds, crystallite size and the identification of lattice parameters for the crystalline materials. The X-ray diffraction patterns are obtained by the interaction of the material with x-rays (Cu K α or Mo K α) and measurement of the angles at which an X-ray beam is diffracted specific directions according to Bragg's equation,

$$n\lambda = 2d\sin\Theta$$

where λ = wavelength of X-rays used, d is the interplanar spacing, n = is the order of reflection which is a usually an integer, θ is the angle between the incoming X-ray.⁴⁹ The identification of phase is based on the comparison of the set of reflections of the sample with that of pure reference phases distributed by International Center for Diffraction Data (ICDD). Unit cell parameter (a) of a cubic lattice can be determined by the following equation: $a = dhkl\sqrt{(h^2 + k^2 + l^2)}$. Scherrer formulae are used to calculate the crystallite size of the particles, Where, D is the crystallite size, λ is the wavelength of X-ray used, θ is the diffracting angle and β is the full width at half maximum of the diffracting peak under consideration. K is a constant which normally is taken as 1. All the Powder XRD samples for the current thesis work has been measured on an Xpert Pro model PAN analytical diffractometer from Philips PAN analytical X'PRET PRO instruments operated at a voltage of 40 kV and a current of 30 mA with Cu Ka radiation ($\lambda = 1.5406 \text{ \AA}$).

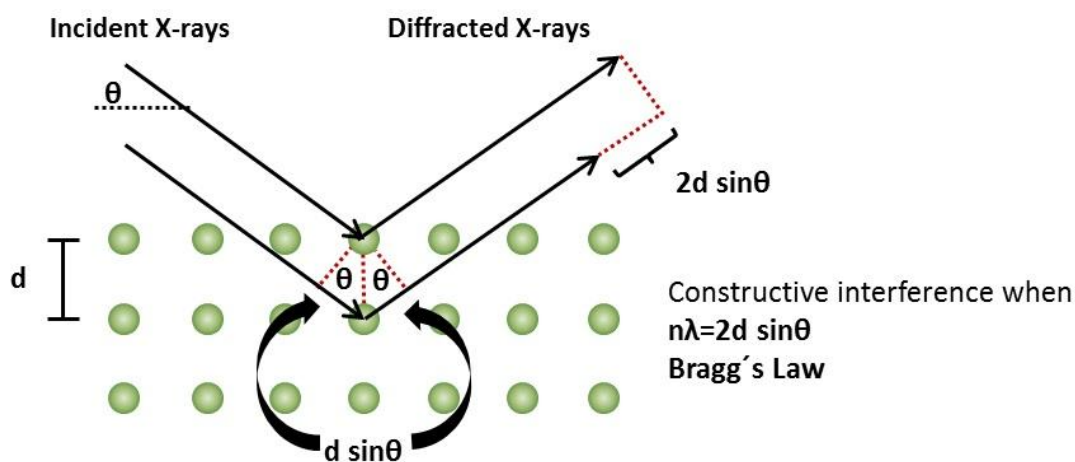


Figure 1.5. Schematic diagram of Bragg's law

1.5.2. X-Ray Photoelectron Spectroscopy

X-ray photoelectron spectroscopy (XPS) is surface science technique widely used for probing the electronic structure of atoms, molecules and precisely identify the chemical composition of the active components in heterogeneous catalysis. XPS spectra are basically obtained by irradiating the sample with X-ray photon of energy $h\nu$ on a solid matter and measuring the kinetic energy of the ejected electrons from the sample surface (E_k).

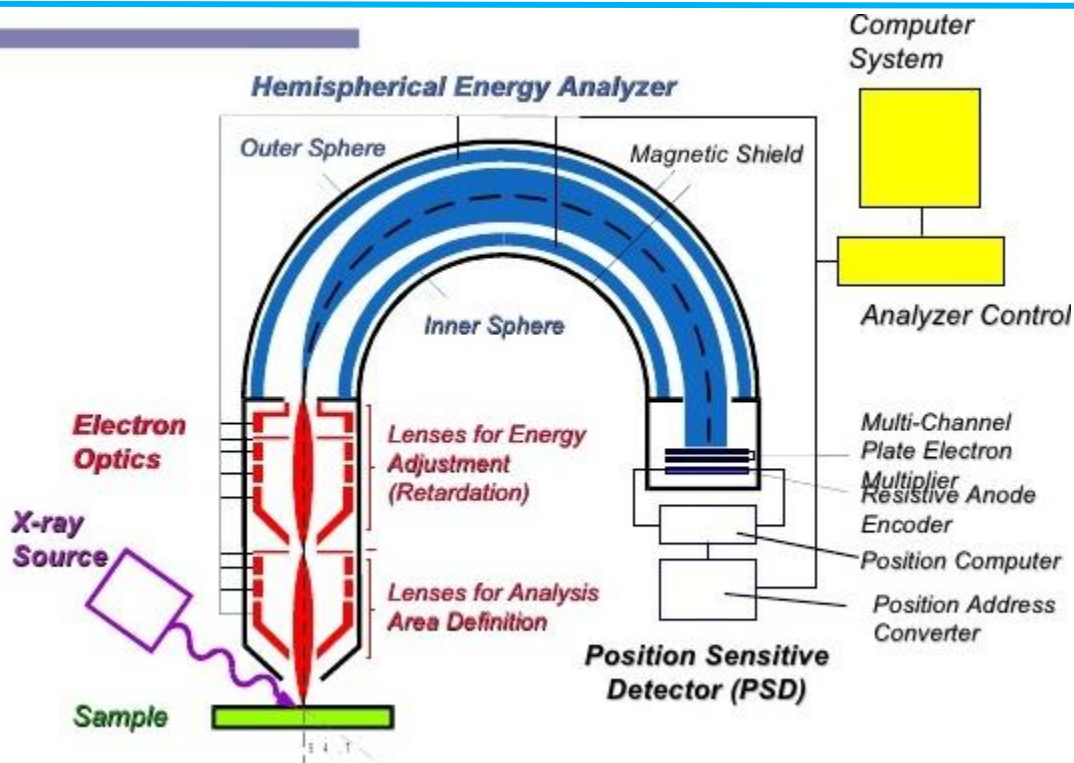


Figure 1.6. Schematic diagram of XPS

The binding energy (E_b) of the ejected photoelectrons can be related as follows: $E_k = h\nu - E_b$. An XPS instrument works based on the principle of the photoelectric effect, where the kinetic energy of the ejected electron will directly give the work function of the materials and thereby indirectly giving the ionization energy of oxidation state of the material/metal under consideration. Where KE is the kinetic energy of the ejected electrons, $h\nu$ is the incident photon energy, BE is the binding energy of the electron and ϕ is the work function of the spectrometer. This kinetic energy distribution of the photoelectrons is fabricated by a series of discrete bands, which symbolizes for the electronic structure of the sample. The core level binding energies of all the elements (other than H and He) in all different oxidation states are unique, which provides instant detection of the chemical composition of the sample after a full range scan. However, to account for the multiplet splitting and satellites accompanying the photoemission peaks, the photoelectron spectra should be interpreted in terms of many-electron states of the final ionized state of the sample, rather than the occupied one-electron states of the neutral species. The chemical nature of the samples discussed in the thesis work were investigated using XPS

analysis XPS was done on a VG Microtech Multilab ESCA 3000 spectrometer that was equipped with a Mg K α X-ray source ($h\nu = 1253.6$ eV).

1.5.3. Inductively coupled Plasma spectroscopy (ICP)

Inductively coupled plasma spectroscopy (ICP), is used to detect the trace metals and to quantify the metal present in the sample under consideration. The main principle is based on emission spectroscopy, in which by utilizing inductively coupled plasma ions of the particular element were generated which emits electromagnetic radiations of specific wavelengths, characteristic of these excited atoms or ions. The emitted radiation will be detected and used for the quantification of a particular element. The intensity of this emission is indicative of the concentration of the element within the sample. The intensity of these emissions is directly proportional to the concentration of the analyte. Plasma is an electrically conducting gas for cations and free electrons in the sample. Mostly argon gas used for the generation of plasma, capable of absorbing energy and to attain high temperatures (up to 10,000 K) and sustain the plasma for prolonged periods.

1.5.4. Scanning Electron Microscopy (SEM)

The scanning electron microscope (SEM) uses a focused beam of high-energy electrons to generate a variety of signals at the surface of solid specimens. The signals that derive from electron-sample interactions reveal information about the sample including external morphology (texture), chemical composition, and crystalline structure and orientation of materials making up the sample. In most applications, data are collected over a selected area of the surface of the sample, and a 2-dimensional image is generated that displays spatial variations in these properties. Areas ranging from approximately 1 cm to 5 microns in width can be imaged in a scanning mode using conventional SEM techniques (magnification ranging from 20X to approximately 30,000X, the spatial resolution of 50 to 100 nm). The SEM is also capable of performing analyses of selected point locations on the sample; this approach is especially useful in qualitatively or semi-quantitatively determining chemical compositions (using EDS), crystalline structure, and crystal orientations (using EBSD).

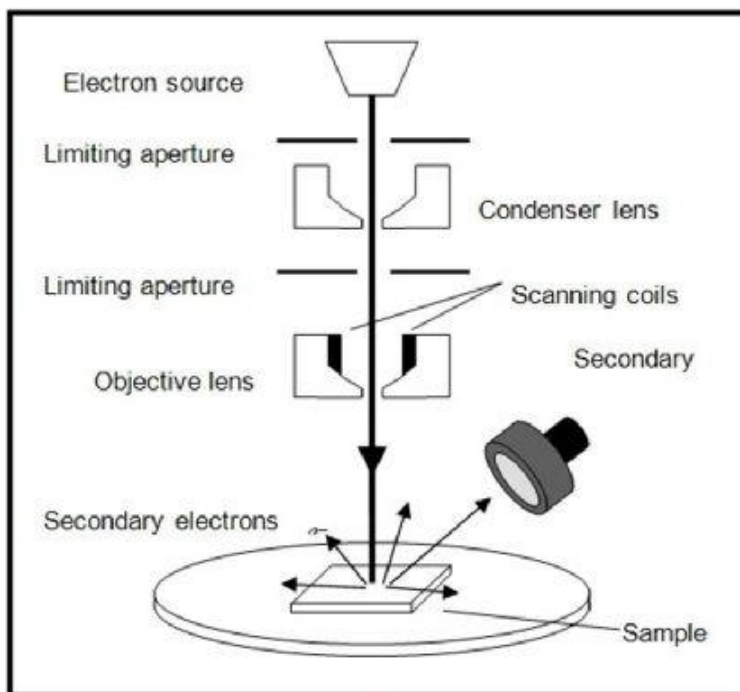


Figure 1.7. Schematic diagram of SEM

1.5.5. Raman Spectroscopy

Raman spectroscopy is the study of the interaction of the material with the light and widely used tools to give finger print features of the molecules. The principle behind the Raman analysis is the interaction of monochromatic light with molecule during which the light gets scattered in elastically and the overall process is called as Raman effect, first described by Sir Chandrasekhara Raman in 1922. The interacted photon will either lose energy or gain energy and its wavelength is either shifted lower or higher (red or blue shifted, respectively). The energy difference will correspond to a spectrum. The scattered photon with high energy showing a blue shift in the wavelength is called anti-stokes lines while the red shifted photon with lesser energy has been subjected to stokes lines.⁴⁹ The monochromatic photon unaffected after scattering having the same wavelength as the incident light is called Rayleigh scattering. This loss of energy is directly related to the functional group, the structure of the molecule to which it is attached, the types of atoms in that molecule and its environment. Change in the polarizability of the bond under monochromatic light is mandatory for showing Raman effect by any molecule.

The greater the change in polarizability of the functional group, the greater the intensity of the Raman scattering effect. Therefore the vibrational or rotational transitions, which exhibit low polarizability, and will not be Raman active. They will not appear in Raman spectra. Heterogeneous catalysis is allied with surface phenomena such as adsorption and desorption. So in determining the catalytic activity of the material Raman spectroscopy can be used to track the catalytic reaction.

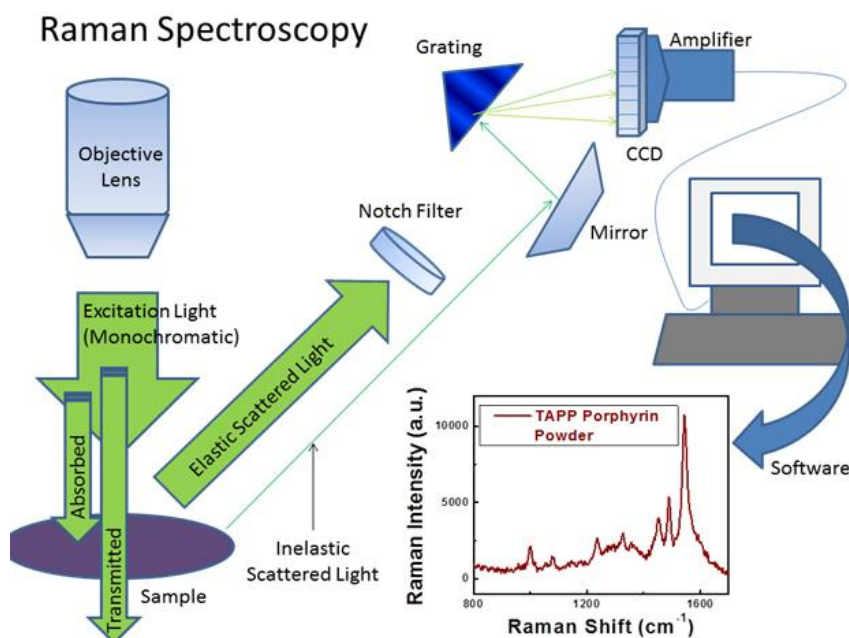


Figure 1.8. Schematic diagram of RAMAN Spectroscopy

1.5.6. Transmission Electron Microscopy (TEM)

Transmission electron microscopy (TEM) is typically used to understanding the absolute morphology, microstructure and compositional analysis under high-resolution imaging using the transmitted beam of incident light through the sample.⁵⁰ The lower de-broglie wavelength of the electron beams allows it to give higher resolution. TEM works based on the principle of optical microscopy but uses focused electron beams as the source instead of light. Following technique involves: (i) irradiation of high-energy electron beam on a thin layer of sample, which gets diffracted by the lattices of a crystalline or semi crystalline material and propagated along different directions, (ii) imaging and angular distribution analysis of the forward scattered electrons and (iii) energy analysis of the emitted X-rays. The images obtained by TEM can be

deployed for structural characterization and identification of various phases of nanomaterials and metal oxides.

In the following thesis, the tem images were collected on Tecnai (Model F20, CMC, CSIR-NCL) operating at 300 kv. Samples were dispersed in ethanol with sonicated before drop casting the sample on a carbon-coated Cu grid for the analysis.

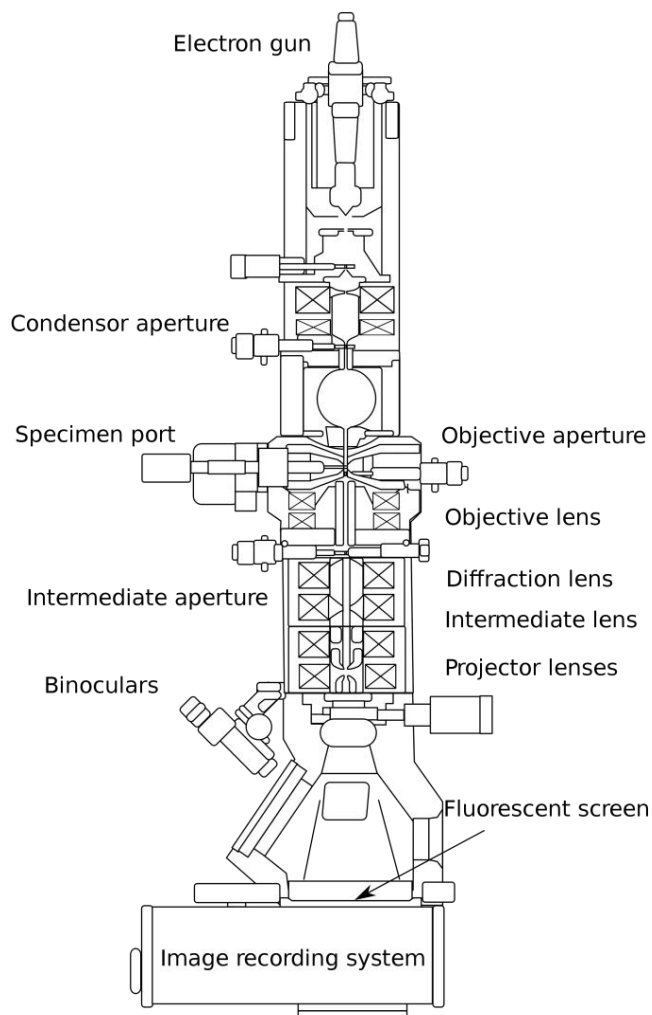


Figure 1.9. Schematic diagram of TEM

1.5.7. Thermal Analyses

The thermoanalytical techniques, *via.*, thermogravimetric analysis (TGA) and differential thermal analysis (DTA) have been widely studied to demonstrate the thermal stability of carbon materials. Both TGA and DTA provide valuable information about the following: (i) temperature programmed desorption (TPD) and removal of physically adsorbed water below 100 °C, (ii) oxidative decomposition of the carboxylic acid, anhydride and release of CO₂ gas, accompanied

by different exotherms within 100 °C to 300°C, (iii) the removal of highly stable oxygen group such as carbonyl, phenol and quinone within the range of 300°C to 500°C and (iv) above 500°C exotherm represent the pyrolysis of carbon skeleton.

1.5.8. Gas Chromatography

Gas chromatography is widely used analytical tool for the separation, identification as well as quantification of the different component present in a sample. This technique based on the differential adsorption of each analyte species over a stationary phase. The mobile phase usually an inert gas (He, Ar or N₂) will carry the sample through the long stationary phase packed in the form a column. The sample will get adsorbed over the stationary phase based on the affinity of the analyte towards the surface polarity. Based on the interaction between the analyte and stationary phase the separation happens and the analyte will reach to the detector and will be identified and quantified. Different types of detectors associated with a gas chromatograph to identify the analyte. To measure a sample with an unknown concentration, a standard sample with known concentration is injected into the instrument. The standard sample peak retention time (appearance time) and area are compared to the test sample to calculate the concentration.

1.5.9. Nuclear Magnetic Resonance Spectroscopy (NMR)

Nuclear magnetic resonance (NMR) spectroscopy is one of the most powerful tools to investigate physical and chemical nature of a material by utilizing the magnetic property of some of the nuclei present in that material. When atomic nuclei consisting of odd number of protons and/or neutrons (Like ¹H, ²⁹Si, ²⁷Al etc) possessing a nuclear spin $I \neq 0$ and consequently a magnetic moment $\mu = \gamma\hbar I$ (γ = gyromagnetic ratio) were kept under magnetic field of strength B_0 , Zeeman interaction results in quantized orientations of the nuclear magnetic moments. The nucleus can adopt $2I + 1$ Eigen states with energies $E(m) = -m\gamma\hbar B_0$, where $m = (I, I-1, \dots, -I)$. Transitions between neighboring energy states ($\Delta m = \pm 1$) can be induced by electromagnetic radiation (energy $E = h\nu$) of frequency $\nu_0 = \gamma B_0/2\pi$. The chemical shift interaction arises from secondary local magnetic fields induced by the interaction of the electrons surrounding the nucleus. The chemical shift values obtained in the spectrum can be used to clearly identify the co-ordination environment of the nuclei under consideration and hence, the structural elucidation of the material or molecule. The shape and width of the spectral lines can directly tell the

bonding pattern in the case of solid state NMR spectra. In the current thesis work ^1H NMR (200, 400 or 500 MHz), $^{13}\text{C}\{^1\text{H}\}$ NMR (50 or 100 MHz) spectra were recorded on the NMR spectrometer. Deuterated chloroform was used as the solvent, and chemical shift values (δ) are reported in parts per million relative to the residual signals of this solvent [δ 7.27 for ^1H (chloroform-d), δ 77.0 for $^{13}\text{C}\{^1\text{H}\}$ (chloroform-d)]. Abbreviations used in the NMR follow-up experiments: br, broad; s, singlet; d, doublet; t, triplet; q, quartet; m, multiplet.

1.6. Scope and objectives of the thesis work

This thesis describes design and development of new catalytic materials based on firstrow transition metals (Mn, Fe, Co) and their applications in dehydrogenation and related reactions with improved activity, selectivity, and stability. The main objective of the thesis is to replace the noble metal catalysts with firstrow transition metal based heterogeneous catalysts, and study the effect of different ligand and supports, and morphology on the catalytic activity in various catalytic reactions such as dehydrogenation and hydrogenation reactions.

1.7. Organization of thesis

The thesis is divided into five chapters. An abstract of each chapter is given below.

Chapter 1: This chapter gives an introduction to heterogeneous nanocatalysis, various method of heterogenizing a homogeneous catalyst, dehydrogenation, and its application in energy and chemical synthesis. This chapter also discusses the analytical methods for the characterization of catalyst and tools used for analyzing catalytic reaction. It gives an outline about the objective of the thesis.

Chapter 2: In this chapter, we have replaced expensive noble metal catalysts with an inexpensive, benign, and sustainable nanoscale iron catalyst for the efficient acceptorless dehydrogenation (AD) and acceptorless dehydrogenative coupling (ADC) reactions. This working chapter has been further divided into two parts.

Subpart A of chapter 2 deals with the heterogenization of the homogeneous metal complex. The heterogeneous catalyst has been well-characterized using the state-of-the-art techniques and then the catalytic material was successfully applied for the catalytic dehydrogenation of

feedstock chemicals, such as alcohols, amines, and *N*-heterocycles to value-added products with the concomitant generation of dihydrogen. The present catalytic approach possesses a dual role; acting as a catalyst as well as can be magnetically separable. The sustainable reuse of heterogeneous iron catalyst is also shown.

Subpart B deals with acceptorless dehydrogenative coupling (ADC) of alcohols with amines to access imine using as synthesized heterogeneous Fe-catalyst. It's an efficient protocol to construct imine bonds with the liberation of molecular hydrogen and water as the byproducts. Imines are an exceptionally versatile functional group and are ubiquitous in pharmaceuticals, biologically active heterocycles, and natural products. The developed ADC strategy is simple, efficient, exhibits wide functional group tolerances and can be scaled up (in gram-scale).

Chapter 3: The third chapter is mainly focused on cobalt nanoparticles deposited on the different supports and their catalytic activity on acceptorless dehydrogenation and transfer hydrogenation reactions. This chapter is also divided into two parts.

In part 3A, of the chapter, in continuation with our interest in the development of efficient heterogeneous catalyst containing sustainable transition metals, we have investigated cobalt based heterogeneous catalyst for the dehydrogenation of *N*-heterocyclic motif.

In part 3B, we reported an operationally simple, mild, and highly *Z*-selective hydrogenation of alkynes and terminal alkyne, applying a reusable cobalt heterogeneous catalyst deposited on graphene *via* transfer hydrogenation strategy.

Chapter 4: In this chapter, we have explored 3d-transition metal-based catalyst, novel manganese-based nanocatalyst for chemo-selective hydrogenation of nitroarenes using amino borane as transfer hydrogenating reagent. The strategy works, under the very mild conditions. To the best our knowledge there is no report on dehydrogenation of ammonia-borane (AB) and subsequent chemo-selective hydrogenation of nitroarenes to anilines either under homogeneous and heterogeneous conditions.

Chapter 5: The Final chapter of the thesis is mainly focused on utilization of iron-based catalyst for partial selective hydrogenation of carbon dioxide to carbon monoxide (RWGS). One of the important strategies is to utilize CO₂ can be partial reduction of CO₂ to produce CO₂-containing syngas (CO₂+SG). Syngas can be used as a feed in crucial energy technologies based on Fischer

Tropsch synthesis, CAMERE process, and fuel cells. Selectivity is the issue as methane is one of the side products in the RWGS reaction. We have successfully used an iron-based heterogeneous catalyst for the selective, and partial hydrogenation of CO₂ to CO (selectivity up to 98%).

1.8. References:

1. *Hydrogen as a Future Energy Carrier*, ed. A. Zuttel, A. Borgschulte and L. Schlapbach, Wiley-VCH, Weinheim, 2008.
2. M. Trincado, D. Banerjee and H. Grützmacher, *Energy Environ. Sci.*, 2014, **7**, 2464-2503.
3. D. Mellmann, P. Sponholz, H. Junge, and M. Beller, *Chem. Soc. Rev.* 2016, **45**, 3954-3988.
4. C. Gunanathan and D. Milstein, *Science*, 2013, **341**, 1229712.
5. D. Wang and D. Astruc, *Chem. Rev.*, 2015, **115**, 6621–6686.
6. C. L. Sun, B.–J. Li and Z.–J. Shi, *Chem. Rev.* 2011, **111**, 1293–1314.
7. A. Quintard and J. Rodriguez, *Angew. Chem. Int. Ed.* 2014, **53**, 4044-4055.
8. R. H. Morris, *Acc. Chem. Res.* 2015, **48**, 1494–1502.
9. T. Zell and D. Milstein, *Acc. Chem. Res.* 2015, **48**, 1979–1994 .
10. I. Bauer and H.-J. Knölker, *Chem. Rev.*, 2015, **115**, 3170–3387.
11. N. Yoshikai, Iron-catalyzed C-C bond formation with C-H bond activation in I. Marek, I., Z. Rappoport, “From Chemistry of Organoiron Compounds” 2014, 499-538, Wiley, ISBN:978-0-470-97359-2.
12. C. Darcel, J. –B. Sortais, S. Q. Duque, *RSC Green Chemistry Series* 2015, 26, 67-92.
13. B. Plietker, Iron-catalysis fundamental and application *Topics in organometallic chemistry*, 2011Springer, Berlin Heidelberg.
14. R. A. Sheldon, I. W. C. E. Arends, G.J. ten Brink and A. Dijkstra, *Acc. Chem. Res.*, 2002, **35**, 774-781.
15. L. Que Jr and W. B. Tolman, *Nature*, 2008, **455**, 333.
16. S. Ott, *Science*, 2011, **333**, 1714-1715.
17. C. Gunanathan and D. Milstein, *Science*, **341**, 1229712.
18. C. Fink, M. Montandon-Clerc, and G. Laurency, *CHIMIA* 2015, **69**, 746-754.
19. A. K. Singh, S. Singh and A. Kumar, *Catal. Sci. Technol.* 2016, **6**, 12-40.

20. S. Enthaler, J. Langermann and T. Schmidt, *Energy Environ. Sci.* 2010, **3**, 1207-1217.
21. C. W. Hamilton, R. T. Baker, A. Staubitzc and I. Manners, *Chem. Soc. Rev.*, 2009, **38**, 279–293.
22. J. Kothandaraman, M. Czaun, A. Goeppert, R. Haiges, J.-P. Jones, R. B. May, G. K. S. Prakash and G. A. Olah, *ChemSusChem*, 2015, **8**, 1442–1451.
23. H. –J. Knölker, E. Baum, H. Goesmann and R. Klauss, *Angew. Chem. Int. Ed.* 1999, **38**, 2064-2066.
24. M. G. Coleman, A. N. Brown, B. A. Bolton and H. Guana, *Adv. Synth. Catal.*, 2010 **352**, 967–970.
25. M. Kamitani, M. Ito, M. Itazaki and H. Nakazawa, *Chem. Commun.*, 2014, **50**, 7941–7944.
26. H. Song, B. Kang and S. H. Hong, *ACS Catal.* 2014, **4**, 2889–2895.
27. S. Chakraborty, P. O. Lagaditis, M. Förster, E. A. Bielinski, N. Hazari, M. C. Holthausen, W. D. Jones and S. Schneider, *ACS Catal.*, 2014, **4**, 3994–4003.
28. M. Pena-Lopez, H. Neumann and M. Beller, *Chem. Cat. Chem.*, 2015, **7**, 865–871.
29. R. Martinez, D. J. Ramon and M. Yus, *Org. Biomol. Chem.*, 2009, **7**, 2176–2181.
30. X. Cui, F. Shi, Y. Zhang and Y. Deng, *Tetrahedron Lett.*, 2010, **51**, 2048–2051.
31. M. Bala, P. K. Verma, U. Sharma, N. Kumar and B. Singh, *Green Chem.*, 2013, **15**, 1687–1693.
32. T. Yan, B. L. Feringa and K. Barta, *Nature Commun.*, 2014, **5**, 5602.
33. H. –J. Knölker, J. Heber and C. H. Mahler, *Synlett* 1992, 1002-1004.
34. H. –J. Knölker and J. Heber, *Synlett* 1993, 924-926.
35. H. –J. Knölker, E. Baum and J. Heber, *Tetrahedron Lett.* 1995, **36**, 7647-7650.
36. H. -J. Knölker, H. Goesmann and R. Klauss, *Angew. Chem. Int. Ed.*, 1999, **38**, 702-705.
37. T. Yan, B. L. Feringa and K. Barta, *ACS Catal.*, 2016, **6**, 381–388.
38. B. Emayavaramban, M. Roy and B. Sundararaju, *Chem. Eur. J.*, 2016, **22**, 3952–3955.
39. A. J. Rawlings, L. J. Diorazio and M. Wills, *Org. Lett.*, 2015, **17**, 1086–1089.
40. M. Wu, X. Hu, J. Liu, Y. Y. Liao and G. –J. Deng, *Org. Lett.*, 2012, **14**, 2722-2725.
41. H. Wang, X. Cao, F. Xiao, S. Liu and G. –J. Deng, *Org. Lett.*, 2013, **15**, 4900-4903.
42. M. Langeron and M. –B. Fleury, *Science*, 2013, **339**, 43-44.

-
-
43. R. Yamaguchi, C. Ikeda, Y. Takahashi, K. Fujita, *J Am Chem Soc.*, 2009, **131**, 8410-8412.
 44. J. Wu, D. Talwar, S. Johnston, M. Yan, J. Xiao, *Angew. Chem. Int. Ed.*, 2013, **52**, 6983-6987.
 45. R. Xu, S. Chakraborty, H. Yuan, W. D. Jones, *ACS Catal.*, 2015, **5**, 6350-6354.
 46. S. Chakraborty, W. W. Brennessel, W. D. Jones, *J. Am. Chem. Soc.*, 2014, **136**, 8564-8567.
 47. J. H. Yun and R. F. Lobo, *J. Catal.*, 2014, **312**, 263–270.
 48. A.J. Medford, A. Vojvodic, J.S. Hummelshøj, J. Voss, F. Abild-Pedersen, F. Studt, T. Bligaard, A. Nilsson, J. K. Nørskov, *J. Catal.*, 2015, **36**, 328.
 49. J.M. Hollas, *Modern spectroscopy*; John Wiley & Sons, 2004.
 50. D. B. Williams, C. B. Carter, *New York, NY* 1996.

Chapter 2

Iron nanocatalyst for the acceptorless dehydrogenation reactions

Part A: Dehydrogenation of *N*-heterocycles and alcohols

2A.1. Introduction

Rapid depletion of limited fossil fuels has directed a significant amount of human efforts to identify alternative renewable, green energy resources. It has been widely accepted that hydrogen as a fuel can be effective to curtail the energy crisis if produced at the proximity of usage without involving long-distance transportation. Thus, the most attractive and efficient hydrogen storage/release media are liquid organic hydrogen carriers (LOHCs), because they have relatively high hydrogen content and can easily be transported. In this context, extraction of H₂ from abundant, renewable feedstocks *via* acceptorless dehydrogenation strategy (AD) is extremely important, but a thermodynamically uphill process.¹⁻⁵ Traditionally, extraction of hydrogen atoms in adjacent positions in an organic molecule can be achieved either by the use of a stoichiometric amount of strong oxidants or sacrificial hydrogen acceptors, which often produce copious waste.⁶⁻⁷ On the other hand, catalytic dehydrogenation with concomitant removal of dihydrogen is a superior strategy and has enabled the direct access to valuable intermediates.

Catalytic acceptorless dehydrogenation by homogeneous transition-metal complexes has been a well-recognized sustainable process in chemistry.⁸⁻¹³ Despite the satisfactory performance at the laboratory scale, homogeneous catalysts face severe limitations such as high-cost, poor recovery, extensive synthesis of ligands and poor stability while scaling up for industrial applications. In comparison, heterogeneous catalysts would be more advantageous with respect to catalyst recycling and reusability. Moreover, tremendous scope for improving step-, atom-economy and benignity of AD strategy that could be more attractive to chemical industries and can be foreseen using novel catalysts. The economical, biorelevant and ample supply of iron salts coupled with their lack of toxicity, makes them ideal candidates to replace precious metals for both the academic and industrial applications.¹⁴⁻¹⁸ However, search for an efficient catalytic system for AD strategy using earth-abundant iron-catalysts is extremely rare due to its propensity to participate in one electron transformation as opposed to the conventional two electron chemistry that is ubiquitous in second- and third-row transition-metals. Indeed, in recent times molecularly-defined iron complexes have been applied successfully under homogeneous conditions as an alternative to noble metal-based catalysts.¹⁶⁻¹⁸ Unfortunately, most of these homogeneous

complexes are rather sensitive and/or sophisticated presenting a synthetically challenging ligand systems.

Acceptorless Dehydrogenation of *N*-Heterocycles

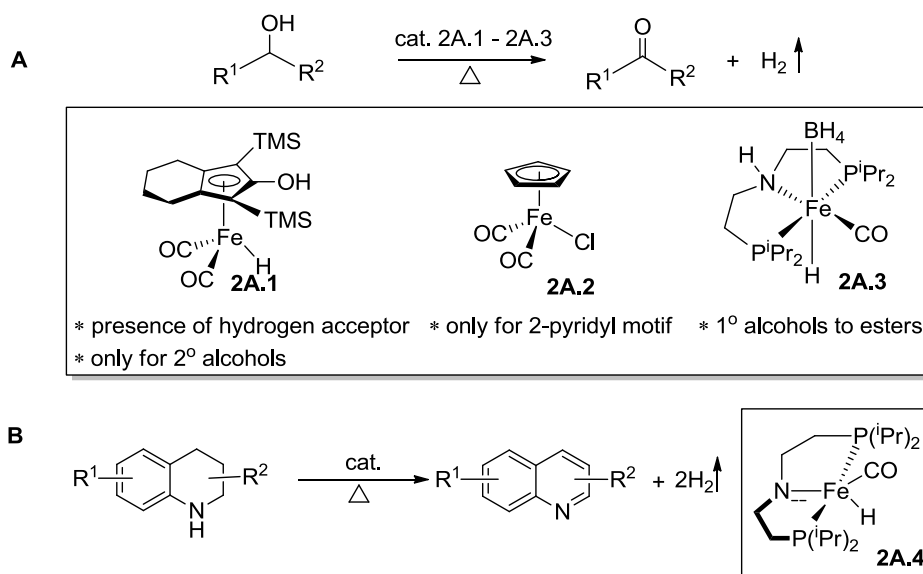
The catalytic dehydrogenation of *N*-heterocycles with concomitant generation of dihydrogen constitutes is not only a fundamental process in synthetic chemistry but also have direct applications in energy storage systems such as liquid organic hydrogen storage materials and fuel cells.¹⁹⁻²¹ Despite several homogeneous catalysts based on iridium (Cp* and pincer-type ligand),²²⁻²⁵ Ru-hydride complexes,^{2,12} Co-pincer complex²⁶ were successfully employed in the catalytic dehydrogenation of *N*-heterocycles without using hydrogen acceptor and additives, there is only one example of an iron-based catalytic system known so far.²⁷ However, the development of stable, inexpensive, reusable heterogeneous system²⁸ for the dehydrogenation *N*-heterocycles operates under practical conditions with the liberation of hydrogen gas is highly desirable and very demanding.

Dehydrogenation of Amines to Imines with Extraction of H₂

Imines serve as a key intermediate for the preparation of fine chemicals, pharmaceuticals, and natural products.²⁹ Traditional methods to access imines involve a condensation reaction of the amine with active carbonyl compounds and often require dehydrating agents as well as Lewis acid catalysts. In a complementary approach, the catalytic dehydrogenative coupling reaction of an alcohol with an amine offers the direct formation of imine derivatives. Nevertheless, this reaction operates at elevated temperature with challenges associated to the competing hydrogen autotransfer (HA) strategy (*in situ* hydrogenation of imine to afford the amine).³⁰ Indeed, acceptorless dehydrogenation of amine to imine by precious metals provides an oxidant-free strategy with extrusion of dihydrogen as a sole byproduct. However, efficient catalytic methods for the direct conversion of primary amines to imines are challenging, due to presence of an α -hydrogen in the intermediate imine, which may be rapidly dehydrogenated to a nitrile and the formation of a mixture of secondary amine (*N*-alkylated amine) and imine products.³⁰ Recently, the selective synthesis of imines from nitroarenes and aldehydes or ketones through hydrogenation has been reported using a reusable cobalt catalyst.³¹

Acceptorless Dehydrogenation: Scope of Primary Alcohols

Casey and co-workers reported the first iron-catalyzed dehydrogenation of alcohols using the Knölker complex, (hydroxycyclopentadienyl) iron dicarbonyl hydride **2A.1**, as a catalyst in the presence of hydrogen acceptor (Scheme 2A.1a).³² Regrettably, the scope of the reaction was limited only to secondary alcohols and conjugated primary alcohols. In 2014, dehydrogenation of 2-pyridylmethanol derivatives catalyzed by an iron–cyclopentadienyl complex **2A.2** (Scheme 2A.1a) has been reported under acceptorless conditions.³³ Of late, Hong and co-workers developed *in situ* generated iron catalytic system (a combination of Fe(III) salt, 1,10-phenanthroline, and K₂CO₃) for dehydrogenation of secondary benzyl alcohols to afford the corresponding ketones.³⁴ However, other unactivated secondary alcohols and primary alcohols were ineffective, and no dehydrogenation was observed. Based on metal-ligand cooperation mechanism, a PNP-iron pincer complex (**2A.3**) catalyzed acceptorless dehydrogenation of alcohols to esters has been reported by the research group of Jones and Schneider (scheme 2A.1a).³⁵ Notably, primary alcohols underwent self-dehydrogenative coupling to form esters presumably *via* Tishchenko reaction. To the best of our knowledge, there have been no reports on reusable, robust iron-based catalytic system for AD strategy of a series of various alcohols under mild conditions. It is important to note that the selective conversion of alcohols to aldehydes *via* AD strategy is very challenging due to competing for ester formation.^{2, 36-37}



Scheme 2A.1. a) Acceptorless dehydrogenation of alcohols and b) Acceptorless dehydrogenation of *N*-heterocycles.

Recently, Fe-based nanocatalysts supported on graphitic carbon has emerged as a valuable catalyst in hydrogenation and related reactions.³⁸⁻⁴² Early works in iron-graphite nanocatalyst systems focused on exploiting the high surface area and excellent transport properties of the graphene layers. Iron-carbon nanocatalyst system is highly sensitive to its microstructure and has been shown to significantly affect the catalytic outcome.⁴²⁻⁴⁴ Thermal decomposition of a molecular complex of a metal on a support is a versatile method to obtain supported nanocatalyst. Based on this approach, Fe₂O₃ and Co-based catalysts encapsulated in *N*-doped graphitic carbon for hydrogenation and oxidation reactions are recently documented.^{40-41, 45-48}

The final composition and the microstructure of the catalyst are observed to vary depending on the ligand, nature of carbon support, decomposition temperature and reaction atmosphere. For instance, the microstructure of the catalyst described in this work is synthesized by thermally pyrolyzing Fe:*N*-rich ligand on graphitic oxide support giving a unique core-shell architecture composed of oxide and carbide of iron without the encapsulating sheath of carbon that is commonly observed in earlier works.⁴⁰⁻⁴⁴ An immediate consequence is the exposure of more catalytic active sites to the reactants. More importantly, we have described in detail the unique catalytic property of our catalyst in an efficient oxidant-free and acceptorless dehydrogenation reactions of partially saturated *N*-heterocycles, relatively abundant alcohols, and amines with the concomitant generation of hydrogen gas. In addition to the concept of liquid organic hydrogen carriers (LOHCs), this elegant system offers a new streamlined strategy for the sustainable production of chemicals with a great step-economy and reduced waste generation. To the best of our knowledge, the acceptorless dehydrogenation of diverse alcohols (1°, 2° alcohols, and diols), amines, and *N*-heterocycles by a single iron-based catalyst either under homogeneous or heterogeneous conditions has not been investigated yet prior to our report.⁴⁹

2A.2. Statement of the Problem

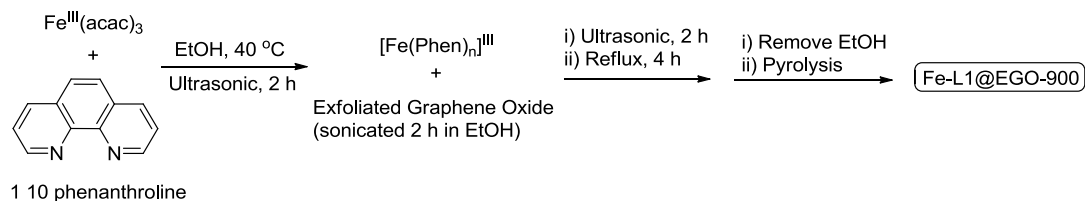
In the present scenario, acceptorless dehydrogenation is mainly reported with organometallic complexes based on noble-metal catalysts under homogeneous condition. However, high-cost, poor recovery, extensive synthesis of ligands and poor stability while scaling up for industrial applications are the potential concern. Indeed, heterogeneous catalysts would be more advantageous with respect to catalyst recycling and reusability. The development of stable, inexpensive, reusable heterogeneous system for the dehydrogenation *N*-heterocycles and

alcohols operates under practical conditions with the liberation of hydrogen gas is highly desirable and very demanding. There are only limited reports based on heterogeneous catalysts.²²⁻²⁷ To the best of our knowledge, the acceptorless dehydrogenation of diverse alcohols (1°, 2° alcohols and diols), amines, and *N*-heterocycles by a single iron-based catalyst either under homogeneous or heterogeneous conditions has not been investigated prior to our report.⁴⁹ The economical, biorelevant and ample supply of iron salts coupled with their lack of toxicity, makes them ideal candidates to replace precious metals for both the academic and industrial applications.

2A.3. Catalyst Synthesis and Characterization

2A.3.1. Synthesis of Fe-L1@EGO-900 catalyst

In a 100 mL beaker Fe(III)acetylacetonate precursor (0.5 mmol) and 1,10-phenanthroline ligand **L1** (0.5 mmol) was dissolved in 30 mL of ethanol and sonicated for 2 h to form Fe-phenanthroline complex. In another 250 mL, beaker 560 mg of EGO support was taken in 70 mL of ethanol and sonicated for 2 h. The above-obtained Exfoliated graphene oxide (EGO) suspension and Fe-phenanthroline complex solution were mixed together in 250 mL beaker and further sonicated for 2 h. The suspension was refluxed at 85 °C for 4 h, and after cooling down to room temperature ethanol was evaporated under vacuum. The solid sample obtained was dried at 80 °C for 14 h. Then, it was ground to a fine powder followed by calcination at 900 °C under a stream of argon with the flow rate of 30 mL/min and the heating rate: 25 °C/min for about 4 h to obtain a catalyst Fe-L1@EGO-900. ICP-AES analysis was done to determine the amount of Iron present and was found to be 5.32%.



Scheme 2A.2. Synthesis procedure of Fe-L1@EGO-900 catalyst.

2A.3.2. Catalyst Characterization

2A.3.2.1. Powder X-ray diffraction (PXRD)

The catalyst Fe-L1@EGO-900 was extensively characterized using several tools. In powder X-ray diffraction (PXRD) pattern of Fe-L1@EGO-900 (Figure 2A.1), a broad peak at $2\theta = 26.5^\circ$ confirmed the presence of few layers of reduced graphene oxide support. Other inorganic phases were confirmed by the presence of diffraction peaks indexed to Fe_3O_4 , Fe_3N , $\beta''\text{-Fe}_2\text{O}_3$, and Fe_7C_3 . Formation of Fe_7C_3 and Fe_3N can be understood in terms of the decomposition of N- and C-rich L1 in the proximity of metal atoms that aggregate to form carbide and nitride nanoparticles. Surprisingly, we could not detect the presence of Fe metal, which is possible under the synthesis conditions in the presence of a reducing agent like graphite. It is likely that smaller nanoparticles of Fe-rich phases could have oxidized to iron oxides when exposed to the ambient conditions.

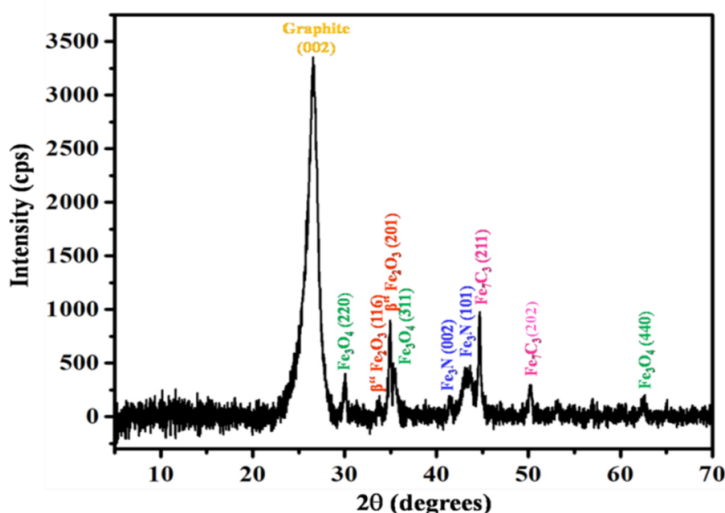


Figure 2A.1. The PXRD pattern of Fe-L1@EGO-900 showing graphite and inorganic phases of the catalyst.

2A.3.2.2. Energy-dispersive X-ray spectroscopy (EDX)

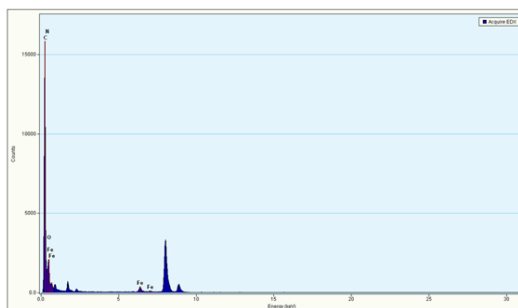


Figure 2A.2. EDX analysis of Fe-L1@EGO-900 catalyst.

Table 2A.1. The weight percent of different elements in the Fe-L1@EGO-900 catalyst

Element	Weight %	Atomic %	Uncert. %	Correction	k-Factor
C(K)	86.67	92.80	0.68	0.26	3.940
N(K)	2.01	1.84	0.12	0.26	3.826
O(K)	4.78	3.84	0.07	0.49	1.974
Fe(K)	6.53	1.50	0.09	0.99	1.403

2A.3.2.3. Scanning Electron Microscopy (SEM) analysis

The morphology of the Fe-L1@EGO-900 catalyst was analyzed using scanning electron microscopy, which clearly showed graphene layers supporting spatially well-separated nanoparticles that are probably rich in iron (Figure 2A.3).

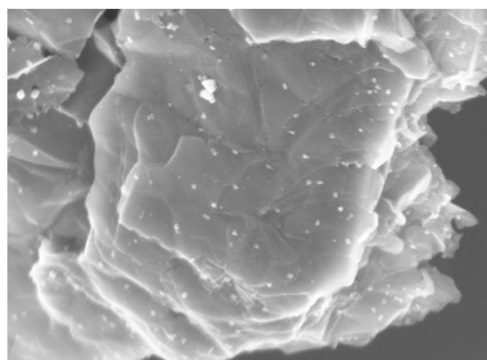


Figure 2A.3. FESEM image of Fe-L1@EGO-900 (scale bar 100 nm).

2A.3.2.4. Transmission Electron Microscope (TEM) Analysis

The microstructure of Fe-L1@EGO-900 catalyst was analyzed using transmission electron microscopy (TEM) and the data are shown in Figure 2A.4. The bright-field image of Fe-L1@EGO-900 showed Fe rich nanoparticles darker in contrast compared to the graphene support. The nanoparticles were distributed throughout the graphene sheets and were of size ranging from 4 to 100 nm with the majority of the particles the range of 11–20 nm as shown in the histogram (Figure 2A.4a). Careful analysis of bright-field TEM image suggested the particles had a core-shell architecture (Figure 2A.4c).

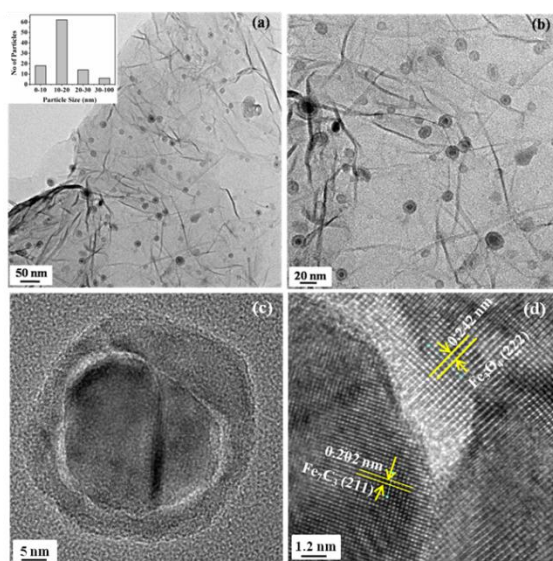


Figure 2A.4. Bright field TEM images of Fe-L1@EGO-900 catalyst. **a**, at the scale bar 50 nm with inset showing a histogram of the size of 100 nanoparticles. **b**, at the scale bar 20 nm. **c**, a single nanoparticle at the scale bar 5 nm. **d**, shows the high-resolution lattice fringes of Fe_7C_3 (211) planes and Fe_3O_4 (222) planes at the scale bar 1.2 nm.

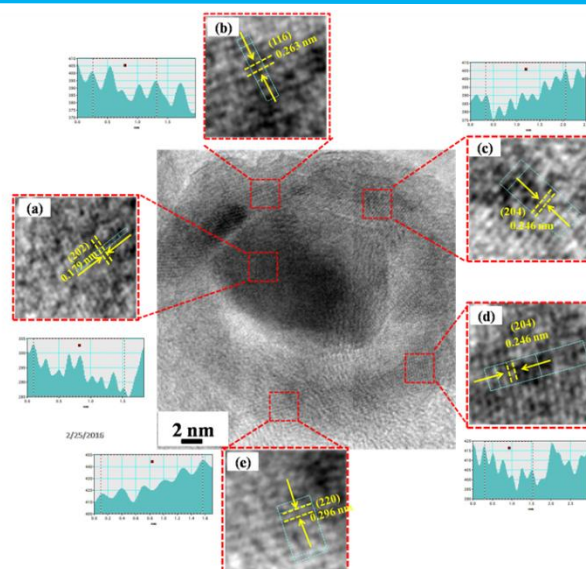


Figure 2A.5. HRTEM of Fe-L1@EGO-900. **a**, Lattice fringes of 1.79 Å corresponding to the d spacing of (202) plane of Fe_7C_3 . **b**, Lattice fringes of 2.63 Å corresponding to the d spacing of (116) plane of Fe_3O_4 phase. **c & d**, Lattice fringes of 2.46 Å corresponding to the d spacing of (204) plane of $\beta\text{-Fe}_2\text{O}_3$. **e**, Lattice fringes of 2.96 Å corresponding to (220) plane of Fe_3O_4 .

High-resolution transmission electron microscopy (HRTEM) image of the sample (Figure 2A.4d) showed lattice fringes of 2.02 Å corresponding to the d spacing of (211) plane of Fe_7C_3 at the core and 2.42 Å corresponding to the d spacing of (222) plane of Fe_3O_4 phase. Further HRTEM image analysis of several particles revealed that the core was composed of iron carbide while the shell was dominated by iron oxides (Figure 2A.4d and Figure 2A.5). Elemental analysis using energy dispersive X-ray analysis under STEM mode further supported the distribution of Fe across the entire particle (Figure 2A.6). Importantly, the graphitic carbon shell which is commonly observed in other reported catalysts^{21–23, 50–52} prepared by thermal pyrolysis of the molecular complex was absent in Fe-L1@EGO-900.

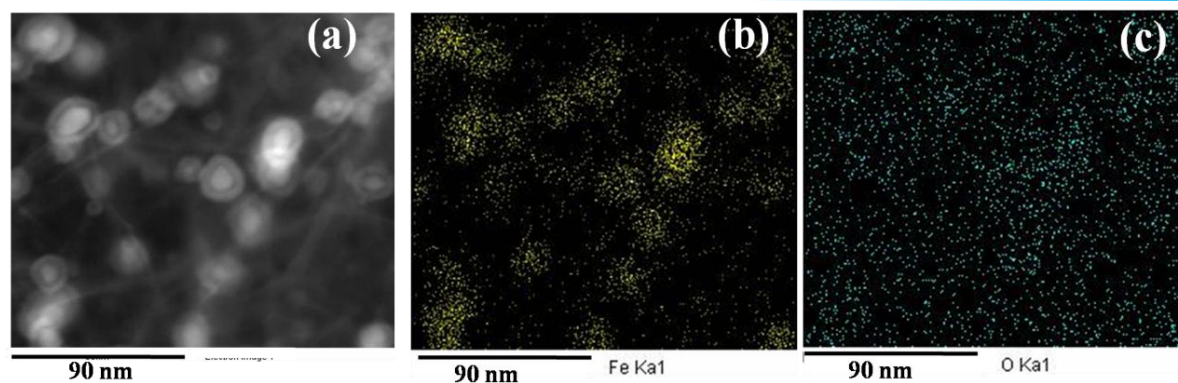


Figure 2A.6A. **a**, STEM image of Fe-L1@EGO-900 catalyst. **b**, EDX elemental maps of iron. **c**, EDX elemental maps of oxygen which were collected from the entire area shown in Figure 2A.2 at the scale bar 90 nm.

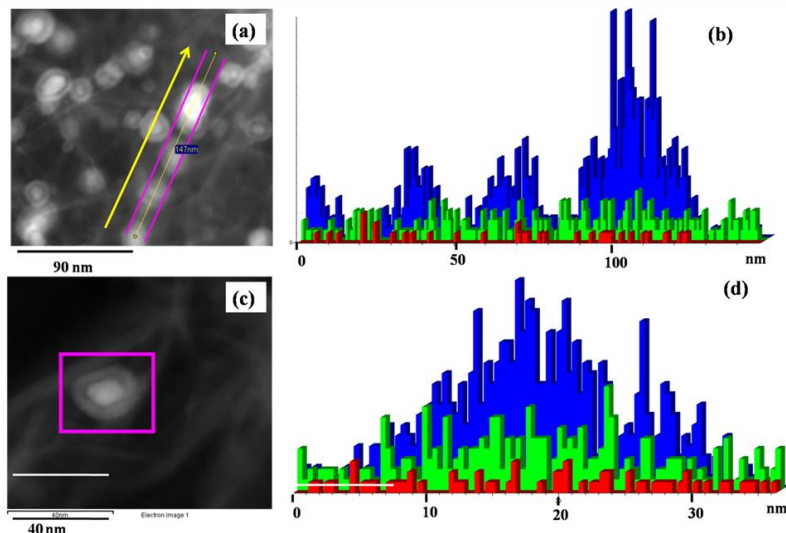


Figure 2A.6B. **a**, STEM image of Fe-L1@EGO-900 catalyst. **b**, Line profile of Iron (blue), Oxygen (green) and Nitrogen (nitrogen) passing through the line. **c**, STEM image of the single particle. **d**, Line profile of single iron nanoparticle iron (blue), oxygen (green) and nitrogen (red) passing through the particle in the given area single particle.

2A.3.2.5. Electron Paramagnetic Resonance (EPR) Analysis

The electron paramagnetic resonance (EPR) spectra of Fe-L1@EGO-900 catalyst recorded in the temperature range 103 - 300 K and showed an intense broad signal at $g \sim 2.19$ and a weak signal at $g \sim 4.3$ at 103K (Figure 2A.7). The line width of the signal at $g \sim 2.19$ increased (from 985 to 1320 G) as the temperature was lowered from 300K to 103 K. Also a marginal change in the g value (from 2.04 to 2.19) was noted at lower temperatures. These observations are indicative of

the ferromagnetic behavior of Fe-L1@EGO-900 containing Fe(III) nanoparticles.^{51, 26} Notably, the presence of metallic iron can be ruled out because their magnetic properties are not in line with the observed EPR intensity behavior.

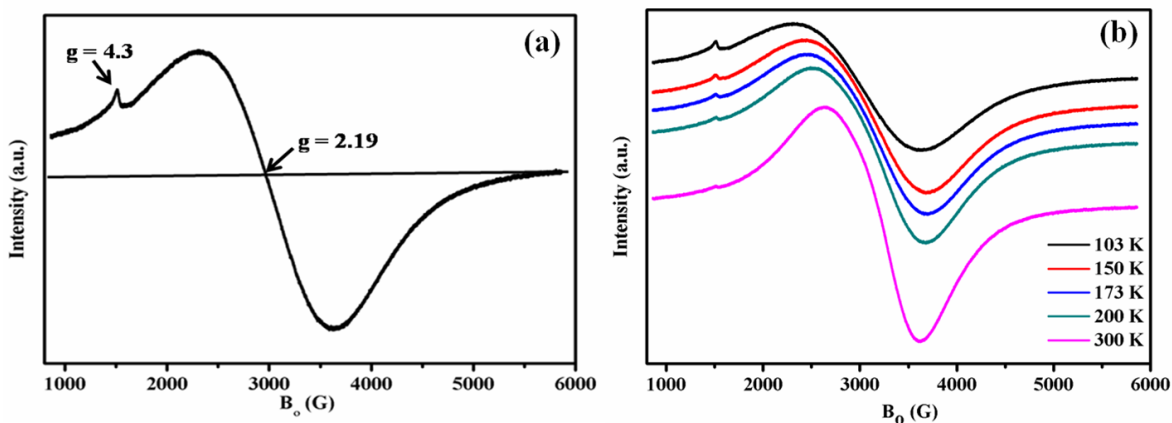


Figure 2A.7. EPR of Fe-L1@EGO-900 catalyst **a**, at 103 K. **b**, at different temperatures.

2A.3.2.6. X-ray photoelectron spectroscopy (XPS)

To obtain further insight into the structure of the catalyst and especially the role of nitrogen from the organic ligand, XPS investigations on the bonding of nitrogen and iron were carried out (Figure 2A.8). XPS clearly showed that nitrogen from L1 was doped into the extended carbon lattice of EGO support and existed as pyridine, pyrrole, and quaternary ammonium groups. Interestingly, five distinct peaks were observed in the N1s spectra of the Fe-L1@EGO-900 catalyst with the binding energy of 397.5 eV, 399.1 eV, 400.1 eV, 401.4 eV and 403.6 eV.⁵¹⁻⁵² The electron binding energy of 399.1 eV and 400.1 eV are characteristic for pyridine-type nitrogen, and pyrrole-type nitrogen contributing two electrons to the carbon matrix.

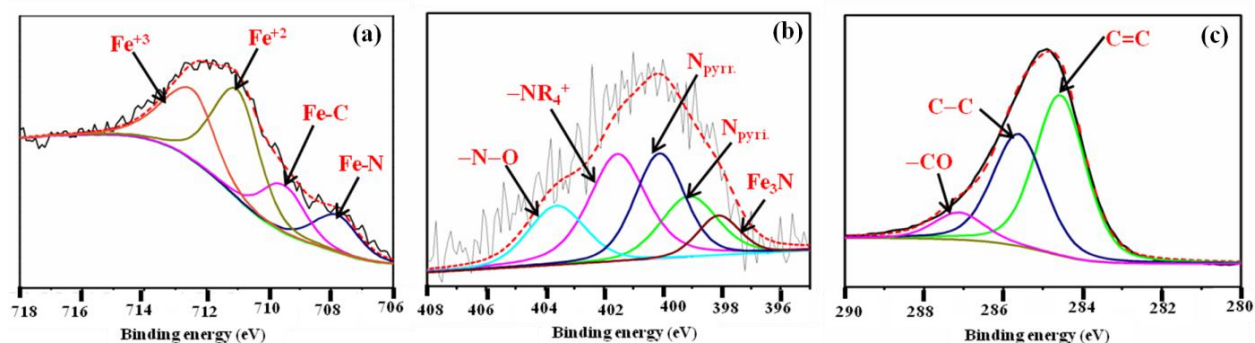


Figure 2A.8. X-ray photoelectron spectra (XPS) of Fe-L1@EGO-900 catalyst. **a**, Iron. **b**, Carbon. **c**, Nitrogen.

The formation Fe_3N and Fe_7C_3 nanoparticles is further supported by XPS measurement with peaks at 707.8 eV and 709.5 eV due to Fe-N and FeC bonds respectively.⁴³ Peak at 711 eV is due to Fe^{+2} and 712.45 for Fe^{+3} confirms the formation of Fe_2O_3 and Fe_3O_4 .

2A.3.2.7. Raman Spectra

Raman spectra of Fe-L1@EGO-900 and reduced graphene (RG) is shown in Figure 2A.9. It shows two characteristic peaks. The first characteristic D band was seen at 1327 cm^{-1} for Fe-L1@EGO-900 and 1330 cm^{-1} for RG arises due to vibration mode of A_{1g} symmetry of the sp^2 carbon of graphite lattice. It characterizes structural defects or edges that can break the symmetry and selection rule. The second characteristic G was located at 1595 cm^{-1} for Fe-L1@EGO-900 and at 1586 cm^{-1} for RG band that appears due to the first-order scattering of the E_{2g} observed for sp^2 carbon domains. G band represents the highly ordered graphite carbon materials. I_D/I_G increased to 1.36 in Fe-L1@EGO-900 compared to $I_D/I_G=1.13$ in RG which may be due to increased in disorderliness of graphene due to deposition of iron nanoparticles in Fe-L1@EGO-900 sample. G band showed a blue shift of 9 cm^{-1} in G band showed of Fe-L1@EGO-900 seen as compared to RG which is due to charge transfer from graphene to iron nanoparticles.⁵³⁻⁵⁴

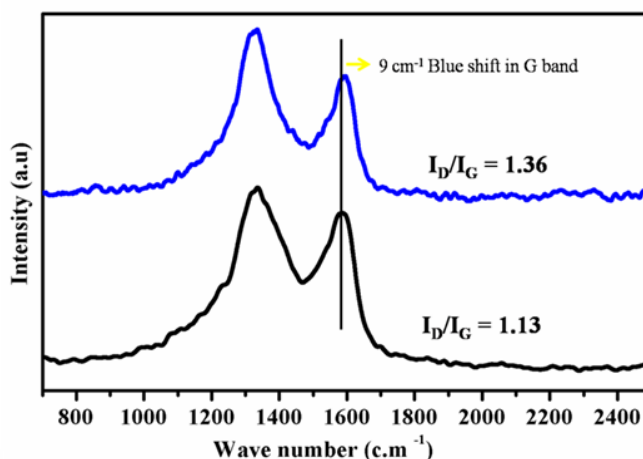


Figure 2A.9 Raman Spectra of reduced graphene (black) and Fe-L1@EGO-900 (Blue).

2A.3.2.7. Thermogravimetric Analysis (TGA)

TGA of the Fe-L1@EGO-900 given in the Figure 2A.10. Weight loss at $150\text{ }^\circ\text{C}$ was due to loss of physisorbed moisture. The weight loss at $350\text{ }^\circ\text{C}$ is characteristic of the loss of oxygen functional groups that are present on the surface of graphitic oxide in the form of epoxide,

alcohol and carbonyl groups. In comparison to trace (i), trace (ii) did not show any weight loss at 150 and 350 °C. Trace (ii) is graphitic oxide loaded with Fe-phenanthroline complex. The percentage weight loss due to loss of functional groups is not seen due to the presence of relatively heavier Fe element. In addition, Fe is also oxidized to Fe₂O₃ and Fe₃O₄.

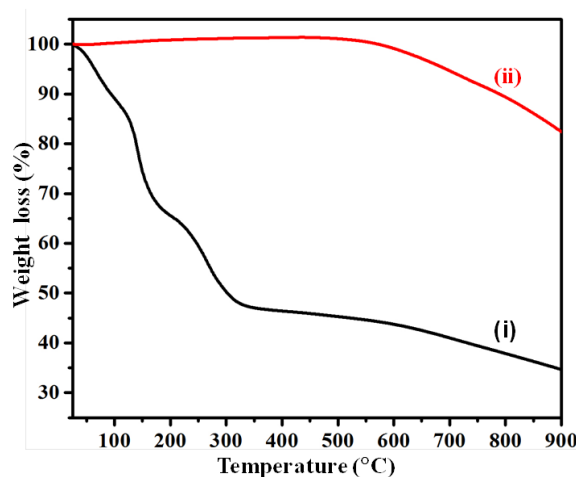


Figure 2A.10. TGA of exfoliated graphene oxide (black) and Fe-phenanthroline complex on graphene oxide support (red).

2A.6.8. Effect of different ligand

In order to understand the role of ligands in the nanocatalyst formation, composition and microstructure two different iron-catalysts Fe-L₂@EGO-900 and Fe-L₃@EGO-900 were prepared under the same conditions using 2,2'-bipyridine (L₂), and pyridine (L₃) as ligands, respectively. The PXRD of the catalytic materials gave an insight into the chemical composition (Figure 2A.11). Notably, the chemical composition of the Fe-L₃@EGO-900, Fe-L₂@EGO-900 and Fe-L₁@EGO-900 were slightly different. In comparison to Fe-L₂@EGO-900 and Fe-L₃@EGO-900, the catalyst Fe-L₁@EGO-900 showed intense peaks suggesting a higher degree of crystallinity. The peaks corresponding to the oxide and the nitride phases were also higher in intensity than the carbide phase in Fe-L₁@EGO-900. The structure and morphology of Fe-L₃@EGO-900, Fe-L₂@EGO-900 and Fe-L₁@EGO-900 were analyzed using TEM (Figure 2A.12). In comparison with Fe-L₁@EGO-900, the microstructure of the nanoparticles synthesized using L₂ and L₃ ligands showed noticeable differences. The TEM analysis of the catalyst Fe-L₁@EGO-900 clearly showed the presence of spherical nanoparticles in the size

range of 4-100 nm. The majority of the particles was in 15 – 20 nm and were supported well on the graphene support.

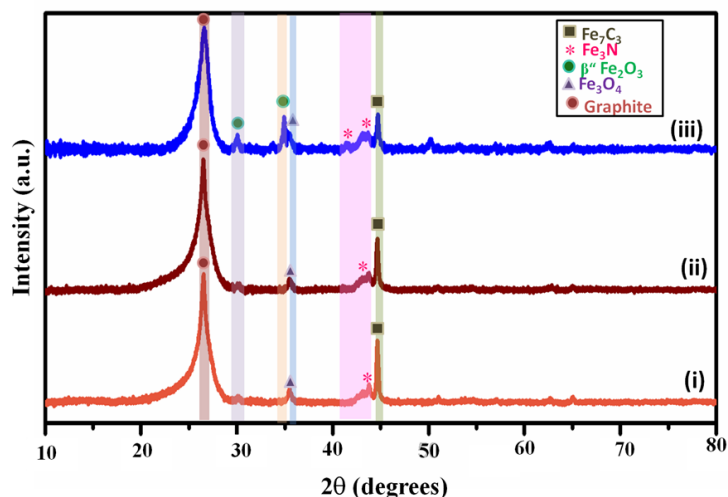


Figure 2A.11. (i) PXRD of Fe-L3@EGO-900, (ii) Fe-L2@EGO-900, (iii) Fe-L1@EGO-900 catalyst.

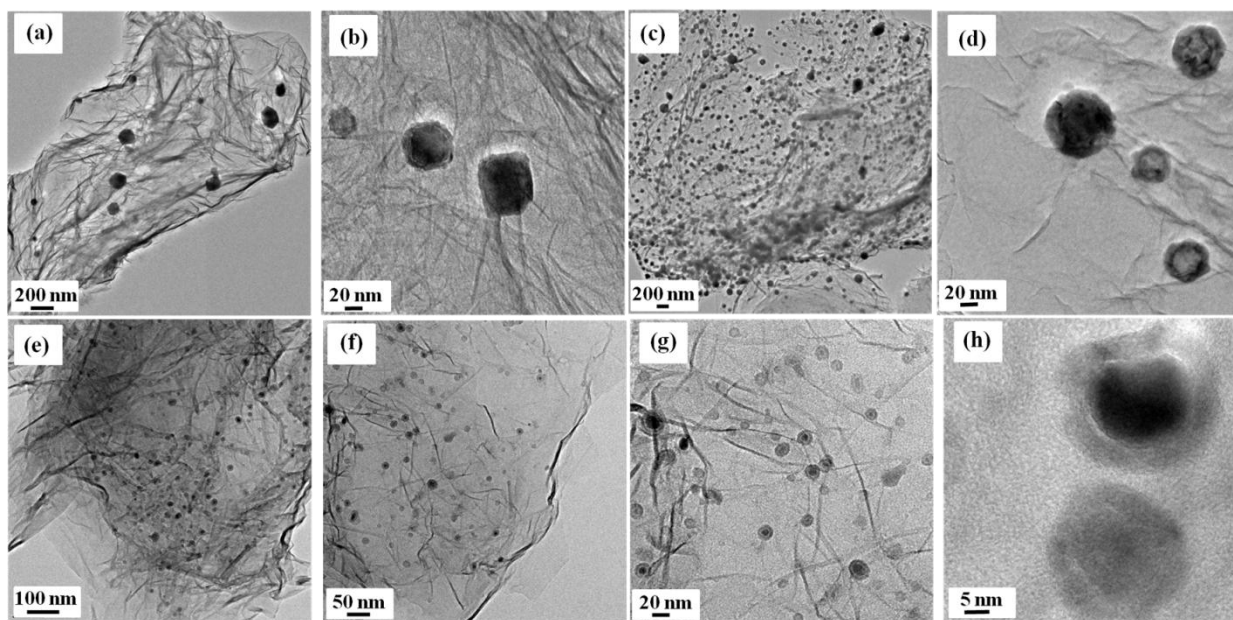


Figure 2A.12. a & b) TEM images of Fe-L3@EGO-900 at the scale bar of 200 nm and scale bar of 20 nm, c & d) TEM images Fe-L2@EGO-900 at the scale bar of 200 nm and the scale bar of 20 nm, e, f, g & h) TEM images of Fe-L1@EGO-900 at the scale bar of 100 nm, scale bar 50 nm, scale bar of 20 nm and scale bar of 5 nm.

On higher magnification, the particles showed a distinguished core-shell structure. In the case of 2,2'-bipyridine (**L2**), we have observed that the catalyst had iron-rich nanoparticles that were reasonably well-distributed and supported on the graphene sheet in the size ranging from 30-300 nm (the majority size of the particles around 50 nm). On careful inspection of TEM images, nanoparticles having the core-shell morphology were seen occasionally. The catalyst precursor with pyridine (**L3**) as a ligand produced larger nanoparticles in the range of 30-300 nm was observed. Interestingly, the nanoparticles were solid and uniform in texture without core-shell type of structure. The extensive analysis also showed not all nanoparticles were supported on the graphene sheet.

2A.6.9. Effect of pyrolysis temperature

The effect of pyrolysis temperature on the composition and microstructure was studied by pyrolyzing Fe-L1 on EGO at various temperatures like 400 °C, 600 °C, and 900 °C. The PXRD patterns showed a broad peak ranging from $2\theta = 20 - 30$ degrees with characteristics of graphitic peak and an unidentified peak in all the samples (Figure 2A.13). At lower pyrolysis temperatures there was overlapping of peaks in this region which could be due to the presence of poorly crystalline carbonaceous materials. Importantly, Fe-L1@EGO-900 that was prepared by pyrolyzing at 900 °C showed a single sharp peak corresponding to the graphitic basal plane at $2\theta = 26.5^\circ$ in addition to clear peaks due to crystalline phases of oxides, nitrides, and carbides. From PXRD data and TGA (Figure 2.A.14), it was clear that high pyrolysis temperature (~900 °C) resulted in the decomposition of the iron-ligand complex to form iron oxide, nitride, and carbide phases.

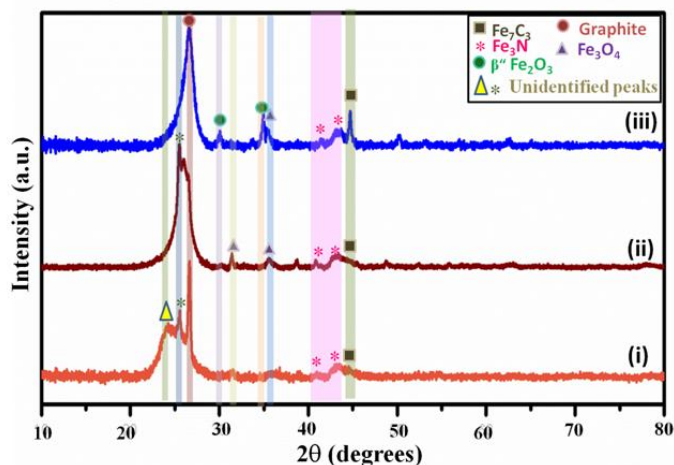


Figure 2A.13. (i) PXRD of Fe-L1@EGO-400, (ii) Fe-L1@EGO-600, (iii) Fe-L1@EGO-900 catalyst.

The effect of pyrolysis temperature on the distribution of size and morphology of the nanoparticles were studied using TEM (Figure 2A.14). The catalyst Fe-L1@EGO-400 showed well distributed small iron nanoparticles in the size range of 2-10 nm. The individual nanoparticles were not in specific shape and no core-shell structure was observed. As the temperature was increased from 400 °C to 600 °C, a few particles agglomerated to form bigger particles with an average size of 10-12 nm. Both PXRD and TEM images strongly indicated that the choice of ligands and pyrolysis temperature affected the composition, size distribution, and microstructure of the individual nanoparticles in the catalyst.

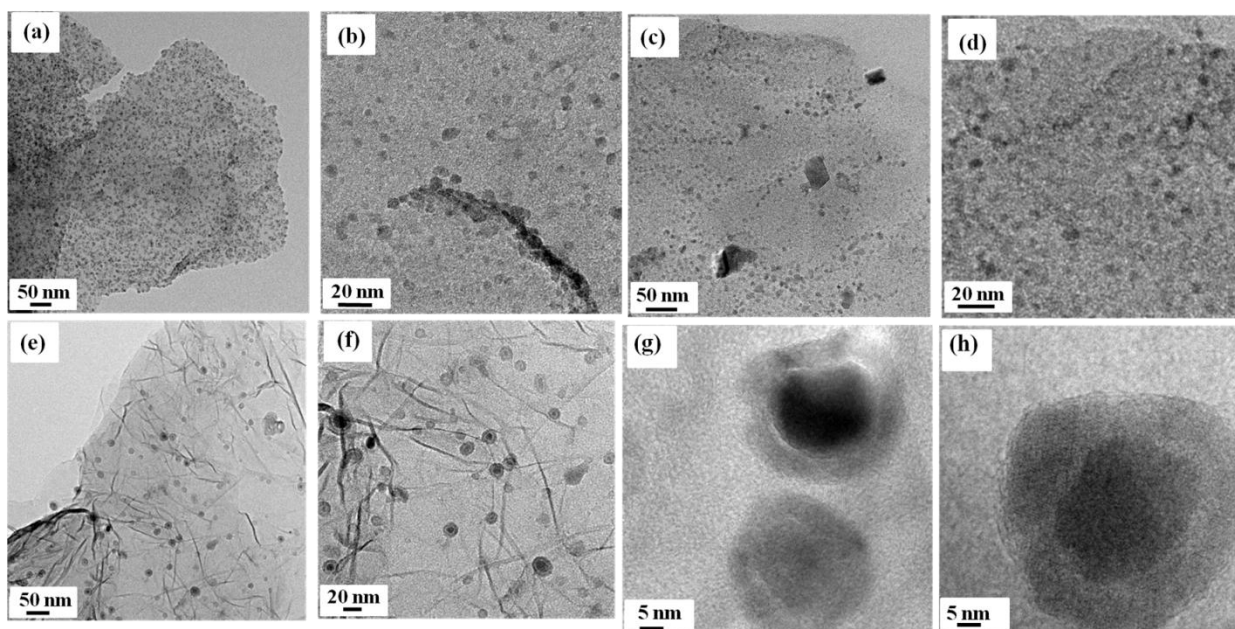


Figure 2A.14. a & b) TEM images of Fe-L1@EGO-400 at the scale bar of 50 nm and scale bar of 20

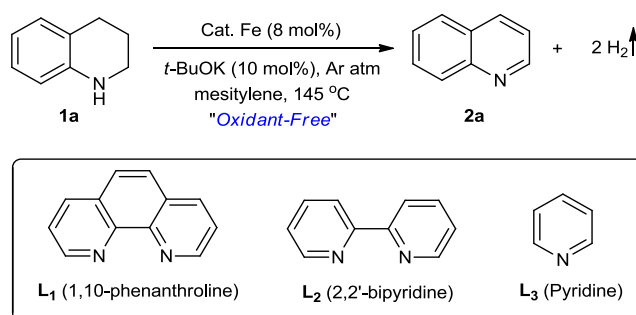
nm, c & d) TEM images Fe-L1@EGO-600 at the scale bar of 50 nm and scale bar of 20 nm. e, f, g & h) TEM images of Fe-L1@EGO-900 at the scale bar of 50 nm, scale bar of 20 nm and scale bar of 5 nm.

2A.4. Result and Discussion

2A.4.1. Optimization Table

To investigate acceptorless dehydrogenation of organic molecule (alcohols and amines) firstly homogeneous complex of iron was deposited on graphene and tested for the acceptorless dehydrogenation of alcohols.

Table 2A.2 Acceptorless dehydrogenation of 1,2,3,4-tetrahydroquinoline (**1a**)



Entry	Catalyst	Conversion (%) ^a	Yield (%) ^a
1	Fe-Phen	trace	trace
2	Fe-Phen@EGO	20	16
3	Fe@EGO	17	15
4	Phen@EGO	6	trace
5	Fe-L ₁ @EGO-400	40	37
6	Fe-L ₁ @EGO-600	52	45 [§]
7	Fe-L ₁ @EGO-900	98	92 (88) ^d
8	Fe-L ₂ @EGO-900	51	40
9	Fe-L ₃ @EGO-900	30	22
10	—	0	0
11	Fe-L ₁ @Al ₂ O ₃ -900	23	19
12	Fe-L ₁ @SiO ₂ -900	15	11
13	Fe-L ₁ @CeO ₂ -900	8	trace
14	Fe-L ₁ @TiO ₂ -900	27	16

Reaction conditions: **1a** (0.5 mmol), cat. Fe-L1@EGO-900 (8 mol%), t-BuOK (10 mol%), and mesitylene (2 mL) heated at 145 °C ^aYields of **2a** and conversion of **1a** were determined by gas chromatography (GC) ^bReaction under homogeneous conditions using the in situ-generated Fe catalyst ^cNon-pyrolyzed materials ^dIsolated yield

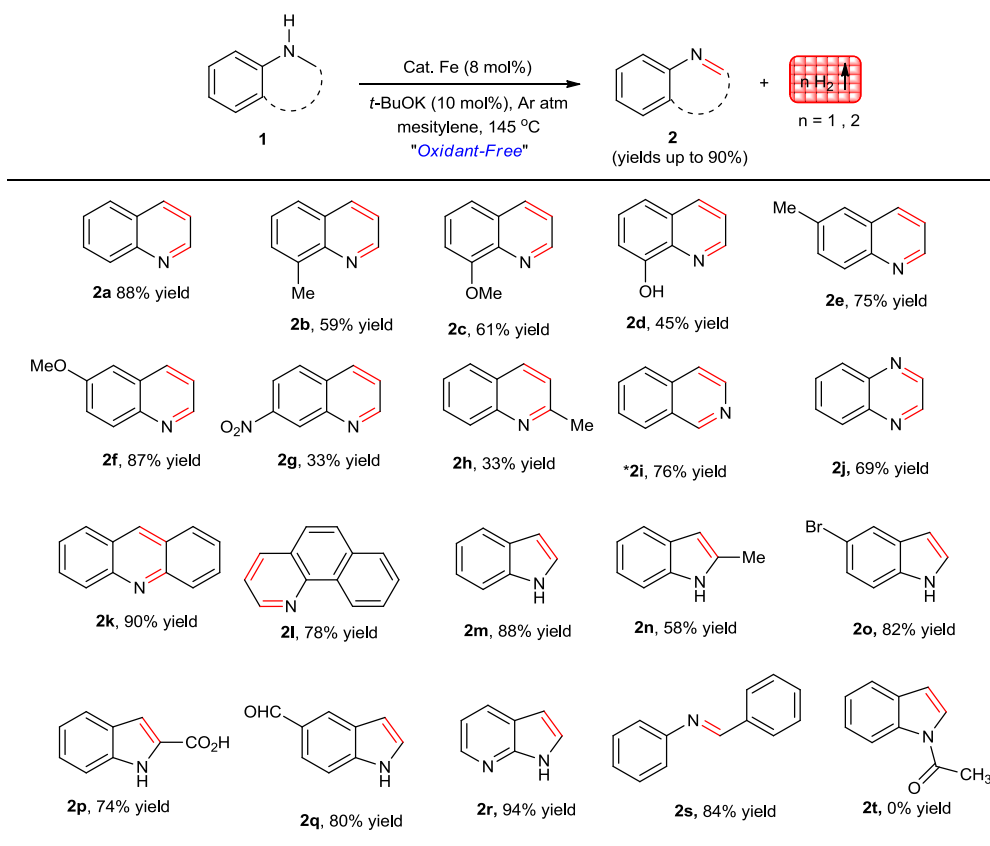
In the preliminary result, it has shown some activity. Later on, several materials were synthesized by changing the ligands and support and tested for their reactivity towards dehydrogenation of *N*-heterocycles with the concomitant generation of dihydrogen under oxidant- and acceptor-free conditions. We began our initial study using 1,2,3,4-tetrahydroquinoline (**1a**) as a benchmark substrate. The effect of each key parameters such as the type of support, nitrogen ligands, Fe: ligand molar ratios, and pyrolysis temperature was carefully investigated (Table 2A.2). As seen from Table 2A.2, *in situ* generated homogeneous metal complex, as well as carbon supported non-pyrolyzed materials, didn't show any catalytic activity under optimal conditions (Table 2A.2, entries 1-2). Similarly, pyrolyzed iron salt (uncomplexed to **L1**), and pyrolyzed **L1** ligand on carbon support were also found to be ineffective (Table 2A.2, entries 3-4). We have observed that the iron- Phenanthroline (Fe-L1) complex pyrolyzed with exfoliated graphitic oxide at 900 °C (Fe-L1@EGO-900) led to a highly active catalytic material for dehydrogenation of **1a** (Table 2A.2, entries 5-7). Under the optimized reaction conditions, the catalyst Fe-L1@EGO-900 selectively formed quinoline (**2a**) in 88% isolated yield with the complete conversion of **1a** (Table 2A.2, entry 7). The generation of molecular hydrogen was qualitatively analyzed by gas chromatography (Figure 2A.15). Other pyrolyzed carbon-supported iron-catalysts using related nitrogen ligands such as 2,2'-bipyridine (**L2**), and pyridine (**L3**) also showed activity yielding the dehydrogenated product (**3a**) in low yields (Table 2A.2, entries 8-9). It was worth noting that under similar experimental conditions, catalysts Fe-L1 prepared on other conventional supports such as SiO₂, Al₂O₃, TiO₂ and CeO₂ showed no activity in the AD with the release of H₂ (Table 2A.2, entries 11-14). The dehydrogenation reaction was also performed with individual phases of iron.

2A.4.2. Substrate scope of *N*-heterocycles

Inspired by the literature reports and with the developed efficient system for AD strategy in hand (Table 2A.2), we sought to apply for oxidant-free, acceptorless dehydrogenation of various *N*-heterocyclic compounds. As expected, Fe-L1@EGO-900 catalyst material displayed the best activity in the complete dehydrogenation of *N*- heterocycles with the liberation of molecular hydrogen. As shown in Table 2A.3, a number of partially saturated *N*-heterocycles containing secondary amines were successfully hydrogenated into corresponding *N*-heteroaromatic

compounds with extrusion of dihydrogen. To our delight, almost all *N*-heterocyclic scaffolds for e.g., 1,2,3,4-tetrahydroquinoline (**1a-1h**), 1,2,3,4-tetrahydroisoquinoline (**1i**), 1,2,3,4-tetrahydroquinoxaline (**1j**), 1,2,3,4-tetrahydrobenzo[*h*]quinoline (**1l**), indoline (**1m-1q**), and 2,3-dihydro-1*H*-pyrrolo[2,3-*b*]pyridine (**1r**) were completely dehydrogenated under oxidant-free acceptorless conditions. Importantly, bromo, formyl, carboxyl, hydroxyl, methoxy, nitro-groups were well tolerated under the optimized conditions and yielded the desired products in moderate to good yields. In order to demonstrate the stability and reusability, the active catalyst was successfully recycled four times without any significant loss of activity for a model substrate (Figure 2A.13). These results evidently demonstrate that our catalyst is highly stable and robust. In addition, the catalyst is conveniently handled under an ambient atmosphere without any deactivation.

Table 2A.3. Nanoscale Iron-Catalyzed Acceptorless Dehydrogenation of *N*-Heterocycles.

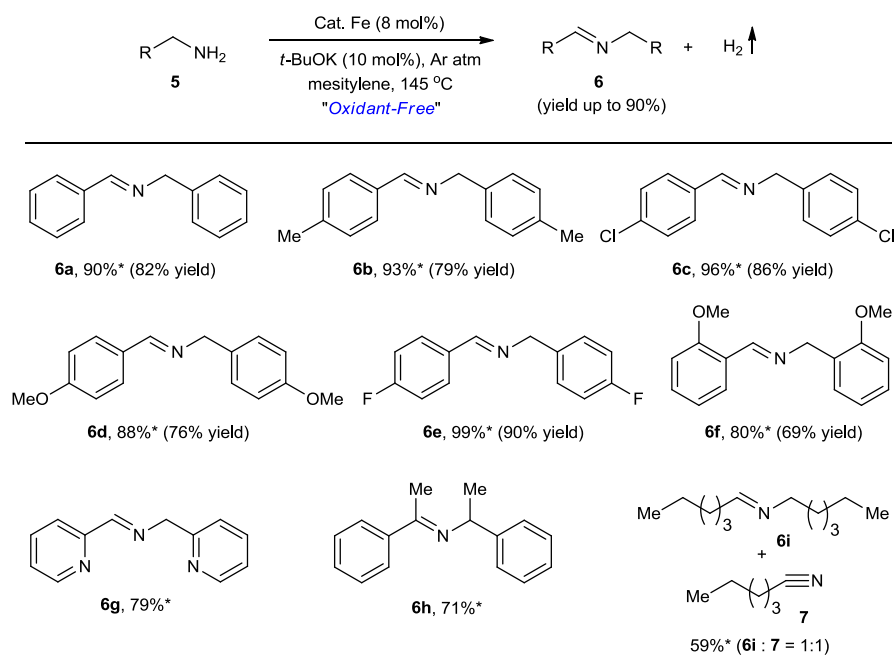


Reaction conditions: **1** (0.5 mmol), cat. Fe-L1@EGO-900 (8 mol%), *t*-BuOK (10 mol%), and mesitylene (2 mL) heated at 145 °C. Yields shown are of isolated products. *Product 3,4-dihydroisoquinoline was observed (8%) on GC.

2A.4.3. Dehydrogenation of Amines to Imines with Extraction of H₂

Various substituted benzylamines (**5a-5e**) and pyridin-2-ylmethanamine (**5g**) were dehydrogenated under optimized conditions and selectively gave the desired imines in good yield. Notably, more sterically hindered benzylamines such as *ortho*-substituted and α -substituted benzylamine were also dehydrogenated (**6f** and **6h**). To our delight, aliphatic amine (**5i**) gave both imine and doubly dehydrogenated product (nitrile compound **7**) in 1:1 ratio under our conditions.

Table 2A.4. Iron-catalyzed Dehydrogenation of Amines to Imines with Extraction of H₂.



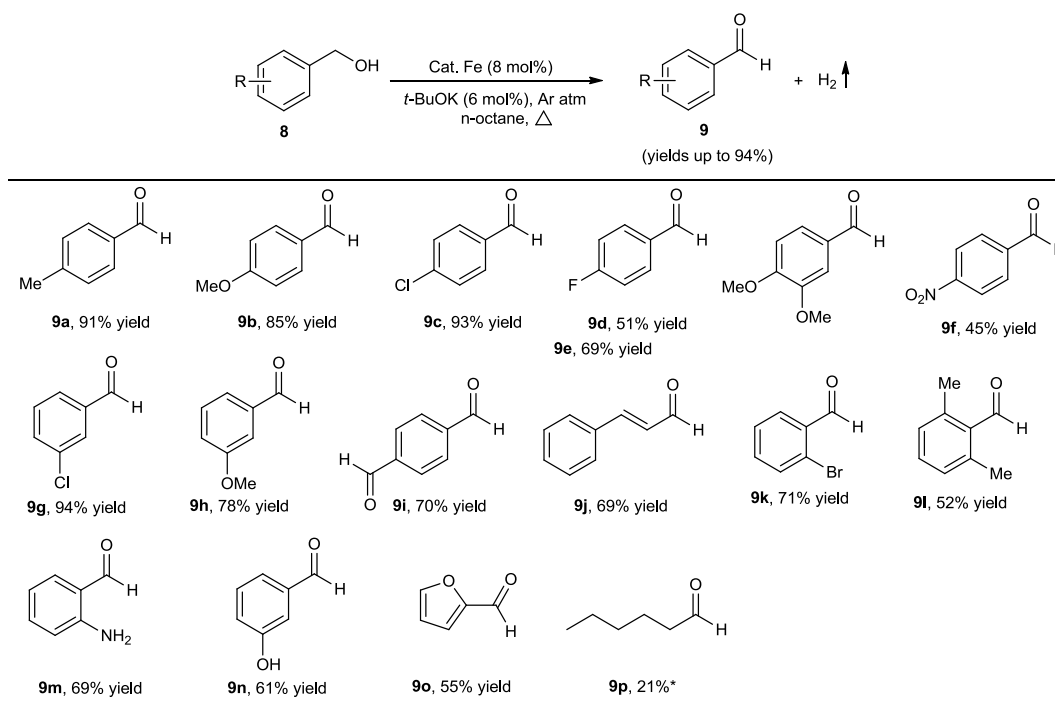
Reaction conditions: **5** (0.5 mmol), cat. Fe-L1@EGO-900 (5 mol%), *t*-BuOK (6 mol%), and mesitylene (2 mL) heated at 145°C.*Yields of **6** was determined by GC using *m*-xylene as an internal standard. Yields shown within brackets are of isolated products.

2A.4.3. Substrate scope of Primary alcohols

Herein, we disclose an efficient, reusable iron-catalyzed oxidant-free, acceptorless dehydrogenation of alcohols such as primary alcohols to aldehydes, secondary alcohols to ketones, and diol to lactone (Table 2A.5). After having demonstrated the excellent activity of the Fe-L1@EGO-900 catalyst in the model reaction (Table 2A.2), we investigated the scope of a series of structurally diverse benzylic alcohols in the acceptorless dehydrogenation. As shown in

Table 2A.5, benzylic alcohols containing electron-donating as well as electron-withdrawing groups are compatible with the catalytic system and good to excellent yields of the corresponding aldehydes are obtained selectively under very mild conditions (up to 94%). Notably, bis-aldehyde (**9i**) can be obtained in a straightforward manner in up to 70% yield. A more sensitive cinnamyl alcohol undergoes dehydrogenation and efficiently gave the corresponding aldehyde **9j** in moderate yield (69%). To our delight, substrates with phenoxy, and amine groups on the aromatic ring also afforded the desired products in good yields (products **9m** in 69% and **9n** in 61% isolated yield respectively). The biomass-derived furfuryl alcohol was readily converted into the corresponding aldehyde in good yield (**9o** in 55% yield). Under optimal conditions, 1-hexanol showed poor reactivity and yielded 1-hexanal (**9p**) in 21% yield. It is important to note that the selective conversion of alcohols to aldehydes *via* acceptorless strategy is very challenging due to competing for ester formation.^{2, 49-50}

Table 2.A.5. Iron-catalyzed Dehydrogenation of Primary Alcohols with Extraction of H₂.

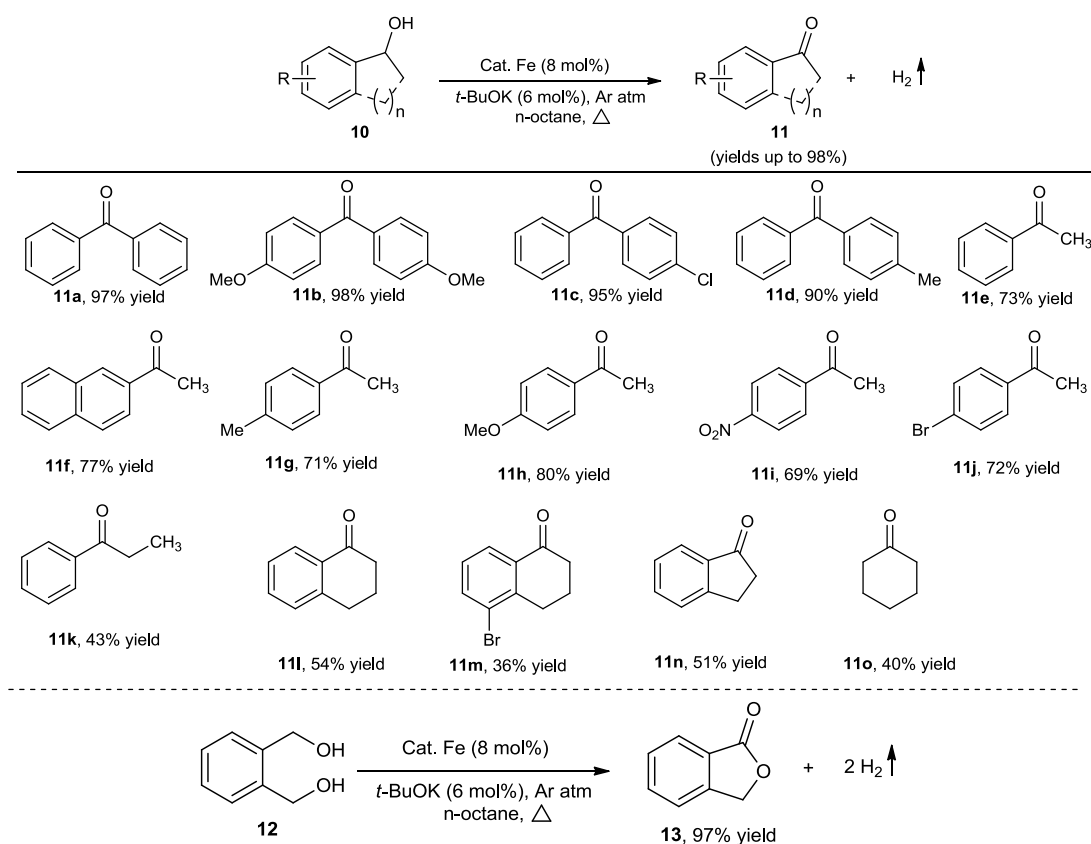


Reaction conditions: Alcohol (0.5 mmol), cat. Fe-L1@EGO-900 (5 mol%), *t*-BuOK (6 mol%), and *n*-octane (2 mL) heated at reflux under open argon atm. Yields shown are of isolated products. *Yields are based on GC.

2A.4.5. Substrate scope of Secondary alcohols and Diol

We examined the scope of secondary alcohols in the catalytic AD strategy using Fe-L1@EGO-900 catalyst (Table 2A.6). Secondary benzylic alcohols are dehydrogenated to the corresponding acetophenone derivatives in good isolated yields (up to 98%). The reaction is tolerant to a variety of functional groups such as -OMe, -Me, and -NO₂ as well as halides (-Cl and -Br). Electronic influence on the dehydrogenation activity seemed to be significant because a substrate containing an electron-donating -OMe group (product **11h** in 80%) gave excellent yield than the one with an electron-withdrawing -NO₂ group (product **11i** in 69%). Importantly, the homologous of 1-(*p*-tolyl)ethan-1-ol gave moderate yield under optimal conditions than **11g** (1-(*p*-tolyl)propan-1-ol) in 71% and 1-(*p*-tolyl)ethan-1-ol **11k** in 43% yield).

Table 2A.6 Iron-catalyzed Dehydrogenation of Secondary Alcohol with Extraction of H₂.



Reaction conditions: Alcohol (0.5 mmol), cat. Fe-L1@EGO-900 (5 mol%), *t*-BuOK (6 mol%), and n-octane (2 mL) heated at reflux under open argon atm. Yields shown are of isolated products. *Yields are based on GC.

In addition to aromatic substrates, the aliphatic secondary alcohol cyclohexanol was successfully dehydrogenated to give cyclohexanone (**11o**) in 40% yield. A substrate with 5- and a 6-membered ring containing 2° alcohols almost gave same yields (products **11l** and **11n** in 54% and 51% yield respectively). Besides primary alcohols and secondary alcohols, diol was also examined. Accordingly, dehydrogenation of 1,2-benzenedimethanol gave 100% conversion and complete selectivity for the corresponding lactone **13** by releasing two equiv. of dihydrogen.² However, the corresponding 1,4-disubstituted derivative gave the corresponding 1,4-dialdehyde derivatives **11i** under the same reaction conditions (Table 2A.6). Perhaps, intramolecular dehydrogenative condensation is more favorable in case of 1,2-disubstituted primary diols and readily produces the corresponding lactone.⁵⁰

Table 2A.7 showing the conversion of 2-chlorobenzyl alcohol and selectivity of 2-chlorobenzaldehyde products using different Fe based catalysts in pure phases. As it is clear, only Fe-L1@EGO-900 with mixed phases in core-shell morphology shows exemplary conversion and selectivity. Other pure single phases of iron are not active for the catalysis. There is a possibility that intermixed phase of iron having specific core-shell morphology is showing catalytic activity.

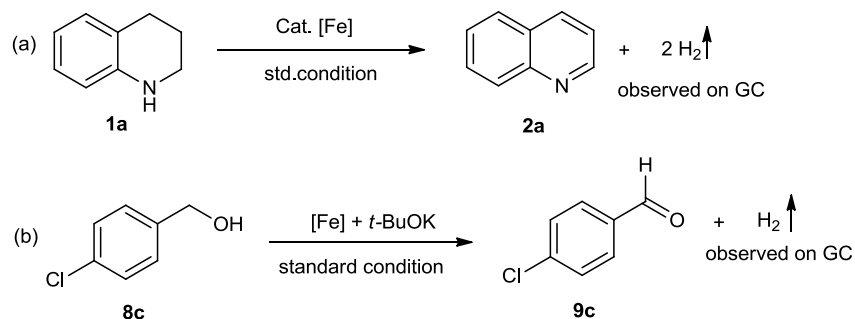
Entry	Catalyst (8 mol%)	Conversion (%)	Selectivity (%)
1	Fe-L1@EGO-900	95	93
2	Fe ₃ O ₄	15	55
3	Fe ₂ O ₃	38	40
4	Fe _x N	15	80
5	Fe ₃ C	12	70

2A.4.6. Mechanistic Studies

2A.4.6.1. Qualitative analysis of hydrogen gas formation

Under standard conditions, the dehydrogenation of 1,2,3,4-tetrahydroquinoline (**1a**), and (4-chlorophenyl)methanol (**8c**) were carried out independently using the J. Young NMR tube. After

24 h, the gas was also collected by a gas-tight syringe and qualitatively analyzed by GC-TCD with a Carbon plot capillary column gas chromatography which shows the presence of H₂ gas at retention time 0.903 (Figure 2A.15).



Scheme 2A.3 Qualitative analysis of hydrogen gas formation.

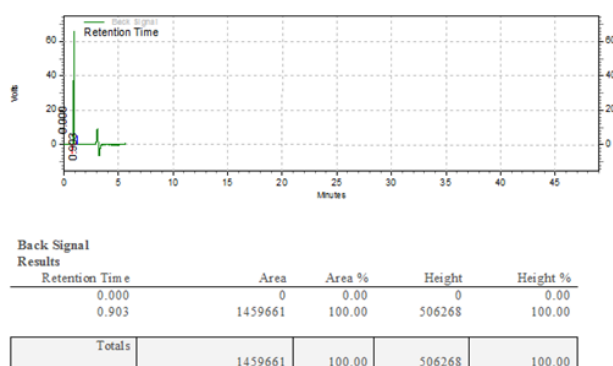


Figure 2A.15. Gas chromatography showing a peak of hydrogen.

2A.4.6.2 Quantitative analysis of hydrogen gas by dual catalysis

(A) For the detection of hydrogen dual reaction involving dehydrogenation of 1,2,3,4-tetrahydroquinoline and hydrogenation of cyclohexene was performed. To schlenk tube, Fe-L1@EGO-900 catalyst (5 mol%), *t*-BuOK (6 mol%), 1,2,3,4-tetrahydroquinoline (0.2 mmol), mesitylene (2 mL) were added under argon atmosphere. The entire system degassed and flushed with argon for 5 minutes (three times) and packed with a rubber septum. To another 25 mL Schlenk tube, RhCl(PPh₃)₃ (3 mol%) catalyst, and cyclohexene (0.4 mmol) were dissolved in benzene (2 mL). Both the flasks were connected through a double-headed syringe and allowed to equilibrate for 5 minutes. The mixture in the former flask was heated at 145 °C, while the mixture in the latter flask was stirred at 50 °C. After 12 hours, the organic entities present in the

latter flask were analyzed by GC-MS which showed a clean conversion (45%) of the cyclohexene to cyclohexane (yield of **2a** = 61%).

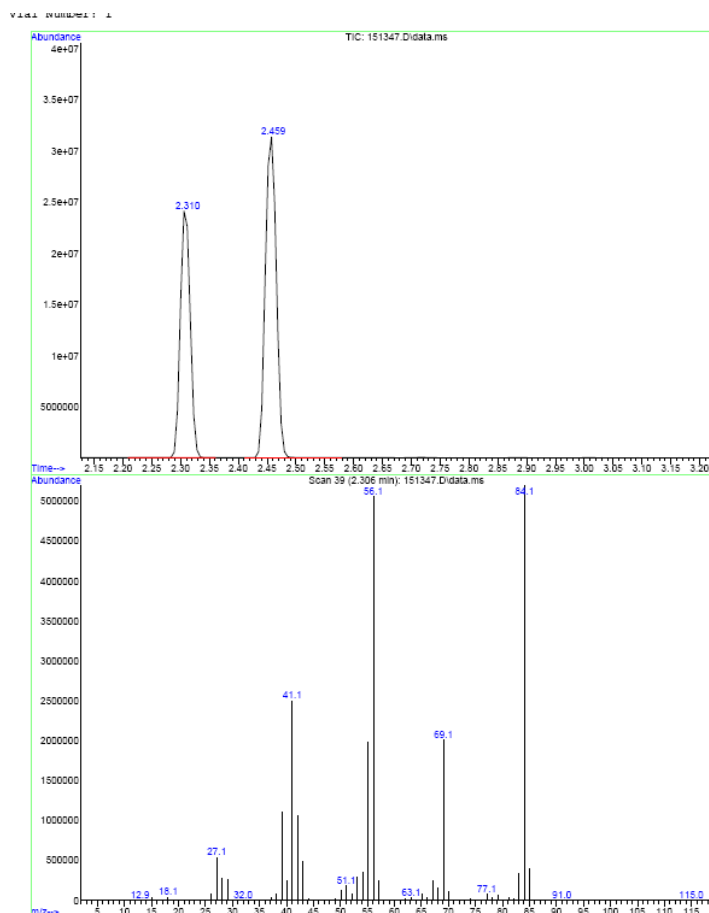
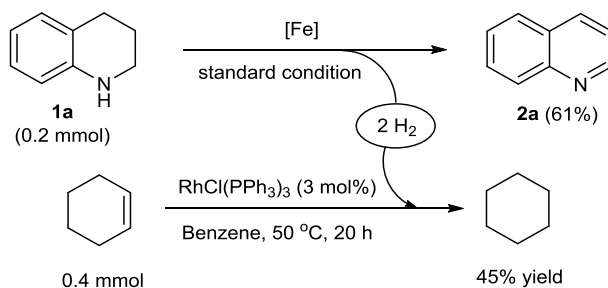
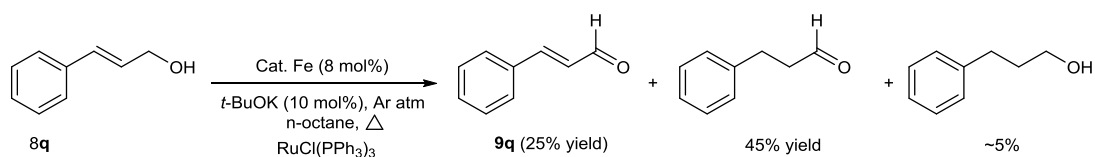


Figure 2A.16. GC-MS of hydrogenation of cyclohexene by *in situ* generated hydrogen gas via dehydrogenation of **1a**.

(B) To an oven dried schlenk tube (25 mL), Fe-L1@EGO-900 catalyst (5 mol%), *t*-BuOK (6 mol%), , cinnamyl alcohol (0.5 mmol), RhCl(PPh₃)₃ (3 mol%), and n-octane (2 mL) were added

under argon atmosphere and packed with rubber septum. The reaction mixture was heated at 120 °C for 24 hours and analyzed. In the reaction mixture cinnamaldehyde (25%) as well as reduced product 3-phenylpropanal (45%), and 3-phenylpropan-1-ol (5%) with the conversion of 74% of **8q**. This result clearly confirms the *in situ* generation of hydrogen (*via* dehydrogenation of alcohol).



Scheme 2A.5. *In situ* generation of hydrogen *via* dehydrogenation of alcohols.

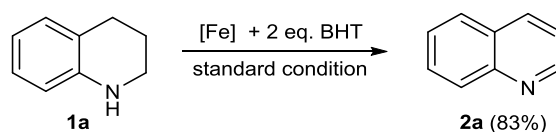
2A.4.6.3. Hydrogen gas quantification: A volumetric quantitative analysis

To an oven dried schlenk tube (25 mL), Fe-L1@EGO-900 catalyst (27 mg, 5 mol%), *t*-BuOK (6 mol%), 1,2,3,4-tetrahydroquinoline **1a** (0.4 mmol), mesitylene (2 mL) was added under argon atmosphere and packed with a rubber septum. The vessel was connected to the gas collection apparatus (standard water displacement apparatus, using a graduated cylinder to determine volume) and the entire system was flushed with argon for 5 minutes and allowed to equilibrate for 5 minutes. The reaction tube was placed preheated oil-bath to the appropriate temperature (145 °C). The reaction was stirred vigorously at a constant temperature until gas evolution ceased. The volume of collected gas was noted and the presence of hydrogen in the collected gas was confirmed by GC. After 24 h, the reaction mixture (contains mesitylene) was removed to give a crude product which was analyzed by ^1H NMR and confirmed 85% yield of the quinoline product (**2a**). The collected volume of gas in the experiment above was 19 mL, which corresponds to 0.80 mmol of dihydrogen and consisted with the release of 2 equivalents of H_2 per mole of 1,2,3,4-tetrahydroquinoline.



Figure 2A.17. Setup for hydrogen gas evolution (a volumetric quantitative analysis).

2A.4.6.4. Reaction under the presence of radical ($O\cdot^{-2}$) scavenger



To a 25 mL oven dried schlenk tube, Fe-L1@EGO-900 catalyst (27 mg, 5 mol%), *t*-BuOK (6 mol%), 1,2,3,4-tetrahydroquinoline (71 mg, 0.5 mmol), 2,6-di-tert-butyl-4-methylphenol (BHT) (242 mg, 1.1 mmol), and *n*-mesitylene (2 mL) were added under argon atmosphere. The schlenk tube was equipped with a reflux condenser and the solution was refluxed under argon atmosphere for 24 h. After cooling to 30 °C the reaction mixture was subjected to centrifugation and the supernatant was collected and the obtained solid was washed with EtOAc (2 x 4 mL) and the washings were collected. The collected reaction mixture was concentrated on rotavapor under reduced pressure. The crude product was purified (deactivated silica gel column chromatography and the eluent is a mixture of petroleum ether and ethyl acetate) and the yield of quinoline is 83%.

2A.4.6.5. Hot Filtration Test

To a 25 mL oven dried schlenk tube, Fe-L1@EGO-900 catalyst (5 mol%), *t*-BuOK (6 mol%), 1,2,3,4-tetrahydroquinoline (71 mg, 0.5 mmol), were added under argon atmosphere. The schlenk tube was equipped with a reflux condenser, and the solution was heated at 145 °C with stirring under open argon flow for 10 h. After cooling to 30 °C the catalyst was separated from the reaction mixture by an external permanent magnet (at this stage the crude reaction mixture was analyzed by GC (43 % of **2a**). Then, the reaction mixture was transferred into another 25 mL oven dried schlenk tube under an argon atmosphere and was equipped with a reflux condenser, and the solution was heated at 145 °C with stirring under open argon flow further 12 h. After cooling to room temperature, the crude reaction mixture was quantitatively analyzed by GC and observed that no change in the yield of **2a**.

2A.4.6.6. Leaching Test

To crude sample (after removal the catalyst) sulfuric acid and aqua regia were added. Then the volume of the residue was adjusted to 50 mL using water to give a sample for Inductively coupled plasma (ICP) for the measurement of the leaching of Iron and the analyses confirmed that the iron concentration in the filtrate was less than 0.24 ppm.

2A.4.6.7. Recyclability of the catalyst

To a oven dried schlenk tube (25 mL) Fe-L1@EGO-900 catalyst (27 mg, 5 mol%), *t*-BuOK (6 mol%), 1,2,3,4- tetrahydroquinoline (0.5 mmol), mesitylene (2 mL) were added under argon atmosphere. The solution was refluxed at 145 °C with stirring under open argon flow for 24 h. After cooling down the reaction mixture to room temperature the catalyst was separated from the reaction mixture by an external permanent magnet and washed several time with mesitylene. Obtained catalyst was dried under vacuum at 60 °C for 12 h. Then the catalyst was reused for the next cycle, and no deactivation of the material was observed up to four cycles. All yields (GC) are averages from at least 2 separate runs.

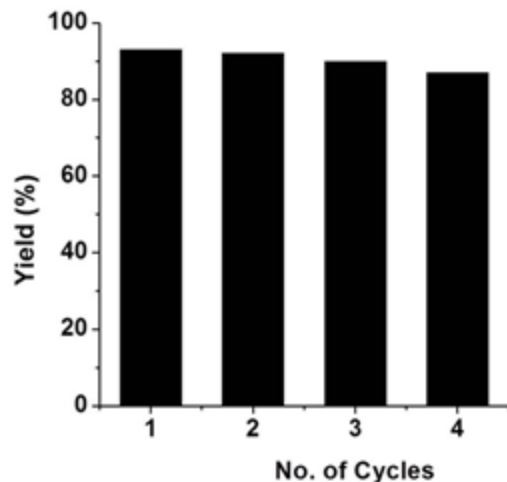


Figure 2A.18. Recyclability experiments.

2A.4.7.2. Magnetic separation of catalyst

The presence of Fe_3O_4 in the catalyst was exploited to magnetically separate them after the reaction. Figure 2A.19(a) digital photograph show the catalyst in highly dispersed form during the reaction. After the reaction was completed, the catalysts were easily separated using a permanent magnet as shown in Figure 2A.19. Efficient magnetic separation of the catalyst was possible even after several cycles of reaction suggesting no phase transformation or leaching of the magnetic phase Fe_3O_4 . This property of the catalyst is a significant advantage compared to the homogeneous and heterogeneous catalysts which are known to catalyze this reaction.

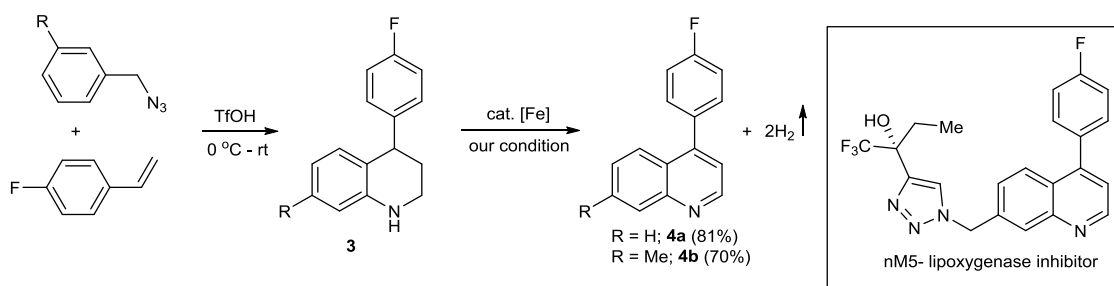


Figure 2A.19. Digital photograph showing **a)** the fine dispersion, and **b)** magnetic separation of Fe-L1@EGO-900.

2A.4.7. Application

2A.4.7.1. Applications in synthesis of drug molecule

The high reactivity of Fe-L1@EGO-900 catalyst towards the acceptorless dehydrogenation of tetrahydroquinoline derivatives encouraged us to extend its application in the synthesis of pharmaceutically important molecules. Thus, dehydrogenation of **3** selectively yielded **4**, a precursor for nM5- lipoxygenase inhibitor (Scheme 2A.6).

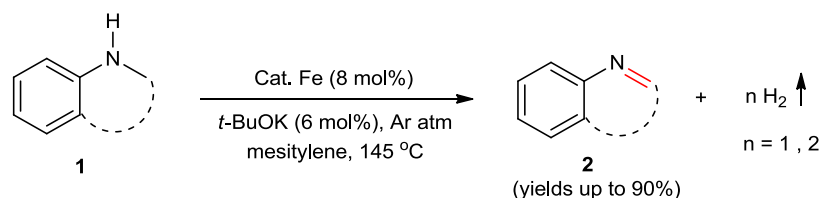


Scheme 2A.6. Application in the synthesis of precursor (**4**) for nM5- lipoxygenase inhibitor.

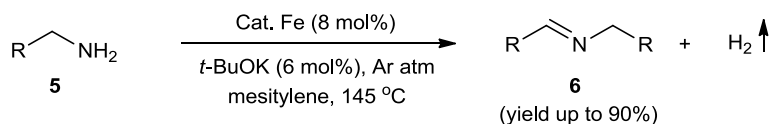
2A.5. Experimental section

2A.5.1. General procedure for the acceptorless dehydrogenation of *N*-heterocycles

To a oven dried schlenk tube (25 mL), Fe-L1@EGO-900 catalyst (27 mg, 5 mol%), *t*-BuOK (6 mol%), *N*-heterocycles (0.5 mmol), mesitylene (2 mL) were added under argon atmosphere. The solution was heated at 145 °C with stirring under open argon flow for 18-24 h. After cooling down the reaction mixture to room temperature the catalyst was separated from the reaction mixture by centrifugation and the reaction mixture was analyzed by GC and GC-MS. The supernatant was transferred to another flask, and the catalyst was washed with EtOAc (2 x 4 mL) and the washings were collected. The solvent was evaporated from the reaction mixture, and the crude product was subjected to silica gel column chromatography using EtOAc : petroleum ether to afford the product.



2A.5.2. General procedure for the acceptorless dehydrogenation of amines to imines



To an oven dried schlenk tube (25 mL), Fe-L1@EGO-900 catalyst (27 mg, 5 mol%), *t*-BuOK (6 mol%), an amine (0.5 mmol), mesitylene (2 mL) were added under argon atmosphere. The solution was heated at 145 °C with stirring under open argon flow for 16-24 h. After cooling down the reaction mixture to room temperature the catalyst was separated from the reaction mixture by centrifugation and the reaction mixture was analyzed by GC and GC-MS. The supernatant was transferred to another flask, and the catalyst was washed with EtOAc (2 x 4 mL) and the washings were collected. The solvent was evaporated from the reaction mixture, and the crude product was subjected to silica gel column chromatography using EtOAc: petroleum ether to afford the product.

2A.5.3. General procedure for the iron-catalyzed alcohol dehydrogenation

To an oven dried schlenk tube (25 mL), Fe-L1@EGO-900 catalyst (27 mg, 5 mol%), *t*-BuOK (6 mol%), alcohol (0.5 mmol), *n*-octane (2 mL) were added under argon atmosphere. The solution was refluxed with stirring under open argon flow for 16-24 h. After cooling down the reaction mixture to room temperature the catalyst was separated from the reaction mixture by centrifugation and the reaction mixture was analyzed by GC and GC-MS. The supernatant was transferred to another flask, and the catalyst was washed with EtOAc (2 x 4 mL) and the washings were collected. The solvent was evaporated from the reaction mixture, and the crude product was subjected to silica gel column chromatography using EtOAc: petroleum ether to afford the corresponding carbonyl compound.

2A.6. Conclusion

In summary, we demonstrated unified strategy for oxidant-free and acceptorless dehydrogenation reactions of relatively abundant alcohols such as primary alcohols to aldehydes, secondary alcohols to ketones, diol to lactone and *N*-heterocycles with the concomitant generation of hydrogen gas catalyzed by iron-based nanocatalyst. The catalytic material described in this work was obtained by thermally pyrolyzing Fe(acac)₃: phenanthroline complex on exfoliated graphitic

oxide support with a unique core-shell architecture composed of oxide and carbide of iron without the encapsulating sheath of carbon. This elegant system offers a new streamlined strategy for the sustainable production of chemicals with a great step-economy and reduced waste generation. In addition to the interesting correlation of microstructure and the catalytic activity of this inexpensive and reusable catalyst, the work also highlights the greenness of the reaction due to the formation of hydrogen gas as the only by-products.

2A.7. References

1. A. J. A. Watson and J. M. J. Williams, *Science*, 2010, **329**, 635-636.
2. C. Gunanathan and D. Milstein, *Science*, **341**, 1229712, (2013).
3. M. Trincado, D. Banerjee and H. r. Grutzmacher, *Energy Environ. Sci.*, 2014, **7**, 2464-2503.
4. M. Yadav and Q. Xu, *Energy Environ. Sci.*, 2012, **5**, 9698-9725.
5. P. J. Bonitatibus, S. Chakraborty, M. D. Doherty, O. Siclovan, W. D. Jones and G. L. Soloveichik, *Proc. Natl. Acad. Sci. USA*, 2015, **112**, 1687-1692.
6. R. A. Sheldon, I. W. C. E. Arends, G.-J. ten Brink and A. Dijkman, *Acc. Chem. Res.*, 2002, **35**, 774-781.
7. L. Que Jr and W. B. Tolman, *Nature*, 2008, **455**, 333.
8. G. E. Dobereiner and R. H. Crabtree, *Chem. Rev.*, 2010, **110**, 681-703.
9. T. C. Johnson, D. J. Morris and M. Wills, *Chem. Soc. Rev.*, 2010, **39**, 81-88.
10. J. Choi, A. H. R. MacArthur, M. Brookhart and A. S. Goldman, *Chem. Rev.*, 2011, **111**, 1761-1779.
11. A. C. Marr, *Catal. Sci. Technol.*, 2012, **2**, 279-287.
12. D. Wang and D. Astruc, *Chem. Rev.*, 2015, **115**, 6621-6686.
13. G. Zeng, S. Sakaki, K.i. Fujita, H. Sano and R. Yamaguchi, *ACS Catal.B*, 2014, **4**, 1010-1020.
14. Plietker, B. *Iron-catalysis fundamental and application. Top.Organomet.Chem.* (Springer, Berlin Heidelberg, 2011).
15. A. Quintard and J. Rodriguez, *Angew. Chem. Int. Ed.*, 2014, **53**, 4044-4055.
16. I. Bauer and H.-J. Knölker, *Chem. Rev.*, 2015, **115**, 3170-3387.
17. R. H. Morris, *Acc. Chem. Res.*, 2015, **48**, 1494-1502.
18. T. Zell and D. Milstein, *Acc. Chem. Res.*, 2015, **48**, 1979-1994.
19. Schlapbach, L. & Züttel *Nature*, 2001, **414**, 353-358.
20. R. H. Crabtree, *Energy Environ. Sci.*, 2008, **1**, 134-138. 19
21. P. Jessop, *Nature chemistry*, 2009, **1**, 350. 20
22. R. Yamaguchi, C. Ikeda, Y. Takahashi and K. i. Fujita, *J Am Chem Soc.*, 2009, **131**, 8410-8412. 21

-
23. H. Li, J. Jiang, G. Lu, F. Huang and Z.-X. Wang, *Organometallics*, 2011, **30**, 3131-3141. 22
 24. J. Wu, D. Talwar, S. Johnston, M. Yan and J. Xiao, *Angew. Chem. Int. Ed.*, 2013, **52**, 6983-6987. 25
 25. K. i. Fujita, Y. Tanaka, M. Kobayashi and R. Yamaguchi, *J. Am. Chem. Soc.*, 2014, **136**, 4829-4832. 25
 26. R. Xu, S. Chakraborty, H. Yuan and W. D. Jones, *ACS Catal.*, 2015, **5**, 6350-6354.
 27. S. Chakraborty, W. W. Brennessel and W. D. Jones, *J. Am. Chem. Soc.*, 2014, **136**, 8564-8567.
 28. D. Forberg, T. Schwob, M. Zaheer, M. Friedrich, N. Miyajima and R. Kempe, *Nat. Commun.*, 2016, **7**, 13201.
 29. M. Langeron and M.-B. Fleury, *Science*, 2013, **339**, 43-44. (53)
 30. T. Yan, B. L. Feringa and K. Barta, *Nat. Commun.*, 2014, **5**, 5602.
 31. T. Schwob, and R. Kempe, *Angew. Chem. Int. Ed.*, 2016, **55**, 15175–15179.
 32. C. P. Casey and H. Guan, *J. Am. Chem. Soc.*, 2007, **129**, 5816-5817. 65
 33. M. Kamitani, M. Ito, M. Itazaki and H. Nakazawa, *Chem. Commun.*, 2014, **50**, 7941-7944.
 34. H. Song, B. Kang and S. H. Hong, *ACS Catal*, 2014, **4**, 2889-2895\
 35. S. Chakraborty, P. O. Lagaditis, M. Förster, E. A. Bielinski, N. Hazari, M. C. Holthausen, W. D. Jones and S. Schneider, *ACS Catal.*, 2014, **4**, 3994-4003. 59
 36. J. Zhao, and J. F. Hartwig, *Organometallics*, 2005, **24**, 2441–2446.
 37. G. Zhang, K. V. Vasudevan, B. L. Scott, and S. K. Hanson, *J. Am. Chem. Soc.*, 2013, **135**, 8668–8681.
 38. S. Enthaler, K. Junge and M. Beller, *Angew. Chem. Int. Ed.*, 2008, **47**, 3317-3321.
 39. R. M. Bullock, *Science*, 2013, **342**, 1054-1055.
 40. R. V. Jagadeesh, A.-E. Surkus, H. Junge, M.-M. Pohl, J. r. Radnik, J. Rabeah, H. Huan, V. Schünemann, A. Brückner and M. Beller, *Science*, 2013, **342**, 1073-1076.
 41. X. Cui, Y. Li, S. Bachmann, M. Scalone, A.-E. Surkus, K. Junge, C. Topf and M. Beller, *J. Am. Chem. Soc.*, 2015, **137**, 10652-10658.
 42. D. Guo, R. Shibuya, C. Akiba, S. Saji, T. Kondo and J. Nakamura, *Science*, 2016, **351**, 361-365.
 43. L. He, F. Weniger, H. Neumann, M. Beller, *Angew. Chem. Int. Ed.*, 2016, **55**, 12582-12594.
-

-
44. M. Li, F. Xu, H. Li and Y. Wang, *Catal. Sci. Technol.*, 2016, **6**, 3670-3693.
 45. F. A. Westerhaus, R. V. Jagadeesh, G. Wienhöfer, M.-M. Pohl, J. r. Radnik, A.-E. Surkus, J. Rabeah, K. Junge, H. Junge and M. Nielsen, *Nat. Chem.*, 2013, **5**, 537-543.
 46. R. V. Jagadeesh, H. Junge and M. Beller, *Nat. Commun.*, 2014, **5**, 4123.
 47. A. V. Iosub and S. S. Stahl, *Org. Lett.*, 2015, **17**, 4404-4407.
 48. F. Chen, A.-E. Surkus, L. He, M.-M. Pohl, J. r. Radnik, C. Topf, K. Junge and M. Beller, *J. Am. Chem. Soc.*, 2015, **137**, 11718-11724.
 49. G. Jaiswal, V. G. Landge, D. Jagadeesan and E. Balaraman, *Nat. Commun.*, 2017, **8**, 2147.
 50. J. R. Pels, F. Kapteijn, J. A. Moulijn, Q. Zhu and K. M. Thomas, *Carbon*, 1995, **33**, 1641-1653.
 51. S. Stankovich, D. A. Dikin, R. D. Piner, K. A. Kohlhaas, A. Kleinhammes, Y. Jia, Y. Wu, S. T. Nguyen and R. S. Ruoff, *Carbon*, 2007, **45**, 1558-1565.
 52. C. D. Wager, M. W. Riggs, L. E. Davis, J. F. Moulder, and G. E. Mullenberg, *Handbook of X-Ray Photoelectron Spectroscopy* (Perkin-Elmer, Eden Prairie, MN, 1979).
 53. R. McCann, S. S. Roy, P. Papakonstantinou, J. A. McLaughlin, and S. C. Ray, *J. Appl. Phys.*, 2005, **97**, 073522.
 54. J. Zhou, H. Song, L. Ma, and X. Chen, *RSC Adv.*, 2011, **1**, 782-791.
 55. R. V. Jagadeesh, G. Wienhoefer, F. A. Westerhaus, A.-E. Surkus, M.-M. Pohl, H. Junge, K. Junge and M. Beller, *Chem. Commun.*, 2011, **47**, 10972–10974.
 56. R. V. Jagadeesh, H. Junge, M.-M. Pohl, J. r. Radnik, A. Bruickner and M. Beller, *J. Am. Chem. Soc.*, 2013, **135**, 10776–10782.
 57. Shimizu, K. i. Shimizu, K. Kon, M. Seto, K. Shimura, H. Yamazaki and J. N. Kondo. *Green Chem.*, 2013, **15**, 418–424.
 58. T. Stemmler, A. E. Surkus, M. M. Pohl, K. Junge, and M. Beller, *ChemSusChem.*, 2014, **7**, 3012–3016.
 59. G. Jaiswal, V. G. Landge, D. Jagadeesan, and E. Balaraman, *Green Chem.*, 2016, **18**, 3232–3238.
 60. D. Formenti, C. Topf, K. Junge, F. Ragaini, and M. Beller, *Catal. Sci. Technol.*, 2016, **6**, 4473–4477.

-
-
61. F. Chen, C. Topf, J. r. Radnik, C. Kreyenschulte, H. Lund, M. Schneider, A.-E. Surkus, L. He, K. Junge and M. Beller, *J. Am. Chem. Soc.*, 2016, **138**, 8781–8788.
 62. Z. Wei, Y. Chen, J. Wang, D. Su, M. Tang, S. Mao and Y. Wang, *ACS Catal.*, 2016, **6**, 5816–5822.
 63. F. Chen, C. Kreyenschulte, J. r. Radnik, H. Lund, A.-E. Surkus, K. Junge and M. Beller, *ACS Catal.*, 2017, **7**, 1526–1532.
 64. D. Wang, and D. Astruc, *Chem. Soc. Rev.*, 2017, **46**, 816–854.

Part B: Acceptorless dehydrogenative coupling of alcohols and amines

2B.1. Introduction

The imine is an exceptionally versatile functional group and is ubiquitous in pharmaceuticals, biologically active heterocycles, and natural products.¹ Traditionally, imine formation was achieved by the condensation reaction of amines with highly reactive carbonyl compounds and often required dehydrating agents as well as Lewis acid catalysts.²⁻³ However, direct formation of imine with easily accessible feedstock chemicals is very attractive and highly desirable in organic synthesis.⁴ In this context, various methods for imine synthesis have been studied based on oxidative dehydrogenation of amines,⁵⁻⁶ and oxidative dehydrogenative coupling of alcohols with amines using various oxidants such as dioxygen, TEMPO, quinine, and iodosylbenzene.⁷ However, several drawbacks remain, for example, the intrinsic self-coupling properties of the substrates, the formation of other side products such as nitrile, amide, azo and a related compound, and the need of stoichiometric amount of oxidants.⁶ Although the use of molecular oxygen as a mild oxidant is an attractive strategy; indeed, there is a need for special equipment while performing reactions under the use of pressurized dioxygen for the large-scale imine production. Thus, the development of an efficient strategy for selective construction of imine scaffolds under the oxidant-free condition is a key motivation in the contemporary science.

Recently, a direct coupling of alcohols with amines by acceptorless dehydrogenative strategy has been developed as an efficient protocol to construct imine bond (C=N) with the liberation of molecular hydrogen and water as the byproducts, which is a greener and more practical method. Although several catalysts reported for the amination of alcohols *via* borrowing hydrogen strategy,⁹ catalytic systems that selectively yield imines are very limited and offer the advantageous possibility of further imine functionalization.^{5z,10} Indeed, heterogeneous catalysts with such activity for the straightforward synthesis of an imine by oxidant-free, acceptorless dehydrogenative coupling of alcohols with amines are rare and very limited. Very recently, Pt nanoparticles loaded on TiO₂ was shown to promote direct synthesis of imines from alcohols and amine under UV irradiation,¹¹ and Pd(0)-immobilized recyclable hydrotalcite catalysts (HT4) for alcohol imination *via* acceptorless dehydrogenation also reported.¹² Notably, catalysts (both

homogeneous and heterogeneous) used for imine synthesis by acceptorless dehydrogenative coupling (ADC) strategy are extensively based on precious metals.

In this regard, the development of novel highly active and selective non-precious metal catalysts; in particular, base metal catalysts is of pivotal importance and a focal point from the perspective of cost, abundance, and sustainable chemistry.¹³ To best of our knowledge, there was no reusable heterogeneous catalysts based on earth-abundant, economical 3d-metals for direct imine formation by acceptorless dehydrogenative coupling of alcohols with amines.

Over the past decade, substantial efforts have been devoted to the replacement of expensive noble metal catalysts by utilizing economical and environmentally benign base metal catalysts. In this regard, earth-abundant, iron catalysts have been intensely used to emulate the selectivity and reactivity of precious-metal catalysts in sustainable catalysis and thus, broaden the scope and practical viability. However, their successful application in the sustainable synthesis of fine chemicals remains at an early stage and can make it difficult to envisage and control catalytic reactivity, as they have the propensity to participate in one electron chemistry as opposed to classical two electron transformation ubiquitous in the second- and third-row transition metals.¹⁴ The present ADC strategy has a broad substrate scope as well as functional group tolerance, and operates under mild conditions with the liberation of hydrogen gas and water as the byproducts, thus making the protocol completely environmentally-benign. An ease of separation and reusability of the heterogeneous iron catalyst is also successfully demonstrated.

2B.2. Statement of problem

To best of our knowledge, there was no reusable heterogeneous catalysts based on earth-abundant, economical 3d-metals for direct imine formation by acceptorless dehydrogenative coupling of alcohols with amines prior to our finding. Development of novel highly active and selective non-precious metal catalysts; in particular, base metal catalysts is of pivotal importance and a focus point from the perspective of cost, abundance, and sustainable chemistry. Over the past decade, substantial efforts have been devoted to the replacement of expensive noble metal catalysts by utilizing economical and environmentally benign base metal catalysts.

2B.3. Catalyst Synthesis and Characterization

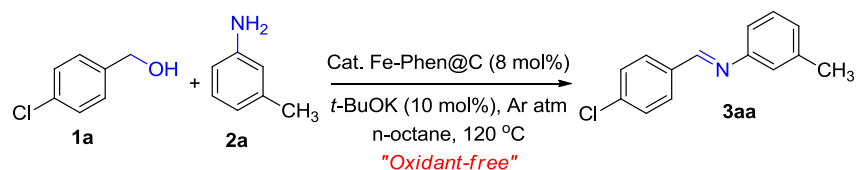
In our previous part of this chapter, we have reported heterogeneous iron-catalyzed acceptorless dehydrogenation of fundamentally important feedstocks such as alcohols to carbonyl compounds and cyclic amines to *N*-heterocycles. Above result prompted us to disclose our first report on a simple, efficient, reusable heterogeneous iron-catalyzed direct imine formation by acceptorless dehydrogenative coupling of alcohols with amines. The catalyst was synthesized and characterized according to the previous part of this chapter (Chapter 2A).

2B.4. Result and Discussion

2B.4.1. Optimization table

Optimization studies on iron-catalyzed direct imine formation by ADC of alcohols with amines are summarized in Table 2B.1

Table 2B.1 Optimization of the reaction conditions.^a



Entry	Cat.	Variation from the initial conditions	Conversion of 1a (%) ^b	Yield of 3aa (%) ^b
1	Fe-Phen@C	none	99	97 (93) ^c
2		closed system	57	40 ^c
3	Fe-Phen@C	without <i>t</i> -BuOK	17	8
4	Fe-Phen@C	K ₂ CO ₃ instead of <i>t</i> -BuOK	35	19
5	Fe-Phen@C	KOH instead of <i>t</i> -BuOK	8	0
6	Fe-Phen@C	CH ₃ CN instead of n-octane	19	15
7	Fe-Phen@C	toluene instead of n-octane	64	46
8	Fe-Phen@C	at 80 °C	40	34 ^{c,d}
9	Fe@C	none	5	0
10	Phen@C	none	0	0
11	---	without Fe-Phen@C	0	0
12 ^o	Fe(acac) ₃ /Phen	under homogeneous condition	8	trace
13 ^o	Fe(CO) ₅ /Phen	under homogeneous condition	trace	0
14	Fe-Phen@SiO ₂	none	31	18
15	Fe-Phen@Al ₂ O ₃	none	17	8
16	Fe-Phen@TiO ₂	none	46	31 ^c

^aReaction conditions: **1a** (0.5 mmol), **2a** (0.55 mmol), cat. Fe-Phen@C (8 mol%), *t*-BuOK(10 mol%), and n-octane (2 mL) heated at 120 °C (oil-bath temperature) for 24 h under open argon atm.

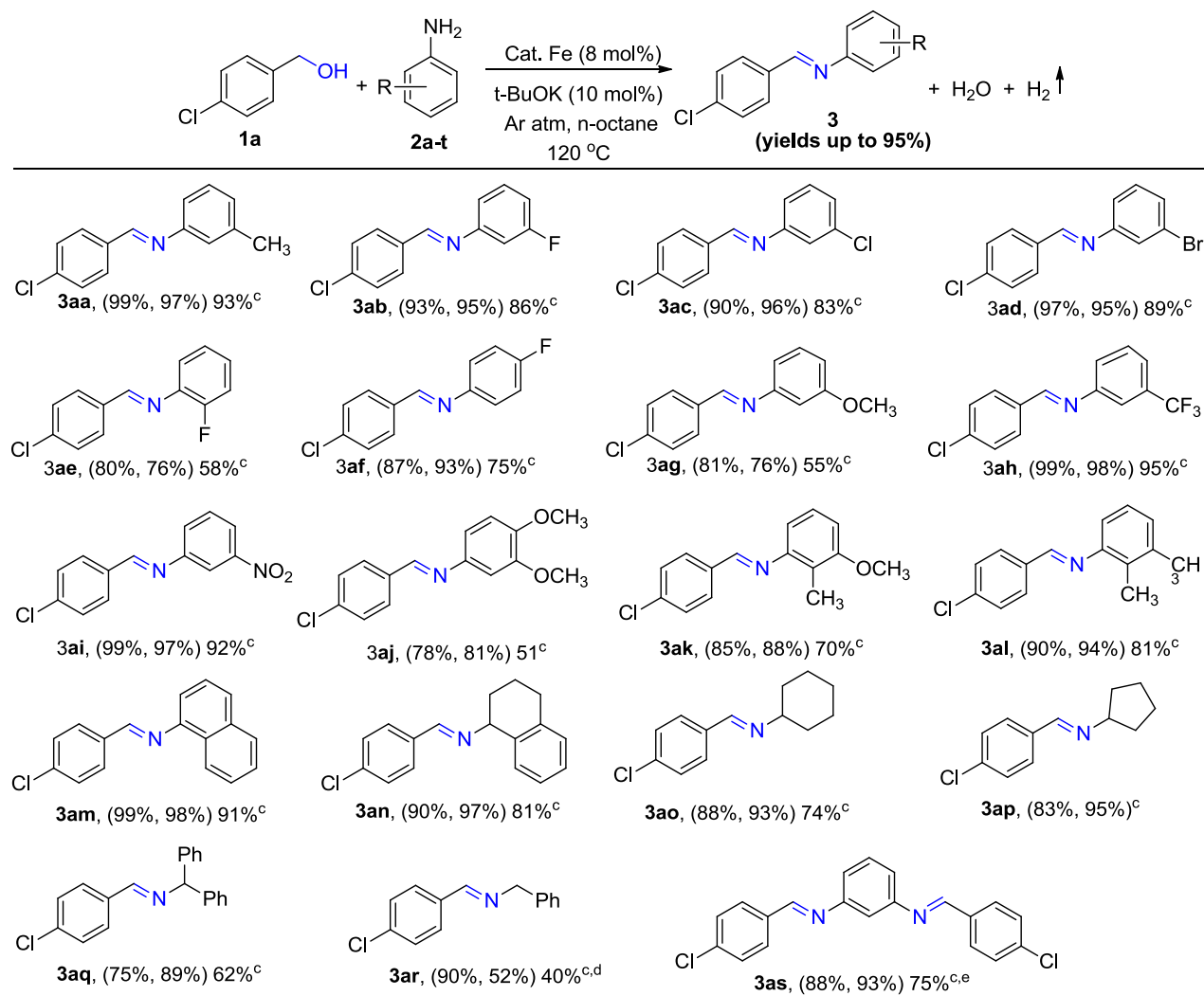
We began our investigation using (4-chlorophenyl)methanol (**1a**) and *m*-toluidine (**2a**) as benchmark substrates in presence of catalytic amount of Fe-Phen@C (8 mol%), and t-BuOK (10 mol%) in n-octane heated at 120 °C (bath temperature) under open Ar atm for 24 h to yield **3aa** in 93% isolated yield with the complete conversion of **1a** (Table 2B.1, entry 1). Indeed, the formation of molecular hydrogen was qualitatively analyzed by gas chromatography (GC). Performing reaction under closed condition yielded **3aa** in lower yield (40%) (Table 2B.1, entry 2) and clearly indicating that the constant removal of H₂ gas from the reaction medium is crucial.^{9-10,19} Notably, the efficiency of the reaction was significantly affected in the absence of t-BuOK (Table 2B.1, entry 3). Other bases like K₂CO₃ and KOH are ineffective under standard reaction conditions (Table 2B.1, entries 4-5). Other bases such as KOAc, CsOAc, Li₂CO₃, Na₂CO₃, K₂CO₃, Cs₂CO₃, Et₃N, DABCO, and DBU proved ineffective and less (~less than 20%), or no formation of **3aa** was observed under optimal conditions. The solvent dependency of the same reaction was carried out (Table 2B.1, entries 1, and 6-7). Further screening using a representative set of common solvents, including apolar arenes (o-xylene, PhCl, anisole), or polar DMF, DMSO, DMA, and DCE proved ineffective and we found that the reaction proceeds efficiently in n-octane compared to other solvents. By lowering the temperature, we obtained the product in lower yield (Table 2B.1, entry 8) and no reaction was observed in the absence of the Fe-Phen@C catalyst (Table 2B.1, entry 11). The reaction was performed under an *in situ* generated soluble Fe-Phen complex by reacting a 1 : 1 mixture of either the readily available Fe(III)-acetylacetonate or Fe(CO)₅ as the iron precursor and 1,10-phenanthroline as a ligand followed by treatment with a catalytic amount of a base (10 mol% of t-BuOK). Notably, either no imine formation or hydrogen gas was observed under homogeneous conditions (Table 2B.1, entries 12-13). It was worth noting that under the similar experimental conditions, catalysts (Fe-Phen) prepared on other conventional supports such as SiO₂, Al₂O₃ and TiO₂ showed lesser activity in the imine formation (Table 2B.1, entries 14-16). These studies show that the special structure of reduced graphene oxide (RGO) may be affected by the reactivity in the environmentally-benign dehydrogenative coupling of alcohols and amines to form imines and H₂

2B.4.2. Substrate scope of alcohols and amine to imine

With an optimized catalytic system in hand (Table 2B.1), we set out to probe its versatility in the direct imine synthesis by ADC strategy of various alcohols and amines. Using (4-

chlorophenyl)methanol **1a** as the benchmark substrate, a number of different anilines were tested using Fe-Phen@C catalyst under standard conditions.

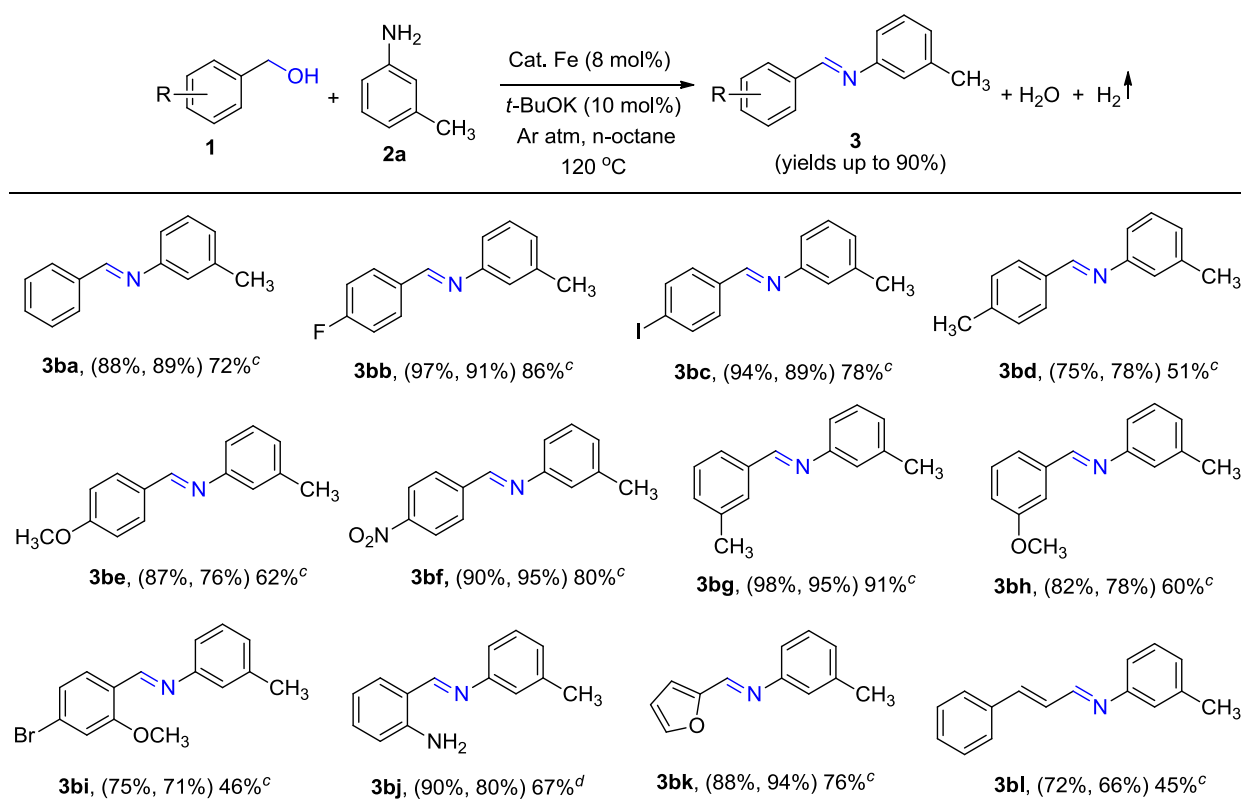
Table 2B.2. Iron-catalyzed direct imine synthesis: Scope of amines.^{a,b}



As shown in Table 2B.2, the present heterogeneous Fe-catalysis is compatible with various anilines containing an electron-rich and electron-deficient substituents, affording the desired

imines in good to excellent yields (up to 95%) under very mild, eco-benign conditions. Interestingly, the reaction proceeded successfully with both cyclic and acyclic secondary amines and gave the desired imines **3an** (81%), **3ao** (74%), **3ap** (73%), and **3aq** (62%) in good yields. It was noteworthy that benzylamine (**2r**) also affording the corresponding imine in moderate yield (40%), along with the formation of (*E*)-*N*-benzyl-1-phenylmethanimine (26% by GC) by dehydrogenative self-coupling of **2r**. The reaction of benzene-1,3-diamine (**2s**) and **1a** selectively gave the corresponding diimine (**3as**) in 75% isolated yield under our catalytic conditions.

Table 2B.3. Iron-catalyzed direct imine synthesis: Scope of alcohols.^{a,b}



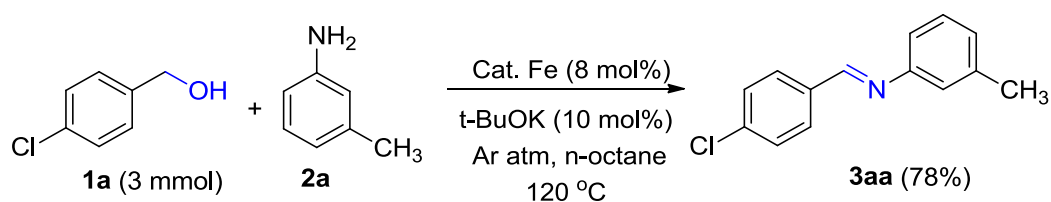
^a Reaction conditions: **1** (0.5 mmol), **2a** (0.55 mmol), cat. Fe-Phen@C (8 mol%), *t*-BuOK (10 mol%), and n-octane (2 mL) heated at 120 °C (oil-bath temperature) for 24 h under open argon atm. ^b Yields are in parentheses are based on the conversion of alcohol and selectivity of **3** respectively and are based on GC using anisole as the internal reference. ^c Isolated yields. ^d Based on ¹H NMR of the crude reaction mixture.

Next, the impact of varying the substituents on the alcohol coupling partner was also assessed (Table 2B.3). The straightforward imine formation reaction proceeded in excellent yields with

either electron donating (4-methyl, 4-methoxy) or electron withdrawing (4-fluoro, 4-nitro) substituents on the benzyl alcohol. Notably, ortho-substituted alcohols yielded the imines (**3bi** and **3bj**) in lower yields, which could be explained by steric effects.²⁵ To our delight, biomass-derived furfuryl alcohol also gave the corresponding imine in good yield (**3bk** in 76% yield). Less reactive cinnamyl alcohol was also tested for the direct imine formation reaction and efficiently gave the corresponding imine in 66% yield. However, 1-hexanol failed to convert into the corresponding aliphatic imine (**3bm**) under optimized conditions.

2B.4.3. Gram-scale synthesis

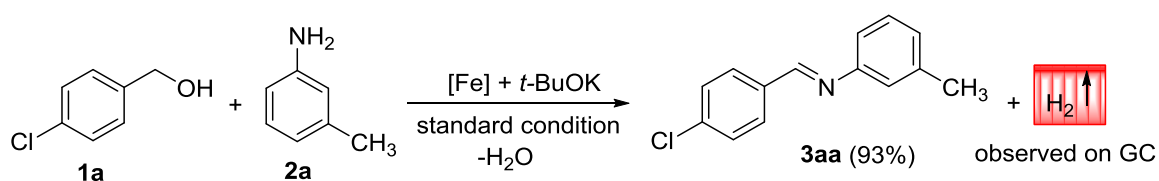
We have successfully shown the scalability and particle viability of this catalytic protocol under standard conditions. In this regard, the present iron-catalyzed direct imine synthesis was tested for the gram-scale synthesis of **3aa**, and it worked excellently with an expected imine in 78% isolated yield after 36 h (Scheme 2B.8). The result implies that the heterogeneous Fe-based catalytic system has a potential in the large-scale production of imines under operationally simple, environmentally benign conditions.



Scheme 2B.1. Gram-scale synthesis of imine (**3aa**).

2B.4.4. Mechanistic Investigation

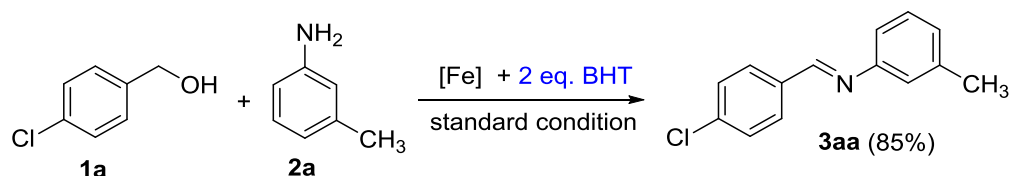
2B.4.4.1. Determination of hydrogen gas formation



To an oven dried 20 mL screw-capped septa vial, Fe-Phen@C catalyst (86 mg, 8 mol%), t-BuOK (11 mg, 10 mol%), (4-chlorophenyl)methanol **1a** (143 mg, 1 mmol), *m*-toluidine **2a** (125 mg, 1.1 mmol), and n-octane (4 mL) were added under argon atmosphere. The vial was heated at

120 °C for 4 h. After cooling to room temperature, the gaseous mixture (formation of hydrogen gas) was qualitatively analyzed by GC-TCD with a Carbon plot capillary column.

2B.4.4.2. Reaction under the presence of radical (O•–2) scavenger



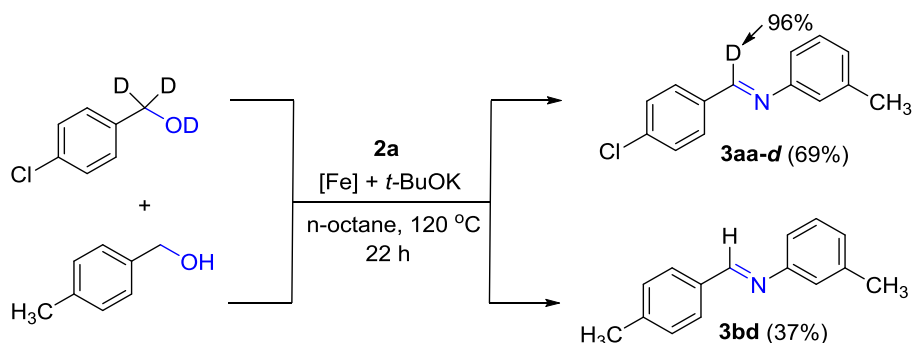
To a 25 mL oven dried schlenk tube, Fe-Phen@C catalyst (43 mg, 8 mol%), t-BuOK (6 mg, 10 mol%), (4-chlorophenyl)methanol (71 mg, 0.5 mmol), *m*-toluidine (62 mg, 0.55 mmol), 2,6-di-tert-butyl-4-methylphenol (BHT) (242 mg, 1.1 mmol), and n-octane (2 mL) were added under argon atmosphere. The schlenk tube was equipped with a reflux condenser and the solution was refluxed under argon atmosphere for 24 h. After cooling to 30 °C the reaction mixture was subjected to centrifugation and the supernatant was collected and the obtained solid was washed with EtOAc (2 x 4 mL) and the washings were collected. The collected reaction mixture was concentrated on rotavapor under reduced pressure. The crude product was purified (deactivated silica gel column chromatography and the eluent is a mixture of petroleum ether and ethyl acetate) and the yield of (*E*)-1-(4-chlorophenyl)-*N*-(*m*-tolyl)methanimine (**3aa**) is 85%.

These experiments (2B.4.4.1 and 2B.4.4.2) reveal that the reaction proceeds only *via* acceptorless dehydrogenation pathway.

2B.4.4.3. Hot filtration test

To a 25 mL oven dried schlenk tube, Fe-Phen@C catalyst (43 mg, 8 mol%), t-BuOK (6 mg, 10 mol%), (4-chlorophenyl)methanol **1a** (71 mg, 0.5 mmol), *m*-toluidine **2a** (62 mg, 0.55 mmol), and n-octane (2 mL) were added under argon atmosphere. The schlenk tube was equipped with a reflux condenser, and the solution was heated at 120 °C (bath temperature) with stirring under open argon flow for 8 h. After cooling to 30 °C the catalyst was separated from the reaction mixture by an external permanent magnet (at this stage the crude reaction mixture was analyzed by GC (67% of **3aa**)). Then, the reaction mixture was transferred into another 25 mL oven dried schlenk tube under an argon atmosphere and was equipped with a reflux condenser, and the solution was heated at 120 °C (bath temperature) with stirring under open argon flow for 24 h.

2B.4.4.6. Deuterium labeling studies



This experiment demonstrates that iron catalyst does not only play a role in the initial dehydrogenation of alcohol and also play a very critical role in initiation due to presence of Lewis acidic sites on the catalyst. However, BET analysis were not performed to to hight weight powdered nature. To a 25 mL oven dried schlenk tube, Fe-Phen@C catalyst (86 mg, 8 mol%), t-BuOK (11 mg, 10 mol%), *p*-tolylmethanol (62 mg, 0.5 mmol), (4-chlorophenyl)methan-d₂-ol-d (73 mg, 0.5 mmol), and *m*-toluidine (138 mg, 1.1 mmol), and n-octane (4 mL) were added under argon atmosphere. The schlenk tube was equipped with a reflux condenser and the solution was refluxed under argon atmosphere for 22 h. After cooling to 30 °C the reaction mixture was subjected to centrifugation and the supernatant was collected and the obtained solid was washed with EtOAc (2 x 4 mL) and the washings were collected. The collected reaction mixture was concentrated under reduced pressure. The crude product was purified, and the yield of (*E*)-1-(4-chlorophenyl)-*N*-(*m*-tolyl)methanimine-*d* and (*E*)-*N*-*m*-tolyl-1-(*p*-tolyl)methanimine are 69% and 37% respectively. This result showed that the initial alcohol dehydrogenation is irreversible.

2B.4.4.7. Kinetic study

Time-dependent experiments on direct imine formation by ADC of alcohols with amines were conducted using heterogeneous iron-catalyst to study the reaction kinetics (Figure 2B.1). Continuous sampling was undertaken with the different time intervals, and the conversion of alcohol (**1a**) and yield of imine (**3aa**) was determined by gas chromatography. Formation of aldehyde intermediate was observed during the reaction pathway, along with the desired imine as the major product.

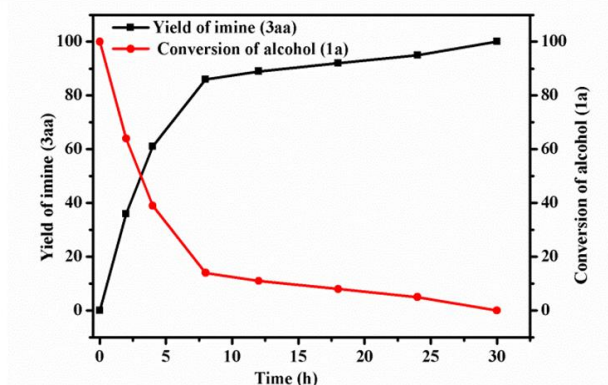


Figure 2B.1. Reaction profile for the iron-catalyzed formation of **3aa**. Reaction conditions: **1a** (0.5 mmol), **2a** (0.55 mmol), cat. Fe-Phen@C (8 mol%), *t*-BuOK (10 mol%), and *n*-octane (2 mL) heated at 120 °C (oil-bath temperature) under open argon atm.

2B.4.4.8. Reusability and Heterogeneity

The significant advantage of heterogeneous catalysts over soluble homogeneous catalysts is its capability for easy separation and recycling. The iron catalyst was easily separated from the reaction medium under the strong magnetic field, as shown in Figure 2B.2a & 2B.2b. The recovered heterogeneous Fe-Phen@C was reused for direct imine synthesis in at least six cycles without a considerable loss in the yield (Figure 2B.2a). The results were within the error limits, and indeed, no deactivation of the catalyst was observed. The hot filtration test was carried out, and it was observed that no further imine formation (**3aa**) took place after the catalyst was filtered off at the conversion of **1a** by 67%. Notably, no imine formation was observed in the reaction under complete homogeneous condition (Table **2B.1**, entries 12-13) and formation of molecular hydrogen was not seen on GC. All these results clearly demonstrate that the present Fe-catalysis is truly heterogeneous in nature.

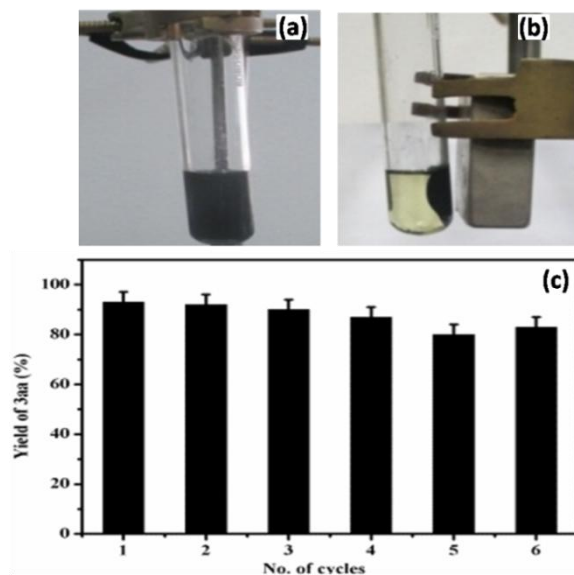
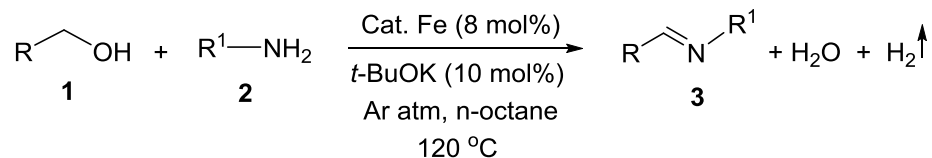


Figure 2B.2. Separation of the catalyst under strong magnetic field **a**: reaction mixture; **b**: under magnetic field). **c**: Recovery and reuse of the Fe-Phen@C catalyst.

2B.5. Experimental section

2B.5.1. General procedure for the iron-catalyzed direct imine formation



To a 25 mL oven dried schlenk tube, Fe-Phen@C catalyst (43 mg, 8 mol%), t-BuOK (10 mol%), alcohol (0.5 mmol), an amine (0.55 mmol), and n-octane (2 mL) were added under argon atmosphere. The schlenk tube was equipped with a reflux condenser, and the solution was heated at 120 °C (bath temperature) with stirring under open argon flow for 24 h. After cooling to 30 °C the catalyst was separated from the reaction mixture by an external permanent magnet and the reaction products were analyzed by GC and GC-MS. The supernatant was transferred into another flask, and the catalyst was washed with EtOAc (2 x 4 mL) and the washings were collected. The solvent was evaporated from the reaction mixture, and the crude product was subjected to deactivated silica gel column chromatography using EtOAc: petroleum ether to afford the imine derivatives.

2B.6. Conclusion

In summary, a more sustainable iron-catalyzed direct imine formation by acceptorless dehydrogenative coupling of alcohols with amines under the oxidant-free condition is reported for the first time. The reaction operates under very mild and environmentally benign conditions with the liberation of dihydrogen and water as the byproducts. The present catalytic approach possesses a dual role; acting as a catalyst as well as can be magnetically separable. The recyclability experiments showed that the catalytic activity for imination can be retained for at least six cycles. The present strategy has great potential for the straightforward synthesis of imines from feedstock chemicals because it tolerates a wide range of substrates with high yields. Mechanistic studies showed the reaction proceeds in a tandem manner (*via* aldehyde formation), and deuterium labeling experiments unambiguously illustrated that the initial alcohol dehydrogenation step is irreversible.

2B.7. References:

1. (a) S. I. Murahashi, *Angew. Chem. Int. Ed. Engl.*, 1995, **34**, 2443-2465; (b) J. P. Adams, *J. Chem. Soc. Perkin Trans. 1* 2000, 125-139; (c) S. Yao, S. Saaby, R. G. Hazell and K. A. Jørgensen, *Chem. -Eur. J.*, 2000, **6**, 2435-2448; (d) S. F. Martin, *Pure Appl. Chem.*, 2009, **81**, 195-204; (e) Z.-Y. Liu, Y.-M. Wang, Z.-R. Li, J.-D. Jiang and D. W. Boykin, *Bioorg. Med. Chem. Lett.* 2009, **19**, 5661-5664.
2. For recent reviews, see (a) R. D. Patil and S. Adimurthy, *Asian J. Org. Chem.*, 2013, **2**, 726-744; (b) R. J. Angelici, *Catal. Sci. Technol.*, 2013, **3**, 279-296; (c) W. Qin, S. Long, M. Panunzio and S. Biondi, *Molecules*, 2013, **18**, 12264-12289.
3. (a) H. Schiff, *Justus Liebigs Ann. Chem.*, 1864, **131**, 118-119; (b) F. Westheimer and K. Taguchi, *J. Org. Chem.*, 1971, **36**, 1570-1572; (c) R. S. Varma, R. Dahiya and S. Kumar, *Tetrahedron Lett.*, 1997, **38**, 2039-2042; (d) G. Liu, D. A. Cogan, T. D. Owens, T. P. Tang and J. A. Ellman, *J. Org. Chem.*, 1999, **64**, 1278-1284; (e) H. Naeimi, F. Salimi and K. Rabiei, *J. Mol. Catal. A: Chem.*, 2006, **260**, 100-104; (f) J. T. Reeves, M. D. Visco, M. A. Marsini, N. Grinberg, C. A. Busacca, A. E. Mattson and C. H. Senanayake, *Org. Lett.*, 2015, **17**, 2442-2445.
4. B. Chen, L. Wang and S. Gao, *ACS Catal.*, 2015, **5**, 5851-5876 and references cited therein.
5. (a) K. Yamaguchi and N. Mizuno, *Angew. Chem. Int. Ed.*, 2003, **42**, 1480-1483; (b) K. Nicolaou, C. J. Mathison and T. Montagnon, *Angew. Chem. Int. Ed.*, 2003, **42**, 4077-4082; (c) K. Nicolaou, C. J. Mathison and T. Montagnon, *J. Am. Chem. Soc.*, 2004, **126**, 5192-5201; (d) B. Zhu and R. J. Angelici, *Chem. Commun.*, 2007, 2157-2159; (e) M. Langeron, A. Chiaroni and M. B. Fleury, *Chem. -Eur. J.*, 2008, **14**, 996-1003; (f) B. Zhu, M. Lazar, B. G. Trewyn and R. J. Angelici, *J. Catal.*, 2008, **260**, 1-6; (g) G. Jiang, J. Chen, J.-S. Huang and C.-M. Che, *Org. Lett.*, 2009, **11**, 4568-4571; (h) L. Aschwanden, B. Panella, P. Rossbach, B. Keller and A. Baiker, *ChemCatChem*, 2009, **1**, 111-115; (i) R. D. Patil and S. Adimurthy, *Adv. Synth. Catal.*, 2011, **353**, 1695-1700; (j) S. Furukawa, Y. Ohno, T. Shishido, K. Teramura and T. Tanaka, *ACS Catal.*, 2011, **1**, 1150-1153; (k) H. Miyamura, M. Morita, T. Inasaki and S. Kobayashi, *Bull. Chem. Soc. Jpn.*, 2011, **84**, 588-599; (l) X. Lang, H. Ji, C. Chen, W. Ma and J. Zhao, *Angew. Chem. Int. Ed.*, 2011, **50**, 3934-3937; (m) H. Yuan, W.-J. Yoo, H. Miyamura and S. Kobayashi, *J. Am. Chem. Soc.*,

- 2012, **134**, 13970-13973; (n) M. Llargeron and M. B. Fleury, *Angew. Chem. Int. Ed.*, 2012, **51**, 5409-5412; (o) L. Liu, Z. Wang, X. Fu and C.-H. Yan, *Org. Lett.*, 2012, **14**, 5692-5695; (p) A. E. Wendlandt and S. S. Stahl, *Org. Lett.*, 2012, **14**, 2850-2853; (q) H. Yuan, W.-J. Yoo, H. Miyamura and S. Kobayashi, *J. Am. Chem. Soc.*, 2012, **134**, 13970-13973; (r) T. Sonobe, K. Oisaki and M. Kanai, *Chem. Sci.*, 2012, **3**, 3249-3255; (s) Z. Hu and F. M. Kerton, *Org. Biomol. Chem.*, 2012, **10**, 1618-1624; (t) L. Al-Hmoud and C. W. Jones, *J. Catal.*, 2013, **301**, 116-124; (u) N. Li, X. Lang, W. Ma, H. Ji, C. Chen and J. Zhao, *Chem. Commun.* 2013, **49**, 5034-5036; (v) K. N. Tayade and M. Mishra, *J. Mol. Catal. A: Chem.* 2014, **382**, 114-125; (w) A. E. Wendlandt and S. S. Stahl, *J. Am. Chem. Soc.*, 2014, **136**, 506-512; (x) A. E. Wendlandt and S. S. Stahl, *J. Am. Chem. Soc.*, 2014, **136**, 11910-11913; (y) B. Chen, L. Wang, W. Dai, S. Shang, Y. Lv and S. Gao, *ACS Catal.*, 2015, **5**, 2788-2794; (z) C. Su, R. Tandiana, J. Balapanuru, W. Tang, K. Pareek, C. T. Nai, T. Hayashi, and K. P. Loh, *J. Am. Chem. Soc.* 2015, **137**, 685-690.
6. For selected reviews, see: (a) S.-I. Murahashi, Y. Okano, H. Sato, T. Nakae and N. Komiya, *Synlett*, 2007, 1675-1678; (b) M. T. Schümperli, C. Hammond and I. Hermans, *ACS Catal.*, 2012, **2**, 1108-1117; (c) M. Llargeron and M. B. Fleury, *Science*, 2013, **339**, 43-44; (d) M. Llargeron, *Eur. J. Org. Chem.* 2013, 5225-5235 and references cited therein.
7. (a) L. Blackburn and R. J. Taylor, *Org. Lett.*, 2001, **3**, 1637-1639; (b) S. Sithambaram, R. Kumar, Y.-C. Son and S. L. Suib, *J. Catal.*, 2008, **253**, 269-277; (c) L. Jiang, L. Jin, H. Tian, X. Yuan, X. Yu and Q. Xu, *Chem. Commun.*, 2011, **47**, 10833-10835; (d) J. Xu, R. Zhuang, L. Bao, G. Tang and Y. Zhao, *Green Chem.*, 2012, **14**, 2384-2387; (e) H. Tian, X. Yu, Q. Li, J. Wang and Q. Xu, *Adv. Synth. Catal.*, 2012, **354**, 2671-2677; (f) Q. Kang and Y. G. Zhang, *Green Chem.*, 2012, **14**, 1016-1019; (g) E. L. Zhang, H. W. Tian, S. D. Xu, X. C. Yu and Q. Xu, *Org. Lett.*, 2013, **15**, 2704-2707; (h) B. Chen, J. Li, W. Dai, L. Wang and S. Gao, *Green Chem.*, 2014, **16**, 3328-3334; (i) L. Han, P. Xing and B. Jiang, *Org. Lett.*, 2014, **16**, 3428-3431; (j) M. Guan, C. Wang, J. Zhang and Y. Zhao, *RSC Adv.* 2014, **4**, 48777-48782; (k) M. Tamura and K. Tomishige, *Angew. Chem. Int. Ed.*, 2015, **54**, 864-867; (l) B. Chen, S. Shang, L. Wang, Y. Zhang and S. Gao, *Chem. Commun.*, 2016, **52**, 481-484.

8. For supported noble-metal heterogeneous catalysts for oxidative dehydrogenation of alcohols with amines using oxygen as the oxidant, see: (a) M. S. Kwon, S. Kim, S. Park, W. Bosco, R. K. Chidrala and J. Park, *J. Org. Chem.*, 2009, **74**, 2877-2879; (b) J. W. Kim, J. He, K. Yamaguchi and N. Mizuno, *Chem. Lett.*, 2009, **38**, 920-921; (c) H. Sun, F. Z. Su, J. Ni, Y. Cao, H. Y. He and K. N. Fan, *Angew. Chem. Int. Ed.*, 2009, **48**, 4390-4393; (d) S. Kegnaes, J. Mielby, U. V. Mentzel, C. H. Christensen and A. Riisager, *Green Chem.*, 2010, **12**, 1437-1441; (e) W. He, L. Wang, C. Sun, K. Wu, S. He, J. Chen, P. Wu and Z. Yu, *Chem. -Eur. J.*, 2011, **17**, 13308-13317; (f) P. Liu, C. Li and E. J. Hensen, *Chem. -Eur. J.*, 2012, **18**, 12122-12129; (g) J.-F. Soulé, H. Miyamura and S. Kobayashi, *Chem. Commun.*, 2013, **49**, 355-357; (h) T. Zhang, L. Zhang, W. Wang, A.-Q. Wang, Y.-T. Cui, X. Yang, Y. Huang, X. Liu, W. Liu and J.-Y. Son, *Green Chem.*, 2013, **15**, 2680-2684.
9. X. Cui, Y. Li, S. Bachmann, M. Scalone, A.-E. Surkus, K. Junge, C. Topf and M. Beller, *J. Am. Chem. Soc.*, 2015, **137**, 10652-10658.
10. For recent review articles on borrowing hydrogen strategy, see: (a) S. Bähn, S. Imm, L. Neubert, M. Zhang, H. Neumann and M. Beller, *ChemCatChem*, 2011, **3**, 1853-1864; (b) C. Gunanathan, D. Milstein, *Science*, 2013, **341**, 1229712; (c) Y. Obora, *ACS Catal.*, 2014, **4**, 3972-3981; (d) J. M. Ketcham, I. Shin, T. P. Montgomery and M. J. Krische, *Angew. Chem. Int. Ed.* 2014, **53**, 9142-9150; (d) Q. Yang, Q. Wang and Z. Yu, *Chem. Soc. Rev.* 2015, **44**, 2305-2329; (e) A. Nandakumar, S. P. Midya, V. G. Landge and E. Balaraman, *Angew. Chem. Int. Ed.*, 2015, **54**, 11022-11034.
11. T. Yan, B. L. Feringa and K. Barta, *Nat. Commun.*, 2014, **5**, 5602-5608.
12. Y. Shiraishi, M. Ikeda, D. Tsukamoto, S. Tanaka and T. Hirai, *Chem. Commun.*, 2011, **47**, 4811-4813.
13. J. Bain, P. Cho and A. V.-Kostal, *Green Chem.*, 2015, **17**, 2271-2280.
14. (a) R. A. Sheldon, *Chem. Soc. Rev.*, 2012, **41**, 1437-1451; (b) I. Delidovich and R. Palkovits, *Green Chem.*, 2016, DOI: 10.1039/c5gc90070k.
15. (a) I. Bauer and H. -J. Knolker, *Chem. Rev.*, 2015, **115**, 3170-3387; (b) C. Darcel, J. -B. Sortais, S. Q. Duque, *RSC Green Chemistry Series* 2015, **26**, 67-92.
16. Selected examples: (a) R. V. Jagadeesh, A.-E. Surkus, H. Junge, M.-M. Pohl, J. Radnik, J. Rabeah, H. Huan, V. Schünemann, A. Brückner and M. Beller, *Science*, 2013, **342**, 1073-1076; (b) F. A. Westerhaus, R. V. Jagadeesh, G. Wienhöfer, M.-M. Pohl, J.

-
-
- Radnik, A.-E. Surkus, J. Rabeah, K. Junge, H. Junge, M. Nielsen, A. Brückner and M. Beller, *Nat Chem*, 2013, **5**, 537-543; (c) F. Chen, A.-E. Surkus, L. He, M.-M. Pohl, J. Radnik, C. Topf, K. Junge and M. Beller, *J. Am. Chem. Soc.*, 2015, **137**, 11718-11724; (d) A. V. Iosub and S. S. Stahl *Org. Lett.*, 2015, **17**, 4404-4407.
17. E. Balaraman, D. Jagadeesan, G. Jaiswal and S. P. Borikar, PCT filled 1494/DEL/2015.
18. X. Cui, Y. Li, S. Bachmann, M. Scalone, A.-E. Surkus, K. Junge, C. Topf and M. Beller, *J. Am. Chem. Soc.*, 2015, **137**, 10652-10658.

Chapter 3

**Cobalt nanocatalyst for the transfer hydrogenation of
alkynes and dehydrogenation reactions**

Part A: Reusable Robust Cobalt-Catalyst for Dehydrogenation of *N*-Heterocycles

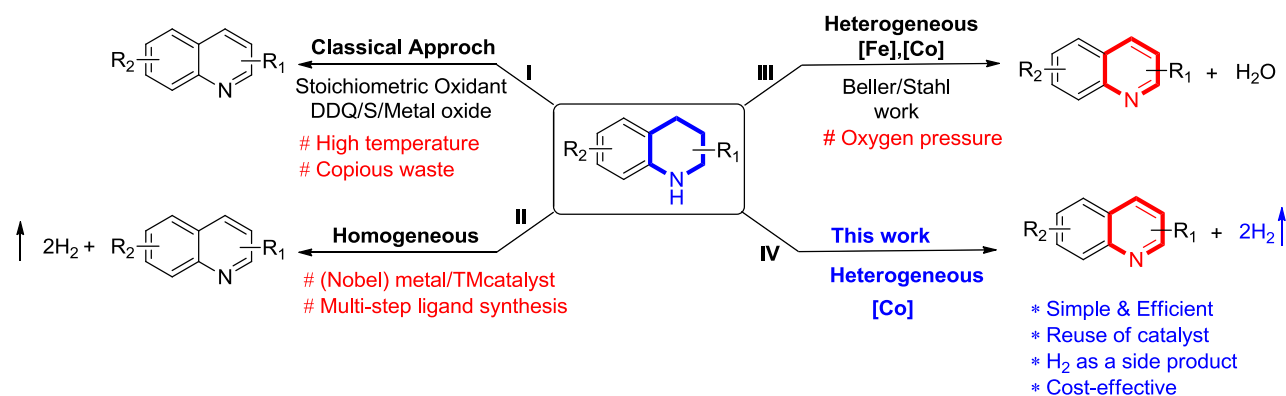
3A.1. Introduction

N-heteroaromatics are extensively used in the synthesis of natural products, bioactive molecules, and pharmaceuticals.¹ Besides, these molecules show profound applications in material science and as LOHCs in fuel cells.² Owing to this, a sustainable catalytic approach for their synthesis is highly demanding. Hence, catalytic dehydrogenation reaction of partially saturated *N*-heterocycles to *N*-aromatics is highly desirable and paid much attention in contemporary science.¹⁻⁴ Conventionally, dehydrogenation reactions were performed using the stoichiometric amount of strong oxidants such as DDQ, peroxides, iodates, chromium (IV) reagents and metal oxides, which often produce excess hazardous waste.⁵ An alternative to one of the toxic oxidants, pressurized air or oxygen were used as green oxidants. Alternatively, catalytic dehydrogenation can also be performed in presence of hydrogen acceptors such as sterically hindered alkenes, and ketones. The overall process is redox neutral and does not involve net hydrogen evolution; however, the byproduct is the stoichiometric amount of sacrificial organic waste.⁸⁻¹⁴ In this context catalytic acceptorless dehydrogenation (ADH) reaction with the liberation of hydrogen gas is the preferred and promising route for many synthetic transformations. The evolved hydrogen; an energy carrier is valuable in itself.¹⁵

Notably, removal of a hydrogen atom from adjacent atomic centers of a saturated organic molecule is extremely challenging and thermodynamically uphill process.¹⁶ Recent DFT calculations and experimental results showed that the presence of nitrogen atom in the cyclic system makes the dehydrogenation process more feasible by lowering the activation energy.¹⁷ Indeed, it is highly demanding to develop an efficient and robust, reusable catalytic system to explore its catalytic performance for the dehydrogenation of *N*-heterocycles.¹⁸⁻²⁰

Significant contributions have been made in transition metal catalyzed ADH reactions by various research groups using well-defined metal complexes under homogeneous conditions.²¹ Alternatively, heterogeneous catalysis could be a better option over

homogeneous catalysis. The significant advantages of heterogeneous catalysis are its capability for easy separation from the reaction mixture and durability of recycling for several runs. However, many heterogeneous catalytic have been well-documented for the oxidative dehydrogenation of *N*-heterocycles using air or oxygen as oxidant.²² Indeed, a robust, reusable catalyst for the ADH reaction of *N*-heterocycles remains an essential goal in chemical research. Very recently, our group reported nano iron-catalyzed ADH reaction of alcohols and amines (chapter 2A).²³ In a continuous effort to discover first-row transition metal catalysts for sustainable catalysis, we have focused our attention on heterogeneous cobalt catalyst.¹³ Notably, a seminal work involved by the research group of Beller and Stahl for the oxidative dehydrogenation of *N*-heterocycles to *N*-aromatics using air/oxygen as sole oxidant. It is Noteworthy that the activity of non-noble metal nanoparticles can be controlled by M:L composition, nature of carbon support, pyrolysis temperature and finally the microstructure of the nanomaterial.^{13, 23, 24} Gratifyingly, the newly synthesized cobalt nanocatalyst has different microstructure as compared to Beller and Stahl's catalysts and superior activity in the ADH of *N*-heterocycles to *N*-heteroarenes. Thus, herein the first cobalt based heterogeneous catalyzed acceptorless dehydrogenation of partially saturated *N*-heterocycles to *N*-aromatics with the liberation of H₂ gas is reported. The present nano-catalyst performs excellently with six-run recycling test.



Scheme 3A.1. Overview of the present work.

3A.2. Statement of the Problem

The various research group has made significant contributions in ADH reactions using well-defined noble metal-based complexes under homogeneous conditions. There are limited reports

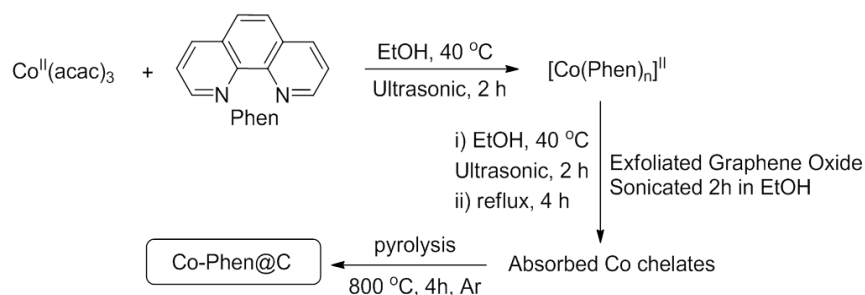
based on first-row transition metal. With respect to homogeneous catalysis main concern is multistep synthesized ligands and difficult to reuse the soluble catalyst. Alternatively, heterogeneous catalysis could be a better option over homogeneous catalysis. However, mostly heterogeneous catalytic have been well-documented for the oxidative dehydrogenation of *N*-heterocycles using air or oxygen as oxidant. Indeed, there is an urgent need of a robust, reusable catalyst for the ADH reaction of *N*-heterocycles in chemical research.

3A.3. Catalyst Synthesis and Characterization

3A.3.1. Synthesis of Co-Phen@C

The active heterogeneous cobalt catalyst for ADH of **1a** was synthesized by our previously reported pyrolysis technique.²³ In a 100 mL beaker Co(II) acetylacetonate precursor (0.5 mmol) and 1,10-phenanthroline ligand (0.5 mmol) were dissolved in 30 mL of ethanol and sonicated for 2 h to form Co-Phenanthroline complex. In another 250 mL, beaker 560 mg of EGO support was taken in 70 mL of ethanol and sonicated for 2 h. The above-obtained EGO suspension and Co-phenanthroline complex solution were mixed together in 250 mL beaker and further sonicated for 2 h. The suspension was refluxed at 85°C for 4 h and after cooling down to room temperature ethanol was evaporated in vacuum. The solid sample obtained was dried at 80 °C for 14 h. Then, it was ground to a fine powder followed by calcination at 800 °C under a stream of argon with the flow rate of 30 mL/min and the heating rate: 25 °C/min for about 4 h to obtain a catalyst Co-Phen@C.

For the synthesis of other conventional based supports (SiO₂, TiO₂, Al₂O₃) synthesis of CoNSiO₂, CoNTiO₂ and CoNAl₂O₃ catalysts were done using 560 mg of the respective support. Other steps in the synthesis were identical as per explained in the synthesis of Co-Phen@C.



Scheme 3A.2. Synthesis procedure of Co-Phen@C catalyst.

3A.3.2. Catalyst Characterization

The Co-Phen@C catalytic material has been characterized thoroughly using PXRD, TEM, SEM, XPS, ICP and Raman spectroscopy analysis.

3A.3.2.1. Powder X-ray Diffraction

The catalyst Co-Phen@C was comprehensively characterized using several tools including XRD, TEM, XPS, ICP-AES, Raman spectroscopy, HRTEM and elemental mapping. In powder X-ray diffraction (PXRD) pattern a broad peak at $2\theta = 26.5$ degree confirm the presence of carbon. The PXRD data displays that Co-Phen@C catalyst contains Co_3C , Co_2N , Co_3O_4 and Co phases (Figure 3A.1). The sharp peak at 31.4 and 36.6, 56.1 degree fits to Co_3O_4 (JCPDS no 80-1541), peaks at 44.2, 51.5, 74.7 degree belongs to metallic cobalt (JCPDS no 15-0806). Also the peaks at 45.1, 56.1, 75.8 degree fits to Co_3C (JCPDS no-26-0450), 34.0 degree assigned to CoO (JCPDS no 75-0419), and a peak at 42.5 degree belongs to Co_2N (JCPDS no 72-1368). Notably, the PXRD peaks of Co_3C were slightly shifted to the higher angle which can be ascribed to lattice shrinkage and comparable to literature.¹² In the active catalyst, Co_3C and Co_2N phases were present which is in accordance with the incorporation of N and C rich ligand in the catalytic system and decomposes in the proximity of metal atoms that aggregate to form cobalt carbide and cobalt nitride nanoparticles.

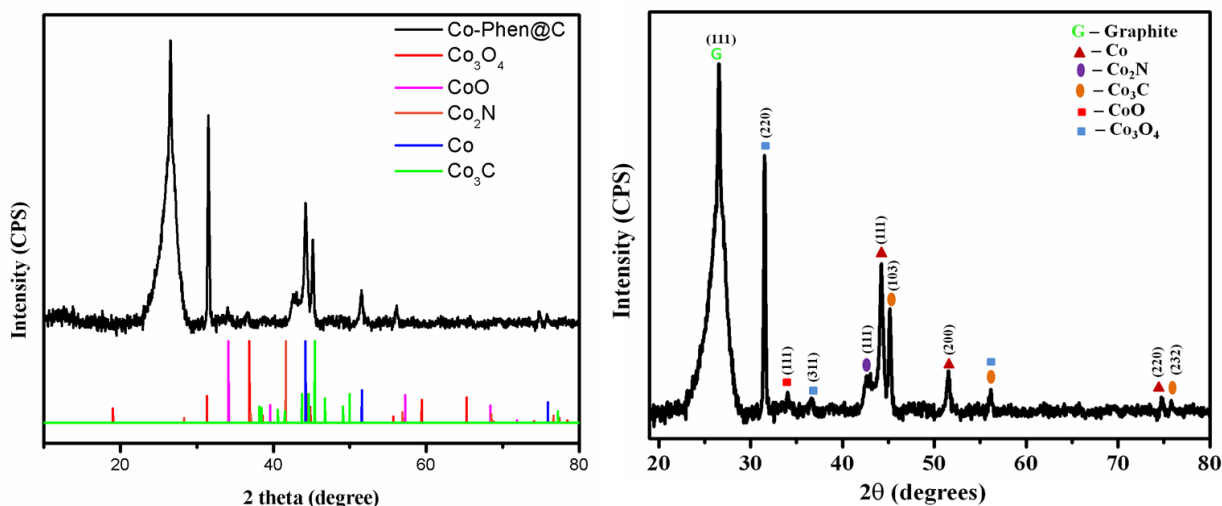


Figure 3A.1. PXRD spectra of Co-Phen@C material with indices of peaks pattern of Co, Co_2N , Co_3C , Co_3O_4 , CoO, and graphite.

3A.3.2.2. SEM and TEM images

The microstructure and EDAX pattern of Co-Phen@C catalyst was analyzed using transmission electron microscopy (TEM). The TEM images (Figure 3A.2a, 3A.2.b.) of the Co-Phen@C catalyst shows that cobalt nanoparticles were supported and distributed throughout the graphene sheets and having a size in the range of 10-50 nm. Nonetheless, the majority of the nanoparticles were in the range of 20-30 nm as shown in the histogram.

The SEM, TEM, and HRTEM clearly support that most of the nanoparticles were spherical and well distributed on graphene (Figure 3A.2).

In the HRTEM image (Figure 3A.2.c), lattice distance of 2.10 Å corresponds to the (111) crystal plane of Co_2N , 4.68 Å corresponds to 111 plane of Co_3O_4 . However, this phase is not seen in PXRD due to low-intensity. The lattice distance of 2.04 Å corresponds to the d spacing of (111) plane of metallic cobalt phase, and 2.82 Å corresponds to the d spacing of (220) plane of Co_3O_4 . The HRTEM image clarifies that center of the nanoparticles mainly consists of metallic cobalt and cobalt nitride while at the ambient conditions the surface of the nanoparticles got oxidized to cobalt oxides.

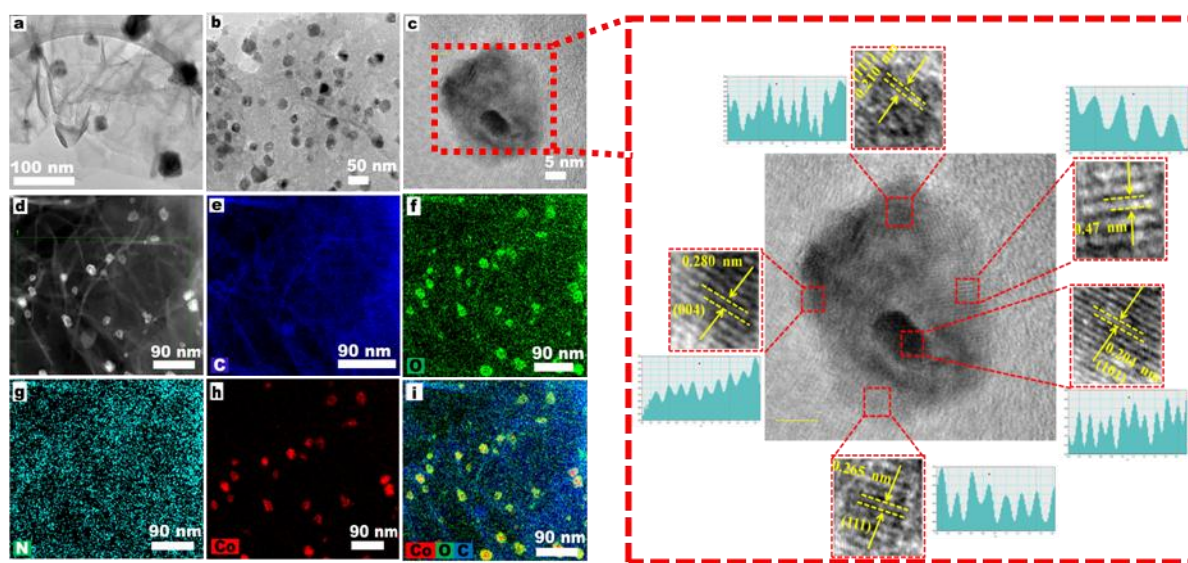


Figure 3A.2. TEM image of Co-Phen@C catalyst (a-b) and elemental mapping showing C, O, N, Co and C, N, Co, and O together (d to i) elemental mapping. HRTEM image of Co-Phen@C catalyst (c) (red marked image).

Furthermore, high-angle annular dark-field scanning transmission electron microscopy (HAADF-STEM) mode supports the distribution of Co nanoparticles across the graphene (Figure 3A.2.d-i). To verify the crystalline nature of the nanoparticles the selected area electron diffraction (SAED) patterns were obtained for the Co-Phen@C catalyst (Figure 3A.3). The ring-like diffraction pattern in SAED image indicates that the particles are partially crystalline. The bright ring arises due to reflection from (111) plane of Co_2N and (232) plane of Co_3C which are supported by the PXRD results.

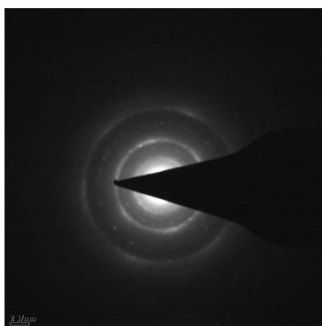


Figure 3A.3. SAED patterns Co-Phen@C catalyst.

3A.3.2.3. XPS analysis

Furthermore, XPS characterizations were conducted to analyze the elemental composition as well as the valence states of the Co-Phen@C catalyst. The survey spectra of the catalyst shows, carbon (94.7%), nitrogen (1.2%), oxygen (3.8%) and cobalt (0.4%). The high resolution XPS spectra of catalyst in C1s region can be deconvoluted in four peaks constituents with binding energy 284.7, 285.9, 286.9 and 287.7 eV corresponding to C-C sp^2 , C-C sp^3 , C-O, and C=O type of carbons with individual atomic % of 84.61, 11.70, 2.89 and 0.80, showing the graphitic nature of carbon material (Figure 3A.4.a).¹⁹ The appearance of specific N1s peak component at 399.6 and 402.6 eV confirms the existence of pyrrolic N, and graphitic N in the catalyst (Figure 3A.4.b).

The deconvoluted O1s spectrum in (Figure 3A.6 c) shows three photoelectron peaks fitted at 530.4, 531.9 and 533.6 eV with an atomic concentration of 15.57%, 28.46%, and 55.98% were attributed to oxygen in hydroxide ions and the oxygen of surface-adsorbed anion correspondingly.²⁰ The two peaks Co 2p_{3/2} and Co 2p_{1/2} positioned at 780.63 and 795.98 eV in the Co 2p spectrum in (Figure 3A.4.d) are attended by two projecting shake-

up satellite peaks (786.2 and 800.3 eV) which noticeably validate the presence of the CoO phase.

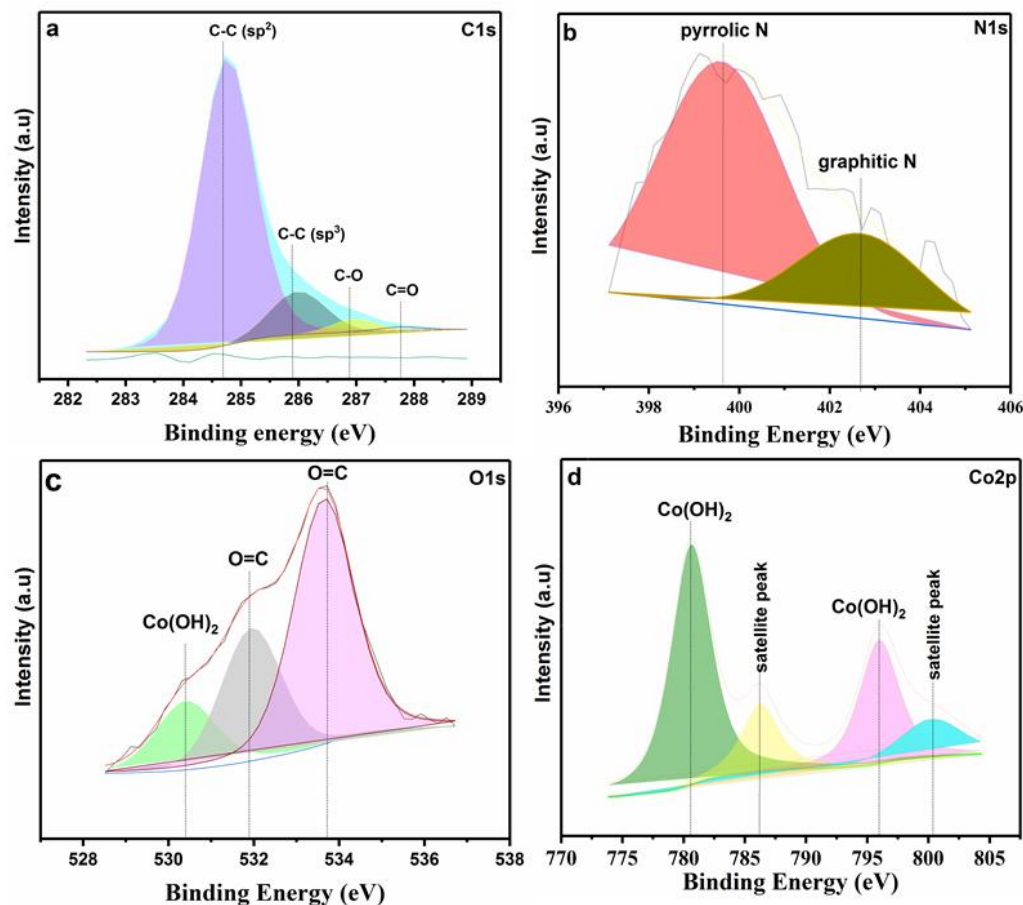


Figure 3A.4. High-resolution XPS spectra of Co-Phen@C catalyst (a) C1s, (b) N1s, (c) O1s, and (d) Co2p region.

3A.3.2.4. EDX analysis

The presence of Co and N was further confirmed by the Energy-Dispersive X-ray spectroscopy (EDAX) spectrum Figure 3A.5 taken in the area shown in Figure 3A.2a of the TEM image, and determined to be 4.57 % Co, 4.79 % N, 3.25 % O, and 86.5 % C. The content was also determined by CHN analysis and revealed an atomic ratio of C, H, N, are 76.3%, 1.2%, and 1.46%, respectively and well matches with the EDAX analysis. To determine the cobalt content of Co-Phen@C, inductively coupled plasma optical emission spectrometry (ICP-AES) was performed and found to be 4.3 wt%.

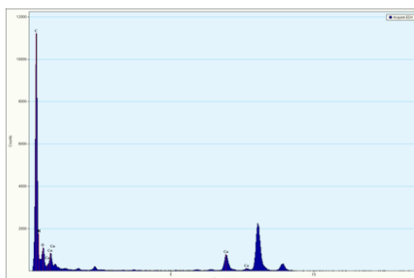


Figure 3A.5. EDX analysis of Co-Phen@C catalyst.

Table 3A.1 showing the weight percent of different elements in the Co-Phen@C

Element	Weight %	Atomic %	Uncert. %	Correction	k-Factor
C(K)	86.52	91.41	0.41	0.26	3.940
N(K)	4.79	4.34	0.12	0.26	3.826
O(K)	4.10	3.25	0.07	0.49	1.974
Co(K)	4.57	0.98	0.05	0.99	1.403

3A.3.2.5. Raman analysis

Raman spectrum of Co-Phen@C Figure 3A.6 clearly shows the D and G bands at 1328 cm^{-1} , 1594 cm^{-1} , respectively. The first characteristic D band is due to vibration mode of A_{1g} symmetry of the sp^2 carbon of graphite lattice, and G band appears due to the first-order scattering of the E_{2g} observed for sp^2 carbon domains. The G band represents the highly ordered graphite carbon materials. The I_D/I_G was found to be 1.12 which shows an increase in the disorderliness of graphene due to deposition of cobalt nanoparticles in Co-Phen@C.

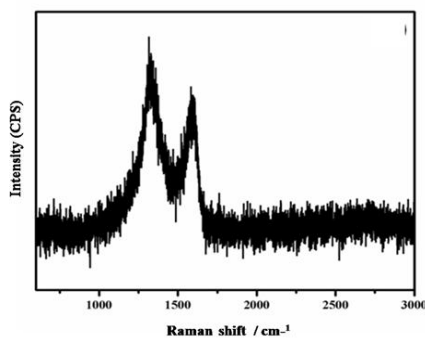


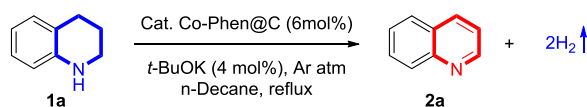
Figure 3A.6 Raman spectra of Co-Phen@C

3A.4. Result and Discussion

3A.4.1. Optimization table

After complete characterization of Co-Phen@C, we have investigated the catalytic activity for ADH reaction and *N*-heterocycles. We have chosen 1,2,3,4-tetrahydroquinoline (**1a**) as the model substrate for the ADH reaction and studied the effect of each component (catalysts, solvents, and bases) to find the optimal conditions (Table 3A.2). After careful screening, we found that substrate **1a** in presence of catalytic amount of Co-Phen@C, and the catalytic amount of *t*-BuOK under argon atm gave the dehydrogenated product **2a** in 93% isolated yield (Table 3A.2, entry 1).

Table 3A.2. Optimization of the reaction conditions^a



Entry	Catalyst	Variation from the initial conditions	Conversion of 1a (%) ^b	Yield of 2a (%) ^b
1	Co-Phen@C	none	99	97 (93) ^c
2	Co-Phen@C	closed system	48	41 ^c
3	Co-Phen@C	without <i>t</i> -BuOK	60	52
4	Co-Phen@C	K ₂ CO ₃ instead of <i>t</i> -BuOK	42	37
5	Co-Phen@C	KOH instead of <i>t</i> -BuOK	24	15
6	Co-Phen@C	CH ₃ CN instead of n-decane	30	22
7	Co-Phen@C	toluene instead of n-decane	60	50
8	Co-Phen@C	at 80 °C	38	32
9	---	without Co-Phen@C	3	0
10	Co(acac) ₃ /Phen	under homogeneous condition	8	trace ^d
11	Co-Phen@SiO ₂	none	36	22
12	Co-Phen@Al ₂ O ₃	none	26	20
13	Co-Phen@TiO ₂	none	32	27
14	Co-Bipy@C	none	65	58 (49) ^c
15	Co-Py@C	none	55	51
16	Co@C	none	62	52 (40) ^c
17	Phen@C	none	8	4
18	Co@vul (Beller catalyst)	none	25	21
19	Stahl catalyst	none	18	15

^aReaction conditions: **1a** (0.50 mmol), cat. Co-Phen@C (6 mol%), *t*-BuOK (4 mol%) and n-decane (2 mL) heated at reflux for 36 h under open argon atm. ^bYields of **2a** and the conversion of **1a** are based on GC using *m*-xylene as an internal standard. ^cYields are in parentheses are based on the isolated yields. ^dReaction under homogeneous condition using *in-situ* generated Co-catalyst by reacting 1:1 mixture of Co-salt and 1,10-phenanthroline (Phen) followed by treatment with *t*-BuOK (4 mol%).

Notably, the generation of hydrogen gas was qualitative analysis on GC analysis. Under similar catalytic conditions in a closed system, a poor yield of **2a** (41% yield) was obtained and the result suggests the necessity of removal of hydrogen gas from the catalytic system (Table 3A.2, entry 2). The base *t*-BuOK was found to be the optimal base for this catalytic transformation. Thus, the reaction in absence of *t*-BuOK or with other bases such as K₂CO₃ or KOH resulted in a moderate yield of **2a**. We firmly believe that the strong base *t*-BuOK accelerates the substrate binding to the catalyst surface by activating the N-H bond.

Notably, control experiments indicated that there is no involvement of radical type mechanism (Table 3A.1, entries 3-5). However, previously reported Beller and Stahl's work to follow radical mechanism. From a variety of solvents screened, *n*-decane was found to be optimal for this ADH reaction (Table 3A.1, entries 1, 6-7). At lower reaction temperature, the product yield decreased drastically; hence, the temperature at reflux is essential for this transformation (Table 3A.1, entry 8). When the reaction was carried out in absence of Co-Phen@C there is no formation of **2a** was observed (Table 3A.1, entry 9). Gratifyingly, heterogeneous Co-catalytic systems, including Beller and Stahl's catalysts gave unsatisfactory results under our optimized conditions (Table 3A.1, entries 9-19). These experiments show the robustness of the present catalytic system for the ADH reaction of **1a**.

Table 3A.3. Showing the conversion of 1,2,3,4- tetrahydroquinoline and selectivity of quinoline products using different Co based catalysts in pure phases.

Entry	Catalyst (8 mol%)	Conversion (%)	Selectivity (%)
1	Co-Phen@C	98	96
2	Co ₃ O ₄	13	73
3	CoO	8	60
4	Co _x N	5	80
5	Co _x C	6	75

3A.4.2. Substrate scope of *N*-heterocycles

With the optimized reaction conditions in hand, next we have investigated the scope of various partially saturated *N*-heterocycles (Table 3A.4). Various tetrahydroquinolines with electron-rich and electron-deficient substituents afforded the corresponding dehydrogenated products in good to excellent yields under optimized conditions.

Table 3A.4. Cobalt-catalyzed direct quinoline synthesis *via* ADH: Scope of tetrahydroquinolines.^a

Reaction scheme: **1a-k** (tetrahydroquinoline with substituents R and R₁) $\xrightarrow[\text{t-BuOK (4 mol\%), Ar atm, n-decane, reflux}]{\text{Cat. Co-Phen@C}}$ **2a-k** (quinoline with substituents R and R₁)

Entry	Product	Conversion (%) ^b	Yield (%) ^c	Entry	Product	Conversion (%) ^b	Yield (%) ^c
1		100	96	7		85	78
2		99	94	8		100	95
3		95	91	9		100	80
4		100	97	10		58	54
5		96	92	11		64	57
6		100	98				

^aReaction conditions: **1a-k** (0.50 mmol), cat. Co-Phen@C (6 mol%), t-BuOK (4 mol%), and n-decane (2 mL) heated at reflux for 36 h under open argon atm. ^bBased on GC. ^cIsolated yields of two independent experiments.

Under standard conditions, the substituted THQ **1a** afforded the dehydrogenated product **2a** in 93% isolated yield (Table 3A.1, entry 1) and THQs with electron-donating groups such as -Me, -OMe gave the desired products **2b-2e** in excellent yields of up to 97% (Table 3A.2, entries 2-5). Notably, the substrate **1f** with a phenolic group (Ar-OH) underwent ADH reaction smoothly and gave the expected product **2f** in 98% of isolated yield (Table 3A.4, entry 6). Similarly, substrates such as 6-FTHQ, 6-BrTHQ, and 7-NO₂THQ having electron-deficient groups were well tolerated and smoothly underwent the dehydrogenation to offer the *N*-aromatics in excellent yields (up to 95%) with the liberation of H₂ gas (Table 3A.4, entries 7-9).

However, the 2-aryl substituted THQ derivatives **1j** and **1k** gave moderate yields under optimized conditions due to a weak *N*-adsorption of the sterically hindered substrate on the catalyst surface (Table 3A.4, entries 10-11). The present catalytic system is superior to the iron-based catalytic system.

Table 3A.5. Cobalt-catalyzed indole synthesis *via* ADH: Scope of indolines.^a

Entry	Product	Conversion (%) ^b	Yield (%) ^c	Entry	Product	Conversion (%) ^b	Yield (%) ^c
1		100	98	5		93	88
2		94	90	6		100	96
3		97	93	7		100	98
4		97	92				

^aReaction conditions: **3a-g** (0.50 mmol), cat. Co-Phen@C (6mol%), t-BuOK (4mol%), and n-decane (2 mL) heated at reflux for 24 h under open argon atm. ^bBased on GC. ^cIsolated yields.

Next, the scope of the ADH strategy was successfully applied for the direct synthesis of indole derivatives (Table 3A.3), a class of highly important pharmaceutically and biologically active

motif. It was found that the electronic nature of the substrates has no significant effect on the ADH reaction under our cobalt catalyzed conditions. The unsubstituted indoline **3a** and dihydroazaindole **3b** gave an excellent yield of the corresponding dehydrogenated products **4a** and **4b** in 98% and 90%, respectively (Table 3A.3 entries 1-2). The electron-rich indolines with -Me or -OMe gave the desired products **4c** in 93% and **4d** in 92% yields (Table 3A.3 entries 3-4). The substrate **3e** with an electron-deficient ester group gave **4e** in 88% isolated yield (Table 3A.3 entry 5). Notably, substrates with sensitive functional groups such as **3f** with an acid group and **3g** with -Br underwent ADH reaction smoothly and gave the expected products in very good yields (Table 3A.3 entries 6-7).

Table 3A.6. Cobalt-catalyzed ADH reaction: Scope of other *N*-heterocycles^a

Reaction scheme: $1a-k \xrightarrow[\text{t-BuOK (4 mol\%), Ar atm, n-decane, reflux}]{\text{Cat. Co-Phen@C}} 2a-k$

Entry	Product	Conversion (%) ^b	Yield (%) ^c	Entry	Product	Conversion (%) ^b	Yield (%) ^c
1		100	96	7		85	78
2		99	94	8		100	95
3		95	91	9		100	80
4		100	97	10		58	54
5		96	92	11		64	57
6		100	98				

^aReaction conditions: **5a-h** (0.50 mmol), cat. Co-Phen@C (6mol%), t-BuOK (4mol%), and n-decane (2 mL) heated at reflux for 24 h under open argon atm. ^bBased on GC. ^cIsolated yields.

Inspired by the excellent results obtained for THQs and indolines, the present heterogeneous Co-catalyzed ADH protocol was successfully applied for the synthesis of other *N*-heteroaromatics such as isoquinoline **6a**, anthracene **6b**, benzo[h]quinoline **6c** and good to excellent yields were obtained under the optimal conditions (Table 4 entries 1-3). Interestingly, the sterically hindered 2-aryl substituted tetrahydroquinoxalines **5d** also underwent ADH reaction under standard conditions and gave the dehydrogenated product in excellent isolated yields (products **6e** in 96%, **6f** in 91% and **6g** in 94% yields). Interestingly, 2-alkyl substituted tetrahydro-quinazolines **5h** with a hexyl group at second position underwent catalytic dehydrogenation smoothly and gave **6h** in 96% yield.

3A.4.3. Mechanistic Investigation

3A.4.3.1. Determination of hydrogen gas formation

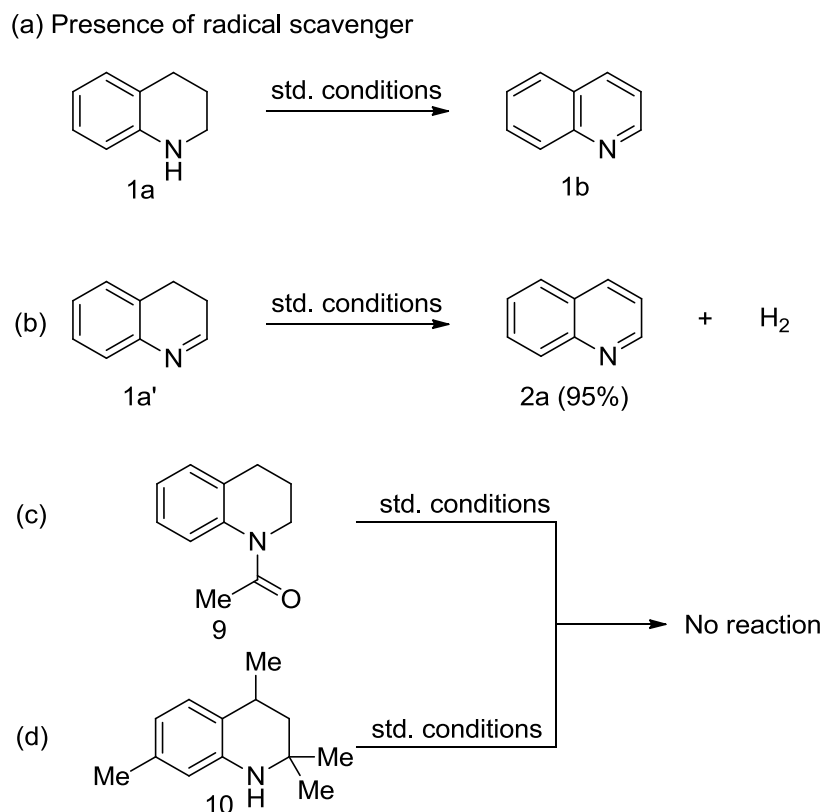
The hydrogen gas was quantified by using the dual catalysis ana volumetric water displacement technique (see chapter 2A).

3A.4.3.2. Reaction under the presence of radical ($O\cdot^{-2}$) scavenger

To get insight into the mechanism, several control experiments were carried out. The presence of radical scavengers does not affect the reactivity of catalyst, and the dehydrogenated product **2a** was isolated in 86% yield. This result ruled out a possibility of the radical mechanism. In addition, a partially dehydrogenated product **1a'** subjected to standard conditions to lead to **2a** in 95% isolated yield. This result indicates that the ADH reaction proceeds *via* the intermediate **1a'** which further undergoes intermediate reaction and lead to partially hydrogenated NH intermediate and subsequent dehydrogenation to give **2a**. When *N*-protected substrate **9** and substrate **10** without N-H and an α -H, respectively subjected to optimized reaction conditions, no dehydrogenated product was formed. These experiments suggest that a proton on N-atom and the α -H of the C-2 position of the cyclic system are crucial for this reaction.

Based on the above results we propose that the amine **1a** will bind to the cobalt surface through nitrogen center. This substrate binding is accelerated by *t*-BuOK. Then, the substrate **1a** undergoes dehydrogenation reaction to give the intermediate **1a'** with the

liberation of one mole of hydrogen. The intermediate **1a'** may undergo isomerization to provide intermediate **1a''**, and subsequent dehydrogenation process will lead to the complete dehydrogenated product **2a**. The formation of H₂ gas in the Co-Phen@C catalyzed the direct synthesis of quinoline was qualitatively observed in gas chromatography and also quantified.



Scheme 3A.3 Control experiments.

3A.4.3.3. Recyclability of the catalyst

The Co-Phen@C catalyst was easily separated from the reaction medium and reused at least for five cycles without a considerable loss in its activity (Figure 3A.7). This suggests that the catalyst is highly robust and does not undergo deactivation during catalysis.

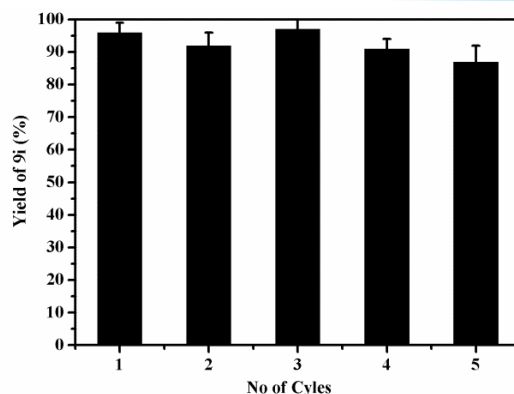
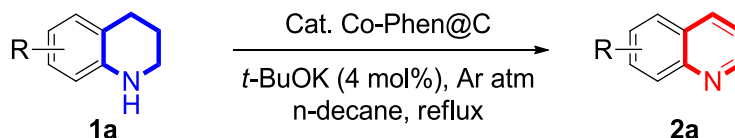


Figure 3A.7 Recyclability of the Co-Phen@C catalyst.

3A.5. Experimental section

3A.5.1. General procedure for the acceptorless dehydrogenation of *N*-heterocycles



To an oven dried schlenk tube (25 mL), Cat. Co-Phen@C catalyst (28 mg, 6 mol%), *t*-BuOK (4 mol%), *N*-heterocycles (0.5 mmol), *n*-decane (2 mL) were added under argon atmosphere. The solution was refluxed with stirring under open argon flow for 24-36 h. After cooling down the reaction mixture to room temperature the catalyst was separated from the reaction mixture by centrifugation and the reaction mixture was analyzed by GC and GC-MS. The supernatant was transferred to another flask, and the catalyst was washed with EtOAc (2 x 4 mL) and the washings were collected. The solvent was evaporated from the reaction mixture, and the crude product was subjected to silica gel column chromatography using EtOAc: petroleum ether to afford the product.

3A.6 Conclusion

In summary, we have developed highly efficient, robust and reusable cobalt based nanocatalyst for catalytic dehydrogenation of various *N*-heterocycles for the first time. Interestingly compared to previously known heterogeneous catalysts, the present catalytic material has a different microstructure and operates under ADH conditions with the liberation of hydrogen gas. The synthetic utility of this reaction is demonstrated explicitly to pharmaceutically relevant molecules.

3A.7. References:

1. C. Gunanathan and D. Milstein, *Science*, 2013, **341**.
2. M. Yadav and Q. Xu, *Energy & Environmental Science*, 2012, **5**, 9698-9725.
3. L. Que Jr and W. B. Tolman, *Nature*, 2008, **455**, 333.
4. G. E. Dobereiner and R. H. Crabtree, *Chemical Reviews*, 2010, **110**, 681-703.
5. (a) P. P. Fu and R. G. Harvey, *Chemical Reviews*, 1978, **78**, 317-361. (b) L. Que Jr and W. B. Tolman, *Nature*, 2008, **455**, 333.
6. H. Yuan, W.-J. Yoo, H. Miyamura and S. Kobayashi, *Journal of the American Chemical Society*, 2012, **134**, 13970-13973.
7. K. Yamaguchi and N. Mizuno, *Angewandte Chemie International Edition*, 2003, **42**, 1480-1483.
8. D. Ge, L. Hu, J. Wang, X. Li, F. Qi, J. Lu, X. Cao and H. Gu, *ChemCatChem*, 2013, **5**, 2183-2186.
9. S. Furukawa, A. Suga and T. Komatsu, *Chem. Commun.* 2014, **50**, 3277-3280.
10. X. Cui, Y. Li, S. Bachmann, M. Scalone, A.-E. Surkus, K. Junge, C. Topf and M. Beller, *J. Am. Chem. Soc.*, 2015, **137**, 10652-10658.
11. (a) A. V. Iosub and S. S. Stahl, *Org. Lett.*, **17**, 4404-4407; (b) F. A. Westerhaus, R. V. Jagadeesh, G. Wienhöfer, M.-M. Pohl, J. r. Radnik, A.-E. Surkus, J. Rabeah, K. Junge, H. Junge, M. Nielsen, A. Brückner and M. Beller, *Nat. Chem.*, 2013, **5**, 537. (b) F. A. Westerhaus, R. V. Jagadeesh, G. Wienhöfer, M.-M. Pohl, J. r. Radnik, A.-E. Surkus, J. Rabeah, K. Junge, H. Junge, M. Nielsen, A. Brückner and M. Beller, *Nat. Chem.*, 2013, **5**, 537.
12. F. Chen, A.-E. Surkus, L. He, M.-M. Pohl, J. r. Radnik, C. Topf, K. Junge and M. Beller, *J. Am. Chem. Soc.*, **137**, 11718-11724.
13. hydrogen energy carrier source
14. (a) A. J. A. Watson and J. M. J. Williams, *Science*, 2010, **329**, 635-636; (b) C. Gunanathan and D. Milstein, *Science*, 2013, **341**; (c) M. Trincado, D. Banerjee and H. Grutzmacher, *Energy Environ. Sci.*, 2014, **7**, 2464-2503. (d) Yadav, M.; Xu, Q., Liquid-phase chemical hydrogen storage materials. *Energy & Environmental Science* **2012**, **5**, (12), 9698-9725; (d) Yadav, M.; Xu, Q., Liquid-phase chemical hydrogen storage materials. *Energy Environ. Sci.*

- 2012**, 5, (12), 9698-9725; (e) Bonitatibus, P. J. Jr. et al. Reversible catalytic dehydrogenation of alcohols for energy storage. *Proc. Natl Acad. Sci. USA* 112, 1687–1692 (2015).
15. (a) Clot, E.; Eisenstein, O.; Crabtree, R. H., Computational structure-activity relationships in H₂ storage: how placement of N atoms affects release temperatures in organic liquid storage materials. *Chem. Commun.* **2007**, (22), 2231-2233; (b) Pez, G. P.; Scott, A. R.; Cooper, A. C.; Cheng, H.; Bagzis, L. D.; Appleby, J. B. WO Appl. Pat. WO 2005/000457 A2, 2005; (c) Pez, G. P.; Scott, A. R.; Cooper, A. C.; Cheng, H. U.S. Patent 7,101,530, 2006; (d) D. E. Schwarz, T. M. Cameron, P. J. Hay, B. L. Scott, W. Tumas and D. L. Thorn, *Chem. Commun.*, 2005, 5919-5921. (e) A. Moores, M. Poyatos, Y. Luo and R. H. Crabtree, *New J. Chem.*, 2006, **30**, 1675-1678; (f) Clot, E.; Eisenstein, O.; Crabtree, R. H., Computational structure-activity relationships in H₂ storage: how placement of N atoms affects release temperatures in organic liquid storage materials. *Chem. Commun.* **2007**, (22), 2231-2233. (g) Y. Cui, S. Kwok, A. Bucholtz, B. Davis, R. A. Whitney and P. G. Jessop, *New J. Chem.*, 2008, **32**, 1027-1037.
16. R. H. Crabtree, *Energy Environ. Sci.*, 2008, **1**, 134-138.
17. P. Jessop, *Nat. Chem.*, 2009, **1**, 350.
18. L. Schlapbach and A. Züttel, *Nature*, 2001, **414**, 353.
19. (a) R. Yamaguchi, C. Ikeda, Y. Takahashi and K.-i. Fujita, *J. Am. Chem. Soc.*, 2009, **131**, 8410-8412; (b) J. Wu, D. Talwar, S. Johnston, M. Yan and J. Xiao, *Angew. Chem. Int. Ed.*, 2013, **52**, 6983-6987; *Angew. Chem.* 2013, 125, 7121–7125; (c) K.-i. Fujita, Y. Tanaka, M. Kobayashi and R. Yamaguchi, *J. Am. Chem. Soc.*, 2014, **136**, 4829-4832; (d) S. Chakraborty, W. W. Brennessel and W. D. Jones, *Journal of the American Chemical Society*, 2014, **136**, 8564-8567; (e) R. Xu, S. Chakraborty, H. Yuan and W. D. Jones, *ACS Catalysis*, 2015, **5**, 6350-6354; (f) M. Kojima and M. Kanai, *Angewandte Chemie*, 2016, **128**, 12412-12415; (g) K. H. He, F. F. Tan, C. Z. Zhou, G. J. Zhou, X. L. Yang and Y. Li, *Angewandte Chemie International Edition*, 2017, **56**, 3080-3084.
20. (a) H. Yuan, W.-J. Yoo, H. Miyamura and S. Kobayashi, *Journal of the American Chemical Society*, 2012, **134**, 13970-13973; (b) K. Yamaguchi and N. Mizuno, *Angewandte Chemie International Edition*, 2003, **42**, 1480-1483; (c) F. Li, J. Chen, Q. Zhang and Y. Wang, *Green Chemistry*, 2008, **10**, 553-562; (d) M. H. So, Y. Liu, C. M. Ho and C. M. Che, *Chem. - Asian J.*, 2009, **4**, 1551-1561; (e) H. Choi and M. P. Doyle, *Chemical Communications*, 2007, 745-

- 747; (f) Ge, D.; Hu, L.; Wang, J.; Li, X.; Qi, F.; Lu, J.; Cao, X.; Gu, H., Reversible Hydrogenation-Oxidative Dehydrogenation of Quinolines over a Highly Active Pt Nanowire Catalyst under Mild Conditions. *ChemCatChem* **2013**, *5*, (8), 2183-2186; (g) Kamata, K.; Kasai, J.; Yamaguchi, K.; Mizuno, N., Efficient Heterogeneous Oxidation of Alkylarenes with Molecular Oxygen. *Organic Letters* **2004**, *6*, (20), 3577-3580; (h) K. Kamata, J. Kasai, K. Yamaguchi and N. Mizuno, *Organic Letters*, 2004, **6**, 3577-3580; (k) V. Jawale Dhanaji, E. Gravel, N. Shah, V. Dauvois, H. Li, N. N. Namboothiri Irishi and E. Doris, *E. Chem. - Eur. J.*, 2015, **21**, 7039-7042;
21. G. Jaiswal, V. G. Landge, D. Jagadeesan and E. Balaraman, *Nature Communications*, 2017, **8**, 2147.
22. (a) H. Fei, J. Dong, M. J. Arellano-Jiménez, G. Ye, N. Dong Kim, E. L. G. Samuel, Z. Peng, Z. Zhu, F. Qin, J. Bao, M. J. Yacaman, P. M. Ajayan, D. Chen and J. M. Tour, *Nature Communications*, 2015, **6**, 8668; (b) Iosub, A. V.; Stahl, S. S., Catalytic Aerobic Dehydrogenation of Nitrogen Heterocycles Using Heterogeneous Cobalt Oxide Supported on Nitrogen-Doped Carbon. *Organic Letters* **2015**, *17*, (18), 4404-4407.
23. Yuan, D.; Martha, T. G.; Chi, Z.; Jian, L., Computational study of precision nitrogen doping on graphene nanoribbon edges. *Nanotechnology* **2017**, *28*, (50), 505602.
24. (a) Dai, X.; Li, Z.; Ma, Y.; Liu, M.; Du, K.; Su, H.; Zhuo, H.; Yu, L.; Sun, H.; Zhang, X., Metallic Cobalt Encapsulated in Bamboo-Like and Nitrogen-Rich Carbonitride Nanotubes for Hydrogen Evolution Reaction. *ACS Applied Materials & Interfaces* **2016**, *8*, (10), 6439-6448.
25. R. V. Jagadeesh, H. Junge, M.-M. Pohl, J. r. Radnik, A. Brückner and M. Beller, *Journal of the American Chemical Society*, 2013, **135**, 10776-10782; (b) E. S. Andreiadis, P.-A. Jacques, P. D. Tran, A. Leyris, M. Chavarot-Kerlidou, B. Jusselme, M. Matheron, J. Pécaut, S. Palacin, M. Fontecave and V. Artero, *Nature Chemistry*, 2013, **5**, 48.
26. (a) J. R. Pels, F. Kapteijn, J. A. Moulijn, Q. Zhu and K. M. Thomas, *Carbon*, 1995, **33**, 1641-1653; (b) S. Stankovich, D. A. Dikin, R. D. Piner, K. A. Kohlhaas, A. Kleinhammes, Y. Jia, Y. Wu, S. T. Nguyen and R. S. Ruoff, *Carbon*, 2007, **45**, 1558-1565.
27. (a) A. Ganguly, S. Sharma, P. Papakonstantinou and J. Hamilton, *The Journal of Physical Chemistry C*, 2011, **115**, 17009-17019; (b) D. Yang, A. Velamakanni, G. I. Bozoklu, S. Park,

-
- M. Stoller, R. D. Piner, S. Stankovich, I. Jung, D. A. Field, C. A. Ventrice and R. S. Ruoff, *Carbon*, 2009, **47**, 145-152.
28. J. Choi, A. H. R. MacArthur, M. Brookhart and A. S. Goldman, *Chemical Reviews*, 2011, **111**, 1761-1779.
29. H. Li, J. Jiang, G. Lu, F. Huang and Z.-X. Wang, *Organometallics*, 2011, **30**, 3131-3141.
30. T. Zell and D. Milstein, *Accounts of Chemical Research*, 2015, **48**, 1979-1994
31. G. Jaiswal, V. G. Landge, D. Jagadeesan and E. Balaraman, *Green Chemistry*, 2016, **18**, 3232-3238.
32. J. R. Pels, F. Kapteijn, J. A. Moulijn, Q. Zhu and K. M. Thomas, *Carbon*, 1995, **33**, 1641-1653.
33. S. Stankovich, D. A. Dikin, R. D. Piner, K. A. Kohlhaas, A. Kleinhammes, Y. Jia, Y. Wu, S. T. Nguyen and R. S. Ruoff, *Carbon*, 2007, **45**, 1558-1565.
34. D. Forberg, T. Schwob, M. Zaheer, M. Friedrich, N. Miyajima and R. Kempe, *Nature Communications*, 2016, **7**, 13201

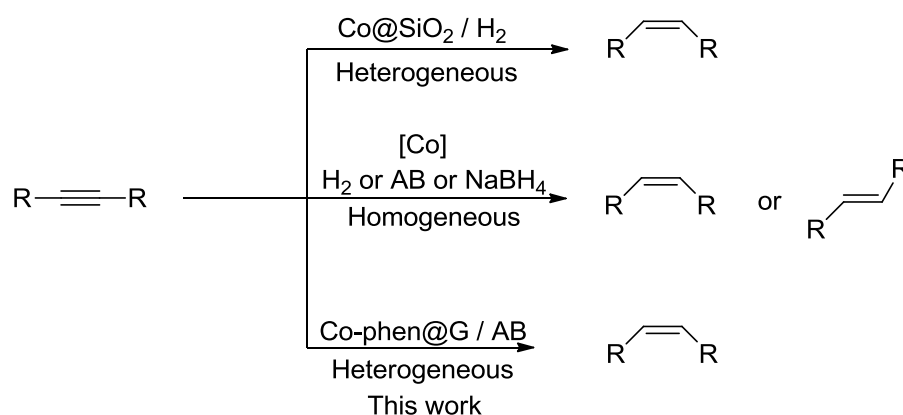
Part B: Cobalt-based nanocatalyst for selective transfer hydrogenation of alkynes

3B.1. Introduction

Development of efficient and selective catalytic system for chemical synthesis is of great demand and fuels the efforts of the present scientific community. In this context, the synthesis of olefins in a stereoselective manner is extremely important and has manifold applications in pharmaceuticals, petrochemical, and fragrance industry.¹ The reduction of alkynes to stereoselective olefins with circumventing the formation of the over-reduced alkane is very challenging.² The semihydrogenation of alkynes to *Z*-selective alkenes found by Lindlar was a significant milestone in the field of catalytic hydrogenation reactions. However, the need for expensive palladium and toxic additives are the potential concern.³ Various noble metal (Pd, Ru, Au) based catalysts have been studied for the semihydrogenation of alkynes.⁴⁻⁵ The high cost and limited reserve of precious metal catalysts impede their large-scale industrial application. As a consequence, the catalytic system based on bio-relevant, cheap metals is highly preferable and demanding.⁶ In recent times, the earth-abundant, non-precious metal-based homogeneous catalysts; in particular, molecularly-defined cobalt complexes have paid much attention in contemporary science.⁷ Continuous efforts have been made for the stereoselective semihydrogenation of alkynes using both homogeneous⁸⁻⁹ and heterogeneous cobalt-based catalysts under a high pressure of H₂.¹⁰⁻¹¹ The significant advantage of heterogeneous catalysts over soluble homogeneous catalysts is its capability for easy separation and recycling; however, structurally less understood.¹² Very recently, Beller and co-workers reported a heterogeneous cobalt catalyst on silica support for semihydrogenation of alkynes at a 30 bar of H₂ pressure.¹⁰

Of late, carbon-based support has paid much attention to material science and electrocatalysis due to its conductive nature, microporous structure, and high stability. Nitrogen-containing carbon materials are known to alter the individual physical and catalytic properties of metal nanoparticles.¹³ Consequently, metal nanoparticles deposited on N-doped carbon material has emerged as a fascinating catalyst in the Fischer-Tropsch process, and electrocatalytic H₂ generation, and various sustainable organic transformations.¹⁴ Recent computational studies illustrate that the N-doping can improve the stability of metal nanoparticles and can influence the

active sites for the nucleation and growth of the metal nanoparticles.¹⁵ Importantly, the activity of these catalysts can be controlled by composition and the microstructure of the nanomaterial. In our previous work (chapter 2), we have synthesized iron-based nanocatalyst obtained by thermally pyrolyzing the molecular iron-complex deposited on exfoliated graphene oxide for the acceptorless dehydrogenation reaction.¹⁶ In recent times, reusable cobalt-based heterogeneous catalysts have paid much attention in the hydrogenation reactions.¹⁷ Inspired by these excellent outcome, the similar synthetic strategy was applied for the synthesis of cobalt nanoparticles deposited on graphene oxide support and displayed excellent catalytic activity for the semihydrogenation of alkynes with high product selectivity (Scheme 3B.1).



Scheme 3B.1. Cobalt-catalyzed semihydrogenation of alkyne.

Notably, the newly synthesized cobalt nanoparticle on nitrogen-doped graphene (Co-Phen@G) has unique nanostructure. The present reusable cobalt-based catalytic system is operationally simple, and effectively catalyzed semihydrogenation of internal alkynes to the corresponding *Z*-alkenes, and terminal alkynes to linear α -olefins using ammonia borane (AB) as the transfer hydrogenating source.¹⁸

3B.2. Statement of the Problem

The stereoselective semi-hydrogenation of alkynes under mild conditions is a great challenge. The reduction of alkynes into stereoselective olefins and avoid the formation of over reduced alkane is very challenging. The contiguous effort has been made for synthesis of olefins using homogeneous and heterogeneous catalysis using H_2 at the high pressure. Herein, There is a

urgent need of catalytic system which is operationally simple, mild, and highly *cis*-selective hydrogenation of alkynes and terminal alkyne. Ammonia-borane (AB) has the advantages of high hydrogen content (19.6 wt.%), low molecular weight and high stability in solutions. It can be safely transported without hydrogen loss, thus making it a highly promising alternative for chemical hydrogen storage material. Herein, we report an operationally simple, mild, and highly *cis*-selective hydrogenation of alkynes and terminal alkyne, applying a reusable cobalt heterogenous catalyst deposited on graphene.

3A.3 Catalyst Synthesis and Characterization

See chapter 3a. The catalyst represents here Co-phen@G is same as mentioned in chapter 3A (Co-phen@C).

3B.4. Result and Discussion

3B.4.1. Optimization table

Optimization studies on Co-phen@G catalyzed semihydrogenation of alkynes to alkenes are summarized in Table 1. We began our investigation using diphenylacetylene (**1a**) as the benchmark substrate. In presence of catalytic amount Co-Phen@G and AB as a transfer hydrogen source, **1a** was selectively hydrogenated to **2a** in 93% isolated yield (only *Z*-selectively) with a complete conversion of **1a** (Table 3B.1, entry 1). The other conventional supports such as Al₂O₃, and SiO₂ gave unsatisfactory results (Table 3B.1, entries 2-3). To know the effect of ligand the cobalt salt (without 1,10-phenanthroline) was deposited on graphene and tested its reactivity under standard conditions. Notably, both Phen@G and Co@G failed to yield the product **2a**, and the starting material **1a** was fully recovered. This result indicates that the importance and the role of Co:L (L:1,10-phenanthroline) for the semihydrogenation reaction (Table 3B.1, entries 4-5. However, the Co-phen@G catalyst with 1,10-phenanthroline ligand was optimal catalyst under standard reaction conditions and gave excellent reactivity in the semihydrogenation of **1a**. The control experiment revealed that there was no formation of **2a** in the absence of a catalyst (Table 3B.1, entry 6). In addition, no reaction occurred in the absence of AB (Table 3B.1, entry 7). It was observed that the reaction proceeded efficiently in methanol.

Table 3B.1. Optimization of the reaction conditions.^a

$\text{Ph}-\text{C}\equiv\text{C}-\text{Ph} \xrightarrow[\text{MeOH, 100 }^\circ\text{C}]{\text{Cat. Co-Phen@G, AB, Ar atm}} \text{Ph}-\text{CH}=\text{CH}-\text{Ph} + \text{Ph}-\text{CH}=\text{CH}-\text{Ph}$

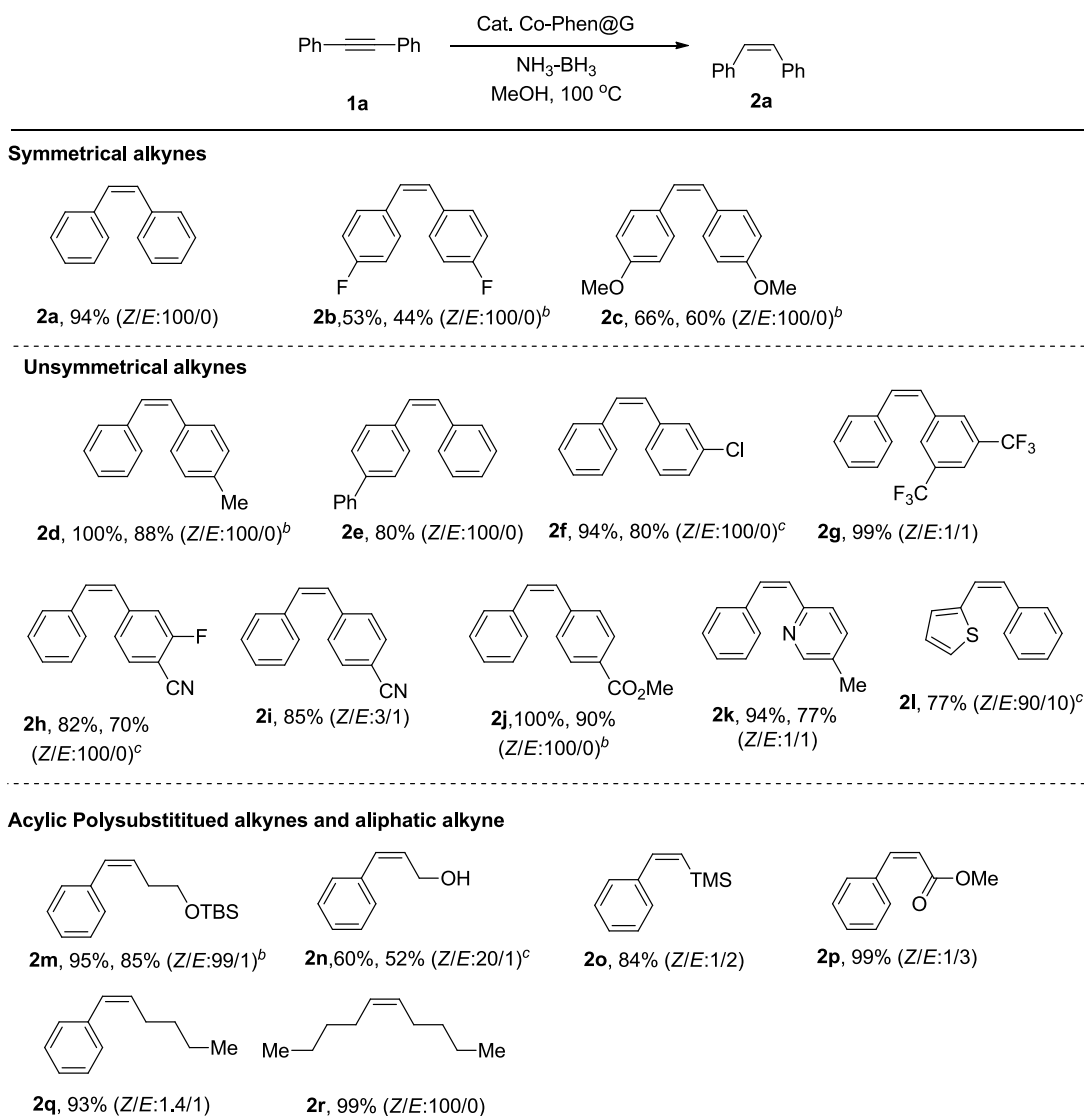
1a **2a** **3a**

Entry	Cat.	Variation from the initial conditions	Conversion of 1a (%) ^b	Yield of 2a/3a (%) ^b
1	Co-Phen@C	none	99	97/0 (93) ^c
2	Co-Phen@Al ₂ O ₃	none	60	20
3	Co-Phen@SiO ₂	none	27	22/78
4	Co@C	none	8	0
5	Phen@C	none	0	0
6	—	without Co-Phen@G	0	0
7	Co-Phen@C	without AB	0	0

^a Reaction conditions: **1a** (0.25 mmol), **AB** (0.5 mmol), cat. Co-Phen@G (8 mol%) and MeOH (2 mL) heated at 100 °C (oil-bath temperature) for 36 h under open argon atm. ^b Conversion of **1a** and yield of **2a** are based on GC. ^c Isolated yields.

3B.4.2. Substrate scope of alkynes

With optimized reaction conditions in hand, the present cobalt-catalyzed semihydrogenation of alkynes was then deployed in the synthesis of a diverse *Z*-alkenes, and the results are summarized in Table 3B.2. The symmetrical alkynes pertaining electron-donating, and electron-withdrawing groups underwent *Z*-selectivity partial hydrogenation smoothly and resulted in the products **2b** in 44% and **2c** in 66% isolated yields with complete *Z*-selectivity. The unsymmetrical alkynes containing electron-donating, electron-withdrawing groups and heterocyclic motifs also underwent semihydrogenation with excellent *Z*-selectivity. A strong electron withdrawing disubstituted trifluoromethyl unsymmetrical alkyne (**1g**) was hydrogenated, and the *Z*-alkene **2g** was produced in 99% yield with 1:1 *Z/E* ratio. Various reducible functional groups such as cyano (**1h** and **1i**), an ester (**1j**) were well tolerated under the standard reaction conditions and yielded the corresponding semi-hydrogenated *Z*-selective alkene in excellent (82-99%) yields. In classical homogeneous conditions, the alkyne-containing heterocyclic motifs challenging to hydrogenate due to strong coordination of heteroatom with the metal center and thus leads to a low yield of the desired product.

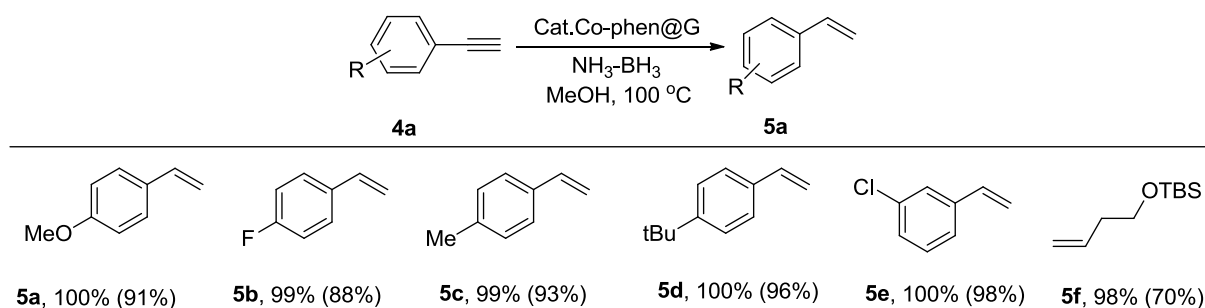
Table 3B.2. The scope of internal alkynes.^a

^aReaction conditions: **1** (0.5 mmol), AB (0.6mmol), and 8.0 mol % of Co-phen@G in 2 mL of MeOH at 100 °C (oil-bath temperature) for 36 h and GC yields of alkenes with *Z/E* ratios are shown (The GC yields are the average of the two independent experiments).^bIsolated yield. ^c¹H NMR of the reaction mixture.

However, the heterocyclic ring containing pyridine (**1k**) and thiophene (**1l**) alkynes proceeded smoothly under the present cobalt-catalyzed conditions and yielded the corresponding semi-hydrogenated products in 77% (*Z:E*=1:1), and 77% (*Z:E*=9:1) yields, respectively. Interestingly, acyclic aliphatic alkynes pertaining ester (**1m**), hydroxyl (**1n**), trimethylsilane (**1o**), and ester (**1p**) group were well-tolerated and gave the semi-hydrogenated products in good yields (up to

99%). Furthermore, unactivated alkynes such as 4-octyne (**1r**) efficiently progressed and converted to the corresponding alkene in 84% yield with excellent a *Z/E* selectivity. Thus, the present catalytic reaction operates under mild, neutral conditions, with no additives being required.

Table 3.B.2 Scope of internal alkynes.^a



^aReaction conditions: **1** (0.5 mmol), AB (0.6 mmol), and 8.0 mol% of Co-phen@G in 2 mL of MeOH at 100 °C for 36 h.

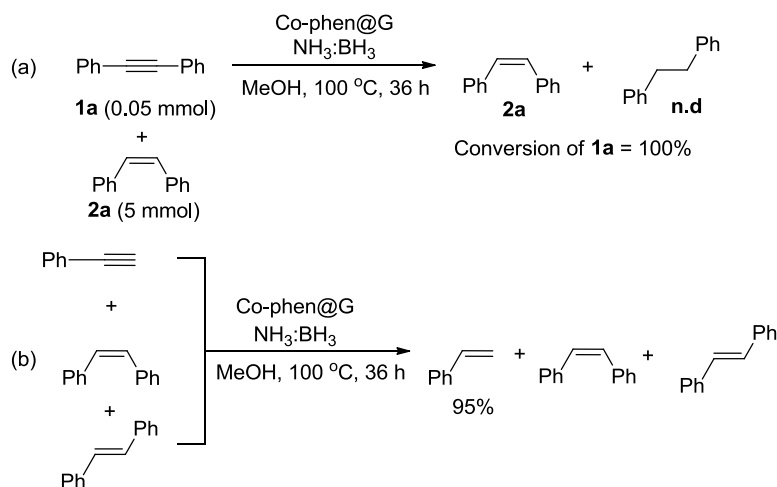
Gratifyingly, we have extended our catalytic system to terminal alkynes (Table 3B.3). The substituted terminal alkynes such as methoxy, methyl, fluoro, and chloro were smoothly proceeded transfer hydrogenation and afforded the corresponding alkenes in moderate to good yields under optimal conditions (52-98%). The unactivated aliphatic terminal alkyne **4f** underwent partial hydrogenation smoothly and resulted in the corresponding linear α -olefin in 70% yield. In most of the cases, no alkane (or a trace amount) formation was detected.

3B.4.3. Application of semihydrogenation

Next, we have explored the potential applications of our current catalytic system in the fine chemical industry. In general, selective removal of alkyne impurities from alkenes is crucial for the valorization of bulk feedstocks, e.g., steam cracking process.¹⁹ Hence, the development of a robust and economical catalytic approach for the selective conversion of the alkyne impurities to alkenes is very important and demanding. In this content, we have carried out the reaction using an excess of alkene in the presence of alkyne under optimized conditions. It was observed that the present cobalt-based catalytic system selectively hydrogenated the internal alkynes and thus, the high purity of α -olefins was obtained (Scheme 3B.2a). In addition, we have carried out the

reaction with a mixture of phenylacetylene, *cis*-stilbene, and *trans*-stilbene under standard reaction conditions (Scheme 3B.2b). Interestingly, only phenylacetylene underwent hydrogenation, and this result demonstrates the potential application of our present system in organic synthesis and purification of alkenes in the chemical industry.

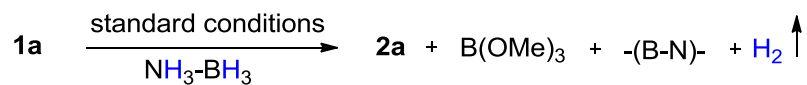
Scheme 3B.2. Applications in selective removal of alkyne impurities from an alkene.



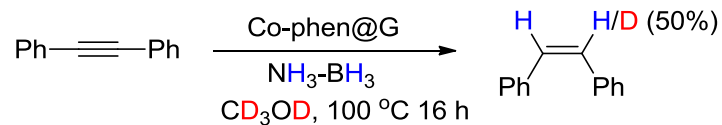
3B.4.4. Mechanistic Investigation

To gain insights into the reaction mechanism, several control experiments, and labelling studies were carried out under standard reaction conditions (Scheme 3B.3). Under standard reaction conditions, the formation of $\text{B}(\text{OMe})_3$, B-N bonded compounds, and the generation of hydrogen was observed. The reaction was carried out using CD_3OD as a solvent, and it was found that 50% deuterium was incorporated in the product **2b** (^1H NMR) which revealed that the proto-demetalation of alkenyl cobalt intermediate occurred in the presence of MeOH (Scheme 3B.3b). Controlled experiments also showed that there was no *Z* to *E* isomerization observed in the absence AB (Scheme 3B.3c).

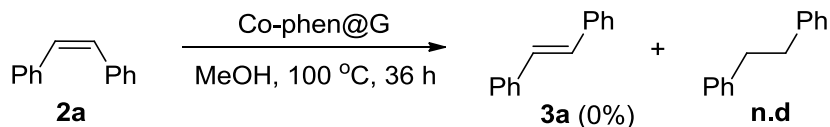
(a) Determination of the dehydrogenated product of AB



(b) Labeling experiment



(c) Isomerization of **2a**



Scheme 3B.3. Mechanistic study

Determination of the dehydrogenation product of ammonia-borane

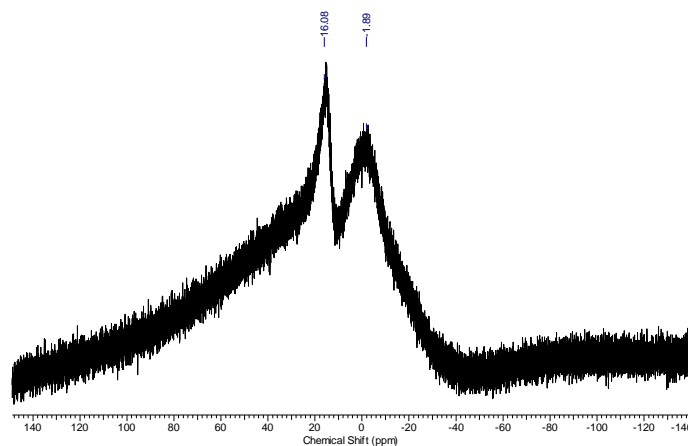
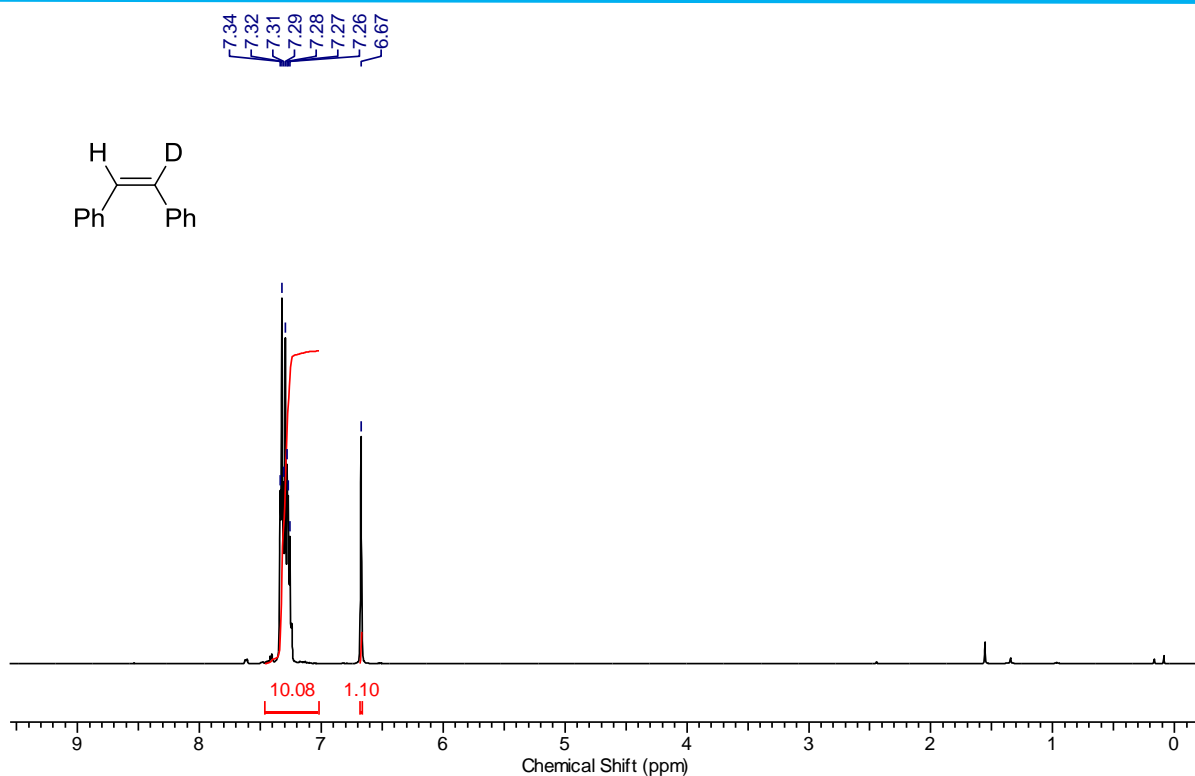
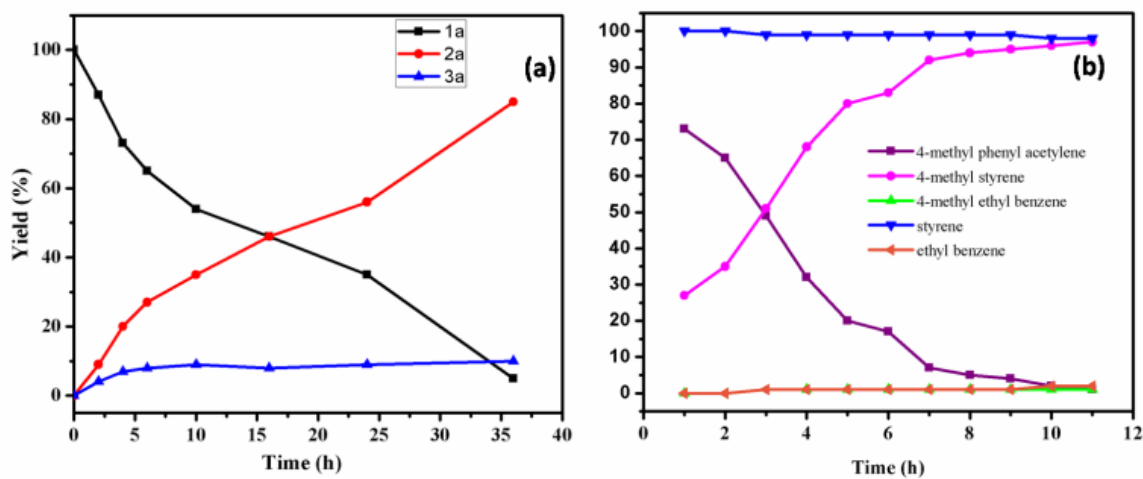


Figure 3B.1. ^{11}B NMR of the crude reaction mixture.

Figure 3B.2. ¹H NMR of [D]-2a.

3B.4.1. Kinetic Studies

Figure 3B.3 (a) Reaction profile for the cobalt-catalyzed formation of **2a**, (b) Competitive experiment for the cobalt-catalyzed formation of 4-methyl styrene (**5c**).

Time-dependent experiments on the reduction of an alkyne with AB were conducted using heterogeneous cobalt-catalyst to study the reaction kinetics further confirms there was no *Z* to *E* isomerization under optimal conditions (Figure 3B.3).

3B.4.4.2. Recyclability of the catalyst

The stability of Co-Phen@G catalyst was tested for the model reaction. After completion of the reaction, the catalyst was easily separated from the reaction medium by simple filtration and the recovered Co-phen@G was reused for semihydrogenation of **1a** in at least six cycles without a considerable loss in the yield/selectivity (Figure 3B.4). The hot filtration test demonstrates that no further hydrogenation took place after the catalyst was filtered off at the conversion of **1a** in 46%. Inductively coupled plasma (ICP) analysis performed from the supernatant after 5th cycle confirmed that the cobalt concentration in the filtrate was less than 0.18 ppm.

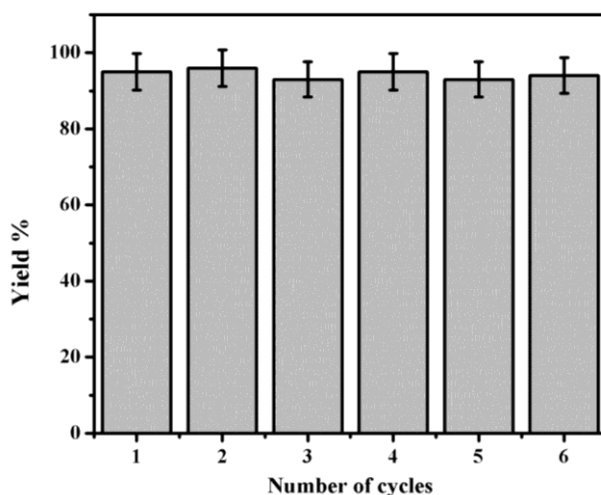
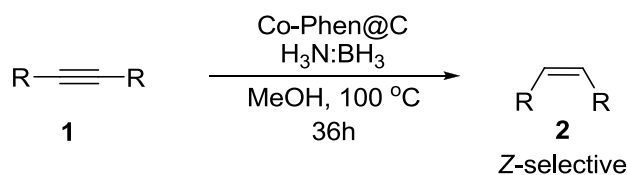


Figure 3B.4. Recyclability of the Co-Phen@C catalyst

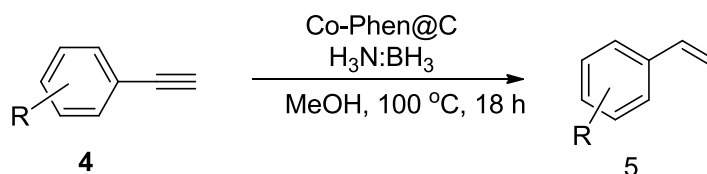
3B.5. Experimental section

3B.5.1. General Procedure for *Z* selective semihydrogenation of internal alkynes



To an oven-dried 10 mL screw-capped vial, alkyne **1** (0.5mmol), ammonia-borane (0.6mmol), Co-Phen@C catalyst (8mol%), and methanol(1 mL) were added under a gentle stream of argon. The mixture was stirred for 36 h at 100 °C (bath temperature) followed by cooling to room temperature. The mixture was filtered through a celite pad with several washings (3 x 3 mL dichloromethane) and concentrated *in vacuo*. The yield of alkene was determined by GC.

3B.5.2. General Procedure for semihydrogenation of terminal alkynes



To an oven-dried 10 mL screw-capped vial, terminal alkyne **4** (0.5 mmol), ammonia-borane (0.6 mmol), Co-Phen@C catalyst (8 mol%), and methanol(1 mL) were added under a gentle stream of argon. The mixture was stirred for 18 h at 100 °C (bath temperature) followed by cooling to room temperature. The mixture was filtered through a celite pad with several washings (3 x 3 mL dichloromethane) and concentrated *in vacuo*. The yield of alkene was determined by GC.

3B.6. Conclusion

In conclusion, a catalytic semihydrogenation of alkynes to configurationally defined Z-alkenes is described using reusable cobalt nanocatalyst. The catalyst is also effective for partial hydrogenation of terminal alkynes to linear α -olefins. The reaction operates under mild, neutral conditions, with no additives being required. This nanocatalyst performs outstandingly with a six-run recycling test. Notably, the newly synthesized cobalt nanocatalyst has unique nanostructure as compared to the literature catalysts.

3B.7. References

1. (a) A. Corma, S. Iborra and A. Velty, *Chem. Rev.*, 2007, **107**, 2411-2502; (b) Handbook of Homogeneous Hydrogenation (Eds.: J. G. de Vries, C. J. Elsevier), Wiley-VCH, Weinheim, 2007; (c) N. B. Johnson, I. C. Lennon, P. H. Moran and J. A. Ramsden, *Acc. Chem. Res.*, 2007, **40**, 1291-1299.
2. (a) H. Lindlar, *Helv. Chim. Acta*, 1952, **35**, 446-450; (b) H. Lindlar and R. Dubuis, *Org. Synth.*, 1966, 89-89.
3. (a) R. Venkatesan, M. H. G. Pechtl, J. D. Scholten, R. P. Pezzi, G. Machado and J. Dupont, *J. Mater. Chem.*, 2011, **21**, 3030-3036; (b) E. D. Slack, C. M. Gabriel and B. H. Lipshutz, *Angew. Chem.*, 2014, **126**, 14275-14278; (c) O. Verho, H. Zheng, P. J. Gustafson Karl, A. Nagendiran, X. Zou and E. Bäckvall Jan, *ChemCatChem*, 2016, **8**, 773-778; (d) W. Niu, Y. Gao, W. Zhang, N. Yan and X. Lu, *Angew. Chem.*, 2015, **54**, 8271-8274; (e) K. Schutte, A. Doddi, C. Kroll, H. Meyer, C. Wiktor, C. Gemel, G. van Tendeloo, R. A. Fischer and C. Janiak, *Nanoscale*, 2014, **6**, 5532-5544; (f) S. Furukawa and T. Komatsu, *ACS Catal.*, 2016, **6**, 2121-2125;
4. (a) D. Köhler, M. Heise, A. I. Baranov, Y. Luo, D. Geiger, M. Ruck and M. Armbrüster, *Chem. Mater.*, 2012, **24**, 1639-1644; (b) T. Mitsudome, M. Yamamoto, Z. Maeno, T. Mizugaki, K. Jitsukawa and K. Kaneda, *J. Am. Chem. Soc.*, 2015, **137**, 13452-13455; (c) G. Li and R. Jin, *J. Am. Chem. Soc.*, 2014, **136**, 11347-11354; (d) S. S. Li, L. Tao, F. Z. R. Wang, Y. M. Liu and Y. Cao, *Adv. Synth. Catal.*, 2016, **358**, 1410-1416; (e) S. Liang, G. B. Hammond and B. Xu, *Chem. Commun.*, 2016, **52**, 6013-6016; (e) Y. S. Wagh and N. Asao, *J. Org. Chem.*, 2015, **80**, 847-851; (f) M. Yan, T. Jin, Y. Ishikawa, T. Minato, T. Fujita, L.-Y. Chen, M. Bao, N. Asao, M.-W. Chen and Y. Yamamoto, *J. Am. Chem. Soc.*, 2012, **134**, 17536-17542.
5. (a) R. M. Bullock, *Science*, 2013, **342**, 1054-1055; (b) A. Fürstner, *ACS Cent. Sci.*, 2016, **2**, 778-789; (c) S. W. M. Crossley, C. Obradors, R. M. Martinez and R. A. Shenvi, *Chem. Rev.*, 2016, **116**, 8912-9000.
6. (a) G. Zhang and S. K. Hanson, *Org. Lett.*, 2013, **15**, 650-653; (b) R. Xu, S. Chakraborty, H. Yuan and W. D. Jones, *ACS Catal.*, 2015, **5**, 6350-6354; (c) S. Rösler, M. Ertl, T. Irrgang and R. Kempe, *Angew. Chem., Int. Ed.*, 2015, **54**, 15046-15050; (d) G. Zhang, Z. Yin and S. Zheng, *Org. Lett.* 2016, **18**, 300-303; (e) M. Mastalir, G.

- Tomsu, E. Pittenauer, G. Allmaier and K. Kirchner, *Org. Lett.* 2016, **18**, 3462-3465; (f) Z. Yin, H. Zeng, J. Wu, S. Zheng and G. Zhang, *ACS Catal.*, 2016, **6**, 6546-6550; (g) N. Deibl and R. Kempe, *J. Am. Chem. Soc.*, 2016, **138**, 10786-10789. (h) G. Zhang and S. K. Hanson, *Chem. Commun.*, 2013, **49**, 10151-10153; (i) S. M. King, X. Ma and S. B. Herzon, *J. Am. Chem. Soc.*, 2014, **136**, 6884-6887; (j) J. K. Pagano, J. P. W. Stelmach and R. Waterman, *Dalton Trans.*, 2015, **44**, 12074- 12077.
7. (a) G. Zhang, B. L. Scott and S. K. Hanson, *Angew. Chem., Int. Ed.*, 2012, **51**, 12102-12106; (b) C. Federsel, C. Ziebart, R. Jackstell, W. Baumann and M. Beller, *Chem.Eur.J.*, 2012, **18**, 72-75; (c) S. M. Jeletic, M. T. Mock, A. M. Appel and J. C. Linehan, *J. Am. Chem. Soc.*, 2013, **135**, 11533-11536; (d) P. Yu, J. M. Darmon, C. Milsmann, G. W. Margulieux, S. C. E. Stieber, S. DeBeer and P. J. Chirik, *J. Am. Chem. Soc.*, 2013, **135**, 13168-13184; (e) M. R. Friedfeld, M. Shevlin, J. M. Hoyt, S. W. Krska, M. T. Tudge and P. J. Chirik, *Science* 2013, **342**, 1076-1080; (f) T.-P. Lin and J. C. Peters, *J. Am. Chem. Soc.*, 2014, **136**, 13672-13683; (g) S. Rösler, J. Obenauf and R. Kempe, *J. Am. Chem. Soc.* 2015, **137**, 7998-8001; (g) D. Srimani, A. Mukherjee, A. F. G. Goldberg, G. Leitus, Y. Diskin-Posner, L. J. W. Shimon, Y. Ben David and D. Milstein, *Angew. Chem., Int. Ed.*, 2015, **54**, 12357-12360; (h) T. J. Korstanje, J. I. van der Vlugt, C. J. Elsevier and B. de Bruin, *Science*, 2015, **350**, 298-302; (i) A. Mukherjee, D. Srimani, S. Chakraborty, Y. Ben-David and D. Milstein, *J. Am. Chem. Soc.*, 2015, **137**, 8888-8891; (j) Z. Shao, S. Fu, M. Wei, S. Zhou and Q. Liu, *Angew. Chem. Int. Ed.*, 2016, **55**, 14653-14657; (k) P. Daw, S. Chakraborty, G. Leitus, Y. Diskin-Posner, Y. Ben-David and D. Milstein, *ACS Catal.*, 2017, **7**, 2500-2504; (l) J. Yuwen, S. Chakraborty, W. W. Brennessel and W. D. Jones, *ACS Catal.*, 2017, **7**, 3735-3740. Chirik, *J. Am. Chem. Soc.*, 2016, **138**, 3314-3324;
8. (a) S. Fu, N. Y. Chen, X. Liu, Z. Shao, S. P. Luo and Q. Liu, *J. Am. Chem. Soc.*, 2016, **138**, 8588-8594; (b) K. Tokmic and A. R. Fout, *J. Am. Chem. Soc.*, 2016, **138**, 13700-13705; (c) B. Raya, S. Biswas and T. V. RajanBabu, *ACS Catal.*, 2016, **6**, 6318-6323; (d) C. Chen, Y. Huang, Z. Zhang, X.-Q. Dong and X. Zhang, *Chem. Commun.*, 2017, **53**, 4612-4615; (e) V. G. Landge, J. Pitchaimani, S. P. Midya, M. Subaramanian, V. Madhu and E. Balaraman, *Catal. Sci. Technol.*, 2018, **8**, 428-433.

-
9. (a) F. Chen, C. Kreyenschulte, J. Radnik, H. Lund, A. E. Surkus, K. Junge and M. Beller, *ACS Catal.*, 2017, **7**, 1526-1532.
 10. S. Nishimura, *Handbook of heterogeneous catalytic hydrogenation for organic synthesis*, Wiley New York etc, 2001.
 11. (a) T. Baramov, P. Loos, J. Hassfeld, H. Alex, M. Beller, T. Stemmler, G. Meier, M. Gottfried and S. Roggan, *Adv. Synth. Catal.*, 2016, **358**, 2903-2911; (b) D. Formenti, C. Topf, K. Junge, F. Ragaini and M. Beller, *Catal. Sci. Technol.*, 2016, **6**, 4473-4477; (c) T. Stemmler, F. Chen, S. Pisiewicz, A. E. Surkus, M. M. Pohl, C. Topf and M. Beller, *J. Mater. Chem.A*, 2015, **3**, 17728-17737; (d) F. Chen, A.-E. Surkus, L. He, M.-M. Pohl, J. Radnik, C. Topf, K. Junge and M. Beller, *J. Am. Chem. Soc.*, 2015, **137**, 11718-11724; (e) F. A. Westerhaus, R. V. Jagadeesh, G. Wienhäfer, M.M. Pohl, J. R. Radnik, A. E. Surkus, J. Rabeah, K. Junge, H. Junge and M. Nielsen, *Nat. Chem.*, 2013, **5**, 537-543.
 12. (a) T. Cheng, H. Yu, F. Peng, H. Wang, B. Zhang and D. Su, *Catal. Sci. Technol.*, 2016, **6**, 1007-1015; (b) M. Li, F. Xu, H. Li and Y. Wang, *Catal. Sci. Technol.*, 2016, **6**, 3670-3693; (c) H. Wang, T. Maiyalagan and X. Wang, *ACS Catal.*, 2012, **2**, 781-794; (d) Z. Wei, Y. Chen, J. Wang, D. Su, M. Tang, S. Mao and Y. Wang, *ACS Catal.*, 2016, **6**, 5816-5822; (e) W. Zhong, H. Liu, C. Bai, S. Liao and Y. Li, *ACS Catal.*, 2015, **5**, 1850-1856; (f) K. Shen, L. Chen, J. Long, W. Zhong and Y. Li, *ACS Catal.*, 2015, **5**, 5264-5271; (g) Y. Wang, Y. Nie, W. Ding, S. G. Chen, K. Xiong, X. Q. Qi, Y. Zhang, J. Wang and Z. D. Wei, *Chem. Commun.*, 2015, **51**, 8942-8945; (h) A. Maleki, N. Ghamari and M. Kamalzare, *RSC Adv.*, 2014, **4**, 9416-9423; (i) R. V. Jagadeesh, A.-E. Surkus, H. Junge, M.-M. Pohl, J. Radnik, J. Rabeah, H. Huan, V. Schänemann, A. Bräckner and M. Beller, *Science*, 2013, **342**, 1073-1076.
 13. (a) D. Yuan, T. G. Martha, Z. Chi and L. Jian, *Nanotechnology*, 2017, **28**, 505-602; (b) J. Lu, L. Yang, B. Xu, Q. Wu, D. Zhang, S. Yuan, Y. Zhai, X. Wang, Y. Fan and Z. Hu, *ACS Catal.*, 2014, **4**, 613-621.
 14. (a) G. Jaiswal, V. G. Landge, D. Jagadeesan and E. Balaraman, *Nat. Commun.*, 2017, **8**, 2147; (b) G. Jaiswal, V. G. Landge, D. Jagadeesan and E. Balaraman, *Green Chem.*, 2016, **18**, 3232-3238.

-
-
15. (a) X. Dai, Z. Li, Y. Ma, M. Liu, K. Du, H. Su, H. Zhuo, L. Yu, H. Sun and X. Zhang, *Acs appl. mater. interfaces*, 2016, **8**, 6439-6448; (b) X. Wang, Q. Li, H. Pan, Y. Lin, Y. Ke, H. Sheng, M. T. Swihart and G. Wu, *Nanoscale*, 2015, **7**, 20290-20298.
16. (a) R. V. Jagadeesh, H. Junge, M.-M. Pohl, J. Radnik, A. Bräckner and M. Beller, *J. Am. Chem. Soc.*, 2013, **135**, 10776-10782; (b) E. S. Andreiadis, P. A. Jacques, P. D. Tran, A. Leyris, M. Chavarot-Kerlidou, B. Joussetme, M. Matheron, J. Păcaut, S. Palacin and M. Fontecave, *Nat. Chem.*, 2013, **5**, 48-53.
17. (a) H. Fei, J. Dong, M. J. Arellano-Jiménez, G. Ye, N. Dong Kim, E. L. G. Samuel, Z. Peng, Z. Zhu, F. Qin, J. Bao, M. J. Yacaman, P. M. Ajayan, D. Chen and J. M. Tour, *Nat. Commun.*, 2015, **6**, 8668; (b) A. V. Iosub and S. S. Stahl, *Org. Lett.*, 2017, **17**, 4404-4407.
18. (a) J. R. Pels, F. Kapteijn, J. A. Moulijn, Q. Zhu and K. M. Thomas, *Carbon*, 1995, **33**, 1641-1653; (b) S. Stankovich, D. A. Dikin, R. D. Piner, K. A. Kohlhaas, A. Kleinhammes, Y. Jia, Y. Wu, S. T. Nguyen and R. S. Ruoff, *Carbon*, 2007, **45**, 1558-1565.
19. (a) A. Ganguly, S. Sharma, P. Papakonstantinou and J. Hamilton, *The J. Phys. Chem. C*, 2011, **115**, 17009-17019; (b) D. Yang, A. Velamakanni, G. I. Bozoklu, S. Park, M. Stoller, R. D. Piner, S. Stankovich, I. Jung, D. A. Field, C. A. Ventrice and R. S. Ruoff, *Carbon*, 2009, **47**, 145-152.

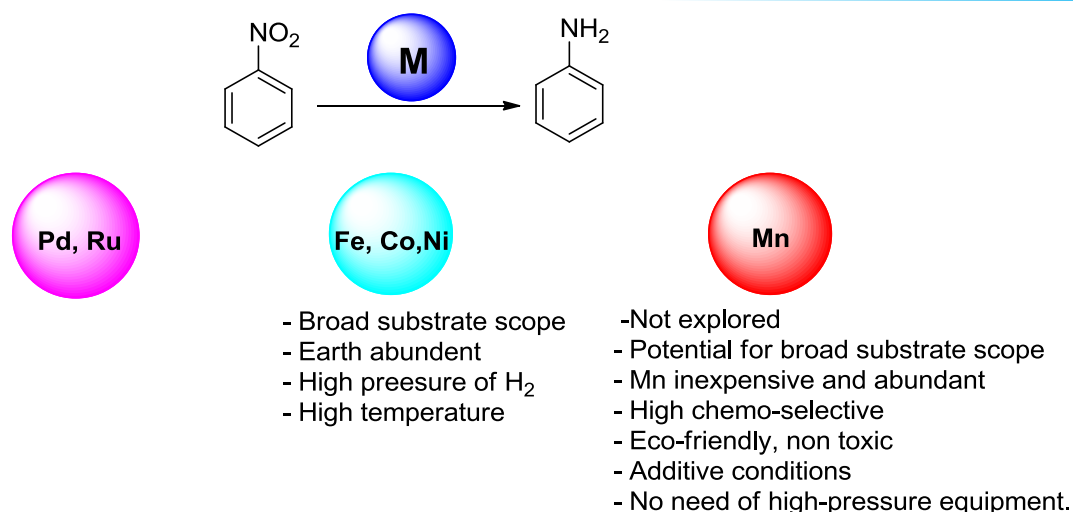
Chapter 4

Chemo-selective catalytic transfer hydrogenation of nitroarenes by reusable manganese nanocatalyst

4.1. Introduction

Aromatic amines serve as industrially important intermediates and play a key role in agrochemicals, biorenewable chemicals, pharmaceuticals, and fine chemicals.¹ The significant growth has been devoted for hydrogenation of nitroarenes to anilines by precious-metal based catalysts, but lack of selectivity and functional group tolerance. In recent times, earth-abundant, non-noble-metal based catalysts have shown promising catalytic performance for hydrogenation reactions and paid considerable momentum in contemporary science.² The high pressure of H₂ gas mainly used for hydrogenation of polar or non-polar compounds but for safety issue nowadays transfers hydrogenation or auto-transfer hydrogenation had received much attention, in which the *in situ* generated hydrogen can be utilized for reduction process.³ Nevertheless, remarkable progress has been made in the area of transfer hydrogenation by using heterogeneous nickel, cobalt, and iron catalysts.⁴ However, the use of the catalytic system based on manganese, the third most abundant after iron and titanium in the earth crust is very limited and rather scarce.⁵ Very recently, Beller and Kirchner independently reported a homogeneous well-defined Mn(I)-pincer complex catalyzed *N*-alkylation of alcohols and heterocyclic formation *via* borrowing hydrogen strategy.⁶

Ammonia borane (AB) the advantages of high hydrogen content (19.6 wt.%), low molecular weight and high stability in solutions, stable material that can be safely transported without hydrogen loss making it a highly promising alternative for chemical hydrogen storage material.⁷ In the last few years, cobalt and iron nanoparticle catalysts, which are easy to handle and separable have been developed for AB dehydrogenation.⁷ To the best of our knowledge there is no report on dehydrogenation of AB as well as chemoselective reduction of nitroarenes to anilines under heterogeneous conditions. Here, we report the preparation of a novel reusable nitrogen-doped manganese-based nanocatalyst (Mn-Phen@G) and its catalytic activity in the tandem dehydrogenation of AB and hydrogenation of nitroarenes under very mild, and benign, conditions. The reaction is general and tolerates various reducible functional groups such as methoxy, halides, esters, nitrile, acids, amides, and olefinic motifs.



Scheme 4.1. Transfer hydrogenation of nitroarenes to anilines.

4.2 Statement of problem

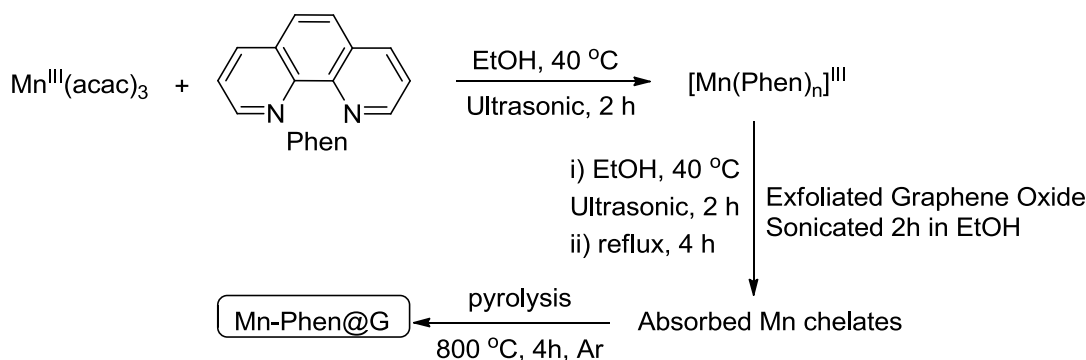
From the above-mentioned literature, it is clear that the dehydrogenation of AB, as well as chemoselective reduction of nitroarenes to anilines either under homogeneous or heterogeneous conditions, are in the primary stage of development. There is no single report based on manganese for the transfer hydrogenation of nitroarenes. Here, we report the preparation of a novel reusable nitrogen-doped manganese-based nanocatalyst (Mn-Phen@G) and its catalytic activity in the tandem dehydrogenation of AB and hydrogenation of nitroarenes under very mild, benign, additive free conditions. The reaction is general and tolerates various reducible functional groups such as methoxy, halides, esters, nitrile, acids, amides, and olefinic motifs.

4.3. Catalyst Synthesis and Characterization

4.3.1. Synthesis of Mn-Phen@G catalyst

In a 100 mL beaker, Mn(III)acetylacetonate precursor (0.5 mmol) and 1,10-phenanthroline ligand (0.5 mmol) were dissolved in 30 mL of ethanol and sonicated for 2 h to form Mn-phenanthroline complex. In another 250 mL, beaker 560 mg of EGO support was taken in 70 mL of ethanol and sonicated for 2 h. The above-obtained EGO suspension and Mn-phenanthroline complex solution were mixed together in 250 mL beaker and further sonicated for 2 h. The suspension was refluxed at 85 °C for 4 h and after cooling down to room temperature ethanol was evaporated in vacuum. The solid sample obtained was dried at 80 °C for 14 h. Then, it was

ground to a fine powder followed by calcination at 800 °C under a stream of argon with the flow rate of 30 mL/min and the heating rate: 25 °C/min for about 4 h to obtain a catalyst Mn-Phen@G



Scheme 4.2. Synthesis procedure of Mn-Phen@G catalyst.

4.3.2. Characterization of catalyst

The complete characterization of the active material (Mn-Phen@G) has been carried out using PXRD, TEM analysis, SEM analysis, XPS, ICP, and Raman spectroscopy. We have observed that the Mn-phenanthroline (Mn-L1) complex pyrolyzed with exfoliated graphitic oxide at 800 °C (Mn-Phen@G) led to a highly active catalytic material towards hydrogenation reactions at atmospheric pressure.

4.3.2.1. Powder X-ray diffraction

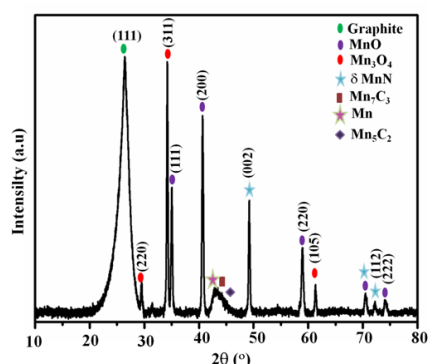


Figure. 4.1. PXRD pattern of Mn-Phen@G showing MnO, Mn₃O₄, Mn₇C₃, MnN, Mn, and graphite.

The PXRD pattern of Mn-Phen@G sample presented in Figure 4.1 showed a broad peak at $2\theta = 26.51$ degrees in and confirmed the presence of a few layers of reduced graphene oxide support. In the given reaction conditions, manganese salt supposed to decomposed on graphitic oxide

support in a pure Ar atmosphere at 800 °C leads to formation MnO and Mn₃O₄ detected in PXRD. In the given PXRD pattern peaks of MnO and Mn₃O₄ were slightly shifted to a higher angle which can be attributed to lattice shrinkage and comparable to literature.⁸ A broad peak between 2θ = 42 to 48 is due to intermix phases of metallic Mn, Mn₅C₂ and Mn₇C₃ phases. Peaks for MnN phase was also observed in PXRD. Formation of metal carbide and MnN can be understood in terms of the decomposition of N and C rich 1,10-phenanthroline L1 in the proximity of metal atoms that aggregate to form a carbide and nitride nanoparticles. The presence of Mn metal is obvious under given reaction conditions in the presence of a reducing agent like graphite.

4.3.2.2. Energy Dispersive X-Ray Analysis (EDX)

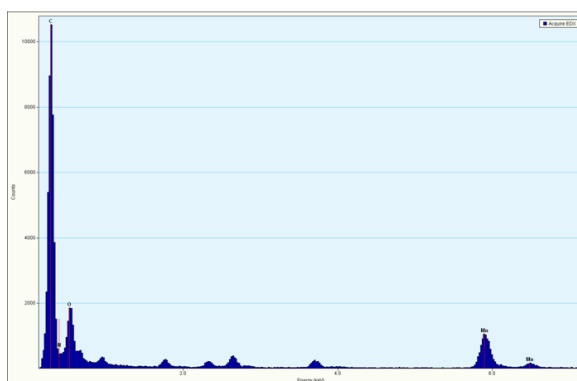


Figure 4.2. EDX analysis of Mn-Phen@G catalyst.

Table 4.1 showing the weight percent of different elements in the Mn-Phen@G catalyst

Element	Weight %	Atomic %	Uncert. %	Correction	k-Factor
C(K)	82.55	90.66	0.47	0.26	3.940
N(K)	1.91	1.76	0.09	0.26	3.826
O(K)	8.27	6.69	0.11	0.49	1.974
Mn(K)	6.25	1.47	0.07	0.99	1.375

4.3.2.3. Scanning Electron Microscopy (SEM), Transmission Electron Microscopy (TEM) and X-ray photoelectron spectroscopy (XPS)

The morphology of the Mn-Phen@G catalyst was analyzed using r (SEM) which clearly showed graphene layers supporting spatially well-separated nanoparticles that are probably rich in Mn

(Figure 4.3). The microstructure of Mn-Phen@G catalyst was analyzed using Transmission Electron Microscopy (TEM) and the data is shown in Figure 4.4.e-h. The nanoparticles were distributed throughout the graphene sheets and were of size ranging from 10 - 300 nm. Few particles were off smaller size while few particles were larger in size.

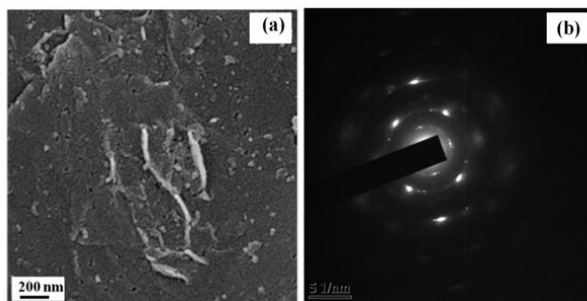


Figure 4.3 (a) SEM images of Mn-Phen@G at the scale of 200nm, (b) SEAD pattern of Mn-Phen@G catalyst.

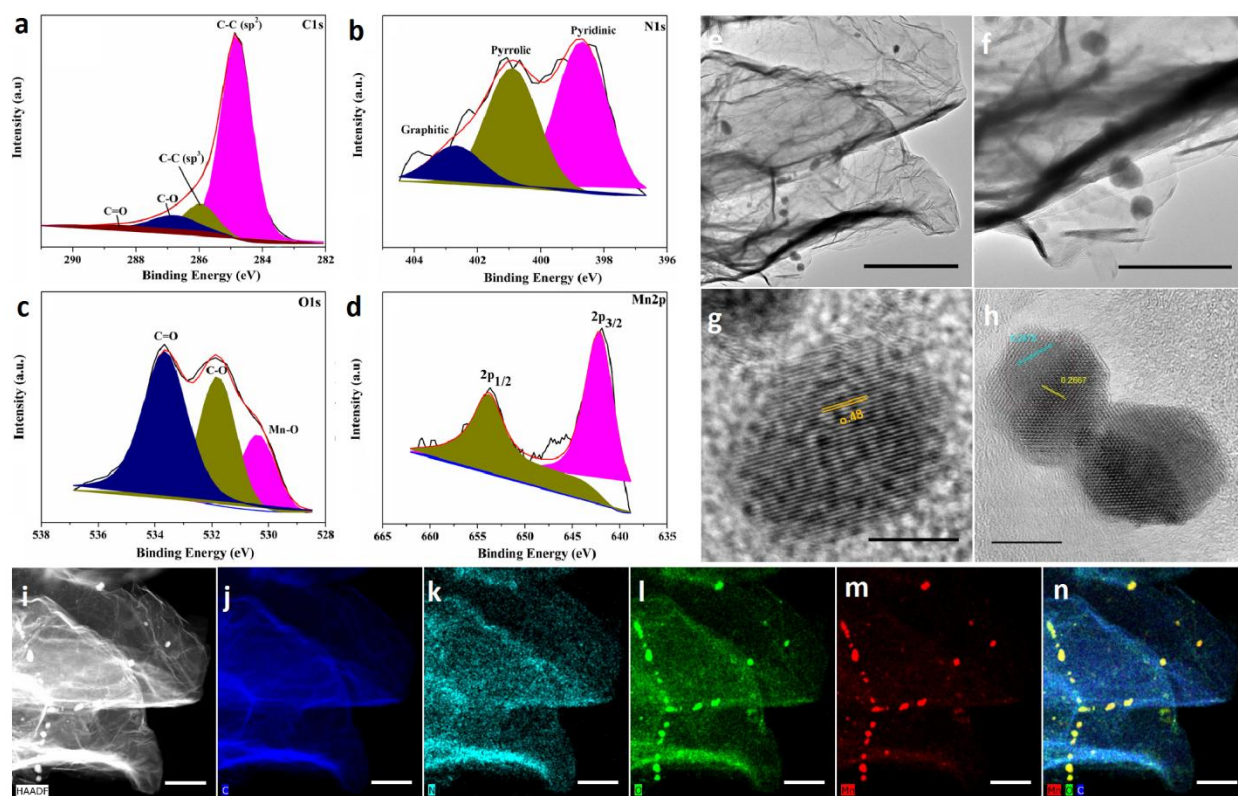


Figure 4.4. a-d) XPS spectra e-h) HRTEM images the Mn-Phen@G sample (Scale bars 500, 200, 10 and 10 nm respectively) i-n) showing HAADF image and elemental mapping of Mn, N, O, and C (Scale bars of 300 nm) in Mn-Phen@G.

Furthermore, X-ray photoelectron spectral (XPS) analysis of Mn-Phen@G catalyst revealed elemental compositions of C, N, O and Mn, which was found to be 90.8, 1.9, 6.4, and 0.9 at.%,

respectively. The high resolution XPS spectra of catalyst in C1s region can be deconvoluted in four peaks components with binding energy 284.7, 285.8, 286.5 and 288.3 eV corresponding to C-C sp^2 , C-C sp^3 , C-O/C-N, and C=O and O=C-O type of carbons with individual atomic % of 80.52, 10.57, 7.69 and 1.429, respectively, and then showing the graphitic nature of carbon material (Figure 4.4.a). The appearance of specific N1s peak component at 398.3, 399.8 and 401.2 eV confirms the presence of pyridinic (48.70%), pyrrolic (38.28%) and pyrolytic nitrogen (13.13%) shows the nitrogen-doped on Mn-Phen@G sample (Figure 4.4.b).⁹ The three peak components at 530.3, 531.8 and 533.6 eV in O1s spectra of material, originated due to the presence of C-O (51.38%), C=O (31.31%) and oxygen on the surface of cobalt (17.31%), which reveal that graphitic carbon is doped with oxygen (Figure 4.4.c). The presence of two-component peaks having binding energy at 642.07 (Mn $2p_{3/2}$) and 653.77 eV (Mn $2p_{1/2}$) confirm the presence of manganese having +4 oxidation state (Figure 4.4.d).¹⁰

HRTEM images of Mn-Phen@G nanocatalyst shows that spherical shape MnO_2 nanoparticles (30-60 nm) are supported on the surface of RGO (Figure 4.4.e and 4.4.f). The close interpretation of single MnO_2 nanoparticle shows the d-spacing of 0.247, 0.266 and 0.48 are related to α - MnO_2 space group (Figure 4.4.g and 4.4h). The elemental mapping of Mn-Phen@G nanocatalyst shows the presence of C, Mn, N and O, mapping, confirms uniform distribution of MnO_2 nanoparticles. This uniform distribution of the MnO_2 nanoparticles over the RGO matrix also demonstrates the fact that the functionalities at the RGO matrix interact strongly with the nanoparticles Figure 4.4.i-n).

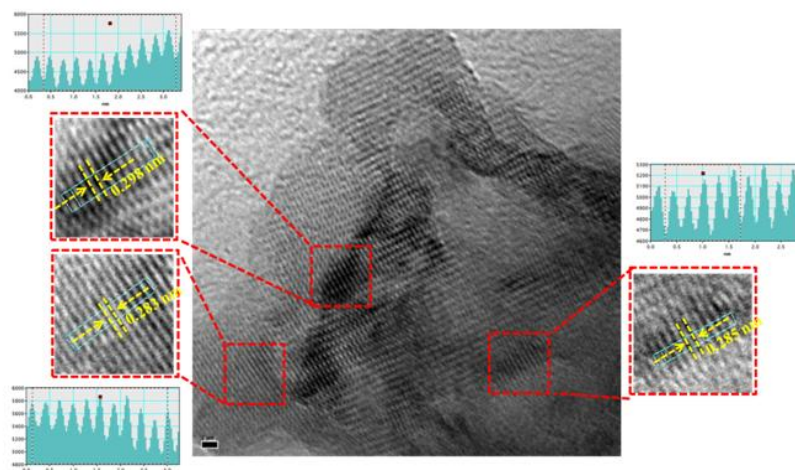


Figure 4.5. HRTEM images of Mn-Phen@G showing high-resolution lattice fringes of Mn_3O_4 (220) planes at the scale bar 5 nm.

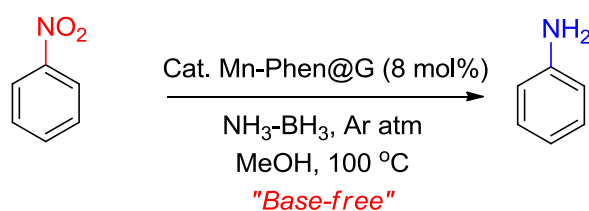
High-resolution transmission electron microscopy (HRTEM) image of the sample showed lattice fringes of 3.02 Å corresponding to the d spacing of (200) plane of Mn₃O₄ (Figure 4.5), and a d spacing of 2.54 Å corresponding to the d spacing of (111) plane of MnO phase.

Selected area electron diffraction (SAED) patterns were obtained for Mn-Phen@G catalyst as shown in Figure 4.3.b which clarifies the crystalline nature of the catalyst. The bright ring arises due to reflection from (111) plane of graphite, (222) plane of MnO, (211) plane of Mn₇C₃ which is in accordance with PXRD.

4.4. Result and Discussion

4.4.1. Optimization Table

Table 4.2: Optimization Studies



Entry	Cat.	Variation from the initial conditions	Conversion of nitrobenzene (%) ^b	Yield of aniline (%) ^b
1	Mn-Phen@G	none	99	97 (93) ^c
2	Mn-Phen@Al ₂ O ₃	none	30	20
3	Mn-Phen@SiO ₂	none	27	15
4	Mn-Phen@TiO ₂	none	20	15
5	Mn@G	none	15	8
6	Phen@G	none	0	0
7	—	without Mn-Phen@C	0	0
8	Mn(acac) ₃ /Phen	under homogeneous condition	0	0
9	Mn-Phen@G	HCO ₂ H+NEt ₃ (1:1) instead of AB	5	0
10	Mn-Phen@G	NaBH ₄ instead of AB	90	80
11	Mn-Phen@G	without AB	0	0
12	Mn-Phen@G	toluene instead of methanol	99	93 ^c
13	Mn-Phen@G	at 80 °C	99	94 ^c

^a Reaction conditions: nitrobenzene (0.25 mmol), AB (0.5 mmol), cat. Mn-Phen@G (8 mol%) and MeOH (2 mL) heated at 100 °C (oil-bath temperature) for 36 h under open argon atm. ^b Conversion of nitrobenzene and yield of aniline are based on GC. ^c Isolated yields.

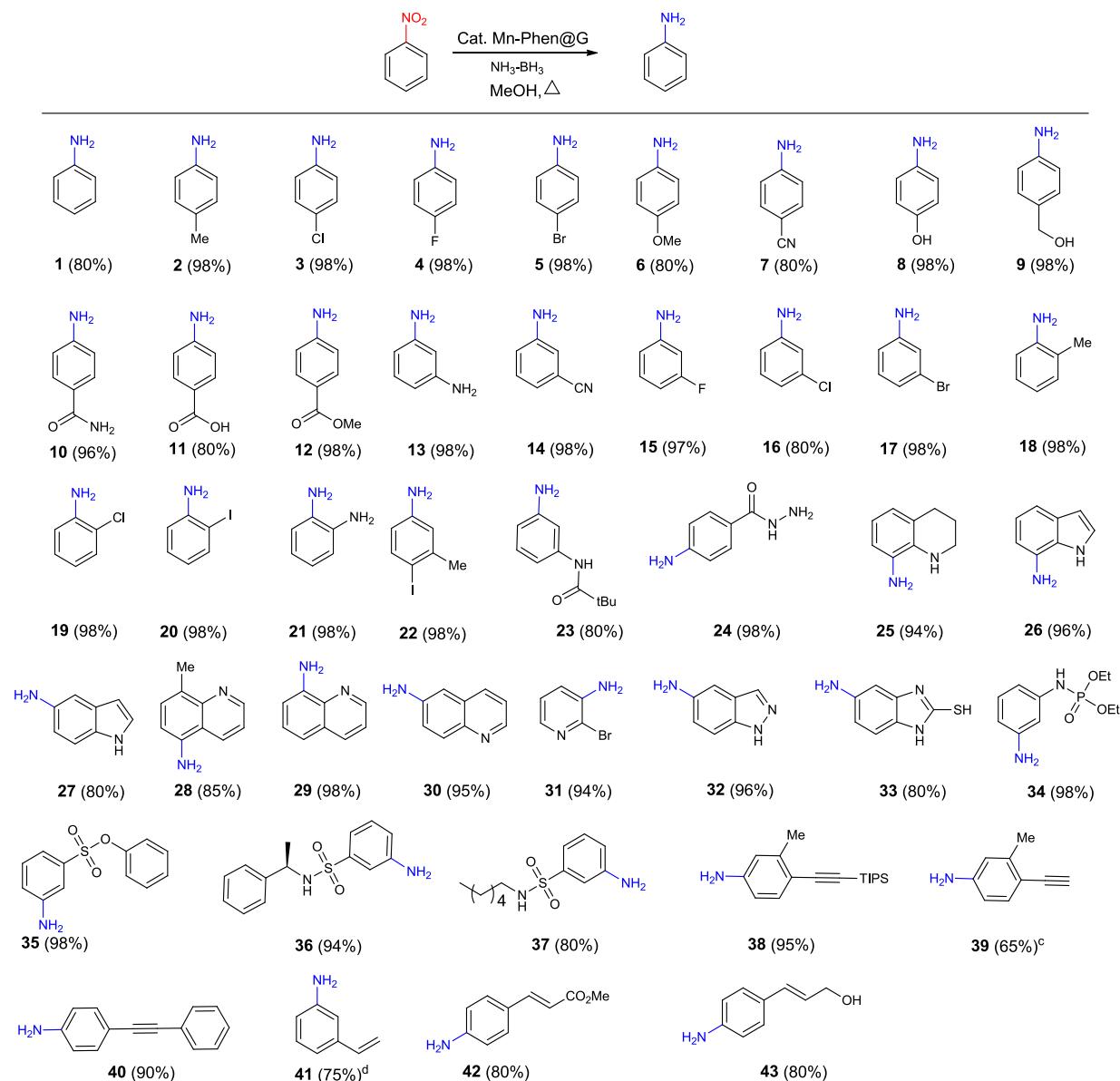
Optimization studies on Mn-catalyzed reduction of nitroarenes to anilines under additive-free conditions are summarized in Table 4.2. We began our investigation using nitrobenzene as the benchmark substrate in presence of catalytic amount of Mn-Phen@G (8 mol%), and AB in methanol heated at 100°C (bath temperature) under Ar atm for 24 h to yield aniline in 93% isolated yield with the complete conversion of nitrobenzene (Table 4.2, entry 1). The catalyst Mn-Phen@G prepared on other conventional supports such as SiO₂, Al₂O₃ and TiO₂ showed lesser activity in the aniline formation under the similar experimental conditions, (Table 4.2, entries 2-4). The control experiment revealed that no formation of hydrogenated product was observed in absence of the catalyst (Table 4.2, entry 7). Under homogeneous condition lower product yield was observed. The screening of different transfer hydrogenating sources such as a mixture of formic acid and triethylamine, sodium borohydride didn't yield the desired product. The variation of solvent showed that the reaction proceeds efficiently in methanol. In addition, no reaction occurred in the absence of AB.

4.4.2. Substrate scope of nitroarenes

With the optimized conditions established (Table 4.2.), the substrate scope was then investigated. As shown in table 4.3, the wide range of nitroarenes bearing different substituents and heteroarenes regardless of their electronic properties underwent chemo-selective hydrogenation reaction smoothly and gave the corresponding anilines in 75-99% yields. Some commonly encountered functional groups such as methoxy, and halides (-F, -Cl, -Br and -I) smoothly underwent hydrogenation reaction under mild reaction conditions and yielded the desired products in excellent yields, thus offers opportunities for further functionalization. Notable, nitrile (-CN) group which is sensitive for hydrogenation by using cobalt and manganese catalyst was chemo-selectively hydrogenated under optimal conditions in 80% yield.¹¹ The acidic functional groups were well tolerated including free (phenolic) alcohol (**8** and **9**), and acid (**11**) thus demonstrating that the anilines derivative could be further functionalized. Interestingly, the amide and ester groups are known to undergo hydrogenation under homogeneous manganese catalysis using PhSiH₃, were also well accommodated, resulting in a high yield of **12**, **23-24**.¹² The substituent at the *meta* position bearing electron-donating and electron-withdrawing groups afforded the corresponding products in good yield (Table 4.3, entries **13-17**). Furthermore, nitroanilines and *ortho*-substituted nitrobenzenes smoothly underwent transfer hydrogenation

under mild reaction conditions, with yields over 88% for the desired products (Table 4.3, entries 18–21).

Table 4.3. Substrate scope of nitroarenes

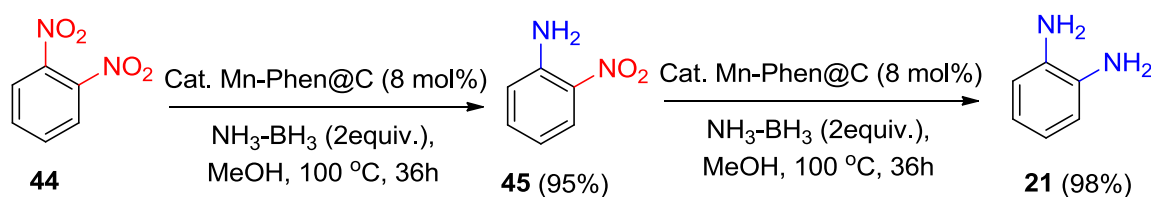


^aReaction conditions: Nitroarene (0.25 mmol), NH₃-BH₃ (2 equiv.), cat. Mn-Phen@G (8 mol%) Methanol at 100 °C for 36 h. ^bIsolated yields. ^cReaction temperature was 50 °C. ^dReaction temperature was 75 °C.

From a synthetic point of view, the retention of halides (-I) is very challenging in presence of heterogeneous catalysis because of it prone to undergo dehalogenation. To our delight, in present

reaction conditions the iodide group remains intact with selective hydrogenation of nitro group in excellent yield, it revealed that practical synthetic utility of heterogeneous manganese catalysis (Table 4.3, entries **20**, and **22**).¹³ The aromatic ring of the substrates could be *N*-Pivalate and *N*-condensed containing nitro arenes were also hydrogenated easily into corresponding amines in 80% and 98% yields (Table 4.3, entries **23-24**).

Furthermore, Mn-Phen@G catalyst also showed its advantages over noble metal-based catalysts on resistance to the poison effect of N or S atoms, and it didn't disturb the hydrogenation rate of corresponding substrates. To our delight, various substituted tetrahydroquinoline, indoles, quinolines, pyridine, indazole and benzimidazole which are very sensitive towards hydrogenations were selectively hydrogenated to corresponding amine derivatives furnishing the products in 70-95% yields (Table 4.3, entries **25-31**). We have also extended scope of reaction towards *N*-Phosphate, O-TS and (chiral or aliphatic) *N*-TS pertaining nitro groups were successfully underwent hydrogenation into corresponding amines in 80-98% high yields (Table 4.3, entries **33-37**). Gratifyingly, very challenging chemo-selective hydrogenation of nitro group in presence of sensitive internal and terminal alkynes underwent smoothly to give good to excellent isolated yields of expected product whereas sensitive groups remain intact during the hydrogenation (Table 4.3, entries **38-40**). The 3-nitro styrene, (*E*)-methyl 3-(4-nitrophenyl) acrylate and 4-nitro cinnamyl alcohol (Table 4.3, entries **41-43**) also underwent smooth chemo-selective reduction with retaining of double bond in the final product.



Scheme 4.3. Sequential reduction of 44

Selective reduction of dinitro group is very important in synthetic point of view and because of high reactivity of noble metals it can reduce both nitro group but our reaction condition **44** has been investigated and pleased to find that only one nitro group was reduced into the respective amine **45** in 95% yields without affecting the other nitro group.

4.4.3. Continuous Flow Setup

The batch process and chemoselective hydrogenation of nitroarenes was successfully extended to continuous flow process. Outstandingly, the reaction worked and yielded the aniline derivative in excellent yield in shorter reaction time.

Continuous Flow a Reaction conditions: 0.3 M solution of 1 in 25 mL MeOH + C₆H₅NO₂ (0.125 mmol) with the flow rate 0.08 mL/min and 0.3 M solution prepared from (NH₃:BH₃ in methanol) in 25 mL were flown with 0.08 mL/min through the 12 mL SS tubular reactor (Vaportec R-series) at 70 °C $t_R=9.3$ minute residence time.

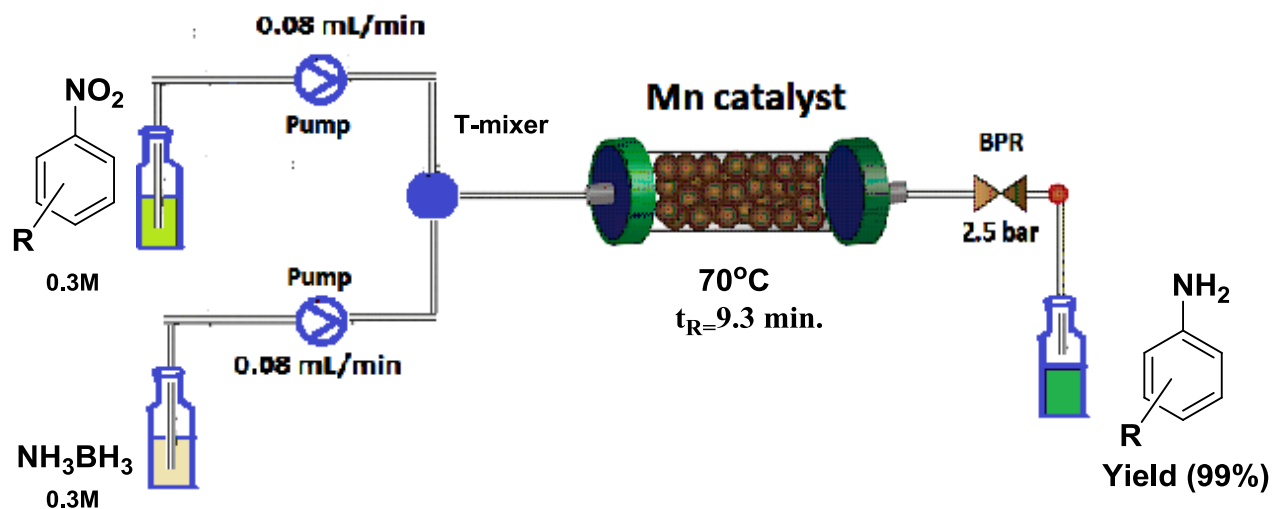


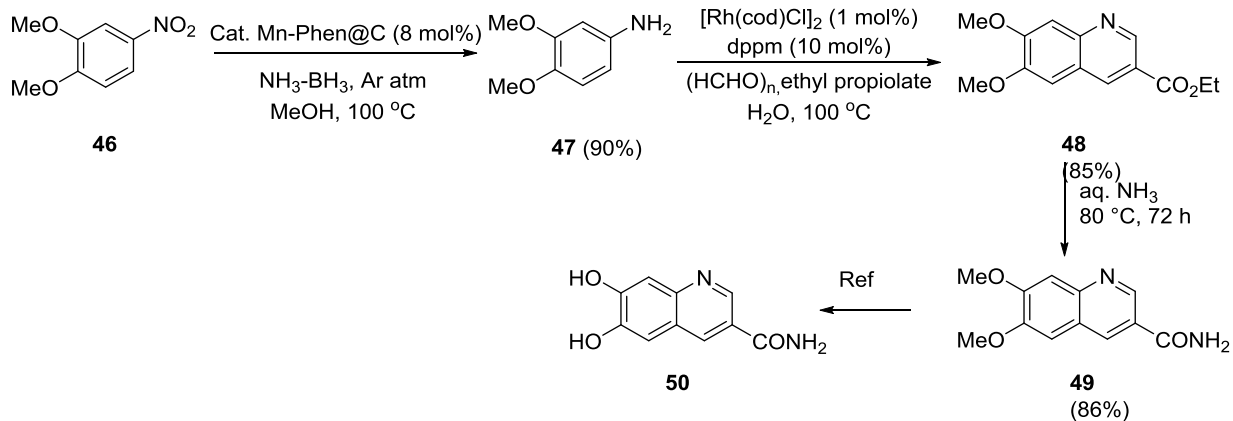
Figure 4.6 setup for continuous flow

4.4.4. Reaction under hydrogen pressure

Here we have also shown the efficient manganese catalyzed hydrogenation of nitro compounds under hydrogen pressure. This protocol operates at 30 bar hydrogen pressure at 100 °C. Nitrobenzene was successfully reduced to aniline under hydrogen pressure (yield 85%).

4.4.5. Application for drug synthesis

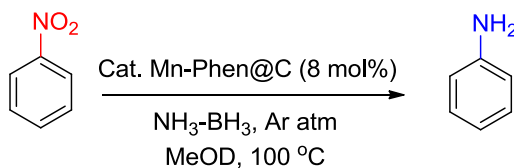
We have also designed a four-step synthetic protocol for 6,7-dihydroxyquinoline-3-carboxamide (**50**), a tyrosine kinase inhibitors (Scheme 4.4); which resulted in a 54% (overall) yield using our strategy.¹⁴



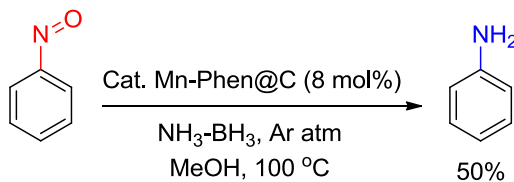
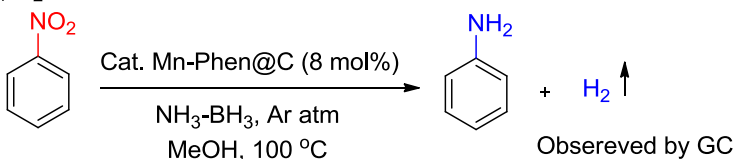
Scheme 4.4. Synthesis of a tyrosine kinase inhibitor

4.4.6. Mechanistic study.

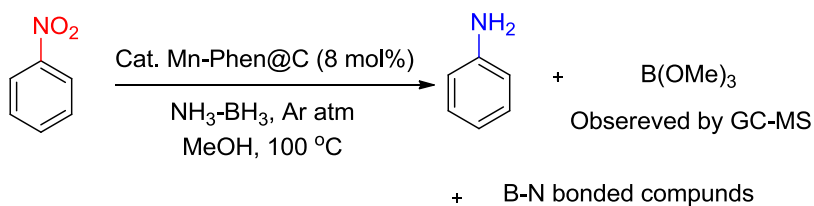
a) Labeling experiment



b) Isomerisation experiment

c) H₂ detection

g) Determination of the dehydrogenation product of AB



Scheme 4.5. Mechanistic study

To shed light on the mechanism, labeling experiment carried out under standard reaction condition in presence of CD_3OD as a solvent. It was observed that no deuterium was incorporated on the basis of ^1H NMR analysis which revealed that methanol does not act as a reductant. To know the reaction intermediate we carried out the reaction with nitrosobenzene under standard reaction condition we found that it can also undergo reduction with 50% yield. Again hydrogen gas generated during the reaction was detected by GC under optimized condition. To know the byproduct of AB during hydrogenation of nitrobenzene GC-MS was recorded which revealed the formation of $\text{B}(\text{OMe})_3$ as the only byproduct

4.4.6.1. EPR Study

To unveil the mechanism of the chemoselective reduction of nitroarenes initiated by the manganese-catalyst (Mn-phen@G) in MeOH solution, in combination with amino borane as transfer hydrogenating reagent, the EPR technique was employed using the spin-trapping technique. The 4-pyridyl-1-oxide-N tetrabutyl nitron (POBN) was used for such purpose as spin trapping agent. POBN was initially dissolved in MeOH together with the amino-borane reagent ($\text{NH}_3\text{-BH}_3$) and the solution warmed for 30 min at 60°C . Under these experimental conditions, we observed that the mixture (MeOH/ $\text{NH}_3\text{-BH}_3$ /POBN) without a catalyst is already capable to release a small amount of H^\bullet radicals, and those can be trapped by POBN, forming the POBN-H radical adduct. The recorded EPR trace ($T = 213\text{ K}$) is shown in Figure 4.6.a and although the EPR signal is very weak compared to the background noise is still possible to simulate the observed EPR trace and the derived spin-Hamiltonian parameters using third-order perturbation theory for the POBN-H radical species are given in Figure 4.6.b. The experimental g_{iso} of 2.0055 and estimated N and H-hyperfine coupling constants (hfcc, $\text{AN} = 15.90\text{ Gauss}$, $\text{AH} = 7.93\text{ Gauss}$) are found here in close similarity to those observed upon trapping H^\bullet radicals with PBN in water from solution of chloramine-T2 under light ($\text{AN} = 15.50\text{ Gauss}$, $\text{AH} = 8.75\text{ Gauss}$). When POBN was added to a solution containing the catalyst suspended in MeOH, after stirring.¹⁵ The reaction mixture (POBN/catalyst/ MeOH) for 30 min at 60°C and collection of the supernatant from centrifugation, the recorded solution EPR spectrum ($T = 213\text{ K}$) evidenced formation of a very strong EPR signal, with resonance, features consistent with POBN trapping a methoxy radical (MeO^\bullet). The MeO^\bullet radical species is therefore produced from the interaction of solvent molecules with the Mn-phen@C catalyst. Simulation of the observed EPR envelope of

the trapped POBN-OMe radical adduct gave the spin-Hamiltonian parameters shown in Figure 1d (g_{iso} of 2.0055, $A_{\text{N}} = 14.40$ Gauss, $A_{\text{H}} = 3.30$ Gauss), with N and H-*hfcc* very similar to those reported in literature by trapping $\text{MeO}\bullet$ radicals with the PBN spin trap in MeOH/water/peroxydisulfate mixture ($A_{\text{N}} = 14.50$ Gauss and $A_{\text{H}} = 2.94$ Gauss).¹⁵

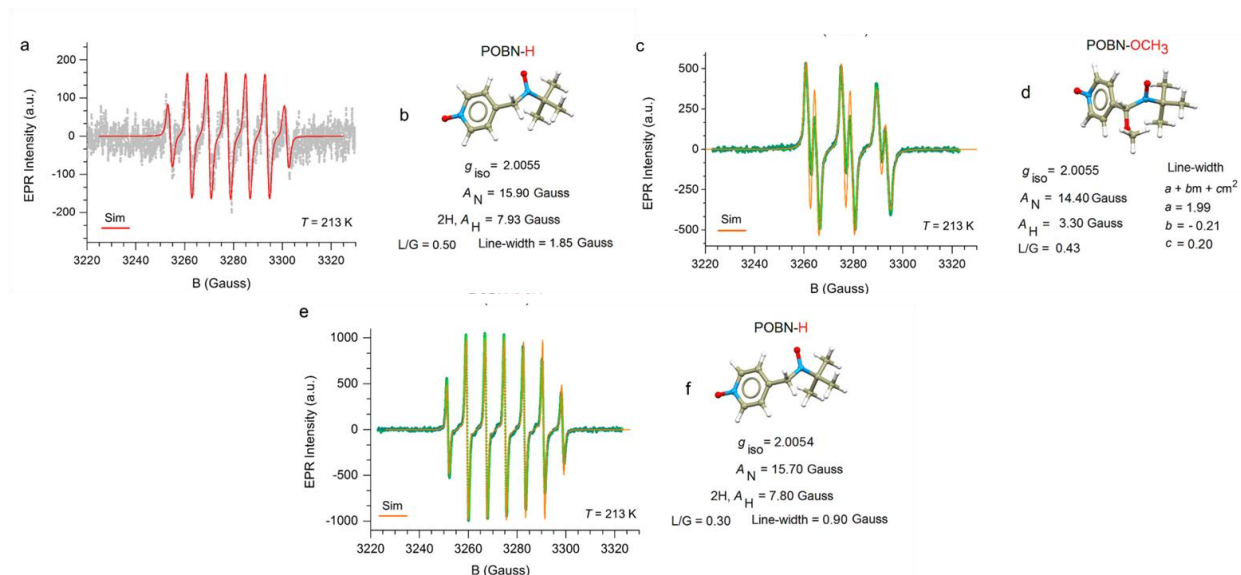
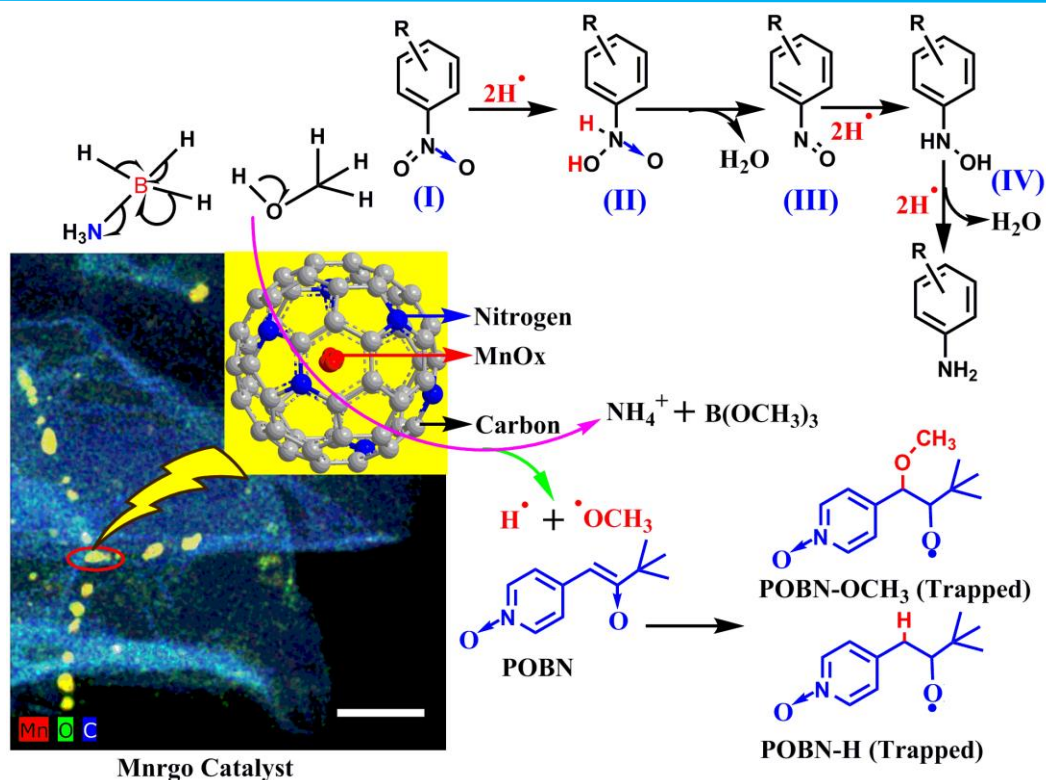


Figure 4.7. X-band (9.16-9.17 GHz) EPR spectra of the trapped radical species. (a) solution spectrum ($T = 213$ K) of the supernatant collected from the $\text{NH}_3\text{-BH}_3/\text{POBN}/\text{MeOH}$ mixture and its EPR simulation (Sim-trace). (c) solution spectrum ($T = 213$ K) of the supernatant collected from the Mn-phen@G catalyst/ POBN/MeOH mixture and its EPR simulation (Sim-trace). e, solution spectrum ($T = 213$ K) of the supernatant collected from the Mn-phen@G catalyst/ $\text{NH}_3\text{-BH}_3/\text{POBN}/\text{MeOH}$ mixture and its EPR simulation (Sim-trace). Panels b,d,f show the correspondent spin-Hamiltonian parameters derived from the simulation of the EPR envelopes shown in a,c and e, respectively. Experimental parameters: 100 KHz modulation frequency, 30 ms time constant, sweep time 1 min, and (a) 3.2 mW power, 2.5 Gauss modulation width, 11 scans accumulated and averaged; (c) 2.59 mW power, 3.0 Gauss modulation width, 21 scans accumulated and averaged; (e) 1.6 mW power, 1.0 Gauss modulation width, 11 scans accumulated and averaged



Scheme 4.8. Schematic Representation of Continuous Flow and Substrate Scope of Nitro compounds

4.4.7. Recyclability of the catalyst

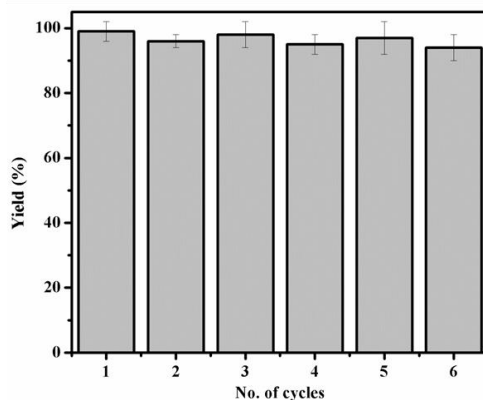


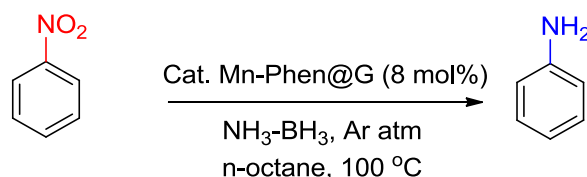
Figure 4.9. Recyclability experiments.

To an oven dried capped sealed tube (15 mL) Mn-Phen@G catalyst (25 mg, 8 mol%), nitro compounds (0.25 mmol), aminoborane (0.5 mmol) and methanol (2 mL) were added under argon atmosphere. The reaction tube was sealed. The reaction mixture was heated at 100 °C (bath temperature) with stirring. After cooling down the reaction mixture to room temperature the catalyst was separated from the reaction mixture by centrifugation and washed several times with

mesitylene. Obtained catalyst was dried under vacuum at 60 °C for 12 h. Then the catalyst was reused for the next cycle, and no deactivation of the material was observed up to four cycles. All yields (GC) are averages from at least 2 separate runs.

4.5. Experimental Details

4.5.1. General procedure for transfer hydrogenation of nitro compounds.



To an oven dried capped sealed tube (15 mL) Mn-Phen@G catalyst (25 mg, 8 mol%), nitro compounds (0.25 mmol), aminoborane (0.5 mmol) and methanol (2 mL) were added under argon atmosphere. The reaction tube was sealed. The reaction mixture was heated at 100 °C (bath temperature) with stirring. After cooling down the reaction mixture to room temperature the catalyst was separated from the reaction mixture by centrifugation and the reaction mixture was analyzed by GC and GC-MS. The supernatant was transferred to another flask, and the catalyst was washed with EtOAc (2 x 4 mL) and the washings were collected. The solvent was evaporated from the reaction mixture, and the crude product was subjected to silica gel column chromatography using EtOAc: petroleum ether to afford the product.

4.5.2. General Procedure for Hydrogenation

In a typical hydrogenation experiment, a stainless steel autoclave (450 mL) equipped with 50 mL high-pressure liquid charging chamber, pressure regulator, and a safety valve was used. Individual vials were charged with metal precursor Mn-phen@G (8 mol %) catalyst, solvent (1 mL), nitrobenzene substrate (0.25 mmol), and stirring bars in a glove box. The vials were transferred to an autoclave and the autoclave was purged three times with hydrogen gas before pressurizing it to the desired pressure. Suitable temperature (110 °C) and 30 bar pressure were maintained during the reaction. After completion of the reaction, the autoclave was cooled to 0 °C, and excess gas was vented off in a well-ventilated fume-hood. The conversion and regioselectivity were determined by using gas chromatography (GC) and proton NMR.

4.6 Conclusion

In conclusion, a robust N-doped Mn-Phen@G stable nanocatalyst has been designed and synthesized by using Manganese precursor and 1,10-phenanthroline ligand. The catalyst delivered excellent performance (yield, and selectivity) for the catalytic transfer hydrogenation of nitro compounds to aniline. The reaction operates under mild, neutral conditions, with no additives being required. This nanocatalyst performs outstandingly with a six-run recycling test. The strategy works, under the very mild condition, and to the best of our knowledge there is no report on dehydrogenation of ammonia borane (AB) and subsequent chemo-selective hydrogenation of nitroarenes to anilines either under homogeneous and heterogeneous conditions.

4.7. References

1. (a) R. S. Downing, P. J. Kunkeler and H. Van Bekkum, *Catal. Today*, 1997, **37**, 121-136; (b) U. Blaser, H. Steiner and M. Studer, *ChemCatChem*, 2009, **1**, 210-221.
2. (a) R. M. Bullock, *Science*, 2013, **342**, 1054-1055; (b) F. A. Westerhaus, R. V. Jagadeesh, G. Wienhofer, M.-M. Pohl, J. r. Radnik, A.-E. Surkus, J. Rabeah, K. Junge, H. Junge and M. Nielsen, *Nat. Chem.*, 2013, **5**, 537-543; (c) Y. g. Wu, M. Wen, Q. s. Wu and H. Fang, *J. Phys. Chem. C*, 2014, **118**, 6307-6313; (d) R. V. Jagadeesh, A.-E. Surkus, H. Junge, M.-M. Pohl, J. r. Radnik, J. Rabeah, H. Huan, V. Schunemann, A. Bruckner and M. Beller, *Science*, 2013, **342**, 1073-1076; (e) D. Cantillo, M. Baghbanzadeh and C. O. Kappe, *Angew. Chem., Int. Ed.*, 2012, **51**, 10190-10193.
3. (a) D. Pinggen, C. Muller and D. Vogt, *Angew. Chem., Int. Ed.*, 2010, **49**, 8130-8133; (b) H. Imai, T. Nishiguchi and K. Fukuzumi, *Chem. Lett.*, 1976, **5**, 655-656; (c) Y. Watanabe, T. Ohta, Y. Tsuji, T. Hiyoshi and Y. Tsuji, *Bull. Chem. Soc. Jpn.*, 1984, **57**, 2440. C. L. Sun, B. J. Li and Z. J. Shi, *Chem. Rev.* 2011, **111**, 1293–1314.
4. (a) K. Junge, B. Wendt, N. Shaikh and M. Beller, *Chem. Commun.*, **46**, 1769-1771; (b) G. Wienhofer, I. n. Sorribes, A. Boddien, F. Westerhaus, K. Junge, H. Junge, R. Llusar and M. Beller, *J. Am. Chem. Soc.*, **133**, 12875-12879; (c) R. V. Jagadeesh, A.-E. Surkus, H. Junge, M.-M. Pohl, J. r. Radnik, J. Rabeah, H. Huan, V. Schunemann, A. Bruckner and M. Beller, *Science*, **342**, 1073-1076; (d) R. V. Jagadeesh, G. Wienhofer, F. A. Westerhaus, A.-E. Surkus, M.-M. Pohl, H. Junge, K. Junge and M. Beller, *Chem. Commun.*, **47**, 10972-10974; (e) Dey, N. Mukherjee, S. Ahammed and B. C. Ranu, *Chem. Commun.*, **48**, 7982-7984; (f) U. Sharma, P. K. Verma, N. Kumar, V. Kumar, M. Bala and B. Singh, *Chem. Eur. J.*, **17**, 5903-5907; (g) U. Sharma, N. Kumar, P. K. Verma, V. Kumar, B. Singh, *Green Chem.*, 2012, **14**, 2289–2293; (h) V. Kumar, U. Sharma, P. K. Verma, N. Kumar and B. Singh, *Adv. Synth. Catal.*, 2012, **354**, 870-878. A. Quintard and J. Rodriguez, *Angew. Chem. Int. Ed.* 2014, **53**, 4044-4055.
5. (a) W. Liu, J. T. Groves, *Acc. Chem. Res.* 2015, **48**, 1727–1735; (b) A. Gunay and K. H. Theopold, *Chem. Rev.*, 2010, **110**, 1060-1081.
6. (a) S. Elangovan, J. Neumann, J.-B. Sortais, K. Junge, C. Darcel and M. Beller, *Nat. Commun.*, 2016, **7**, 12641; (b) M. Mastalir, M. Glatz, N. Gorgas, B. Stoger, E.

-
- Pittenauer, G. n. Allmaier, L. F. Veiros and K. Kirchner, *Chem. Eur. J.*, 2016, **22**, 12316-12320.
7. Ammonia-borane ($\text{NH}_3\text{:BH}_3$), an easy to prepare and manipulate solid, has attracted interest as a potential dihydrogen (H_2) storage material, see: (a) C. W. Hamilton, R. T. Baker, A. Staubitz and I. Manners, *Chem. Soc. Rev.*, 2009, **38**, 279-293; (b) A. Staubitz, A. P. M. Robertson and I. Manners, *Chem. Rev.*, 2010, **110**, 4079-4124; (c) J. Yang, A. Sudik, C. Wolverton and D. J. Siegel, *Chem. Soc. Rev.*, 2010, **39**, 656-675; (d) H. L. Jiang and Q. Xu, *Catal. Today*, 2011, **170**, 56-63.
8. (a) J. X. Guo, Y. F. Qu, S. Shu, X.-J. Wang, H.-Q. Yin and Y.-H. Chu, *New Journal of Chemistry*, 2015, **39**, 5997-6015; (b) 49 F. T. Wang, Y. C. Wu and T. G. Wang, *Adv. Funct. Mater.*, 2007, **38**, 2062–2065.
9. (a) J. R. Pels, F. Kapteijn, J. A. Moulijn, Q. Zhu and K. M. Thomas, *Carbon*, 1995, **33**, 1641-1653; (b) S. Stankovich, D. A. Dikin, R. D. Piner, K. A. Kohlhaas, A. Kleinhammes, Y. Jia, Y. Wu, S. T. Nguyen and R. S. Ruoff, *Carbon*, 2007, **45**, 1558-1565.
10. (a) M. Meng, S. X. Wu, L. Z. Ren, W. Q. Zhou, Y. J. Wang, G. L. Wang and S. W. Li, . *J. Appl. Phys.*, 2014, **116**, 173911; (b) S. Rong, P. Zhang, Y. Yang, L. Zhu, J. Wang and F. Liu, *ACS Catal.*, 2017, **7**, 1057-1067.
11. (a) J. Long, K. Shen and Y. Li, *ACS Catal.*, 2016, **7**, 275-284; (b) Z. Shao, S. Fu, M. Wei, S. Zhou and Q. Liu, *Angew. Chem. Int. Ed.*, 2016, **55**, 14653-14657; (c) F. Kallmeier, T. Irrgang, T. Dietel and R. Kempe, *Angew. Chem. Int. Ed.*, 2016, **55**, 11806-11809.
12. C. M. Kelly, R. McDonald, O. L. Sydora, M. Stradiotto and L. Turculet, *Angew. Chem. Int. Ed.*, 2017, **129**, 16117-16120.
13. L. Zhou, H. Gu and X. Yan, *Catal. Lett.*, 2009, **132**, 16-21.
14. (a) S. P. Midya, M. K. Sahoo, V. G. Landge, P. R. Rajamohan and E. Balaraman, *Nat. Commun.*, 2015, **6**, 8591; (b) T. R. Burke Jr, B. Lim, V. E. Marquez, Z. H. Li, J. B. Bolen, I. Stefanova and I. D. Horak, *J. Med. Chem.*, 1993, **36**, 425-432.
15. A. Ledwith, P. Russell and L. H. Sutcliffe, *Proc. R. Soc. Lond. A*, 1973, **332**, 151-166.
16. J. C. Evans, S. K. Jackson, C. C. Rowlands and M. D. Barratt, *Tetrahedron*, 1985, **41**, 5191-5194.
-

Chapter 5

**Fe Based nanocatalyst for the partial hydrogenation of
CO₂ to CO**

5.1. Introduction

Climate change and global warming is one of the most concerned issue for the scientific community, industries and environmental agencies.¹⁻² CO₂ is the main active component of green house gas which leads to increase in atmospheric temperature. CO₂ Utilization by catalytic conversion to value-added products is an important technological frontier with a high potential to address both energy and environmental pollution crises.³⁻⁵ In response to the suppress the demand of carbon foot prints across the globe, an immense research output is evident in this field focusing on the chemical conversion of CO₂ to hydrocarbons, syngas, organic carbonates and urethanes.⁶⁻⁹ CO₂ is a highly stable molecule and shows very less reactivity which makes the hydrocarbon production from CO₂ very strenuous process. Another important strategy to utilize CO₂ is to produce CO₂-containing syngas (CO₂+SG) that can be used as a feed in Fischer Tropsch synthesis, CAMERE process, and fuel cells.¹⁰⁻¹¹ Traditionally syngas is produced by steam reformation of natural gas, biomass or coal.¹²⁻¹³ Syngas produced by above process contains impurities of CH₄, NO_x, H₂S and traces of metals depending on the source.¹⁴ One of the efficient routes to produce CO₂+SG is by partial reduction of CO₂ through reverse water gas shift reaction (RWGS).¹⁵⁻¹⁶ Therefore, it would be an advantageous to produce CO₂+SG from CO₂ with high purity and reliable composition rather than purifying the syngas produced *via* steam reformation of fossil fuels. Mostly RWGS reaction has been explored with Mo, Co, Fe, Ni, and Cu.¹⁷⁻²⁰ The above catalyst shows selectivity towards CO in the range between 30-90%. Iron can be a promising RWGS catalyst because of its high thermal stability, earth-abundance, low cost and high activity over a wide range of reaction temperature.²¹ A wide range of the already known iron-based catalyst selectively converts CO₂ to hydrocarbon.²² According to the prior art in most of the case, Fe₃O₄ catalyzes the formation of higher hydrocarbons in addition to the formation of CO. However, it suffers from deactivation of the catalyst with time. There are limited reports based on iron for the selective conversion of CO₂ to CO.

In the present work iron nanoparticles supported on graphene has been explored for the selective conversion of CO₂ to CO. In recent year catalysis is mostly focused on supported metal nanocatalyst due to its high surface area, chemical reactivity, dispersion of nanoparticles and unique structure. Thermal decomposition of metal salt is a well-known synthesis technique adopted in solid state chemistry to synthesize supported nanoparticles.²³ The above method

offers an efficient way to control the particle size and electronic environment of Fe-rich phases by changing the organometallic precursor. As per the previous study, the electronic environment around the metal nanoparticles can be changed by doping a ligand containing heteroatoms.²⁴⁻²⁵ We have used exfoliated graphene oxide as a support instead of Vulcan carbon which is mostly used as a carbon support. Several iron-based catalysts were synthesized and tested for the reactivity. The catalysts with specific metal to ligand ratio showed an unusual enhancement in the RWGS activity with excellent stability and an unprecedented selectivity to CO in comparison to conventional Iron catalysts. It has been observed that Fe-based catalysts in Fischer-Tropsch reaction using syngas with a distinct CO₂:CO ratio operates with improved life time due to lesser deposition of carbon on the catalyst.²⁶

5.2. Statement of problem

As per literature survey, various types of catalyst have been reported for catalytic conversion of CO₂ to CO *via* thermal, photochemical and electrochemical procedure. Mostly noble metals such as Pt, Pd, Au and Cu have been reported to catalyze RWGS under the H₂ stream. Therefore it is highly demanding to discover 3d-transition metal catalyst for this transformation, to make it more economically viable. A well designed and engineered material with good stability and its capability to activate highly inner CO₂ molecule would be a better choice for chemical conversion of CO₂.

5.3. Catalyst Synthesis and Characterization

In the previous chapter 2, we have synthesized and studied iron-based heterogeneous catalyst for dehydrogenation reaction, in which metal: ligand ratio we maintained to 1:1. However, in the present chapter, we have tested above material for hydrogenation reaction and M:L ratio was also varied to check its effect on catalytic activity. Above material was tested for the selective hydrogenation of CO₂ to CO. In this present chapter, the catalyst was synthesized as per the procedure described in chapter 2. The catalytic material presented in this study labeled as FeNGR

5.3.1. Catalyst Characterization

The active catalyst and other standard catalyst were characterized by several tools such as PXRD, SEM, TEM, XPS and Raman analysis to see the structural activity correlation. To understand the different phases of iron in the catalytic material PXRD was analyzed for Fe_2O_3 , FeGr and FeNGR-1:3 catalysts (Figure 5.1). On careful analysis, it has been observed that iron nanoparticles deposited on graphene is forming extensive intermix phases of Fe_7C_3 , Fe_3N , Fe_2O_3 and Fe_3O_4 . Pure Fe_3O_4 nanoparticles were showing crystalline phases belongs to Fe_3O_4 only (Figure 5.1, trace 3). In case of FeGR intermix phases of Fe_7C_3 , Fe_2O_3 and Fe_3O_4 have been seen. In a similar way, as expected in the FeNGR-1:3 catalyst Fe_3N was also seen which is due to the incorporation of nitrogen-containing ligand.

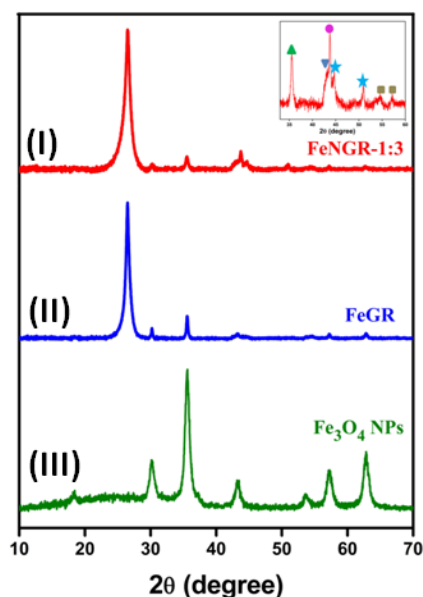


Figure.5.1. PXRD of FeNGr-1:3 (I), FeGr catalyst (II) and Fe_3O_4 (III) catalyst.

TEM images of Fe_3O_4 , FeGR and FeNGR-1:3 were given in Figure 5.2 to do the comparative analysis. It is clear from the TEM image that Fe_3O_4 catalyst is having size in the range of 15-20 nm, giving 6.3% conversion. While iron nanoparticles supported on graphene (FeGR) is having size in the range 20-200 nm, giving 12% conversion. On careful analysis, it has been seen in the TEM analysis that, as the nitrogen was doped in the catalyst, the catalyst started forming core-shell structure with uniform distribution of nanoparticles over graphene surface. The detailed analysis of core-shell morphology is discussed in chapter 2 and is under progress. Other

characterization such as XPS, EDX, Raman of the active catalyst is already discussed in chapter 2a.

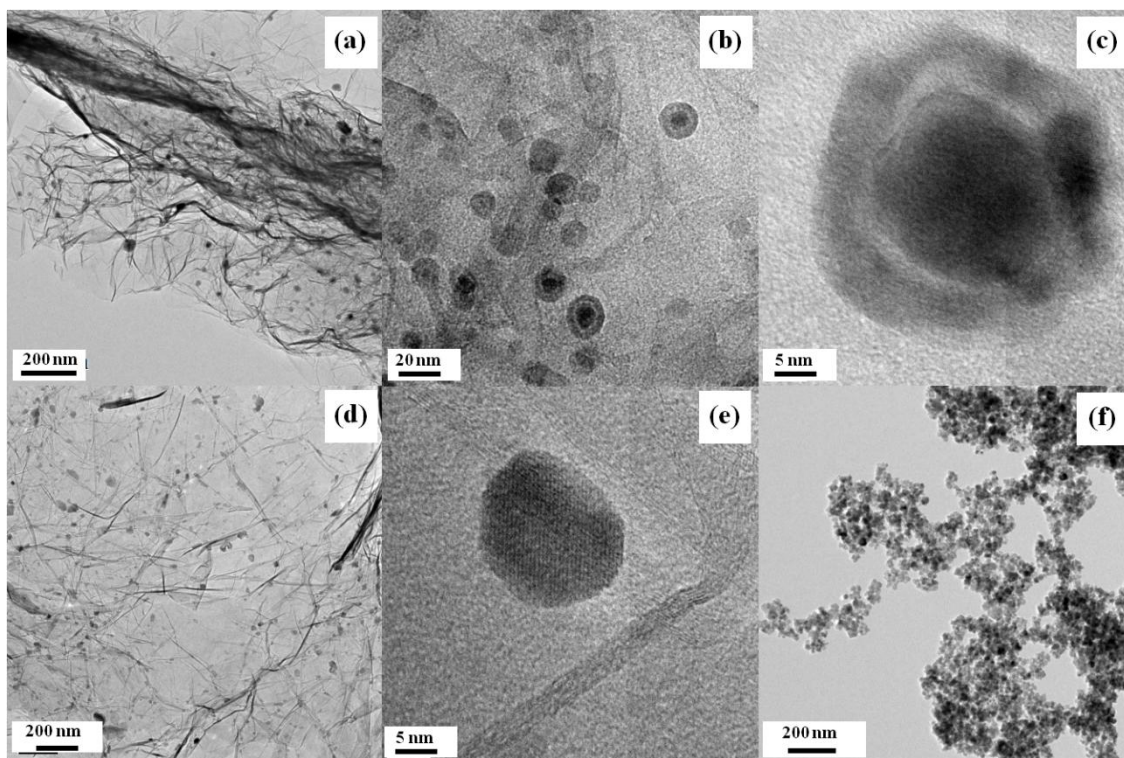


Figure. 5.2 (a), (b), (c), TEM image of FeNGR-1:3 at 200 nm, 20 nm and 5 nm respectively, (d), (e) TEM image of FeGR at the scale of 200 nm and 5 nm respectively, and (f) TEM image of Fe_3O_4 .

5.4. Result and Discussion

5.4.1. Catalytic performance of catalysts

Catalytic performances of the catalysts in RWGS were tested and the results are tabulated in Table 5.1. Fe-GR, Fe_3O_4 and FeNGR (1:1, 1:3 and 1:5) were tested for reactivity in which FeNGR (1:3) (entry 3) showed good activity towards RWGS with a high selectivity towards CO (97.2%).

Table 5.1. Iron time yield (FTY), CO₂ Conversion and Selectivity of different iron catalyst.

Entry No.	Catalyst	FTY mol g ⁻¹ sec ⁻¹ (10 ⁻⁴)	CO ₂ Conversion (%)	Selectivity (%)		
				CO	CH ₄	C ²⁺
1	FeGR	10.4	12.1	72.5	26.9	0.6
2	FeNGR-1:1	13.9	14	93.2	6.6	0.2
3	FeNGR-1:3	16.5	17.5	97.2	2.8	0.0
4	FeNGR-1:5	6.9	7.5	95.6	4.4	0.0
5	Fe ₃ O ₄ NPs	1.1	6.3	65.1	32.6	2.3
6*	FeNGR-1:3	-	0.0	-	-	-

The RWGS was studied over the reduced iron graphene catalyst between 300 to 500 °C temperature, under 5800 h⁻¹ gas hourly space velocities and atmospheric pressure condition. Under the studied reaction condition carbon monoxide (CO) was the main product and only very small amount of methane (CH₄) has been observed as a function of temperature. The catalytic behavior of the different iron catalyst (FeNGR, FeGR, Fe₃O₄) has been shown in Figure 5.3 as a function of reaction temperature, in which FeNGR-1:3 has shown maximum activity. It has been observed that CO₂ conversion has been increased with increase in the temperature in all the studied catalyst. The most active FeNGR-1:3 catalyst has achieved 17.5% conversion at 450 °C, a value near to expected from the thermodynamic equilibrium at this condition. However, Fe₃O₄ nanoparticles show only 6.2% conversion under same reaction condition. We have also studied the effect of different support and quantitative effect of the ligand with respect to metal for RWGS reaction. Catalyst prepared by decomposition of iron organometallic complex on graphene surface (FeGR) has shown 12.1% conversion at 450 °C. As the nitrogen-containing ligand has been incorporated into the system, conversion and selectivity got increased. Similarly, to show the effect of nitrogen-containing ligand, the metal to ligand ratio has been changed. As

ratio of metal to nitrogen-containing 1,10-phenanthroline ligand has been increased, catalytic conversion got increased from 14% (FeNGR-1:1) to 17.5% (FeNGR-1:3); however, after certain limit further increase in the metal to ligand ratio was not effective as conversion got decreased from 17.5% (FeNGR-1:3) to 7.5% (FeNGR-1:5). On selectivity point of view at 450 °C, FeNGR-1:3 showed 97.2% selectivity for CO, which is slightly higher than other nitrogen contain Fe catalyst (FeNGR-1:1, FeNGR-1:5). Iron catalysts which were not chelated with ligand such as (FeGR) and Fe₃O₄ nanoparticles show low to moderate selectivity for RWGS. Above results show the crucial role of nitrogen ligand for tuning the selectivity towards CO.

In the previous section, it was clearly observed by TEM data that ligand has a significant role in the catalyst composition, its morphology and its activity. for CO production. An apparent activation energy of 45 KJ/mol for FeNGR-1:3 was calculated from Arrhenius plot at the low-temperature regime (300-400 °C).

Figure 5.3 d shows the CO₂ conversion and CO selectivity variation under different gas hour space velocity (GHSV) condition for FeNGR-1:3 catalyst. At 450°C, under a GHSV of 11600 h⁻¹, a decrease of CO₂ conversion to 13.4% was observed; however, selectivity toward CO reached nearly 99%. However, decrease in GHSV to 3000 h⁻¹, not much affected CO₂ conversion (18.1%) and selectivity (97%).

In a separate experiment a fresh FeNGR-1:3 sample was treated with Ar and H₂ at 500°C for 3h (Table 5.1, entry 6). During the treatment, no CO was detected in the effluent. This result confirms the stability of graphene support under reaction condition; however, if graphene is not stable under the given reaction condition, it will produce quantitative amount of CO. As discussed in experimental section the Ar treatment at 800°C produce a partial transformation of Fe-ligand complex to iron carbide over graphene.

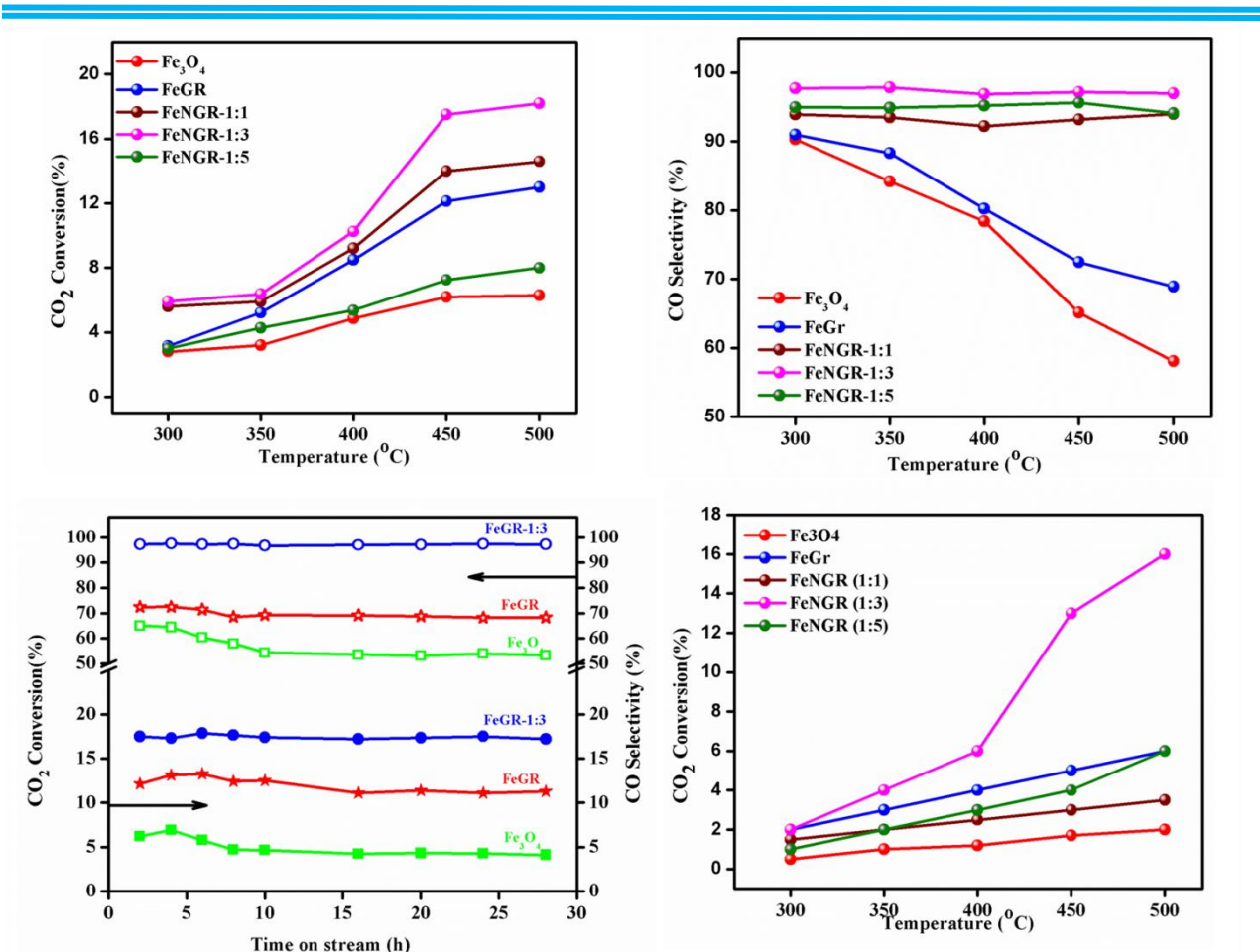


Figure 5.3. (a) Catalytic conversion of CO₂ with respect to temperature, (b) CO selectivity with respect to temperature, (c) Catalytic conversion and CO selectivity with respect to time, (d) Activation energy against temperature (K) for different iron-based catalyst.

In order to verify the stability of the catalysts (Fe₃O₄ NPS, FeGR and FeNGR-1:3) under RWGS reaction conditions, a separate experiment was carried for a longer time (GSHV of 5400h⁻¹ and 450 °C.). Figure 5.3 (c) shows the CO₂ conversion and selectivity towards CO as a function of reaction time. It is clear from the graph that CO₂ conversion has been decreased drastically from 6.3% to 4.7% for Fe₃O₄ NPS after 8h. However, under the same reaction condition FeGR catalyst has shown slightly decrease in the activity initially from 12.1% to 11.5% after 24h of reaction. However, FeNGR-1:3 has shown excellent stability for 28h under the given reaction condition and maintained the conversion to 17.5% and CO selectivity (99%).

Figure 5.4 shows the TEM images of different iron-based catalyst after the reaction. It is clear from the images that Fe_3O_4 NPS (Figure 5.4) showed a drastic change in morphology after RWGS reaction. It got agglomerated in the given reaction condition and average particle size increased to 60 nm. In case of FeGR and FeNGR-1:3 used iron nanoparticles was intacted on the surface of graphene even after the reaction and core-shell morphology was also retained. These results are in comparison to the CO selectivity over time on stream under reaction condition.

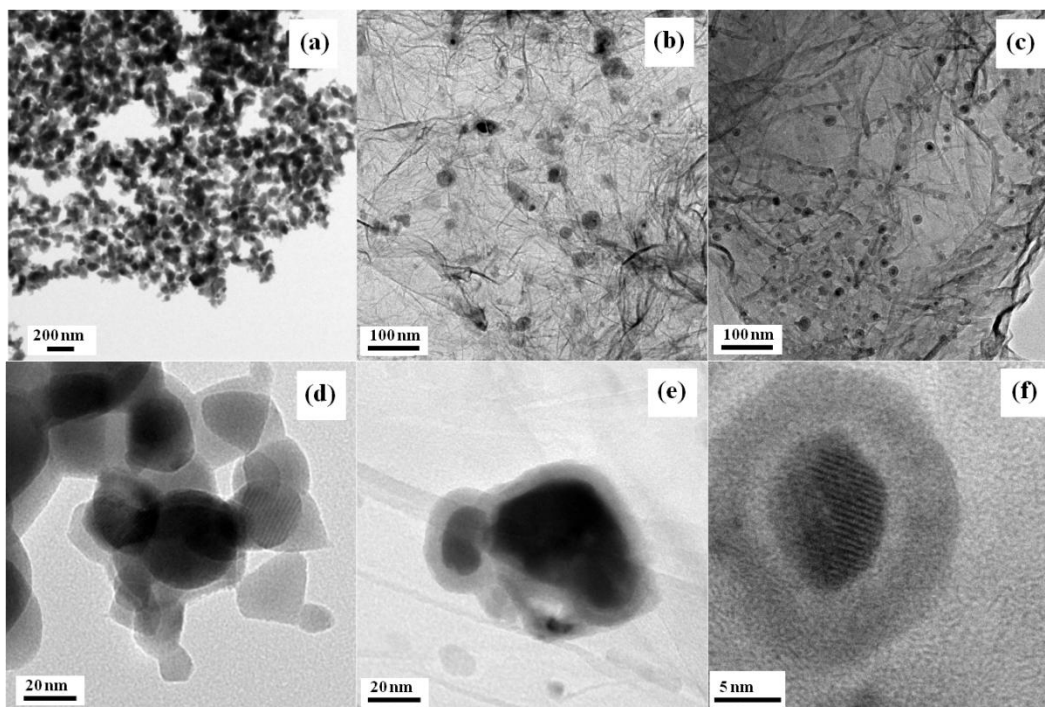


Figure 5.4 TEM images of spent catalyst (a) Fe_3O_4 , (b) FeGR, and (c) FeNGR-1:3 at low magnification; (d) Fe_3O_4 , (e) FeGR, and (f) FeNGR-1:3 at higher magnification.

It is also in correlation with activity, as it has been seen in RWGS reaction that nitrogen doping has influenced the conversion and selectivity in the given reaction condition. In the similar way it has been observed from the TEM images that nitrogen doping in FeNGR-1:3 catalysts promotes the formation of a new structure having the core-shell type of morphology. The iron nanoparticles in FeNGF-1:3 catalyst were uniformly distributed spherical in shape and forming a core-shell type of structure. On magnification, it has been observed that after nitrogen incorporation, nanoparticles are forming a core-shell type of structure which was not observed in the case of FeGR catalyst. It may be concluded that the core-shell type of morphology has strong correlation with the high conversion and high selectivity for CO.

5.5. Experimental section

5.5.1 Activity Test

Hydrogenation of CO₂ was carried out in a long tube quartz tube reactor installed in Carbolite tube furnace that can be heated to a high temperature range. A standard 100 mg of the catalyst has loaded for catalytic testing and the catalyst were activated in the same reactor under a 10 mL/min H₂ flow (Purity >99.999 %) hydrogenation at 450°C at atmospheric pressure for 2 h before the CO₂ and then cooled down up to 400 °C and subsequently CO₂ hydrogenation started by switching the gas ratio CO₂:H₂ (1:2) with the total flow rate of 6 SCCM (CO₂ > 99.995 %) to the reaction temperature of 450°C. Two Alicat MFC (MC-100SCCM-D) installed to control the flow of H₂ and CO₂. A Nucon 5765 GC was installed for the online gas phase analysis of product which equipped with Porapak-Q packed column attached to TCD for detection of CO₂, CO and CH₄ and HP-PLOT Q capillary column attached to FID for hydrocarbon detection. A condenser was set in place on the outlet of the reactor to condensed water vapor formed during the course of the reaction. The conversion is reported as mole % of CO₂ converted into product and it is determined by dividing the carbon mole converted including all the product to the carbon mole injected as CO₂. Selectivity is simply calculated by the number of moles of a particular product formed divided by the total number of moles of the entire product. FTY has reported as the number of moles of product formed per gram of iron loading per second of the reaction and the absolute amount of Iron present in the catalyst determined by ICP-AES analysis.

5.6 Conclusion

Iron nanocatalyst having core-shell type of morphology has been efficiently used for the selective reduction of CO₂ to CO under moderate and practical condition. The core-shell structure supported on graphene attributed to the synergistic interaction between the metal and graphitic carbon. Furthermore, the electron-rich nitrogen ligand plays a crucial role in the formation of active catalyst (for the reduction of CO₂). In short nitrogen doped iron graphene catalyst could be considered as an economically viable, highly efficient and selective catalyst for CO production from CO₂ via the reverse water gas shift reaction. The activity result makes a significant contribution to the green transformation of CO₂ as a renewable resource. It is very interesting that the while changing the M:L ratio from 1:1 to 1:3, we have observed the core-

shell structure vary clearly. After several hours of the reaction, the microstructure (i.e, core-shell structure) was retained. Above catalytic material has shown excellent activity and selectivity for the hydrogenation of CO₂ to CO with FeNGR-1:3 (Fe:L ratio in 1:3). Further analysis is under progress in our laboratory.

5.7. References

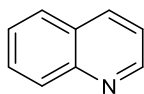
1. O. S. Joo, K.-D. Jung, I. Moon, A. Y. Rozovskii, G. I. Lin, S.-H. Han and S.-J. Uhm, *J. Ind. Eng. Chem.*, 1999, **38**, 1808-1812.
2. Y. K. M. Kerry, C. Igor, G. Joseph and T. S. C. Edman, *ChemSusChem*, 2008, **1**, 893-899.
3. Q. Liu, L. Wu, R. Jackstell and M. Beller, *Nat. Commun.*, 2015, **6**, 5933.
4. N. Z. Muradov and T. N. Veziroğlu, *Int. J. Hydrogen Energy*, 2008, **33**, 6804-6839.
5. S. Saeidi, N. A. S. Amin and M. R. Rahimpour, *Journal of CO2 Utilization*, 2014, **5**, 66-81.
6. C. Song, *Catal. Today*, 2006, **115**, 2-32.
7. W. Wang, S. Wang, X. Ma and J. Gong, *Chem Soc Rev*, 2011, **40**, 3703-3727.
8. X. Xiaoding and J. A. Moulijn, *Energy & Fuels*, 1996, **10**, 305-325.
9. R. Zevenhoven, S. Eloneva and S. Teir, *Catal.Today*, 2006, **115**, 73-79.
10. H. Zhenhong, Q. Qingli, M. Jun, M. Qinglei, Z. Huacong, S. Jinliang, L. Zhimin and H. Buxing, *Angew. Chem. Int. Ed*, 2016, **55**, 737-741.
11. G. Centi and S. Perathoner, *Catal. Today*, 2009, **148**, 191-205.
12. C.-S. Chen, W.-H. Cheng and S.-S. Lin, *Catal Lett.*, 2000, **68**, 45-48.
13. C.-S. Chen, W.-H. Cheng and S.-S. Lin, *Appl. Catal., A*, 2004, **257**, 97-106.
14. M. J. L. Ginés, A. J. Marchi and C. R. Apesteguía, *Appl. Catal., A*, 1997, **154**, 155-171.
15. D. A. Hickman and L. D. Schmidt, *Science*, 1993, **259**, 343-346.
16. J. Kopyscinski, T. J. Schildhauer and S. M. A. Biollaz, *Fuel*, 2010, **89**, 1763-1783.
17. Y. Liu, Z. Li, H. Xu and Y. Han, *Catal. Commun.*, 2016, **76**, 1-6.
18. G. Maschio, A. Lucchesi and G. Stoppato, *Bioresour Technol.*, 1994, **48**, 119-126.

-
19. L. Pastor-Pérez, F. Baibars, E. Le Sache, H. Arellano-García, S. Gu and T. R. Reina, *Journal of CO2 Utilization*, 2017, **21**, 423-428.
 20. L. Wang, H. Liu, Y. Liu, Y. Chen and S. Yang, *Journal of Rare Earths*, 2013, **31**, 559-564.
 21. X. Cui, Y. Li, S. Bachmann, M. Scalone, A.-E. Surkus, K. Junge, C. Topf and M. Beller, *J. Am. Chem. Soc.*, 2015, **137**, 10652-10658.
 22. S. C. Kang, K.-W. Jun and Y.-J. Lee, *Energy & Fuels*, 2013, **27**, 6377-6387.
 23. A. G. Kharaji, A. Shariati and M. A. Takassi, *Chin. J. Chem. Eng.*, 2013, **21**, 1007-1014.
 24. D. H. Kim, S. W. Han, H. S. Yoon and Y. D. Kim, *J. Ind. Eng. Chem.*, 2015, **23**, 67-71.
 25. Z. Li, J. Liu, Z. Huang, Y. Yang, C. Xia and F. Li, *ACS Catal.*, 2013, **3**, 839-845.
 26. D. C. Marcano, D. V. Kosynkin, J. M. Berlin, A. Sinitskii, Z. Sun, A. Slesarev, L. B. Alemany, W. Lu and J. M. Tour, *ACS Nano*, 2010, **4**, 4806-4814.

Appendix a

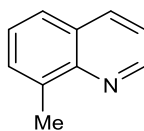
NMR of compounds synthesized compounds

Chapter 2a



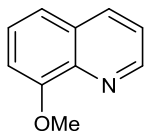
Quinoline (2a)

Compound **2a** was prepared according to the general procedure as described and was purified by silica gel column chromatography using petroleum ether/ethyl acetate. Yield: 88% (57.2 mg); ^1H NMR (200 MHz, CDCl_3) δ 7.27-7.79 (m, 4H), 8.09-8.15 (m, 2H), 8.90 (s, 1H); ^{13}C NMR (125 MHz, CDCl_3) δ 120.9, 126.4, 127.6, 128.1, 129.2, 135.96, 148.03, 150.173; HRMS (ESI) calculated for $\text{C}_9\text{H}_7\text{N}$ $[\text{M}+\text{H}]^+$: 130.0651; found: 130.0651.



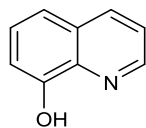
8-Methylquinoline (2b)

Compound **2b** was prepared according to the general procedure as described and was purified by silica gel column chromatography using petroleum ether/ethyl acetate. Yield: 59% (42 mg); ^1H NMR (500 MHz, CDCl_3) δ 2.83 (s, 3H), 7.35-7.45 (m, 2H), 7.53-7.57 (d, $J = 8.0$ Hz, 1H), 7.66-7.62 (d, $J = 8.0$ Hz, 1H), 8.08-8.12 (d, $J = 8.0$ Hz, 1H), 8.93-8.96 (m, 1H); ^{13}C NMR (125 MHz, CDCl_3) δ 18.0, 120.6, 125.7, 126.1, 128.0, 129.4, 136.1, 136.8, 147.1, 149.0; HRMS (ESI) calculated for $\text{C}_{10}\text{H}_9\text{N}$ $[\text{M}+\text{H}]^+$: 144.0807; found 144.0808.



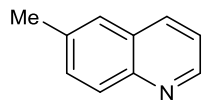
8-Methoxyquinoline (2c)

Compound **2c** was prepared according to the general procedure as described and was purified by silica gel column chromatography using petroleum ether/ethyl acetate; Yield: 61%. ^1H NMR (300 MHz, $\text{DMSO-}d_6$) δ : 3.96 (s, 3H), 7.17 (m, 1H), 7.51 (m, 3H), 8.29 (m, 1H), 8.84 (m, 1H). The spectral data is identical with the literature compound.⁶



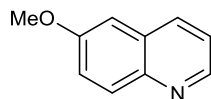
Quinolin-8-ol (2d)

Compound **2d** was prepared according to the general procedure as described and was purified by silica gel column chromatography using petroleum ether/ethyl acetate. Yield: 45% (33.5 mg); ^1H NMR (500 MHz, CDCl_3) δ 7.18-7.52 (m, 4H), 8.17 (dd, $J = 8.4$ Hz 1H), 8.80 (dd, $J = 4.2$ Hz 1H); ^{13}C NMR (126 MHz, CDCl_3) δ 76.7, 77.3, 110.0, 117.9, 121.8, 127.7, 128.5, 136.1, 138.3, 147.9, 152.2.



6-Methylquinoline (2e)

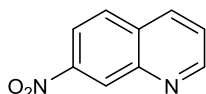
Compound **2e** was prepared according to the general procedure as described and was purified by silica gel column chromatography using petroleum ether/ethyl acetate. Yield: 75% (53.6 mg); ^1H NMR (500 MHz, CDCl_3) δ 2.47 (s, 3H), 7.26-7.29 (d, $J = 4.2$ Hz, 1H), 7.48-7.49 (m, 2H), 7.97-8.00 (t, $J = 8.5$ Hz, 2H), 7.80-8.81 (dd, $J = 3.9$ Hz, 1H); ^{13}C NMR (125 MHz, CDCl_3) δ 21.3, 120.8, 126.4, 128.1, 128.8, 131.5, 135.1, 136.1, 146.6, 149.2. HRMS (ESI) calculated for $\text{C}_{10}\text{H}_9\text{N}$ $[\text{M}+\text{H}]^+$ 144.0807; found: 144.0808.



6-Methoxyquinoline (2f)

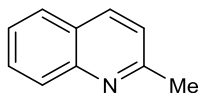
Compound **2f** was prepared according to the general procedure as described and was purified by silica gel column chromatography using petroleum ether/ethyl acetate. Yield: 87% (61.3 mg); ^1H

NMR (500 MHz, CDCl₃) δ 3.92 (s, 3H), 7.05-7.06 (d, J = 2.7 Hz, 1H), 7.32-7.34 (q, J = 4.2 Hz, 1H), 7.35-7.38 (dd, J = 9.1 Hz, 1H), 7.99-8.01 (d, J = 9.1 Hz, 1H), 8.02-8.04 (d, J = 8.2 Hz, 1H), 8.75-8.76 (d, J = 4.2 Hz, 1H); ¹³C NMR (125 MHz, CDCl₃) δ 55.4, 105.1, 121.3, 122.2, 129.3, 130.8, 134.7, 144.4, 147.9, 157.7; HRMS (ESI) calculated for C₁₀H₉NO [M+H]⁺: 160.0756; found: 160.0756.



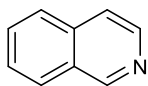
7-Nitroquinoline (2g)

Compound **2g** was prepared according to the general procedure as described and was purified by silica gel column chromatography using petroleum ether/ethyl acetate. Yield: 33% (28.7 mg); ¹H NMR (200 MHz, CDCl₃) δ 7.61-7.63 (q, J = 4.1 Hz, 1H), 7.96-8.01 (q, J = 8.9 Hz, 1H), 8.26-8.35 (dt, J = 8.9 Hz, 2H), 9.00-9.10 (d, J = 2.1 Hz, 1H), 9.07-9.10 (dd, J = 1.6 Hz, 1H); ¹³C NMR (125 MHz, CDCl₃) δ 120.1, 123.9, 125.8, 129.5, 131.4, 135.9, 147.1, 148.1, 152.7; HRMS (ESI) calculated for C₉H₆N₂O₂ [M+H]⁺: 175.0501; found: 175.0502.



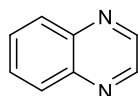
2-Methylquinoline (2h)

Compound **2h** was prepared according to the general procedure as described and was purified by silica gel column chromatography using petroleum ether/ethyl acetate. Yield: 33% (23.5 mg); ¹H NMR (500 MHz, CDCl₃) δ 2.70 (s, 1H), 7.18-7.20 (t, J = 8.2 Hz, 1H), 7.40-7.43 (t, J = 7.9 Hz, 1H), 7.61-7.64 (t, J = 8.5 Hz, 1H), 7.68-7.70 (d, J = 7.9 Hz, 1H), 7.94-7.95 (d, J = 8.5 Hz, 1H), 7.99-8.01 (d, J = 8.5 Hz, 1H); ¹³C NMR (125 MHz, CDCl₃) δ 25.2, 121.8, 124.4, 126.3, 127.3, 128.4, 129.2, 135.9, 147.7, 158.8; HRMS (ESI) calculated for C₁₀H₉N [M+H]⁺: 144.087144.087; found: 144.0808.



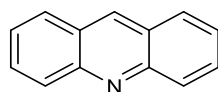
Isoquinoline (2i)

Compound **2i** was prepared according to the general procedure as described and was purified by silica gel column chromatography using petroleum ether/ethyl acetate. Yield: 76% (50 mg); ^1H NMR (200 MHz, CDCl_3) δ 7.63-7.95 (m, 4H), 8.09-8.13 (m, 2H), 9.24 (s, 1H); ^{13}C NMR (25 MHz, CDCl_3) δ 120.3, 126.3, 127.1, 127.5, 128.5, 130.26, 130.64, 142, 152, HRMS (ESI) calculated for $\text{C}_9\text{H}_7\text{N}$ $[\text{M}+\text{H}]^+$: 130.0651; found: 130.0651.



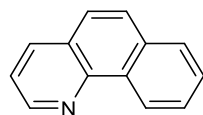
Quinoxaline (2j)

Compound **2j** was prepared according to the general procedure as described and was purified by silica gel column chromatography using petroleum ether/ethyl acetate. Yield: 69% (44.8 mg): ^1H NMR (500 MHz, CDCl_3) δ 7.41 (s, 2H), 7.78-7.81 (m, 2H), 8.51-8.54 (m, 2H); ^{13}C NMR (125 MHz, CDCl_3) δ 128.8, 129.3, 142.2, 144.3. HRMS (ESI) calculated for $\text{C}_8\text{H}_6\text{N}_2$ $[\text{M}+\text{H}]^+$: 131.0606; found: 131.0604.



Acridine (2k)

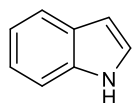
Compound **2k** was prepared according to the general procedure as described and was purified by silica gel column chromatography using petroleum ether/ethyl acetate. Yield: 90% (81 mg); ^1H NMR (500 MHz, CDCl_3) δ 7.49-7.51 (q, $J = 5.4$ Hz, 2H), 7.74-7.78 (m, 2H), 7.94-7.97 (t, $J = 8.2$ Hz, 2H), 8.24-8.25 (t, $J = 8.8$ Hz, 2H), 8.69-8.71 (d, $J = 9.7$ Hz, 1H); ^{13}C NMR (125 MHz, CDCl_3) δ 125.6, 126.5, 128.1, 129.3, 130.1, 149.0.



Benzo[h]quinoline (2l)

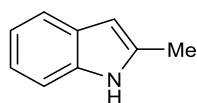
Compound **2l** was prepared according to the general procedure as described and was purified by silica gel column chromatography using petroleum ether/ethyl acetate. Yield: 78% (71.7 mg); ^1H

NMR (500 MHz, CDCl₃) δ 7.49-7.51 (q, J = 4.2 Hz, 1H), 7.65-7.67 (d, J = 8.8 Hz, 1H), 7.70-7.73 (td, J = 6.7 Hz, 1H), 7.75-7.81 (m, 2H), 7.91-7.92 (d, J = 8.2 Hz, 1H), 8.13-8.15 (dd, J = 7.9 Hz, 1H), 9.02-9.03 (dd, J = 4.5 Hz, 1H), 9.34-9.36 (d, J = 7.6 Hz, 1H); ¹³C NMR (125 MHz, CDCl₃) δ 121.6, 124.3, 125.2, 126.3, 126.9, 127.7, 128.1, 131.4, 133.5, 135.6, 146.5, 146.5, 148.7.



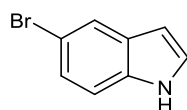
1H-indole (2m)

Compound **2m** was prepared according to the general procedure as described and was purified by silica gel column chromatography using petroleum ether/ethyl acetate. Yield: 88% (51.5 mg); ¹H NMR (200 MHz, CDCl₃) δ 6.62-6.65 (m, 1H), 7.15-7.32 (m, 3H), 7.44-7.49 (d, J = 8.2 Hz, 1H), 7.70-7.75 (d, J = 7.5 Hz, 1H), 8.19 (s, 1H); ¹³C NMR (25 MHz, CDCl₃) δ 102.6, 110.9, 119.8, 121.9, 124.1, 127.8, 135.7.



2-Methyl-1H-indole (2n)

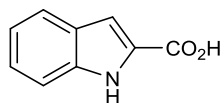
Compound **2n** was prepared according to the general procedure as described and was purified by silica gel column chromatography using petroleum ether/ethyl acetate. Yield: 58% (38 mg); ¹H NMR (500 MHz, CDCl₃) δ 2.46 (s, 3H), 6.29 (s, 1H), 7.15-7.21 (m, 2H), 7.30-7.31 (d, J = 7.6 Hz, 1H), 7.60-7.11 (d, J = 7.6 Hz, 1H), 7.75 (s, 1H); ¹³C NMR (125 MHz, CDCl₃) δ 13.6, 100.2, 110.2, 119.5, 120.8, 128.9, 135.1, 135.9.



5-Bromo-1H-indole (2o)

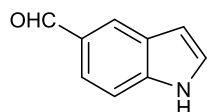
Compound **2o** was prepared according to the general procedure as described and was purified by silica gel column chromatography using petroleum ether/ethyl acetate. Yield 82% (38 mg); ¹H

NMR (500 MHz, CDCl₃) δ 6.52-6.53 (s, 1H), 7.27-7.30 (m, 3H), 7.29 (s, 1H), 8.22 (bs, 1H); ¹³C NMR (125 MHz, CDCl₃) δ 120.3, 112.4, 113.0, 123.2, 124.8, 125.3, 129.6, 134.4.



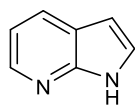
1H-indole-2-carboxylic acid (2p)

Compound **2p** was prepared according to the general procedure as described and was purified by silica gel column chromatography using petroleum ether/ethyl acetate. Yield 74% (60 mg); ¹H NMR (500 MHz, CDCl₃) δ 7.18-7.21 (t, *J* = 7.6 Hz, 1H), 7.36-7.40 (m, 2H), 7.46-7.47 (d, *J* = 8.2 Hz, 1H), 7.73-7.75 (d, *J* = 8.2 Hz, 1H), 8.97 (bs, 1H); ¹³C NMR (125 MHz, CDCl₃) δ 110.8, 111.9, 121.1, 122.9, 126.1, 127.4, 137.3, 166.1; HRMS (ESI) calculated for C₉H₇NO₂ [M+H]⁺: 162.0546; found: 162.0550.



1H-indole-5-carbaldehyde (2q)

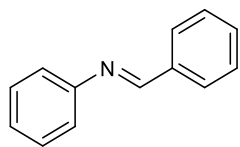
Compound **2q** was prepared according to the general procedure as described and was purified by silica gel column chromatography using petroleum ether/ethyl acetate. Yield 80% (58 mg); ¹H NMR (500 MHz, CDCl₃) δ 6.72-6.73 (s, 1H), 7.33-7.34 (t, *J* = 3.0 Hz, 1H), 7.49-7.50 (d, *J* = 8.2 Hz, 1H), 7.78-7.80 (dd, *J* = 8.5 Hz, 1H), 8.20 (s, 1H), 8.95 (bs, 1H), 10.06 (s, 1H); ¹³C NMR (125 MHz, CDCl₃) δ 104.3, 111.8, 122.2, 126.3, 127.7, 129.6, 139.4, 192.8; HRMS (ESI) calculated for C₉H₇NO [M+H]⁺: 146.0599; found: 146.0600.



1H-pyrrolo[2,3-b]pyridine (2r)

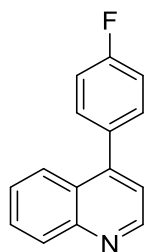
Compound **2r** was prepared according to the general procedure as described and was purified by silica gel column chromatography using petroleum ether/ethyl acetate. Yield: 94% (58 mg); ¹H NMR (500 MHz, CDCl₃) δ 6.54-6.54 (d, *J* = 3.0 Hz, 1H), 7.11-7.14 (q, *J* = 4.8 Hz, 1H), 7.41-

7.41 (q, $J = 3.3$ Hz, 1H), 8.00-8.02 (d, $J = 7.6$ Hz, 1H), 8.35-8.35 (d, $J = 4.5$ Hz, 1H), ^{13}C NMR (125 MHz, CDCl_3) δ 100.8, 115.8, 120.7, 125.4, 129.4, 141.9, 148.2.

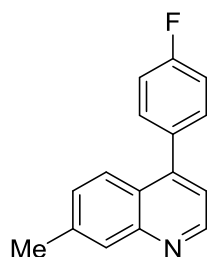


(E)-N-benzylideneaniline (2s)

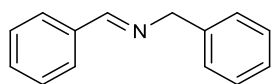
Compound **2s** was prepared according to the general procedure as described and was purified by silica gel column chromatography using petroleum ether/ethyl acetate. 84% (38 mg); ^1H NMR (500 MHz, CDCl_3) δ 7.25-7.29 (m, 3H), 7.42-7.45 (t, $J = 7.6$ Hz, 2H), 7.50-7.51 (m, 3H), 7.93-7.95 (dd, $J = 3.6$ Hz, 2H), 8.49 (s, 1H); ^{13}C NMR (125 MHz, CDCl_3) δ 120.8, 125.9, 128.7, 128.8, 129.1, 131.3, 136.1, 152.0, 160.4.



Compound **4a** was prepared according to the general procedure as described and was purified by silica gel column chromatography using petroleum ether/ethyl acetate. Yield: 81%; ^1H NMR (500 MHz, CDCl_3) δ = 7.29-7.16 (m, 3 H), 7.32 (d, $J = 4.3$ Hz, 1 H), 7.57 - 7.45 (m, 3 H), 7.75 (ddd, $J = 1.2, 6.9, 8.3$ Hz, 1 H), 7.98-7.83 (m, 1 H), 8.19 (d, $J = 8.5$ Hz, 1 H), 8.95 (d, $J = 4.3$ Hz, 1 H), ^{13}C NMR (125 MHz, CDCl_3) δ 115.6, 115.7, 121.4, 125.6, 126.7, 126.8, 129.4, 129.9, 131.2, 133.9, 147.4, 148.6, 149.9, 161.9, 163.9.

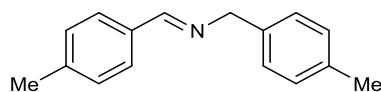


Compound **4b** was prepared according to the general procedure as described and was purified by silica gel column chromatography using petroleum ether/ethyl acetate. Yield: 70%; $^1\text{H NMR}$ (500 MHz, CDCl_3) δ 2.60 (s, 3H), 7.30-7.20 (m, 3H), 7.36 (d, $J = 4.5$ Hz, 1H), 7.47-7.38 (m, 1H), 7.55-7.46 (m, 2H), 7.82 (d, $J = 8.6$ Hz, 1H), 8.15 (brs, 1H), 8.90 (m, 1H). The spectral data is identical with the literature compound.⁵



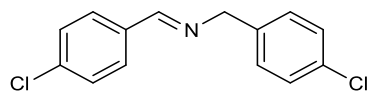
(E)-N-benzylidene-1-phenylmethanamine (6a)

Yield: 82% (41 mg); $^1\text{H NMR}$ (200 MHz, CDCl_3) δ 4.74 (s, 2H), 7.15-7.35 (m, 8H), 7.68-7.72 (m, 2H), 8.31 (s, 1H); $^{13}\text{C NMR}$ (125 MHz, CDCl_3) δ 65.0, 126.9, 127.9, 128.2, 128.5, 128.6, 130.7, 136.1, 139.2, 162.0; HRMS (ESI) calculated for $\text{C}_{14}\text{H}_{13}\text{N}$ $[\text{M}+\text{H}]^+$: 196.1181; found: 196.1121.



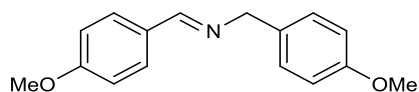
(E)-N-(4-methylbenzylidene)-1-p-tolylmethanamine (6b)

Yield: 79% (44.3 mg); $^1\text{H NMR}$ (500 MHz, CDCl_3) δ 2.35 (s, 3H), 2.39 (s, 3H), 4.78 (s, 2H), 7.15-7.17 (d, $J = 7.9$ Hz, 2H), 7.22-7.28 (d, $J = 6.4$ Hz, 4H), 7.67-7.68 (d, $J = 7.9$ Hz, 2H), 8.35 (s, 1H); $^{13}\text{C NMR}$ (125 MHz, CDCl_3) δ 21.1, 21.4, 64.7, 27.9, 128.2, 129.1, 129.3, 133.6, 136.3, 136.5, 140.9, 161.7; HRMS (ESI) calculated for $\text{C}_{16}\text{H}_{17}\text{N}$ $[\text{M}+\text{H}]^+$: 224.1433; found: 224.1434.



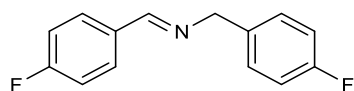
(E)-N-(4-chlorobenzylidene)-1-(4-chlorophenyl)methanamine (6c)

Yield: 86% (57 mg); $^1\text{H NMR}$ (200 MHz, CDCl_3) δ 4.66 (s, 2H), 7.11-7.28 (m, 6H), 7.49-7.53 (m, 1H), 7.69-7.70 (s, 1H), 8.20 (s, 1H); $^{13}\text{C NMR}$ (125 MHz, CDCl_3) δ 64.1, 125.9, 126.6, 127.2, 127.8, 129.9, 129.7, 129.8, 130.8, 134.3, 134.8, 137.6, 141.0, 160.8; HRMS (ESI) calculated for $\text{C}_{14}\text{H}_{11}\text{Cl}_2\text{N}$ $[\text{M}+\text{H}]^+$: 264.0338; found: 264.0341.



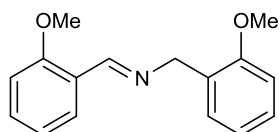
(E)-N-(4-methoxybenzylidene)-1-(4-methoxyphenyl)methanamine (6d)

Yield: 76% (48.5 mg); ^1H NMR (500 MHz, CDCl_3) δ 3.69 (s, 3H), 3.72 (s, 3H), 4.63 (s, 2H), 6.76-6.84 (m, 4H), 7.15 (d, $J = 8.6$ Hz, 4H), 7.62 (d, $J = 8.6$ Hz, 2H), 8.19 (s, 1H); ^{13}C NMR (125 MHz, CDCl_3) δ 55.2, 55.2, 64.3, 113.8, 113.9, 129.1, 129.7, 131.6, 158.5, 160.8, 161.6. HRMS (ESI) calculated for $\text{C}_{16}\text{H}_{17}\text{NO}_2$ $[\text{M}+\text{H}]^+$: 256.1328; found: 256.1332.



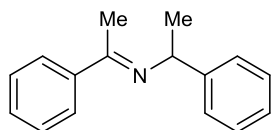
(E)-N-(4-fluorobenzylidene)-1-(4-fluorophenyl)methanamine (6e)

Yield: 90% (52 mg); ^1H NMR (500 MHz, CDCl_3) δ 4.78 (s, 2H), 7.04-7.07 (t, $J = 8.5$ Hz, 2H), 7.10-7.14 (t, $J = 8.5$ Hz, 2H), 7.30-7.33 (q, $J = 5.4$ Hz, 2H), 7.78-7.81 (q, $J = 5.4$ Hz, 2H), 8.35 (s, 1H); ^{13}C NMR (125 MHz, CDCl_3) δ 64.0, 115.1, 115.6, 115.7, 129.3, 129.4, 130.0, 130.1, 132.2, 132.3, 134.8, 134.9, 160.4, 160.9, 162.9, 163.3, 165.3; HRMS (ESI) calculated for $\text{C}_{12}\text{H}_{13}\text{N}_2$ $[\text{M}+\text{H}]^+$: 232.0943; found: 232.0932.



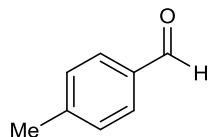
(E)-N-(2-methoxybenzylidene)-1-(2-methoxyphenyl)methanamine (6f)

Yield: 69% (44 mg); ^1H NMR (500 MHz, CDCl_3) δ 3.77-3.80 (m, 6H), 4.76(s, 2H), 6.78-6.94 (m, 4H), 7.13-7.31 (m, 3H), 7.94-7.98 (m, 1H), 8.77 (s, 1H); ^{13}C NMR (125 MHz, CDCl_3) δ 55.3, 55.5, 59.6, 110.1, 110.9, 120.5, 120.7, 127.5, 127.9, 129.1, 131.7, 158.3; HRMS (ESI) calculated for $\text{C}_{16}\text{H}_{17}\text{NO}_2$ $[\text{M}+\text{H}]^+$: 256.1328; found: 256.1332.



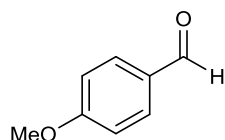
(E)-1-phenyl-N-(1-phenylethylidene)ethanamine (6h)

Yield: 71 % (40 mg); ^1H NMR (500 MHz, CDCl_3) δ 1.57-1.58 (m, 3H), 2.28(s, 3H), 4.85 (q, J = 6.4 Hz, 1H), 7.31-7.50 (m, 8H), 7.83-7.88 (m, 2H), 8.26 (s, 1H); HRMS (ESI) calculated for $\text{C}_{16}\text{H}_{17}\text{N}[\text{M}+\text{H}]^+$: 224.1433; found: 224.1434.



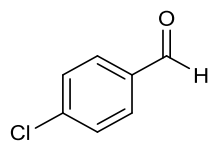
4-Methylbenzaldehyde (9a)

Yield: 91 % (54.6 mg); ^1H NMR (500 MHz, CDCl_3) δ 2.45 (s, 3H), 7.34-7.35 (d, J = 7.9 Hz, 2H), 7.78-7.80 (d, J = 7.9 Hz, 2H), 9.97 (s, 1H); ^{13}C NMR (125 MHz, CDCl_3) δ 21.8, 129.7, 129.8, 134.1, 145.5, 192.0.; HRMS (ESI) calculated For $\text{C}_8\text{H}_8\text{O} [\text{M}+\text{H}]^+$: 121.651; found 121.0648.



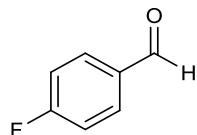
4-Methoxybenzaldehyde (9b)

Yield: 85 % (57.8 mg); ^1H NMR (200 MHz, CDCl_3) δ 3.87 (s, 3H), 6.96-7.01 (d, J = 8.8Hz, 2H), 7.80-7.84 (d, J = 8.8Hz, 2H), 9.86 (s, 1H); ^{13}C NMR (125 MHz, CDCl_3) 55.5, 114.2, 132.0, 190.9; HRMS (ESI) calculated for $\text{C}_8\text{H}_8\text{O}_2 [\text{M}+\text{H}]^+$: 137.0598; found: 137.0597.

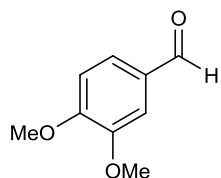


4-Chlorobenzaldehyde (9c)

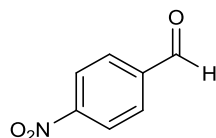
Yield: 93% (65.1 mg); ^1H NMR (500 MHz, CDCl_3) δ 7.50-7.52 (d, J = 8.5 Hz, 2H), 7.81-7.83 (d, J = 8.5 Hz, 2H), 9.98 (s, 1H); ^{13}C NMR (125 MHz, CDCl_3) δ 129.4, 130.9, 134.6, 140.9, 190.0; HRMS (ESI) calculated for $\text{C}_7\text{H}_5\text{ClO} [\text{M}+\text{H}]^+$: 141.0103; found: 141.0102.

**4-Fluorobenzaldehyde (9d)**

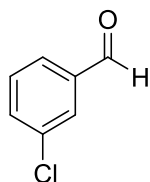
Yield: 51% (31.6 mg); $^1\text{H NMR}$ (500 MHz, CDCl_3) δ 7.18-7.22 (t, $J = 8.5\text{ Hz}$, 2H), 7.89-7.91 (q, $J = 5.4\text{ Hz}$, 2H), 9.95 (s, 1H); $^{13}\text{C NMR}$ (125 MHz, CDCl_3) δ 116.2, 116.4, 132.1, 132.2, 132.8, 132.9, 165.4, 167.5, 190.5; HRMS (ESI) calculated for $\text{C}_7\text{H}_5\text{FO}$ $[\text{M}+\text{H}]^+$: 125.0399; found: 125.0397.

**3,4-Dimethoxybenzaldehyde (9e)**

Yield: 69% (57.3 mg); $^1\text{H NMR}$ (200 MHz, CDCl_3) δ 3.94 (s, 3H), 3.96 (s, 3H), 6.96-7.00 (d, $J = 8.2\text{ Hz}$, 1H), 7.40-7.48 (m, 2H), 9.85 (1H); $^{13}\text{C NMR}$ (125 MHz, CDCl_3) δ 55.9, 56.1, 108.7, 110.3, 126.8, 130.1, 149.5, 154.4, 190.8; HRMS (ESI) calculated for $\text{C}_9\text{H}_{10}\text{O}_3$ $[\text{M}+\text{H}]^+$: 167.0701; found: 167.0703.

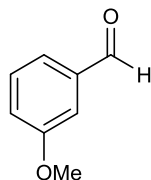
**4-Nitrobenzaldehyde (9f)**

Yield: 45% (34 mg); $^1\text{H NMR}$ (200 MHz, CDCl_3) δ 8.05-8.10 (d, $J = 8.7\text{ Hz}$, 2H), 8.38-8.41 (d, $J = 8.7\text{ Hz}$, 2H), 10.16 (s, 1H); $^{13}\text{C NMR}$ (25 MHz, CDCl_3) δ 124.2, 130.4, 139.9, 151.0, 190.2.

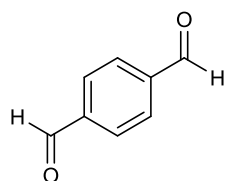


3-Chlorobenzaldehyde (9g)

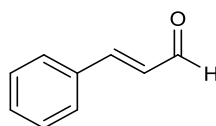
Yield: 94%; ^1H NMR (400 MHz, CDCl_3): δ 7.49 (t, $J = 7.9$ Hz, 1H), 7.61 (m, 1H), 7.77 (dt, $J = 7.9$ Hz, 1.3 Hz, 1H), 7.86 (t, $J = 2.0$ Hz, 1H), 9.98 (s, 1H). ^{13}C NMR (125 MHz, CDCl_3): δ 127.9, 129.3, 130.3, 134.4, 135.4, 137.8, 190.8.

**3-Methoxybenzaldehyde (9h)**

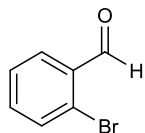
Yield: 78% (53 mg); ^1H NMR (200 MHz, CDCl_3) δ 3.85 (s, 3H), 7.14-7.19 (m, 1H), 7.37-7.38 (t, $J = 2.2$ Hz, 1H), 7.42-7.45 (m, 2H), 9.86 (s, 1H); ^{13}C NMR (125 MHz, CDCl_3) δ 55.4, 112.0, 121.4, 123.5, 129.9, 137.7, 160.1, 192.1.

**Terephthalaldehyde 9i**

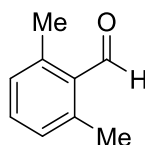
Yield: 70% (47 mg); ^1H NMR (200 MHz, CDCl_3) δ 8.05 (s, 4H), 10.12 (s, 2H); ^{13}C NMR (125 MHz, CDCl_3) δ 130.1, 139.9, 191.5; HRMS (ESI) calculated for $\text{C}_8\text{H}_6\text{O}_2$ $[\text{M}+\text{H}]^+$: 135.0440; found: 135.0441.

**Cinnamaldehyde (9j)**

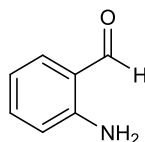
Yield: 69 % (42 mg); ^1H NMR (500 MHz, CDCl_3) δ 7.69-7.74 (q, $J = 7.6$ Hz, 1H), 7.43-7.49 (m, 4H), 7.56-7.58 (m, 2H), 9.70-9.71 (t, $J = 7.6$ Hz, 1H); ^{13}C NMR (125 MHz, CDCl_3) δ 128.4, 129.0, 131.1, 133.9, 152.7, 193.6.

**2-Bromobenzaldehyde (9k)**

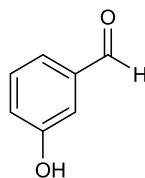
Yield: 71% (65 mg); ^1H NMR (200 MHz, CDCl_3) δ 7.39-7.49 (m, 3H), 7.60-7.65 (m, 1H), 7.86-7.92 (m, 1H), 10.33 (s, 1H); ^{13}C NMR (125 MHz, CDCl_3) δ 127.8, 129.7, 133.7, 135.2, 191.7; HRMS (ESI) calculated for $\text{C}_7\text{H}_5\text{BrO}$ $[\text{M}+\text{H}]^+$: 184.9595; found: 184.9597.

**2,6-Dimethylbenzaldehyde (9l)**

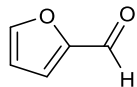
Yield: 52%. ^1H NMR (200 MHz, CDCl_3) δ 2.62 (s, 6H), 7.10 (d, $J = 7.5$ Hz, 2H), 7.33 (t, $J = 7.5$ Hz, 1H), 10.64 (s, 1H), ^{13}C NMR (125 MHz, CDCl_3) δ 20.7, 129.9, 132.7, 133.2, 141.3, 193.8.

**2-Aminobenzaldehyde (9m)**

^1H NMR (400 MHz, CDCl_3): δ 9.86 (s, 1H), 7.46 (d, $J = 7.2$ Hz, 1H), 7.30 (t, $J = 6.8$ Hz, 1H), 6.73 (t, $J = 6.6$ Hz, 1H), 6.64 (d, $J = 8.0$ Hz, 1H), 6.13 (s, 2H). ^{13}C NMR (125 MHz, CDCl_3): δ 116.1, 116.4, 118.9, 135.2, 135.7, 150.0, 194.1.

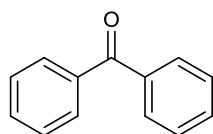
**3-Hydroxybenzaldehyde (9n)**

Yield: 61% (37 mg); ^1H NMR (200 MHz, CDCl_3) δ 6.42 (s, 1H), 7.14-7.20 (m, 1H) 7.40-7.46 (m, 3H), 9.95 (s, 1H); ^{13}C NMR (125 MHz, CDCl_3) δ 114.7, 122.2, 123.5, 130.4, 137.7, 156.5, 192.7; HRMS (ESI) calculated for $\text{C}_7\text{H}_6\text{O}_2$ $[\text{M}+\text{H}]^+$: 123.0443; found: 123.0441.



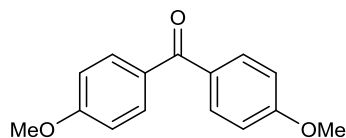
Furan-2-carbaldehyde (9o)

Yield: 55% (26.5 mg); ^1H NMR (200 MHz, CDCl_3) δ 6.61-6.64 (q, $J = 1.6$ Hz, 1H), 7.27-7.29 (q, $J = 3.6$ Hz, 1H), 7.71-7.72 (t, $J = 0.7$ Hz, 1H), 9.67 (s, 1H); ^{13}C NMR (125 MHz, CDCl_3) δ 112.5, 121.1, 147.9, 152.8, 177.7; HRMS (ESI) calculated for $\text{C}_5\text{H}_4\text{O}_2$ $[\text{M}+\text{H}]^+$: 97.0289; found: 97.0284.



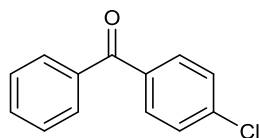
Benzophenone (11a)

Yield: 97% (88 mg); ^1H NMR (200 MHz, CDCl_3) δ 7.42-7.60 (m, 6H), 7.76-7.81 (m, 4H); ^{13}C NMR (125 MHz, CDCl_3) δ 128.2, 129.9, 132.3, 137.5, 196.6. HRMS (ESI) calculated for $\text{C}_{13}\text{H}_{10}\text{O}$ $[\text{M}+\text{H}]^+$: 183.0803; found: 183.0804.



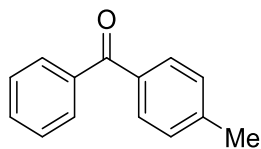
Bis(4-methoxyphenyl)methanone (11b)

Yield: 98% (118 mg); ^1H NMR (200 MHz, CDCl_3) δ 3.90 (s, 6H), 6.97 (d, $J = 9$ Hz, 4H), 7.80 (d, $J = 9$ Hz, 4H); ^{13}C NMR (50 MHz, CDCl_3) δ 55.5, 113.4, 130.7, 132.2, 162.8.

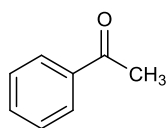


(4-Chlorophenyl)(phenyl)methanone (11c)

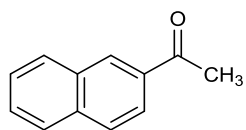
Yield: 95% (102 mg); ^1H NMR (200 MHz, CDCl_3) δ 7.45-7.54 (m, 4H), 7.58-7.66 (m, 1H), 7.75-7.80 (m, 4H); HRMS (ESI) calculated for $\text{C}_{13}\text{H}_9\text{ClO}$ $[\text{M}+\text{H}]^+$: 217.0415; found: 217.0415.

**Phenyl(p-tolyl)methanone (11d)**

Yield: 90% (88 mg); ^1H NMR (200 MHz, CDCl_3) δ 2.44 (s, 3H), 7.26-7.30 (d, $J = 8.4$ Hz, 2H), 7.43-7.62 (m, 3H), 7.70-7.81 (m, 4H); ^{13}C NMR (125 MHz, CDCl_3) δ 21.6, 128.2, 128.9, 129.9, 130.2, 132.1, 134.8, 137.9, 143.2, 196.5; HRMS (ESI) calculated for $\text{C}_{14}\text{H}_{12}\text{O}$ $[\text{M}+\text{H}]^+$: 197.0961; found: 197.0961.

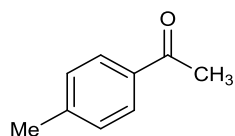
**Acetophenone (11e)**

Yield: 73 % (43.8 mg); ^1H NMR (200 MHz, CDCl_3) δ 2.60 (s, 3H), 7.42-7.56 (m, 3H), 7.93-7.88 (m, 2H); ^{13}C NMR (25 MHz, CDCl_3) δ 26.6, 128.3, 128.5, 133.0, 137.0, 198.1; HRMS (ESI) calculated for $\text{C}_8\text{H}_8\text{O}$ $[\text{M}+\text{H}]^+$: 120.0651; found: 120.648.

**1-(Naphthalen-2-yl)ethanone (11f)**

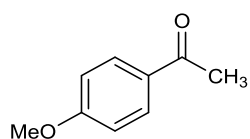
Yield: 77% (65.5 mg); ^1H NMR (500 MHz, CDCl_3) δ 2.72 (s, 3H), 7.54-7.62 (m, 2H), 7.86-7.89 (d, $J = 7.3$ Hz, 2H), 7.95-7.97 (d, $J = 7.9$ Hz, 1H), 8.02-8.04 (d, $J = 8.5$ Hz, 1H), 8.46 (s, 1H);

^{13}C NMR (125 MHz, CDCl_3) δ 26.6, 123.8, 126.7, 127.7, 128.3, 128.4, 129.5, 130.1, 132.4, 134.3, 135.5, 198.0; HRMS (ESI) calculated for $\text{C}_{12}\text{H}_{10}\text{O}$ $[\text{M}+\text{H}]^+$: 171.804; found: 171.0804.



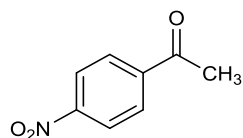
1-*p*-tolylethanone (11g)

Yield: 71% (46.8 mg); ^1H NMR (200 MHz, CDCl_3) δ 2.40 (s, 3H), 2.57 (s, 3H), 7.23-7.27 (d, J = 8.3 Hz, 2H), 7.84-7.88 (d, J = 8.0 Hz, 2H); ^{13}C NMR (125 MHz, CDCl_3) δ 21.5, 26.4, 128.3, 129.1, 134.6, 143.8, 197.7; HRMS (ESI) calculated for $\text{C}_9\text{H}_{10}\text{O}$ $[\text{M}+\text{H}]^+$: 135.0804; found: 135.0804.



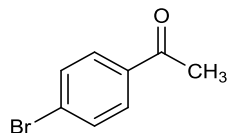
1-(4-Methoxyphenyl)ethanone (11h)

Yield: 80% (60 mg); ^1H NMR (200 MHz, CDCl_3) δ 2.53 (s, 3H), 3.84 (s, 3H), 6.89-6.93 (d, J = 8.9 Hz, 2H), 7.89-7.94 (d, J = 8.9 Hz, 1H); ^{13}C NMR (125 MHz, CDCl_3) δ 26.2, 55.3, 113.6, 130.2, 130.4, 163.4, 196.7; HRMS (ESI) calculated for $\text{C}_9\text{H}_{10}\text{O}_2$ $[\text{M}+\text{H}]^+$: 151.0752; found: 151.0754.

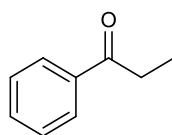


1-(4-Nitrophenyl)ethanone (11i)

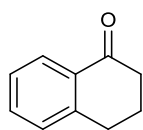
Yield: 69% (57 mg); ^1H NMR (200 MHz, CDCl_3) δ 2.68 (s, 3H), 8.09-8.13 (t, J = 8.8 Hz, 2H), 8.29-8.33 (d, J = 8.8 Hz, 2H); ^{13}C NMR (25 MHz, CDCl_3) δ 26.9, 123.8, 129.2, 141.3, 150.3, 196.3; HRMS (ESI) calculated for $\text{C}_8\text{H}_7\text{NO}_3$ $[\text{M}+\text{H}]^+$: 166.0498; found: 166.0499.

**1-(4-Bromophenyl)ethanone (11j)**

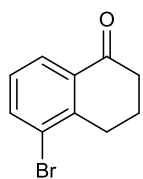
Yield: 72% (71 mg); ^1H NMR (200 MHz, CDCl_3) δ 2.56 (s, 2H), 7.55-7.59 (d, $J = 8.5$ Hz, 2H), 7.77-7.81 (d, $J = 8.5$ Hz, 2H); ^{13}C NMR (125 MHz, CDCl_3) δ 26.4, 128.1, 129.7, 131.7, 135.8, 196.8; HRMS (ESI) calculated for $\text{C}_8\text{H}_7\text{BrO}$ $[\text{M}+\text{H}]^+$: 198.9751; found: 198.9753.

**Propiophenone (11k)**

Yield: 43% (29 mg); ^1H NMR (200 MHz, CDCl_3) δ 1.19-1.26 (t, $J = 7.3$ Hz, 3H), 2.95-3.05 (d, $J = 7.2$ Hz, 2H), 7.40-7.55 (m, 3H), 7.54-7.55 (m, 2H); ^{13}C NMR (125 MHz, CDCl_3) δ 8.1, 31.6, 127.8, 128.4, 132.7, 136.8, 200.7.

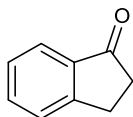
**3,4-Dihydronaphthalen-1(2H)-one (11l)**

Yield: 54% (39.5 mg); ^1H NMR (200 MHz, CDCl_3) δ 2.07-2.20 (m, $J = 6.5$ Hz, 2H), 2.63-2.69 (t, $J = 6.9$ Hz, 2H), 2.94-3.00 (t, $J = 6.0$ Hz, 2H), 7.23-7.34 (m, 2H), 7.43-7.51 (m, 1H), 8.01-8.06 (d, $J = 7.8$ Hz, 1H); ^{13}C NMR (125 MHz, CDCl_3) δ 23.1, 29.6, 39.1, 126.5, 127.0, 128.7, 132.5, 133.2, 144.4, 198.2; HRMS (ESI) calculated for $\text{C}_{10}\text{H}_{10}\text{O}$ $[\text{M}+\text{H}]^+$: 147.0803; found: 147.0804.

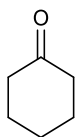


5-Bromo-3,4-dihydronaphthalen-1(2H)-one (11m)

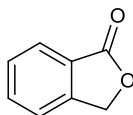
Yield: 36%; ^1H NMR: δ 2.1-2.2 (m, 2H), 2.65 (m, 2H), 3.0 (t, $J = 7.0$ Hz, 2H), 7.15-7.25 (t, $J = 6.9$ Hz, 1H) 7.7 (d, $J = 7.5$ Hz, 1H), 8.0 (d, $J = 8.0$ Hz, 1H).

**2,3-Dihydro-1H-inden-1-one (11n)**

Yield: 51% (31.11 mg); ^1H NMR (200 MHz, CDCl_3) δ 2.65-2.71 (t, $J = 6.2$ Hz, 2H), 3.11-3.17 (t, $J = 6.2$ Hz, 2H), 7.36-7.40 (t, $J = 7.7$ Hz, 1H), 7.45-7.49 (d, $J = 7.7$ Hz, 1H), 7.54-7.62 (t, $J = 6.9$ Hz, 1H), 7.73-7.74 (d, $J = 7.7$ Hz, 1H); ^{13}C NMR (125 MHz, CDCl_3) δ 25.7, 36.1, 123.6, 126.6, 127.2, 134.5, 137.0, 155.1, 207.0; HRMS (ESI) calculated for $\text{C}_9\text{H}_8\text{O}$ $[\text{M}+\text{H}]^+$: 133.0648; found: 133.0648.

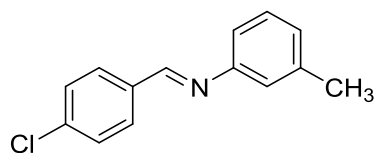
**Cyclohexanone (11o)**

Yield: 40% (20 mg); ^1H NMR (500 MHz, CDCl_3) δ 1.69-1.73 (m, 2H), 1.83-1.88 (m, 4H), 2.31-2.34 (m, 4H); ^{13}C NMR (125 MHz, CDCl_3) δ 128.2, 129.9, 132.3, 137.5, 196.6; HRMS (ESI) calculated for $\text{C}_6\text{H}_{10}\text{O}$ $[\text{M}+\text{H}]^+$: 99.0808; found: 99.0804.

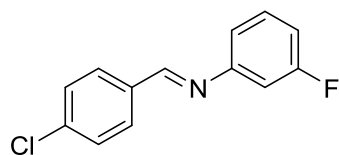
**Isobenzofuran-1(3H)-one (13)**

Yield: 97 % (65 mg); ^1H NMR (200 MHz, CDCl_3) δ 5.33 (s, 2H), 7.49-7.57 (t, $J = 7.5$ Hz, 2H), 7.65-7.73 (d, $J = 7.5$ Hz, 1H), 7.90-7.94 (d, $J = 7.5$ Hz, 1H); ^{13}C NMR (125 MHz, CDCl_3) δ 69.6, 120.0, 125.6, 128.9, 133.9, 146.5, 171.1; HRMS (ESI) calculated for $\text{C}_8\text{H}_6\text{O}$ $[\text{M}+\text{H}]^+$: 135.0440; found: 135.0441.

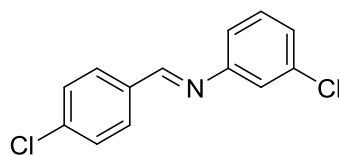
Chapter 2b

**(E)-N-(4-chlorobenzylidene)-3-methylaniline (3aa)**

106 mg, 93% isolated yield. ^1H NMR (CDCl_3 , 500 MHz) δ 8.43 (s, 1H), 7.85 (d, $J = 8.4$ Hz, 2H), 7.46 (d, $J = 8.4$ Hz, 2H), 7.30 (t, $J = 7.5$ Hz, 1H), 7.08 (d, $J = 7.2$ Hz, 1H), 7.04-7.02 (m, 2H), 2.41 (s, 3H). ^{13}C NMR (CDCl_3 , 125 MHz) δ 158.61, 151.62, 139.02, 137.25, 134.69, 129.89, 129.02(d, $J = 4.8$ Hz), 126.95, 121.58, 117.79, 21.38; HRMS Calcd for $\text{C}_{14}\text{H}_{12}\text{NCl}$ $[\text{M}+\text{H}]^+$: 230.0731; Found: 230.0734.

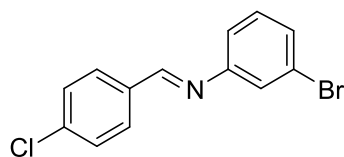
**N-(4-chlorobenzylidene)-3-fluoroaniline (3ab)**

100 mg, 86% isolated yield. ^1H NMR (CDCl_3 , 200 MHz) δ 8.29 (s, 1H), 7.74 (d, $J = 8.5$ Hz, 2H), 7.36 (d, $J = 8.4$ Hz, 2H), 7.23-7.16 (m, 1H), 6.90-6.81 (m, 3H). ^{13}C NMR (CDCl_3 , 125 MHz) δ 164.23, 162.27, 159.58, 153.48, 153.40, 130.32, 130.05, 129.08, 116.66, 116.64, 112.88, 112.70, 108.09, 107.91; HRMS Calcd for $\text{C}_{13}\text{H}_9\text{NClF}$ $[\text{M}+\text{H}]^+$: 234.0480; Found: 234.0482.

**(E)-3-chloro-N-(4-chlorobenzylidene)aniline (3ac)**

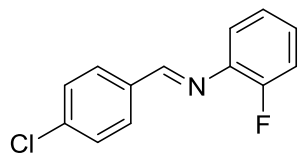
103 mg, 83% isolated yield. ^1H NMR (CDCl_3 , 200 MHz) δ 8.29 (s, 1H), 7.74 (d, $J = 8.6$ Hz, 2H), 7.36 (d, $J = 8.5$ Hz, 2H), 7.23-7.10 (m, 3H), 6.98 (d, $J = 7.91$, 1H). ^{13}C NMR (CDCl_3 , 50

(MHz) δ 159.76, 152.95, 137.81, 134.78, 134.31, 130.89, 130.18, 130.09, 129.46, 129.15, 126.05, 120.87, 119.36; HRMS Calcd for $C_{13}H_9NCl_2$ $[M+H]^+$: 250.0185; Found: 250.0187.



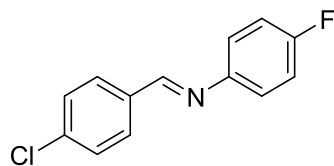
(E)-3-bromo-N-(4-chlorobenzylidene)aniline (3ad)

130 mg, 89% isolated yield. 1H NMR ($CDCl_3$, 500 MHz) δ 8.31 (s, 1H), 7.76 (d, $J = 8.3$ Hz, 2H), 7.38 (d, $J = 8.3$ Hz, 2H), 7.31–7.14 (m, 3H), 7.06 (d, $J = 7.8$ Hz, 1H); ^{13}C NMR ($CDCl_3$, 125 MHz) δ 159.76, 153.01, 137.77, 134.23, 130.85, 130.54, 130.44, 130.07, 129.41, 129.11, 128.92, 123.64, 119.90; HRMS Calcd for $C_{13}H_9NBrCl$ $[M+H]^+$: 293.9680; Found: 293.9684.



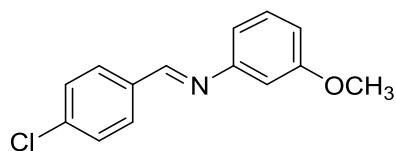
(E)-N-(4-chlorobenzylidene)-2-fluoroaniline (3ae)

68 mg, 58% isolated yield. 1H NMR ($CDCl_3$, 500 MHz) δ 8.50 (s, 1H), 7.87 (d, $J = 8.6$ Hz, 2H), 7.46 (d, $J = 8.6$ Hz, 2H), 7.27 - 7.15 (m, 4H). ^{13}C NMR ($CDCl_3$, 125 MHz) δ 161.33, 156.15, 154.16, 139.61, 139.53, 137.77, 134.50, 130.08, 129.06, 126.94, 126.88, 124.50, 124.47, 122.02, 116.37, 116.21; HRMS Calcd for $C_{13}H_9NCIF$ $[M+H]^+$: 234.0480; Found: 234.0482.

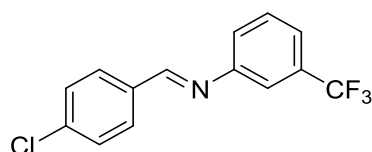


(E)-N-(4-chlorobenzylidene)-4-fluoroaniline (3af)

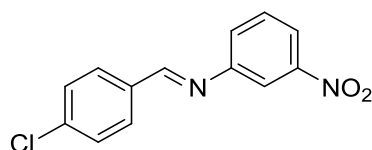
87 mg, 75% isolated yield. 1H NMR ($CDCl_3$, 200 MHz) δ 8.41 (s, 1H), 7.85 (d, $J = 8.7$ Hz, 2H), 7.47 (d, $J = 8.7$ Hz, 2H), 7.37 (d, $J = 8.5$ Hz, 2H), 7.15 (d, $J = 8.7$ Hz, 2H). ^{13}C NMR ($CDCl_3$, 125 MHz) δ 159.12, 150.10, 137.65, 134.44, 131.75, 130.90, 130.01, 129.46, 129.29, 129.14, 122.17; HRMS Calcd for $C_{13}H_9NCIF$ $[M+H]^+$: 234.0480; Found: 234.0482.

**(E)-N-(4-chlorobenzylidene)-3-methoxyaniline (3ag)**

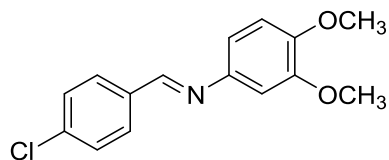
68 mg, 55% isolated yield. ^1H NMR (CDCl_3 , 500 MHz) δ 8.43 (s, 1H), 7.85 (d, $J = 8.6$ Hz, 2H), 7.46 (d, $J = 8.2$ Hz, 2H), 7.31 (t, $J = 8.2$ Hz, 1H), 6.82 - 6.78 (m, 3H), 3.85 (s, 3H). ^{13}C NMR (CDCl_3 , 125 MHz) δ 160.31, 159.01, 153.08, 137.42, 134.56, 129.97, 129.94, 129.08, 112.79, 112.02, 106.62, 55.33; HRMS Calcd for $\text{C}_{14}\text{H}_{12}\text{NClO}$ $[\text{M}+\text{H}]^+$: 246.0680; Found: 246.0683.

**(E)-N-(4-chlorobenzylidene)-3-(trifluoromethyl)aniline (3ah)**

134 mg, 95% isolated yield. ^1H NMR (CDCl_3 , 500 MHz) δ 8.44 (s, 1H), 7.87 (d, $J = 8.6$ Hz, 2H), 7.53-7.45 (m, 4H), 7.39 - 7.37 (m, 2H). ^{13}C NMR (CDCl_3 , 125 MHz) δ 160.24, 152.12, 137.96, 134.19, 130.14, 129.73, 129.20, 128.32, 124.15, 122.66, 117.71; HRMS Calcd for $\text{C}_{14}\text{H}_9\text{NClF}_3$ $[\text{M}+\text{H}]^+$: 284.0448; Found: 284.0450.

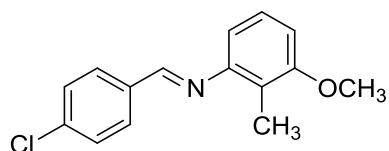
**(E)-N-(4-chlorobenzylidene)-3-nitroaniline (3ai)**

120 mg, 92% isolated yield. ^1H NMR (CDCl_3 , 500 MHz) δ 8.47 (s, 1H), 8.11 (dt, $J = 8.2, 2.2$ Hz, 1H), 8.05 (t, $J = 2.2$ Hz, 1H), 7.88 (d, $J = 8.5$ Hz, 2H), 7.58 (t, $J = 7.7$ Hz, 1H), 7.54 (dt, $J = 8.5, 1.6$ Hz, 1H), 7.50 (d, $J = 8.5$ Hz, 2H). ^{13}C NMR (CDCl_3 , 125 MHz) δ 161.08, 152.75, 138.33, 133.88, 130.29, 129.96, 129.27, 129.11, 127.62, 120.67, 115.31; HRMS Calcd for $\text{C}_{13}\text{H}_9\text{N}_2\text{O}_2$ $[\text{M}+\text{H}]^+$: 261.0425; Found: 261.0733.



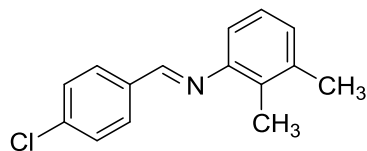
(E)-N-(4-chlorobenzylidene)-3,4-dimethoxyaniline (3aj)

71 mg, 51% isolated yield. ^1H NMR (CDCl_3 , 400 MHz) δ 8.44 (s, 1H), 7.81 (d, $J = 8.6$ Hz, 2H), 7.42 (d, $J = 8.6$ Hz, 2H), 6.89-6.87 (m, 2H), 6.82 (dd, $J = 8.2, 2.3$ Hz, 1H), 3.92 (s, 3H), 3.90 (s, 3H). ^{13}C NMR (CDCl_3 , 100 MHz) δ 156.80, 149.26, 147.83, 144.74, 136.92, 134.73, 129.64, 128.93, 112.12, 111.30, 105.51, 55.99, 55.80; HRMS Calcd for $\text{C}_{15}\text{H}_{15}\text{NO}_2\text{Cl}$ $[\text{M}+\text{H}]^+$: 276.0786; Found: 276.0787.



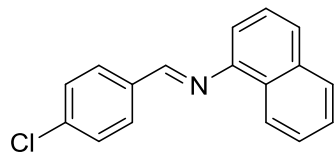
(E)-N-(4-chlorobenzylidene)-3-methoxy-2-methylaniline (3ak)

91 mg, 70% isolated yield. ^1H NMR (CDCl_3 , 500 MHz) δ 8.33 (s, 1H), 7.87 (d, $J = 7.4$ Hz, 2H), 7.46 (d, $J = 8.1$ Hz, 2H), 7.18 (t, $J = 7.5$ Hz, 1H), 6.77 (d, $J = 7.3$ Hz, 1H), 6.60 (d, $J = 7.7$ Hz), 3.88 (s, 3H), 2.25 (s, 3H). ^{13}C NMR (CDCl_3 , 125 MHz) δ 158.13, 151.62, 137.20, 134.98, 129.86, 129.01, 126.56, 120.40, 110.50, 107.79, 55.68, 10.32; HRMS Calcd for $\text{C}_{15}\text{H}_{14}\text{ONCl}$ $[\text{M}+\text{H}]^+$: 260.0764; Found: 260.0837.



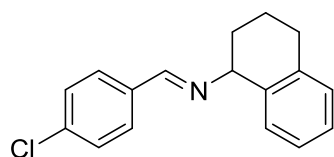
(E)-N-(4-chlorobenzylidene)-2,3-dimethylaniline (3al)

97 mg, 81% isolated yield. ^1H NMR (CDCl_3 , 200 MHz) δ 8.32 (s, 1H), 7.87 (d, $J = 8.7$ Hz, 2H), 7.46 (d, $J = 8.2$ Hz, 2H), 7.17 - 7.04 (m, 2H), 6.79 (d, $J = 7.2$ Hz, 1H), 2.33 (s, 3H), 2.30 (s, 3H). ^{13}C NMR (CDCl_3 , 50 MHz) δ 157.69, 150.67, 137.51, 137.05, 135.01, 130.47, 129.80, 128.98, 127.46, 126.02, 115.33, 20.09, 13.79; HRMS Calcd for $\text{C}_{15}\text{H}_{14}\text{NCl}$ $[\text{M}+\text{H}]^+$: 244.0888; Found: 244.0890.



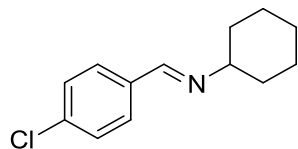
(E)-N-(4-chlorobenzylidene) naphthalen-1-amine (3am)

121 mg, 91% isolated yield. ^1H NMR (CDCl_3 , 500 MHz) δ 8.6 (s, 1H), 7.91-7.86 (m, 5H), 7.62 (s, 1H), 7.53 - 7.45 (m, 5H). ^{13}C NMR (CDCl_3 , 125 MHz) δ 158.92, 149.16, 137.38, 134.66, 134.00, 132.05, 129.97, 129.08, 129.00, 127.92, 127.71, 126.45, 125.47, 120.89, 117.93; HRMS Calcd for $\text{C}_{17}\text{H}_{12}\text{NCl}$ $[\text{M}+\text{H}]^+$: 266.0731; Found: 266.0733.



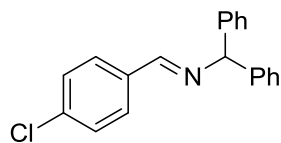
(E)-N-(4-chlorobenzylidene)-1,2,3,4-tetrahydronaphthalen-1-amine (3an)

109 mg, 81% isolated yield. ^1H NMR (CDCl_3 , 500 MHz) δ 8.4 (s, 1H), 7.74 (d, $J = 8.2$ Hz, 2H), 7.40 (d, $J = 8.9$ Hz, 2H), 7.19 - 7.14 (m, 3H), 7.02 (2, $J = 8.2$ Hz, 1H), 4.54 (t, $J = 7$ Hz, 1H), 2.96 - 2.84 (m, 2H), 2.13 - 2.02 (m, 3H), 1.91 - 1.84 (m, 1H). ^{13}C NMR (CDCl_3 , 125 MHz) δ 159.15, 137.15, 136.96, 136.56, 134.80, 129.56, 129.25, 128.84, 128.58, 127.01, 125.83, 68.52, 31.52, 29.49, 20.10; HRMS Calcd for $\text{C}_{17}\text{H}_{16}\text{NCl}$ $[\text{M}+\text{H}]^+$: 270.1044; Found: 270.1042.



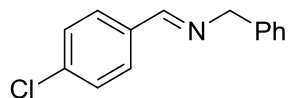
(E)-N-(4-chlorobenzylidene)cyclohexanamine (3ao)

82 mg, 74% isolated yield. ^1H NMR (CDCl_3 , 500 MHz) δ 8.27 (s, 1H), 7.67 (d, $J = 7.7$ Hz, 2H), 7.37 (d, $J = 7.7$ Hz, 2H), 3.19 (s, 1H), 1.85 - 1.82 (m, 2H), 1.74 - 1.67 (m, 3H), 1.62 - 1.55 (m, 2H), 1.40 - 1.33 (m, 2H), 1.30 - 1.25 (m, 1H). ^{13}C NMR (CDCl_3 , 125 MHz) δ 157.25, 136.16, 135.01, 129.20, 128.72, 69.92, 34.25, 25.55, 24.71; HRMS Calcd for $\text{C}_{13}\text{H}_{16}\text{NCl}$ $[\text{M}+\text{H}]^+$: 222.1044; Found: 222.1042.



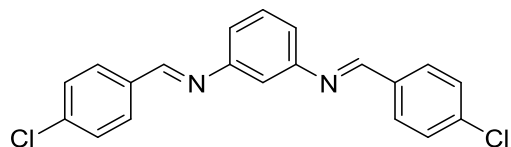
(E)-N-(4-chlorobenzylidene)-1,1-diphenylmethanamine (3aq)

94 mg, 62% isolated yield. ^1H NMR (CDCl_3 , 500 MHz) δ 8.40 (s, 1H), 7.80 (d, $J = 8.5$ Hz, 2H), 7.42 – 7.30 (m, 11H), 7.26 – 7.20 (m, 1H), 5.62 (s, 1H). ^{13}C NMR (CDCl_3 , 125 MHz) δ 159.44, 143.65, 136.70, 134.74, 129.62, 128.79, 128.46, 127.60, 127.05, 77.84; HRMS Calcd for $\text{C}_{20}\text{H}_{16}\text{NCl}$ $[\text{M}+\text{H}]^+$: 306.1044; Found: 306.1042.



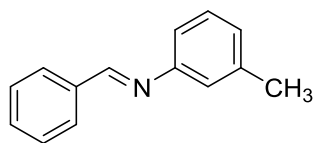
(E)-N-(4-chlorobenzylidene)-1-phenylmethanamine (3ar)

46 mg, 40% isolated yield. ^1H NMR (CDCl_3 , 200 MHz) δ 8.25 (s, 1H), 7.63 (d, $J = 8.5$ Hz, 2H), 7.31 – 7.21 (m, 7H), 4.73 (d, $J = 1.1$ Hz, 1H). ^{13}C NMR (CDCl_3 , 50 MHz) δ 160.47, 139.01, 136.66, 134.60, 129.41, 128.83, 128.50, 127.95, 127.04, 64.94; HRMS Calcd for $\text{C}_{14}\text{H}_{12}\text{NCl}$ $[\text{M}+\text{H}]^+$: 230.0731; Found: 230.0730.



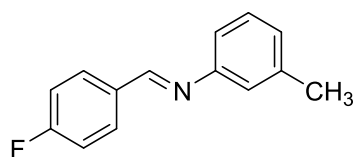
(E,E)-N¹,N³-bis(4-chlorobenzylidene)benzene-1,3-diamine (3as)

132 mg, 75% isolated yield. ^1H NMR (CDCl_3 , 500 MHz) δ 8.48 (s, 2H), 7.86 (d, $J = 8.5$ Hz, 4H), 7.47 (d, $J = 8.5$ Hz, 4H), 7.42 (t, $J = 8.1$ Hz, 1H), 7.11 (dd, $J = 7.6, 1.8$ Hz, 2H), 7.06 (s, 1H). ^{13}C NMR (CDCl_3 , 125 MHz) δ 159.25, 152.64, 137.52, 134.53, 129.99, 129.86, 129.10, 129.01, 118.77, 113.04; HRMS Calcd for $\text{C}_{20}\text{H}_{14}\text{N}_2\text{Cl}_2$ $[\text{M}+\text{H}]^+$: 353.0607; Found: 353.0603.



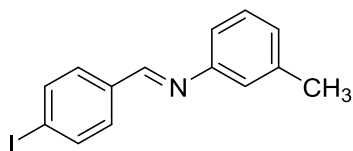
(E)-N-benzylidene-3-methylaniline (3ba)

70 mg, 72% isolated yield. ^1H NMR (CDCl_3 , 200 MHz) δ 8.47 (s, 1H), 7.94 – 7.89 (m, 2H), 7.50–7.47 (m, 3H), 7.33 – 7.29 (m, 1H), 7.09 – 7.01 (m, 3H), 2.41 (s, 3H). ^{13}C NMR (CDCl_3 , 50 MHz) δ ppm 160.25, 131.35, 129.79, 129.01, 128.80, 126.75, 121.66, 117.87, 21.45; HRMS Calcd for $\text{C}_{14}\text{H}_{13}\text{N}$ $[\text{M}+\text{H}]^+$: 196.1121; Found: 196.1121.

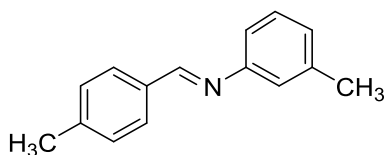


(E)-N-(4-fluorobenzylidene)-3-methylaniline (3bb)

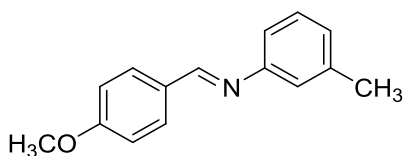
92 mg, 86% isolated yield. ^1H NMR (CDCl_3 , 200 MHz) δ 8.31 (s, 1H), 7.79 (d, $J = 8.1$ Hz, 2H), 7.23 - 6.90 (m, 6H), 2.30 (s, 3H). ^{13}C NMR (CDCl_3 , 50 MHz) δ 167.12, 162.12, 158.52, 151.81, 138.96, 132.58, 130.77, 130.60, 128.95, 126.75, 121.55, 117.76, 116.07, 115.63, 21.34; HRMS Calcd for $\text{C}_{14}\text{H}_{12}\text{NF}$ $[\text{M}+\text{H}]^+$: 214.1027; Found: 214.1027.

**(E)-N-(4-iodobenzylidene)-3-methylaniline (3bc)**

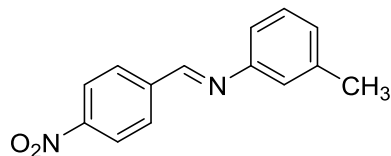
125 mg, 78% isolated yield. ^1H NMR (CDCl_3 , 400 MHz) δ 8.37 (s, 1H), 7.81 (d, $J = 8.2$ Hz, 2H), 7.61 (d, $J = 8.2$ Hz, 2H), 7.26 (s, 1H), 7.06-6.99 (m, 1H), 2.38 (s, 3H); ^{13}C NMR (CDCl_3 , 100 MHz) δ 158.91, 151.62, 139.04, 137.97, 135.70, 130.14, 129.01, 127.00, 121.57, 117.79, 98.09, 21.38; HRMS Calcd for $\text{C}_{14}\text{H}_{12}\text{NI}$ $[\text{M}+\text{H}]^+$: 322.0087; Found: 322.0086.

**(E)-3-methyl-N-(4-methylbenzylidene)aniline (3bd)**

53 mg, 51% isolated yield. ^1H NMR (CDCl_3 , 200 MHz) δ 8.32 (s, 1H), 7.70 (d, $J = 8.8$ Hz, 2H), 7.20-7.15 (m, 3H), 6.97-6.91 (m, 3H), 2.33 (s, 3H), 2.30 (s, 3H). ^{13}C NMR (CDCl_3 , 50 MHz) δ 160.07, 152.22, 141.72, 138.87, 133.71, 129.45, 128.90, 128.74, 126.47, 121.60, 117.81, 21.56, 21.36; HRMS Calcd for $\text{C}_{15}\text{H}_{15}\text{N}$ $[\text{M}+\text{H}]^+$: 210.1277; Found: 210.1277.

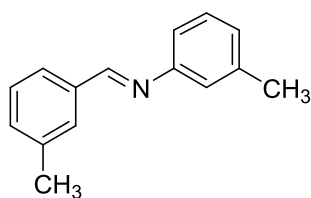
**(E)-N-(4-methoxybenzylidene)-3-methylaniline (3be)**

70 mg, 62% isolated yield. ^1H NMR (CDCl_3 , 200 MHz) δ 8.38 (s, 1H), 7.84 (d, $J = 8.9$ Hz, 2H), 7.31-7.23 (m, 1H), 7.04 - 6.96 (m, 5H), 3.87 (s, 3H), 2.38 (s, 3H). ^{13}C NMR (CDCl_3 , 125 MHz) δ 162.15, 159.53, 152.30, 138.90, 130.44, 129.25, 128.91, 126.31, 121.61, 117.81, 114.13, 55.41, 21.40.



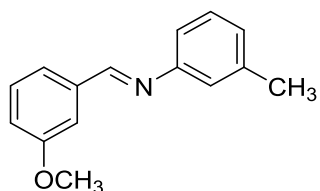
(E)-3-methyl-N-(4-nitrobenzylidene)aniline (3bf)

96 mg, 80% isolated yield. ^1H NMR (CDCl_3 , 400 MHz) δ 8.56 (s, 1H), 8.34 (d, $J = 8.7$ Hz, 2H), 8.08 (d, $J = 8.7$ Hz, 2H), 7.33 (t, $J = 7.3$ Hz, 1H), 7.14-7.07 (m, 3H), 2.42 (s, 3H). ^{13}C NMR (CDCl_3 , 100 MHz) δ 157.19, 151.01, 149.34, 141.74, 139.32, 129.43, 129.23, 127.93, 124.09, 121.78, 118.00, 77.08, 21.47; HRMS Calcd for $\text{C}_{14}\text{H}_{12}\text{O}_2\text{N}_2$ $[\text{M}+\text{H}]^+$: 241.0972; Found: 241.0972.



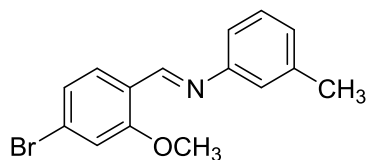
(E)-3-methyl-N-(3-methylbenzylidene)aniline (3bg)

95 mg, 91% isolated yield. ^1H NMR (CDCl_3 , 200 MHz) δ 8.33 (s, 1H), 7.67 (s, 1H), 7.56 (d, $J = 7.8$ Hz, 1H), 7.22-7.15 (m, 3H), 6.97-6.90 (m, 3H), 2.33 (s, 3H), 2.30 (s, 3H). ^{13}C NMR (CDCl_3 , 50 MHz) δ 160.42, 152.16, 138.94, 138.52, 136.23, 132.15, 128.93, 128.62, 126.62, 126.37, 121.61, 117.81, 21.38, 21.28; HRMS Calcd for $\text{C}_{15}\text{H}_{15}\text{N}$ $[\text{M}+\text{H}]^+$: 210.1277; Found: 210.1279.



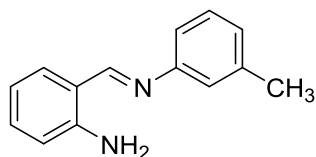
(E)-N-(3-methoxybenzylidene)-3-methylaniline (3bh)

67 mg, 60% isolated yield. ^1H NMR (CDCl_3 , 200 MHz) δ 8.37 (s, 1H), 7.47-7.31 (m, 3H), 7.23-7.19 (dd, $J = 7.3, 2.6$ Hz, 1H), 7.02-6.69 (m, 4H), 3.84 (s, 3H), 2.34 (s, 3H). ^{13}C NMR (CDCl_3 , 125 MHz) δ 162.15, 159.53, 152.30, 138.90, 130.44, 129.25, 128.91, 126.31, 121.61, 117.81, 114.13, 55.41, 21.40; HRMS Calcd for $\text{C}_{15}\text{H}_{15}\text{NO}$ $[\text{M}+\text{H}]^+$: 226.1226; Found: 226.1227.



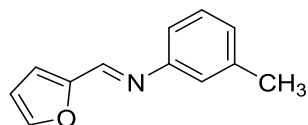
(E)-N-(4-bromo-2-methoxybenzylidene)-3-methylaniline (3bi)

70 mg, 46% isolated yield. ^1H NMR (CDCl_3 , 500 MHz) δ 8.78 (s, 1H), 7.97 (d, $J = 8.2$ Hz, 1H), 7.23-6.96 (m, 6H), 3.86 (s, 3H), 2.35 (s, 3H). ^{13}C NMR (CDCl_3 , 125 MHz) δ 159.66, 155.14, 152.33, 138.90, 128.89, 128.65, 126.67, 126.46, 124.15, 123.79, 121.71, 118.01, 115.33, 114.69, 55.83, 21.38; HRMS Calcd for $\text{C}_{15}\text{H}_{14}\text{ONBr}$ $[\text{M}+\text{H}]^+$: 304.0332; Found: 304.0333.



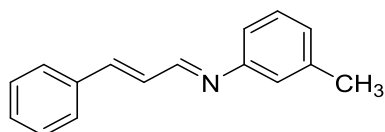
(E)-N-(2-aminobenzylidene)-3-methylaniline (3bj)

70 mg, 67% isolated yield. ^1H NMR (CDCl_3 , 500 MHz) δ 8.53 (s, 1H), 7.35 (d, $J = 8.0$ Hz, 1H), 7.20 (d, $J = 8.0$ Hz, 1 H), 7.06-6.99 (m, 3H), 6.77-6.70 (m, 3H), 6.53(s, 1H), 2.40 (s, 3H). HRMS Calcd for $\text{C}_{14}\text{H}_{14}\text{N}_2$ $[\text{M}+\text{H}]^+$: 211.1230; Found: 211.1230.



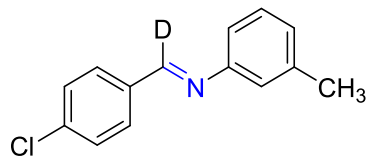
(E)-N-(furan-2-ylmethylene)-3-methylaniline (3bk)

70 mg, 76% isolated yield. ^1H NMR (CDCl_3 , 200 MHz) δ 8.24 (s, 1H), 7.57 (s, 1H), 7.24-7.19 (m, 1H), 7.03-6.99 (m, 3H), 6.90 (d, $J = 3.5$ Hz, 1H), 6.52-6.50 (m, 1H), 2.34 (s, 3H). ^{13}C NMR (CDCl_3 , 100 MHz) δ 152.10, 151.32, 147.49, 145.52, 138.94, 128.93, 126.97, 121.65, 118.02, 116.04, 112.08, 21.35; HRMS Calcd for $\text{C}_{12}\text{H}_{11}\text{ON}$ $[\text{M}+\text{H}]^+$: 186.0913; Found: 186.0914.



(E)-3-methyl-N-((E)-3-phenylallylidene)aniline (3bl)

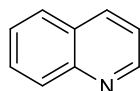
50 mg, 45% Isolated yield. ^1H NMR (CDCl_3 , 500 MHz) δ 8.26 (d, $J = 7.5$ Hz, 1H), 7.53 (d, $J = 7.5$ Hz, 1H), 7.40-7.34 (m, 3H), 7.25 (d, $J = 6.5\text{Hz}$, 1H), 7.16-6.97 (m, 3H), 2.37 (s, 3H). ^{13}C NMR (CDCl_3 , 125 MHz) δ 161.44, 151.71, 143.83, 138.99, 135.62, 129.54, 128.98, 128.91, 128.65, 127.47, 126.89, 121.61, 117.95, 21.39; HRMS Calcd for $\text{C}_{16}\text{H}_{15}\text{N}$ $[\text{M}+\text{H}]^+$: 222.1277; Found: 222.1277.



(E)-1-(4-chlorophenyl)-N-(m-tolyl)methanimine-d (3aa-d)

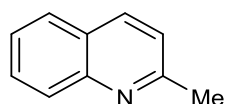
^1H NMR (CDCl_3 , 500 MHz) δ 7.85 (d, $J = 8.4$ Hz, 2H), 7.46 (d, $J = 8.4$ Hz, 2H), 7.29 (t, $J = 7.2$ Hz, 1H), 7.08-7.02 (m, 3H), 2.40 (s, 3H); HRMS Calcd for $\text{C}_{14}\text{H}_{11}\text{NClD}$ $[\text{M}+\text{H}]^+$: 231.0794; Found: 231.0794.

Chapter 3A



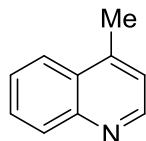
Quinoline (2a)

Compound **2a** was prepared according to the general procedure as described and was purified by silica gel column chromatography using petroleum ether/ethyl. Yield: 93% (60 mg); ^1H NMR (200 MHz, CDCl_3) δ 7.27-7.79 (m, 4H), 8.09-8.15 (m, 2H), 8.90 (s, 1H); ^{13}C NMR (125 MHz, CDCl_3) δ 120.9, 126.4, 127.6, 128.1, 129.2, 135.96, 148.03, 150.173; HRMS (ESI) calculated for $\text{C}_9\text{H}_7\text{N}$ $[\text{M}+\text{H}]^+$: 130.0651; found: 130.0651.



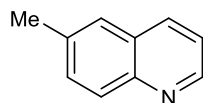
2-Methylquinoline (2b)

Compound **2b** was prepared according to the general procedure as described and was purified by silica gel column chromatography using petroleum ether/ethyl acetate. Yield: 94% (67 mg); ^1H NMR (500 MHz, CDCl_3) δ 2.70 (s, 1H), 7.18-7.20 (t, $J = 8.2$ Hz, 1H), 7.40-7.43 (t, $J = 7.9$ Hz, 1H), 7.61-7.64 (t, $J = 8.5$ Hz, 1H), 7.68-7.70 (d, $J = 7.9$ Hz, 1H), 7.94-7.95 (d, $J = 8.5$ Hz, 1H), 7.99-8.01 (d, $J = 8.5$ Hz, 1H); ^{13}C NMR (125 MHz, CDCl_3) δ 25.2, 121.8, 124.4, 126.3, 127.3, 128.4, 129.2, 135.9, 147.7, 158.8; HRMS (ESI) calculated for $\text{C}_{10}\text{H}_9\text{N}$ $[\text{M}+\text{H}]^+$ 144.0808; found: 144.0809.



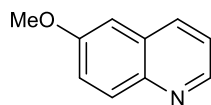
4-Methylquinoline (2c)

Compound **2c** was prepared according to the general procedure as described and was purified by silica gel column chromatography using petroleum ether/ethyl acetate. Yield: 91% (65 mg); δ = 2.65 (s, 3H), 7.18 (d, J = 3.5 Hz, 1H), 7.52 (t, J = 7.6 Hz, 1H), 7.68 (t, J = 7.7 Hz, 1H), 7.95 (d, J = 8.3 Hz, 1H), 8.10 (d, J = 8.3 Hz, 1H), 8.76 (s, 1H); ^{13}C NMR (126 MHz, CDCl_3): δ = 18.48, 121.74, 123.68, 126.13, 128.17, 128.95, 129.90, 144.10, 147.88, 150.01; HRMS (ESI) m/z calculated for $\text{C}_{10}\text{H}_{10}\text{N}$ $[\text{M}+\text{H}]^+$ 144.0808; found 144.0808.



6-Methylquinoline (2d)

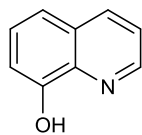
Compound **2d** was prepared according to the general procedure as described and was purified by silica gel column chromatography using petroleum ether/ethyl acetate. Yield: 97% (69 mg); ^1H NMR (500 MHz, CDCl_3) δ 2.47 (s, 3H), 7.26-7.29 (d, J = 4.2 Hz, 1H), 7.48-7.49 (m, 2H), 7.97-8.00 (t, J = 8.5 Hz, 2H), 7.80-8.81 (dd, J = 3.9 Hz, 1H); ^{13}C NMR (125 MHz, CDCl_3) δ 21.3, 120.8, 126.4, 128.1, 128.8, 131.5, 135.1, 136.1, 146.6, 149.2. HRMS (ESI) calculated for $\text{C}_{10}\text{H}_9\text{N}$ $[\text{M}+\text{H}]^+$ 144.0807; found: 144.0808.



6-Methoxyquinoline (2e)

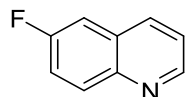
Compound **2e** was prepared according to the general procedure as described and was purified by silica gel column chromatography using petroleum ether/ethyl acetate. Yield: 92% (73 mg); ^1H NMR (500 MHz, CDCl_3) δ 3.92 (s, 3H), 7.05-7.06 (d, J = 2.7 Hz, 1H), 7.32-7.34 (q, J = 4.2 Hz, 1H), 7.35-7.38 (dd, J = 9.1 Hz, 1H), 7.99-8.01 (d, J = 9.1 Hz, 1H), 8.02-8.04 (d, J = 8.2 Hz, 1H),

8.75-8.76 (d, $J = 4.2$ Hz, 1H); ^{13}C NMR (125 MHz, CDCl_3) δ 55.4, 105.1, 121.3, 122.2, 129.3, 130.8, 134.7, 144.4, 147.9, 157.7; HRMS (ESI) calculated for $\text{C}_{10}\text{H}_9\text{NO}$ $[\text{M}+\text{H}]^+$: 160.0757; found: 160.0756.



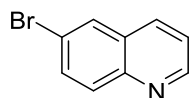
Quinolin-8-ol (2f)

Compound **2f** was prepared according to the general procedure as described and was purified by silica gel column chromatography using petroleum ether/ethyl acetate. Yield: 98% (71 mg); ^1H NMR (500 MHz, CDCl_3) δ 7.18-7.52 (m, 4H), 8.17 (dd, $J = 8.4$ Hz 1H), 8.80 (dd, $J = 4.2$ Hz 1H); ^{13}C NMR (126 MHz, CDCl_3) δ 76.7, 77.3, 110.0, 117.9, 121.8, 127.7, 128.5, 136.1, 138.3, 147.9, 152.2.



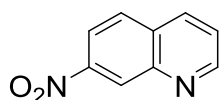
6-Fluoroquinoline (2g)

Compound **2g** was prepared according to the general procedure as described and was purified by silica gel column chromatography using petroleum ether/ethyl. Yield: 78% (57 mg); ^1H NMR (500 MHz, CDCl_3): $\delta = 7.42$ -7.38 (m, 2H), 7.47 (dt, $J = 9.1, 2.7$ Hz, 1H), 8.11-8.07 (m, 2H), 8.87 (dd, $J = 4.1, 1.1$ Hz, 1H); ^{13}C NMR (126 MHz, CDCl_3): $\delta = 110.62$ (d, $J_{\text{C-F}} = 21.9$ Hz), 119.68 (d, $J_{\text{C-F}} = 25.8$ Hz), 121.70, 128.81 (d, $J_{\text{C-F}} = 9.5$ Hz), 131.92 (d, $J_{\text{C-F}} = 9.5$ Hz), 135.33 (d, $J_{\text{C-F}} = 5.6$ Hz), 145.33, 149.62 (d, $J_{\text{C-F}} = 2.8$ Hz), 160.32 (d, $J_{\text{C-F}} = 248.2$ Hz); HRMS (ESI) m/z calculated for $\text{C}_9\text{H}_7\text{FN}$ $[\text{M}+\text{H}]^+$ 148.0557; found 148.0556.



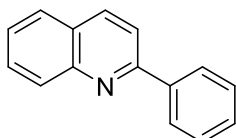
6-Bromoquinoline (2h)

Compound **2h** was prepared according to the general procedure as described and was purified by silica gel column chromatography using petroleum ether/ethyl acetate. Yield: 95% (97 mg); ^1H NMR (500 MHz, CDCl_3): $\delta = 7.42$ (dd, $J = 8.3, 4.1$ Hz, 1H), 7.78 (dd, $J = 9.0, 2.3$ Hz, 1H), 7.99 - 7.97 (m, 2H), 8.06 (d, $J = 8.1$ Hz, 1H), 8.92 (dd, $J = 4.2, 1.5$ Hz, 1H); ^{13}C NMR (126 MHz, CDCl_3): $\delta = 120.42, 121.85, 129.31, 129.76, 131.18, 132.91, 135.01, 146.79, 150.69$; HRMS (ESI) m/z calculated for $\text{C}_9\text{H}_7\text{BrN}[\text{M}+\text{H}]^+$ 207.9756; found 207.9759.



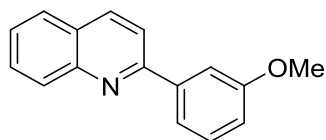
7-Nitroquinoline (2i)

Compound **2i** was prepared according to the general procedure as described and was purified by silica gel column chromatography using petroleum ether/ethyl acetate. Yield: 80% (69 mg); ^1H NMR (200 MHz, CDCl_3) $\delta = 7.61$ - 7.63 (q, $J = 4.1$ Hz, 1H), 7.96 - 8.01 (q, $J = 8.9$ Hz, 1H), 8.26 - 8.35 (dt, $J = 8.9$ Hz, 2H), 9.00 - 9.10 (d, $J = 2.1$ Hz, 1H), 9.07 - 9.10 (dd, $J = 1.6$ Hz, 1H); ^{13}C NMR (125 MHz, CDCl_3) $\delta = 120.1, 123.9, 125.8, 129.5, 131.4, 135.9, 147.1, 148.1, 152.7$; HRMS (ESI) calculated for $\text{C}_9\text{H}_6\text{N}_2\text{O}_2 [\text{M}+\text{H}]^+$: 175.0501; found: 175.0502.



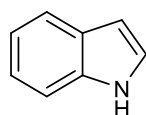
2-phenylquinoline (2j)

Compound **2j** was prepared according to the general procedure as described and was purified by silica gel column chromatography using petroleum ether/ethyl acetate. Yield: 54% (55 mg); ^1H NMR (500 MHz, CDCl_3) $\delta = 7.49$ (t, $J = 7.2$ Hz, 1H), 7.57 - 7.53 (m, 3H), 7.75 (t, $J = 8.0$ Hz, 1H), 7.83 (d, $J = 8.0$ Hz, 1H), 7.88 (d, $J = 8.4$ Hz, 1H), 8.21 (t, $J = 9.2$ Hz, 4H); ^{13}C NMR (126 MHz, CDCl_3) $\delta = 118.94, 126.22, 127.13, 127.41, 127.52, 128.79, 129.26, 129.59, 129.70, 136.70, 139.64, 148.24, 157.29$.



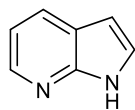
2-(3-Methoxyphenyl)quinoline (2k)

Compound **2k** was prepared according to the general procedure as described and was purified by silica gel column chromatography using petroleum ether/ethyl acetate. Yield: 57% (67 mg); ^1H NMR (400 MHz, CDCl_3): δ = 3.94 (s, 3H), 7.05 (dd, J = 8.5, 1.9 Hz, 1H), 7.45 (t, J = 8.0 Hz, 1H), 7.54 (t, J = 8.0 Hz, 1H), 7.76-7.72 (m, 2H), 7.84-7.80 (m, 2H), 7.86 (d, J = 8.6 Hz, 1H), 8.21 (dd, J = 8.5, 3.7 Hz, 2H); ^{13}C NMR (126 MHz, CDCl_3): δ = 55.34, 112.66, 115.30, 119.02, 119.95, 126.25, 127.20, 127.39, 129.58, 129.68, 129.74, 136.68, 141.09, 148.15, 157.04, 160.08. HRMS (ESI) m/z calculated for $\text{C}_{16}\text{H}_{14}\text{NO}$ $[\text{M}+\text{H}]^+$ 236.1070; found 236.1068.



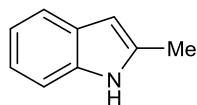
1H-indole (4a)

Compound **4a** was prepared according to the general procedure as described and was purified by silica gel column chromatography using petroleum ether/ethyl acetate. Yield: 98% (57 mg); ^1H NMR (200 MHz, CDCl_3) δ 6.62-6.65 (m, 1H), 7.15-7.32 (m, 3H), 7.44-7.49 (d, J = 8.2 Hz, 1H), 7.70-7.75 (d, J = 7.5 Hz, 1H), 8.19 (s, 1H); ^{13}C NMR (25 MHz, CDCl_3) δ 102.6, 110.9, 119.8, 121.9, 124.1, 127.8, 135.7.

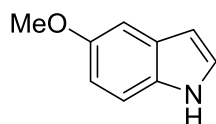


1H-pyrrolo[2,3-b]pyridine (4b)

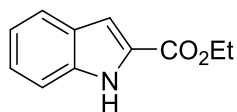
Compound **4b** was prepared according to the general procedure as described and was purified by silica gel column chromatography using petroleum ether/ethyl acetate. Yield: 90% (53 mg); ^1H NMR (500 MHz, CDCl_3) δ 6.54-6.54 (d, J = 3.0 Hz, 1H), 7.11-7.14 (q, J = 4.8 Hz, 1H), 7.41-7.41 (q, J = 3.3 Hz, 1H), 8.00-8.02 (d, J = 7.6 Hz, 1H), 8.35-8.35 (d, J = 4.5 Hz, 1H), ^{13}C NMR (125 MHz, CDCl_3) δ 100.8, 115.8, 120.7, 125.4, 129.4, 141.9, 148.2.

**2-Methyl-1H-indole (4c)**

Compound **4c** was prepared according to the general procedure as described and was purified by silica gel column chromatography using petroleum ether/ethyl acetate. Yield: 93% (61 mg); ^1H NMR (500 MHz, CDCl_3) δ 2.46 (s, 3H), 6.29 (s, 1H), 7.15-7.21 (m, 2H), 7.30-7.31 (d, $J = 7.6$ Hz, 1H), 7.60-7.11 (d, $J = 7.6$ Hz, 1H), 7.75 (s, 1H); ^{13}C NMR (125 MHz, CDCl_3) δ 13.6, 100.2, 110.2, 119.5, 120.8, 128.9, 135.1, 135.9.

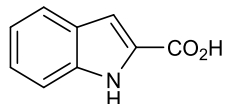
**5-Methoxy 1H-indole (4d)**

Compound **4d** was prepared according to the general procedure as described and was purified by silica gel column chromatography using petroleum ether/ethyl acetate. Yield: 92% (67 mg); ^1H NMR (500 MHz, CDCl_3): $\delta = 3.90$ (s, 3H), 6.52 (s, 1H), 6.92 (d, $J = 8.7$ Hz, 1H), 7.16 (s, 1H), 7.18 (t, $J = 2.6$ Hz, 1H), 7.29 (d, $J = 8.7$ Hz, 1H), 8.07 (brs, 1H); ^{13}C NMR (126 MHz, CDCl_3): $\delta = 55.81, 102.29, 111.69, 112.29, 124.87, 128.23, 130.92, 154.12$; HRMS (ESI) m/z calculated for $\text{C}_9\text{H}_{10}\text{NO}[\text{M}+\text{H}]^+$ 148.0757; found 148.0758.

**Ethyl 1H-indole-2-carboxylate (4e)**

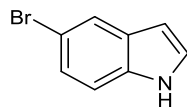
Compound **4e** was prepared according to the general procedure as described and was purified by silica gel column chromatography using petroleum ether/ethyl acetate. Yield: 88% (83 mg); ^1H NMR (400 MHz, CDCl_3): $\delta = 1.45$ (t, $J = 7.3$ Hz, 3H), 4.46 (q, $J = 6.8$ Hz, 2H), 7.18 (t, $J = 8.0$ Hz, 1H), 7.35 (t, $J = 7.7$ Hz, 1H), 7.27 (s, 1H), 7.46 (d, $J = 8.0$ Hz, 1H), 7.72 (d, $J = 7.7$ Hz, 1H), 9.32 (brs, 1H); ^{13}C NMR (101 MHz, CDCl_3): $\delta = 14.35, 61.04, 108.60, 111.90, 120.70, 122.54,$

125.26, 127.43, 136.91, 162.22; HRMS (ESI) m/z calculated for $C_{11}H_{11}NNaO_2[M+Na]^+$ 212.0682; found 212.0682.



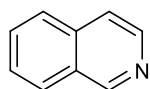
1*H*-indole-2-carboxylic acid (4f)

Compound **4f** was prepared according to the general procedure as described and was purified by silica gel column chromatography using petroleum ether/ethyl acetate. Yield 96% (77 mg); ¹H NMR (500 MHz, CDCl₃) δ 7.18-7.21 (t, $J = 7.6$ Hz, 1H), 7.36-7.40 (m, 2H), 7.46-7.47 (d, $J = 8.2$ Hz, 1H), 7.73-7.75 (d, $J = 8.2$ Hz, 1H), 8.97 (bs, 1H); ¹³C NMR (125 MHz, CDCl₃) δ 110.8, 111.9, 121.1, 122.9, 126.1, 127.4, 137.3, 166.1; HRMS (ESI) calculated for $C_9H_7NO_2 [M+H]^+$: 162.0546; found: 162.0550.



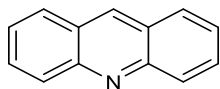
5-Bromo-1*H*-indole (4g)

Compound **4g** was prepared according to the general procedure as described and was purified by silica gel column chromatography using petroleum ether/ethyl acetate. Yield 98% (95 mg); ¹H NMR (500 MHz, CDCl₃) δ 6.52-6.53 (s, 1H), 7.27-7.30 (m, 3H), 7.29 (s, 1H), 8.22 (bs, 1H); ¹³C NMR (125 MHz, CDCl₃) δ 120.3, 112.4, 113.0, 123.2, 124.8, 125.3, 129.6, 134.4.

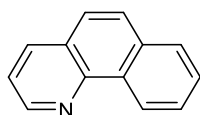


Isoquinoline (6a)

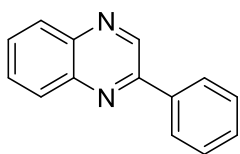
Compound **6a** was prepared according to the general procedure as described and was purified by silica gel column chromatography using petroleum ether/ethyl acetate. Yield: 93% (60 mg); ¹H NMR (200 MHz, CDCl₃) δ 7.63-7.95 (m, 4H), 8.09-8.13 (m, 2H), 9.24 (s, 1H); ¹³C NMR (25 MHz, CDCl₃) δ 120.3, 126.3, 127.1, 127.5, 128.5, 130.26, 130.64, 142, 152, HRMS (ESI) calculated for $C_9H_7N [M+H]^+$: 130.0651; found: 130.0651.

**Acridine (6b)**

Compound **6b** was prepared according to the general procedure as described and was purified by silica gel column chromatography using petroleum ether/ethyl acetate. Yield: 89% (80 mg); ^1H NMR (500 MHz, CDCl_3) δ 7.49-7.51 (q, $J = 5.4$ Hz, 2H), 7.74-7.78 (m, 2H), 7.94-7.97 (t, $J = 8.2$ Hz, 2H), 8.24-8.25 (t, $J = 8.8$ Hz, 2H), 8.69-8.71 (d, $J = 9.7$ Hz, 1H); ^{13}C NMR (125 MHz, CDCl_3) δ 125.6, 126.5, 128.1, 129.3, 130.1, 149.0.

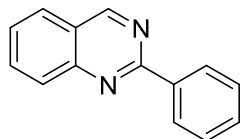
**Benzo[h]quinoline (6c)**

Compound **6c** was prepared according to the general procedure as described and was purified by silica gel column chromatography using petroleum ether/ethyl acetate. Yield: 74% (66 mg); ^1H NMR (500 MHz, CDCl_3) δ 7.49-7.51 (q, $J = 4.2$ Hz, 1H), 7.65-7.67 (d, $J = 8.8$ Hz, 1H), 7.70-7.73 (td, $J = 6.7$ Hz, 1H), 7.75-7.81 (m, 2H), 7.91-7.92 (d, $J = 8.2$ Hz, 1H), 8.13-8.15 (dd, $J = 7.9$ Hz, 1H), 9.02-9.03 (dd, $J = 4.5$ Hz, 1H), 9.34-9.36 (d, $J = 7.6$ Hz, 1H); ^{13}C NMR (125 MHz, CDCl_3) δ 121.6, 124.3, 125.2, 126.3, 126.9, 127.7, 128.1, 131.4, 133.5, 135.6, 146.5, 146.5, 148.7; HRMS (ESI) m/z calculated for $\text{C}_{13}\text{H}_{10}\text{N}[\text{M}+\text{H}]^+$ 180.0808; found 180.0806.

**2-Phenylquinoxaline (6d)**

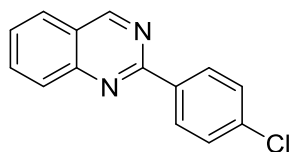
Compound **6d** was prepared according to the general procedure as described and was purified by silica gel column chromatography using petroleum ether/ethyl acetate. (96 mg, 99%); ^1H NMR (500 MHz, CDCl_3): $\delta = 7.59-7.51$ (m, 3H), 7.80-7.73 (m, 2H), 8.13 (d, $J = 8.0$ Hz, 1H), 8.16 (d, $J = 8.0$ Hz, 1H), 8.20 (d, $J = 8.3$ Hz, 2H), 9.33 (s, 1H), 8.16); ^{13}C NMR (126 MHz, CDCl_3): $\delta =$

127.50, 129.08, 129.10, 129.48, 129.58, 130.13, 130.22, 136.73, 141.53, 142.25, 143.31, 151.78, HRMS (ESI) m/z calculated for $C_{14}H_{11}N_2[M+H]^+$ 207.0917; found 207.0917.



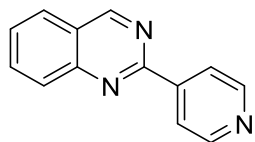
2-Phenylquinazoline (6e)

Compound **6e** was prepared according to the general procedure as described and was purified by silica gel column chromatography using petroleum ether/ethyl acetate. Yield: 96% (99 mg); 1H NMR (500 MHz, $CDCl_3$): δ = 7.57-7.51 (m, 3H), 7.63 (t, J = 7.6 Hz, 1H), 7.95-7.91 (m, 2H), 8.11 (d, J = 8.4 Hz, 1H), 8.63 (d, J = 8.4 Hz, 2H), 9.49 (s, 1H), ^{13}C NMR (126 MHz, $CDCl_3$): δ = 123.61, 127.12, 127.26, 128.57, 128.64, 130.60, 134.11, 138.04, 150.79, 160.50, 161.08; HRMS (ESI) m/z calculated for $C_{14}H_{11}N_2[M+H]^+$ 207.0917; found 207.0917.



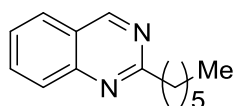
2-(4-Chlorophenyl)quinazoline (6f)

Compound **6f** was prepared according to the general procedure as described and was purified by silica gel column chromatography using petroleum ether/ethyl acetate. Yield: 91% (109 mg); 1H NMR (500 MHz, $CDCl_3$): δ = 7.50 (d, J = 8.4 Hz, 2H), 7.60 (t, J = 7.7 Hz, 1H), 7.91-7.88 (m, 2H), 8.06 (d, J = 8.8 Hz, 1H), 8.57 (d, J = 8.4 Hz, 2H), 9.41 (s, 1H); ^{13}C NMR (126 MHz, $CDCl_3$): δ = 123.49, 127.04, 127.34, 128.49, 128.70, 129.82, 134.13, 136.42, 136.72, 150.55, 159.87, 160.39; HRMS (ESI) m/z calculated for $C_{14}H_{10}ClN_2[M+H]^+$ 241.0527; found 241.0528.



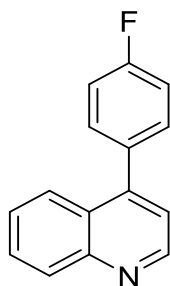
2-(Pyridin-4-yl)quinazoline (6g)

Compound **6g** was prepared according to the general procedure as described and was purified by silica gel column chromatography using petroleum ether/ethyl acetate. Yield: 94% (97 mg); ^1H NMR (500 MHz, CDCl_3): $\delta = 7.62(\text{t}, J = 7.6 \text{ Hz}, 1\text{H}), 7.90\text{-}7.88 (\text{m}, 2\text{H}), 8.05 (\text{d}, J = 9.1 \text{ Hz}, 1\text{H}), 8.40 (\text{d}, J = 5.5 \text{ Hz}, 2\text{H}), 8.77(\text{d}, J = 5.0 \text{ Hz}, 2\text{H}), 9.41 (\text{s}, 1\text{H})$; ^{13}C NMR (126 MHz, CDCl_3): $\delta = 122.20, 123.99, 127.04, 128.16, 128.72, 134.36, 145.14, 150.32, 150.38, 158.73, 160.57$; HRMS (ESI) m/z calculated for $\text{C}_{13}\text{H}_{10}\text{N}_3[\text{M}+\text{H}]^+$ 208.0869; found 208.0869.



2-Hexylquinazoline (**6h**)

Compound **6h** was prepared according to the general procedure as described and was purified by silica gel column chromatography using petroleum ether/ethyl acetate. Yield: 93% (73 mg); ^1H NMR (500 MHz, CDCl_3): $\delta = 0.82 (\text{s}, 3\text{H}), 1.40\text{-}1.24 (\text{m}, 6\text{H}), 1.87 (\text{quin}, J = 7.3 \text{ Hz}, 2\text{H}), 3.07 (\text{t}, J = 8.1 \text{ Hz}, 2\text{H}), 7.51 (\text{t}, J = 7.8 \text{ Hz}, 1\text{H}), 7.80 (\text{t}, J = 7.2 \text{ Hz}, 2\text{H}), 7.92 (\text{d}, J = 7.7 \text{ Hz}, 1\text{H}), 9.28 (\text{s}, 1\text{H})$; ^{13}C NMR (126 MHz, CDCl_3): $\delta = 13.93, 22.42, 28.85, 29.10, 31.57, 39.87, 122.89, 126.73, 126.91, 167.76, 127.73, 133.82, 150.20, 160.21$; HRMS (ESI) m/z calculated for $\text{C}_{14}\text{H}_{19}\text{N}_2[\text{M}+\text{H}]^+$ 215.1543; found 215.1541.

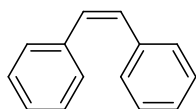


Compound **8** was prepared according to the general procedure as described and was purified by silica gel column chromatography using petroleum ether/ethyl acetate. Yield: 62% (27 mg); ^1H NMR (500 MHz, CDCl_3): $\delta = 7.23 (\text{t}, J = 8.5 \text{ Hz}, 2\text{H}), 7.32 (\text{d}, J = 4.2 \text{ Hz}, 1\text{H}), 7.54\text{-}7.47 (\text{m}, 3\text{H}), 7.74 (\text{t}, J = 8.2 \text{ Hz}, 1\text{H}), 7.88 (\text{d}, J = 8.5 \text{ Hz}, 1\text{H}), 8.19 (\text{d}, J = 8.9 \text{ Hz}, 1\text{H}), 8.95 (\text{d}, J = 4.4 \text{ Hz}, 1\text{H})$; ^{13}C NMR (126 MHz, CDCl_3): $\delta = 115.64 (\text{d}, J_{\text{C-F}} = 21.1 \text{ Hz}), 121.36, 125.56, 126.69, 126.76, 129.41, 129.89, 131.21 (\text{d}, J_{\text{C-F}} = 8.5 \text{ Hz}), 133.90 (\text{d}, J_{\text{C-F}} = 3.8 \text{ Hz}), 147.39, 148.63$,

149.91, 162.89 (d, $J_{C-F} = 247.7$ Hz); ^{19}F NMR (376 MHz, D_2O): $\delta = -113.26$; HRMS (ESI) m/z calculated for $\text{C}_{15}\text{H}_{11}\text{FN}$ $[\text{M}+\text{H}]^+$ 224.0870; found 224.0871.

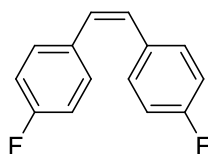
Chapter 3B

(Z)-1,2-diphenylethene (2a)



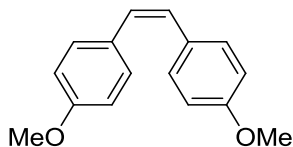
^1H NMR (400MHz, CDCl_3) $\delta = 7.30$ (d, $J = 9.2$ Hz, 10 H), 6.67 (s, 2 H).

(Z)-1,2-bis(4-fluorophenyl)ethane (2b)⁴



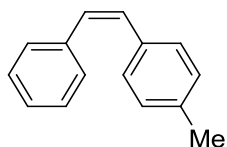
^1H NMR (500MHz, CDCl_3) $\delta = 7.24 - 7.15$ (m, 4 H), 6.93 (t, $J = 8.8$ Hz, 4 H), 6.55 (s, 2 H). ^{13}C NMR (126MHz, CDCl_3) $\delta = 162.8, 160.9, 133.0, 133.0, 130.5, 130.4, 129.1, 115.3, 115.2$.

(Z)-1,2-bis(4-methoxyphenyl)ethane (2c)⁵



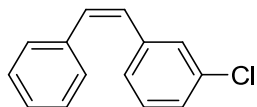
^1H NMR (500MHz, CDCl_3) $\delta = 7.23$ (d, $J = 8.8$ Hz, 4 H), 6.80 (d, $J = 8.8$ Hz, 4 H), 6.47 (s, 2 H), 3.81 (s, 7 H). ^{13}C NMR (126MHz, CDCl_3) $\delta = 158.5, 130.0, 129.3, 128.4, 113.7, 113.6, 55.1$.

(Z)-1-methyl-4-styrylbenzene (2d)



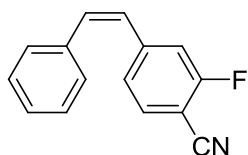
^1H NMR (400MHz, CDCl_3) δ = 7.40 - 7.35 (m, 2 H), 7.35 - 7.21 (m, 5 H), 7.12 (d, J = 7.9 Hz, 2 H), 6.65 (s, 2 H), 2.40 (s, 3 H). ^{13}C NMR (101MHz, CDCl_3) δ = 137.5, 136.8, 134.3, 130.2, 129.5, 128.9, 128.8, 128.8, 128.2, 126.9, 21.2.

(Z)-1-chloro-3-styrylbenzene (2f)



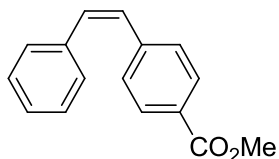
^1H NMR (500MHz, CDCl_3) δ = 7.32 - 7.23 (m, 6 H), 7.23 - 7.13 (m, 3 H), 6.70 (d, J = 12.2 Hz, 1 H), 6.57 (d, J = 12.2 Hz, 1 H).

(Z)-2-fluoro-4-styrylbenzotrile (2h)



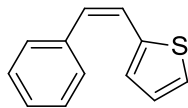
^1H NMR (500MHz, CDCl_3) δ = 7.30 (br. s., 4 H), 7.22 (br. s., 2 H), 7.17 - 7.01 (m, 3 H), 6.85 (d, J = 12.2 Hz, 1 H), 6.55 (d, J = 12.2 Hz, 1 H).

(Z)-methyl 4-styrylbenzoate (2j)



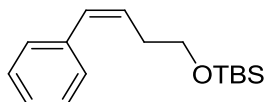
^1H NMR (500 MHz, CDCl_3) δ = 7.92 (d, J = 8.4 Hz, 2 H), 7.33 (d, J = 8.0 Hz, 2 H), 7.28 - 7.21 (m, 5 H), 6.74 (d, J = 12.2 Hz, 1 H), 6.64 (d, J = 12.6 Hz, 1 H), 3.95 - 3.87 (m, 3 H). ^{13}C NMR (126 MHz, CDCl_3) δ = 166.9, 142.1, 136.6, 132.2, 129.5, 129.2, 128.8, 128.3, 127.5, 52.0. HRMS (EI): m/z Calcd for $\text{C}_{16}\text{H}_{15}\text{O}_2$: 239.1072; Found: 239.1067.

(Z)-2-styrylthiophene (2l)



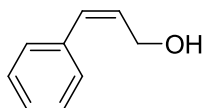
^1H NMR (500MHz, CDCl_3) δ = 7.42 - 7.35 (m, 5 H), 7.12 (d, J = 5.0 Hz, 1 H), 7.00 (d, J = 3.4 Hz, 1 H), 6.92 (dd, J = 3.8, 5.0 Hz, 1 H), 6.73 (d, J = 11.8 Hz, 1 H), 6.61 (d, J = 12.2 Hz, 1 H).

(Z)-tert-butyldimethyl(4-phenylbut-3-enyloxy)silane (2m)



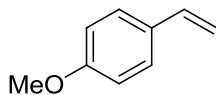
^1H NMR (500 MHz, CDCl_3) δ = 7.43 - 7.30 (m, 4 H), 7.24 (dt, J = 2.9, 5.8 Hz, 1 H), 6.53 (d, J = 11.8 Hz, 1 H), 5.73 (td, J = 7.4, 11.5 Hz, 1 H), 3.74 (t, J = 6.7 Hz, 2 H), 2.64 - 2.54 (m, 2 H), 0.95 - 0.90 (m, 10 H), 0.19 - 0.03 (m, 7 H). ^{13}C NMR (126 MHz, CDCl_3) δ = 137.5, 130.4, 129.0, 128.7, 128.1, 126.6, 62.9, 32.2, 25.9, 18.4. HRMS (EI): m/z Calcd for $\text{C}_{16}\text{H}_{17}\text{OSi}$: 263.1831; Found: 263.1826.

(Z)-3-phenylprop-2-en-1-ol (2n)³



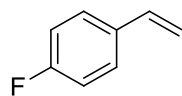
^1H NMR (200MHz, CDCl_3) δ = 7.39 - 7.10 (m, 6 H), 6.54 (d, J = 11.7 Hz, 1 H), 5.85 (td, J = 6.4, 11.8 Hz, 1 H), 4.41 (d, J = 6.2 Hz, 3 H), 2.22 (br. s., 1 H).

1-methoxy-4-vinylbenzene (5a)



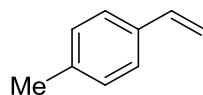
^1H NMR (200 MHz, CDCl_3) δ = 7.45 - 7.30 (m, 2 H), 6.99 - 6.82 (m, 2 H), 6.70 (dd, J = 10.9, 17.6 Hz, 1 H), 5.64 (dd, J = 1.0, 17.6 Hz, 1 H), 5.16 (dd, J = 1.0, 10.9 Hz, 1 H), 3.89 - 3.78 (m, 3 H).

1-fluoro-4-vinylbenzene (5b)



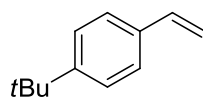
^1H NMR (200 MHz, CDCl_3) δ = 7.56 - 7.34 (m, 2 H), 7.19 - 6.93 (m, 2 H), 6.72 (dd, J = 10.9, 17.6 Hz, 1 H), 5.70 (d, J = 17.6 Hz, 1 H), 5.26 (d, J = 10.9 Hz, 1 H).

1-methyl-4-vinylbenzene (5c)



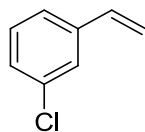
^1H NMR (200 MHz, CDCl_3) δ = 7.47 - 7.31 (m, J = 8.2 Hz, 2 H), 7.25 - 7.04 (m, J = 8.0 Hz, 2 H), 6.76 (dd, J = 10.9, 17.6 Hz, 1 H), 5.77 (dd, J = 1.0, 17.6 Hz, 1 H), 5.25 (dd, J = 1.0, 10.9 Hz, 1 H), 2.41 (s, 3 H).

1-*tert*-butyl-4-vinylbenzene (5d)



^1H NMR (200 MHz, CDCl_3) δ = 7.55 - 7.59 (m, 4 H), 6.86–7.01 (m, 1 H), 5.93 (dd, J = 1.0, 17.6 Hz, 1 H), 5.41 (dd, J = 1.0, 10.9 Hz, 1 H), 1.53 (s, 9 H).

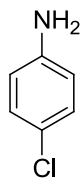
1-chloro-3-vinylbenzene (5e)



^1H NMR (200 MHz, CDCl_3) δ = 7.44 - 7.32 (m, 1 H), 7.32 - 7.08 (m, 3 H), 6.65 (dd, J = 10.9, 17.6 Hz, 1 H), 5.75 (d, J = 17.6 Hz, 1 H), 5.29 (d, J = 10.9 Hz, 1 H).

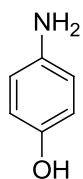
Chapter 4

4-chloroaniline (1)



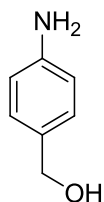
31 mg, 98% isolated yield. $R_f = 0.32$ (hexane/EtOAc = 10/1). Yellow Liquid. $^1\text{H NMR}$ (500MHz, CHLOROFORM-d) $\delta = 7.20 - 7.01$ (m, $J = 8.5$ Hz, 2 H), $6.68 - 6.53$ (m, $J = 8.5$ Hz, 2 H), 3.65 (br. s., 2 H). $^{13}\text{C NMR}$ (126MHz, CHLOROFORM-d) $\delta = 144.9, 129.1, 123.1, 116.2$.

4-aminophenol (8)



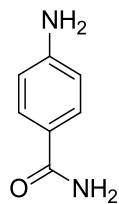
28 mg, 98% isolated yield. $R_f = 0.32$ (hexane/EtOAc = 1/1). yellow solid. $^1\text{H NMR}$ (500MHz, DMSO- d_6) $\delta = 7.41$ (br. s., 1 H), 5.47 (d, $J = 7.6$ Hz, 2 H), 5.41 (d, $J = 7.6$ Hz, 2 H), 3.35 (br. s., 2 H). $^{13}\text{C NMR}$ (126MHz, DMSO- d_6) $\delta = 148.4, 140.7, 115.7, 115.5$.

(4-aminophenyl)methanol (9)



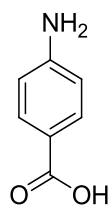
30 mg, 98% isolated yield. $R_f = 0.32$ (hexane/EtOAc = 1/1). yellow solid. $^1\text{H NMR}$ (500 MHz, DMSO- d_6) δ ppm 6.06 (d, $J=8.5$ Hz, 2 H), 5.62 (d, $J=7.9$ Hz, 2 H), 4.01 (br. s., 2 H), 3.90 (s, 1 H), 3.39 (d, $J=5.5$ Hz, 2 H). $^{13}\text{C NMR}$ (126 MHz, DMSO- d_6) δ ppm $147.5, 129.6, 127.9, 113.6, 63.2$

4-aminobenzamide (10)



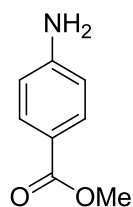
33 mg, 96% isolated yield. $R_f = 0.32$ (hexane/EtOAc = 1/1). white solid. $^1\text{H NMR}$ (500MHz, CHLOROFORM-d) $\delta = 7.29$ (s, 1 H), 7.10 (t, $J = 7.6$ Hz, 1 H), 6.78 (d, $J = 7.9$ Hz, 1 H), 6.72 (t, $J = 7.6$ Hz, 1 H), 4.06 (br. s., 2 H). $^{13}\text{C NMR}$ (126MHz, CHLOROFORM-d) $\delta = 142.9, 129.3, 127.6, 119.2, 118.9, 115.8$.

4-aminobenzoic acid (11)

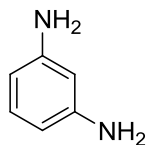


27 mg, 80% isolated yield. $R_f = 0.32$ (hexane/EtOAc = 1/1). Yellow solid. $^1\text{H NMR}$ (500MHz, DMSO-d₆) $\delta = 11.05$ (br. s., 1 H), 6.69 (s, 2 H), 5.62 (s, 2 H), 4.93 (br. s., 2H). $^{13}\text{C NMR}$ (126MHz, DMSO-d₆) $\delta = 167.6, 153.2, 131.3, 117.0, 112.6$.

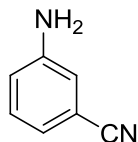
methyl 4-aminobenzoate (12)



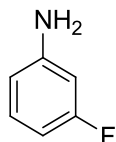
37 mg, 98% isolated yield. $R_f = 0.32$ (hexane/EtOAc = 10/1). White solid. $^1\text{H NMR}$ (500MHz, CHLOROFORM-d) $\delta = 7.85$ (d, $J = 8.5$ Hz, 2 H), 6.64 (d, $J = 8.5$ Hz, 2 H), 4.08 (br. s., 2 H), 3.86 (s, 3 H). $^{13}\text{C NMR}$ (126MHz, CHLOROFORM-d) $\delta = 167.1, 150.8, 131.6, 119.7, 113.7, 51.6$.

benzene-1,3-diamine (13)

26 mg, 98% isolated yield. $R_f = 0.32$ (hexane/EtOAc = 1/1). Yellow solid. $^1\text{H NMR}$ (500MHz, CHLOROFORM-d) $\delta = 6.96$ (t, $J = 7.8$ Hz, 1 H), 6.13 (dd, $J = 2.3, 8.0$ Hz, 2 H), 6.02 (s, 1 H), 3.53 (br. s., 4 H). $^{13}\text{C NMR}$ (126MHz, CHLOROFORM-d) $\delta = 147.4, 130.0, 105.8, 101.9$.

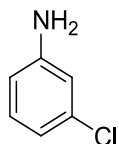
3-aminobenzonitrile (14)

28 mg, 98% isolated yield. $R_f = 0.32$ (hexane/EtOAc = 10/1). Yellow solid. $^1\text{H NMR}$ (500MHz, CHLOROFORM-d) $\delta = 7.25 - 7.18$ (m, 1 H), 7.01 (d, $J = 7.3$ Hz, 1 H), 6.95 - 6.82 (m, 2 H), 3.91 (br. s., 2 H). $^{13}\text{C NMR}$ (126MHz, CHLOROFORM-d) $\delta = 146.9, 130.0, 121.9, 119.1, 117.4, 112.8$.

3-fluoroaniline (15)

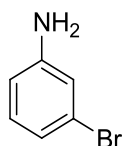
27 mg, 97% isolated yield. $R_f = 0.32$ (hexane/EtOAc = 10/1). White liquid. $^1\text{H NMR}$ (500MHz, CHLOROFORM-d) $\delta = 7.10$ (q, $J = 7.9$ Hz, 1 H), 6.50 - 6.26 (m, 3 H), 3.75 (br. s., 2 H). $^{13}\text{C NMR}$ (126MHz, CHLOROFORM-d) $\delta = 164.8, 162.9, 148.3, 148.2, 130.4, 130.4, 110.6, 110.6, 105.1, 104.9, 102.0, 101.9$.

3-chloroaniline (16)



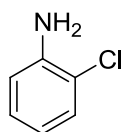
25 mg, 80% isolated yield. $R_f = 0.32$ (hexane/EtOAc = 10/1). White liquid. $^1\text{H NMR}$ (500MHz, CHLOROFORM-d) $\delta = 7.08$ (t, $J = 8.2$ Hz, 1 H), 6.75 (d, $J = 7.9$ Hz, 1 H), 6.68 (t, $J = 1.8$ Hz, 1 H), 6.55 (dd, $J = 1.8, 7.9$ Hz, 1 H), 3.72 (br. s., 2 H). $^{13}\text{C NMR}$ (126MHz, CHLOROFORM-d) $\delta = 147.6, 134.7, 130.2, 118.3, 114.8, 113.1$.

3-bromoaniline (17)



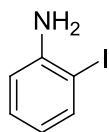
42 mg, 98% isolated yield. $R_f = 0.32$ (hexane/EtOAc = 10/1). White liquid. $^1\text{H NMR}$ (500MHz, CHLOROFORM-d) $\delta = 7.02$ (t, $J = 6.7$ Hz, 1 H), 6.95 - 6.86 (m, 1 H), 6.84 (br. s., 1 H), 6.66 - 6.46 (m, 1 H), 3.72 (br. s., 2 H). $^{13}\text{C NMR}$ (126MHz, CHLOROFORM-d) $\delta = 147.8, 147.8, 130.6, 122.9, 121.2, 117.7, 113.6$.

2-chloroaniline (19)



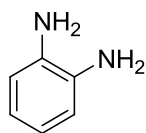
31 mg, 98% isolated yield. $R_f = 0.32$ (hexane/EtOAc = 10/1). White liquid. $^1\text{H NMR}$ (500MHz, CHLOROFORM-d) $\delta = 7.29$ (s, 1 H), 7.10 (t, $J = 7.6$ Hz, 1 H), 6.84 - 6.68 (m, 2 H), 4.06 (br. s., 2 H). $^{13}\text{C NMR}$ (126MHz, CHLOROFORM-d) $\delta = 142.9, 129.3, 127.6, 119.2, 118.9, 115.8$.

2-iodoaniline (20)



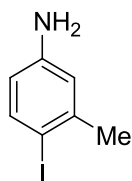
53 mg, 98% isolated yield. $R_f = 0.32$ (hexane/EtOAc = 10/1). White liquid. $^1\text{H NMR}$ (500MHz, CHLOROFORM-d) $\delta = 8.11$ (d, $J = 8.5$ Hz, 1 H), 7.36 (t, $J = 7.6$ Hz, 1 H), 6.82 (d, $J = 8.5$ Hz, 1 H), 6.70 (t, $J = 7.6$ Hz, 1 H), 6.08 (br. s., 2 H). $^{13}\text{C NMR}$ (126MHz, CHLOROFORM-d) $\delta = 144.6, 135.6, 126.1, 118.7, 116.9$.

benzene-1,2-diamine (21)



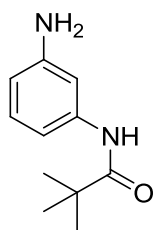
26 mg, 98% isolated yield. $R_f = 0.32$ (hexane/EtOAc = 1/1). Yellow solid. $^1\text{H NMR}$ (500MHz, CHLOROFORM-d) $\delta = 6.79 - 6.62$ (m, 4 H), 3.40 (br. s., 4 H). $^{13}\text{C NMR}$ (126MHz, CHLOROFORM-d) $\delta = 134.7, 120.2, 116.7$.

4-iodo-3-methylaniline (22)



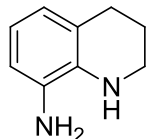
57 mg, 98% isolated yield. $R_f = 0.32$ (hexane/EtOAc = 10/1). White liquid. $^1\text{H NMR}$ (500MHz, CHLOROFORM-d) $\delta = 7.52$ (d, $J = 8.4$ Hz, 1 H), 6.62 (d, $J = 2.7$ Hz, 1 H), 6.28 (dd, $J = 2.7, 8.4$ Hz, 1 H), 3.44 (br. s., 2 H), 2.34 (s, 3 H). $^{13}\text{C NMR}$ (126MHz, CHLOROFORM-d) $\delta = 146.6, 141.9, 139.2, 116.7, 114.7, 86.4, 27.9$.

N-(3-aminophenyl)pivalamide (23)



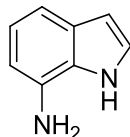
38 mg, 80% isolated yield. $R_f = 0.32$ (hexane/EtOAc = 10/1). Yellow liquid. $^1\text{H NMR}$ (500MHz, CHLOROFORM- d) $\delta = 7.22$ (br. s., 1 H), 7.07 (t, $J = 8.0$ Hz, 1 H), 6.67 (d, $J = 8.0$ Hz, 1 H), 6.43 (d, $J = 8.0$ Hz, 1 H), 3.44 (br. s., 2 H), 1.30 (s, 9 H). $^{13}\text{C NMR}$ (126MHz, CHLOROFORM- d) $\delta = 176.5, 147.2, 139.0, 129.6, 110.9, 109.7, 106.7, 39.6, 27.6$.

1,2,3,4-tetrahydroquinolin-8-amine (25)



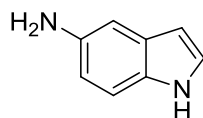
36 mg, 94% isolated yield. $R_f = 0.32$ (hexane/EtOAc = 10/1). Yellow liquid. $^1\text{H NMR}$ (500MHz, CHLOROFORM- d) $\delta = 6.76$ (d, $J = 7.6$ Hz, 1 H), 6.03 (d, $J = 8.0$ Hz, 1 H), 5.86 (s, 1 H), 3.45 (br. s., 3 H), 3.31 - 3.20 (m, 2 H), 2.68 (t, $J = 6.1$ Hz, 2 H), 2.01 - 1.87 (m, 2 H). $^{13}\text{C NMR}$ (126MHz, CHLOROFORM- d) $\delta = 145.3, 145.2, 130.1, 112.2, 104.9, 100.7, 41.9, 26.2, 22.6$.

1H-indol-7-amine (26)



32 mg, 98% isolated yield. $R_f = 0.32$ (hexane/EtOAc = 10/1). Yellow solid. $^1\text{H NMR}$ (500MHz, CHLOROFORM- d) $\delta = 8.06$ (br. s., 1 H), 7.24 (d, $J = 8.0$ Hz, 1 H), 7.10 - 6.97 (m, 2 H), 6.59 (d, $J = 7.6$ Hz, 1 H), 6.56 - 6.47 (m, 1 H), 3.53 (br. s., 2 H). $^{13}\text{C NMR}$ (126MHz, CHLOROFORM- d) $\delta = 130.8, 128.9, 126.8, 124.1, 120.5, 112.7, 108.5, 103.2$.

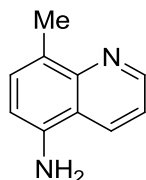
1H-indol-5-amine (27)



27 mg, 80% isolated yield. $R_f = 0.32$ (hexane/EtOAc = 10/1). Yellow solid. $^1\text{H NMR}$ (500MHz, DMSO- d_6) $\delta = 10.56$ (br. s., 1 H), 7.20 - 7.01 (m, 2 H), 6.74 - 6.60 (m, 1 H), 6.49 (dd, $J = 2.1,$

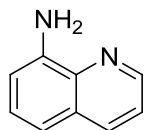
8.6 Hz, 1 H), 6.13 (br. s., 1 H), 4.40 (br. s., 2 H). ^{13}C NMR (126MHz, DMSO- d_6) δ = 141.0, 129.8, 128.6, 124.7, 111.8, 111.4, 103.2, 99.6.

8-methylquinolin-5-amine (28)



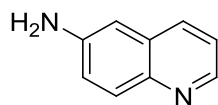
39 mg, 85% isolated yield. R_f = 0.32 (hexane/EtOAc = 10/1). Yellow liquid. ^1H NMR (500MHz, CHLOROFORM- d) δ = 9.04 - 8.83 (m, 1 H), 8.16 (dd, J = 1.1, 8.4 Hz, 1 H), 7.44 - 7.30 (m, 2 H), 6.73 (d, J = 7.6 Hz, 1 H), 4.01 (br. s., 1 H), 2.70 (s, 3 H). ^{13}C NMR (126MHz, CHLOROFORM- d) δ = 149.0, 147.7, 140.3, 129.8, 129.7, 127.3, 119.3, 119.2, 110.0, 17.6.

quinolin-8-amine (29)



35 mg, 98% isolated yield. R_f = 0.32 (hexane/EtOAc = 10/1). Yellow solid. ^1H NMR (500 MHz, CHLOROFORM- d) δ ppm 8.77 (dd, J =4.01, 1.34 Hz, 1 H), 8.08 (dd, J =8.39, 1.14 Hz, 1 H), 7.30 - 7.45 (m, 2 H), 7.17 (d, J =8.01 Hz, 1 H), 6.94 (d, J =7.25 Hz, 1 H), 5.00 (br. s., 2 H). ^{13}C NMR (126MHz, CHLOROFORM- d) δ = 147.4, 143.9, 138.4, 136.0, 128.8, 127.3, 121.3, 116.0, 110.0.

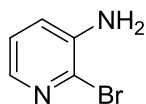
quinolin-6-amine (30)



34 mg, 95% isolated yield. R_f = 0.32 (hexane/EtOAc = 10/1). Yellow liquid. ^1H NMR (500MHz, CHLOROFORM- d) δ = 8.66 (br. s., 1 H), 7.91 (br. s., 2 H), 7.17 (d, J = 7.9 Hz, 1 H), 6.91 (br.

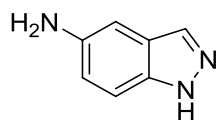
s., 1 H), 3.97 (br. s., 2 H). ^{13}C NMR (126MHz, CHLOROFORM-d) δ = 146.9, 144.6, 133.7, 130.6, 129.8, 121.5, 121.4, 107.4.

2-bromopyridin-3-amine (31)



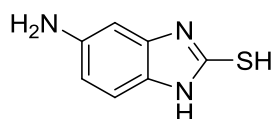
40 mg, 94% isolated yield. R_f = 0.32 (hexane/EtOAc = 5/1). Yellow liquid. ^1H NMR (500MHz, CHLOROFORM-d) δ = 7.77 (d, J = 3.4 Hz, 1 H), 7.12 - 6.93 (m, 2 H), 4.10 (br. s., 1 H). ^{13}C NMR (126MHz, CHLOROFORM-d) δ = 141.4, 139.1, 129.6, 123.6, 121.8.

1H-indazol-5-amine (32)



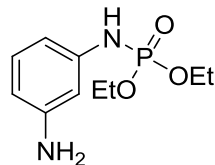
32 mg, 96% isolated yield. R_f = 0.32 (hexane/EtOAc = 1/2). Yellow liquid. ^1H NMR (500 MHz, DMSO- d_6) δ ppm 12.60 (br. s., 1 H), 7.73 (s, 1 H), 7.25 (d, J = 8.77 Hz, 1 H), 6.73 - 6.83 (m, 2 H). ^{13}C NMR (126MHz, DMSO- d_6) δ = 142.2, 131.6, 124.0, 118.3, 110.4, 100.7.

5-amino-1H-benzo[d]imidazole-2-thiol (33)



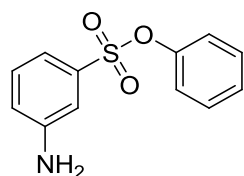
33 mg, 80% isolated yield. R_f = 0.32 (hexane/EtOAc = 1/3). Yellow liquid. ^1H NMR (500MHz, DMSO- d_6) δ = 12.04 (s, 1 H), 12.06 (s, 1 H), 6.81 (d, J = 9.2 Hz, 1 H), 6.44 - 6.28 (m, 2 H), 5.12 - 4.88 (m, 2H). ^{13}C NMR (126MHz, DMSO- d_6) δ = 165.9, 144.9, 133.4, 123.8, 110.0, 109.9, 94.6.

diethyl 3-aminophenylphosphoramidate (34)



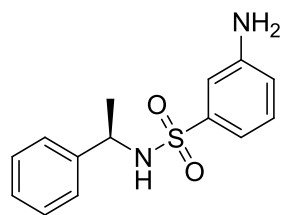
59 mg, 98% isolated yield. $R_f = 0.32$ (hexane/EtOAc = 5/1). Yellow liquid. $^1\text{H NMR}$ (500MHz, CHLOROFORM-d) $\delta = 6.99$ (t, $J = 7.8$ Hz, 1 H), 6.59 (d, $J = 8.0$ Hz, 1 H), 6.46 - 6.34 (m, 2 H), 6.32 - 6.24 (m, 1 H), 4.23 - 4.11 (m, 2 H), 4.11 - 3.98 (m, 2 H), 3.54 (br. s., 1 H), 1.30 (t, $J = 6.9$ Hz, 6 H). $^{13}\text{C NMR}$ (126MHz, CHLOROFORM-d) $\delta = 147.4, 140.8, 129.9, 108.5, 107.7, 107.6, 104.0, 103.9, 62.6, 62.5, 16.1, 16.0$.

phenyl 3-aminobenzenesulfonate (35)



61 mg, 98% isolated yield. $R_f = 0.32$ (hexane/EtOAc = 5/1). Yellow liquid. $^1\text{H NMR}$ (500MHz, CHLOROFORM-d) $\delta = 7.40 - 7.25$ (m, 4 H), 7.19 (d, $J = 8.0$ Hz, 1 H), 7.17 - 7.12 (m, 1 H), 7.05 (d, $J = 7.6$ Hz, 2 H), 6.94 (dd, $J = 1.5, 8.0$ Hz, 1 H), 4.10 - 3.86 (m, 1 H). $^{13}\text{C NMR}$ (126MHz, CHLOROFORM-d) $\delta = 149.7, 147.2, 136.1, 129.9, 129.5, 127.1, 122.3, 120.2, 117.9, 113.7$.

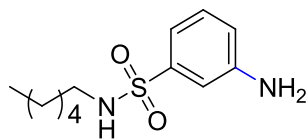
(R)-3-amino-N-(1-phenylethyl)benzenesulfonamide (36)



65 mg, 94% isolated yield. $R_f = 0.32$ (hexane/EtOAc = 5/1). Yellow liquid. $^1\text{H NMR}$ (500MHz, CHLOROFORM-d) $\delta = 7.26 - 7.07$ (m, 7 H), 7.03 (s, 1 H), 6.78 - 6.66 (m, 1 H), 5.35 (d, $J = 7.2$ Hz, 1 H), 4.50 - 4.39 (m, 1 H), 3.86 (br. s., 2 H), 1.40 (d, $J = 6.9$ Hz, 3 H). $^{13}\text{C NMR}$ (126MHz

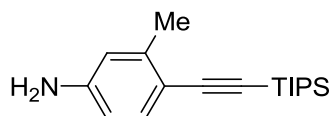
,CHLOROFORM-d) δ = 147.0, 142.2, 141.2, 129.7, 128.4, 127.4, 126.1, 118.6, 116.5, 112.9, 53.6, 23.4

3-amino-N-propylbenzenesulfonamide (37)



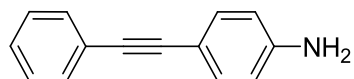
43 mg, 80% isolated yield. R_f = 0.32 (hexane/EtOAc = 5/1). Yellow liquid. ^1H NMR (500MHz, CHLOROFORM-d) δ = 7.31 - 7.07 (m, 3 H), 6.88 - 6.75 (m, 1 H), 4.77 (t, J = 5.9 Hz, 1 H), 3.99 (br. s., 2 H), 2.92 (q, J = 6.9 Hz, 2 H), 1.51 - 1.37 (m, 2 H), 1.32 - 1.09 (m, 6 H), 0.85 (t, J = 6.9 Hz, 3 H). ^{13}C NMR (126MHz, CHLOROFORM-d) δ = 147.3, 140.5, 129.9, 118.7, 116.5, 112.7, 43.3, 31.2, 29.4, 26.1, 22.4, 13.9.

3-methyl-4-((triisopropylsilyl)ethynyl)aniline (38)



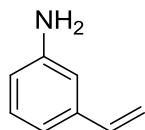
68 mg, 95% isolated yield. R_f = 0.32 (hexane/EtOAc = 10/1). Yellow liquid. ^1H NMR (500MHz, CHLOROFORM-d) δ = 7.29 (s, 2 H), 6.57 - 6.50 (m, 1 H), 6.45 (dd, J = 2.3, 8.0 Hz, 1 H), 3.75 (br. s., 2 H), 2.40 (s, 3 H), 1.15 (s, 21H). ^{13}C NMR (126MHz, CHLOROFORM-d) δ = 146.6, 142.1, 133.7, 115.7, 113.3, 112.1, 106.6, 91.4, 21.0, 18.7, 18.6, 11.4.

4-(phenylethynyl)aniline (40)



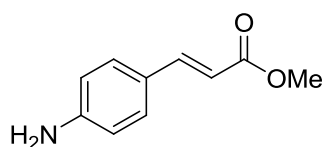
43 mg, 90% isolated yield. R_f = 0.32 (hexane/EtOAc = 5/1). Yellow liquid. ^1H NMR (500MHz, CHLOROFORM-d) δ = 7.51 (d, J = 6.9 Hz, 2 H), 7.43 - 7.23 (m, 5 H), 6.65 (d, J = 8.4 Hz, 2 H), 3.82 (br. s., 2 H). ^{13}C NMR (126MHz, CHLOROFORM-d) δ = 146.6, 132.9, 131.3, 128.2, 127.6, 123.9, 114.7, 112.6, 90.1, 87.3.

3-vinylaniline (41)



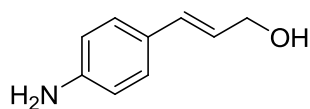
22 mg, 75% isolated yield. $R_f = 0.32$ (hexane/EtOAc = 10/1). Yellow liquid. $^1\text{H NMR}$ (500MHz, CHLOROFORM-d) $\delta = 7.14$ (t, $J = 7.6$ Hz, 1 H), 6.85 (d, $J = 7.6$ Hz, 1 H), 6.76 (s, 1 H), 6.72 - 6.56 (m, 2 H), 5.72 (d, $J = 17.5$ Hz, 1 H), 5.23 (d, $J = 11.1$ Hz, 1 H), 3.67 (br. s., 2 H). $^{13}\text{C NMR}$ (126MHz, CHLOROFORM-d) $\delta = 146.5, 138.6, 137.0, 129.4, 116.9, 114.7, 113.6, 112.7$.

(E)-methyl 3-(4-aminophenyl)acrylate (42)



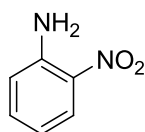
35 mg, 80% isolated yield. $R_f = 0.32$ (hexane/EtOAc = 5/1). Yellow liquid. $^1\text{H NMR}$ (500MHz, DMSO-d₆) $\delta = 7.47 - 7.50$ (d, $J = 15.6$ Hz, 1 H), 7.42 - 7.32 (m, 2 H), 6.62 - 6.52 (m, 2 H), 6.21 - 6. (d, $J = 15.6$ Hz, 1 H), 5.75 (br. s., 2 H), 3.43 (s, 3 H). $^{13}\text{C NMR}$ (126MHz, DMSO-d₆) $\delta = 167.5, 151.6, 145.6, 130.2, 128.6, 121.3, 113.6, 110.7, 51.0$.

(E)-3-(4-aminophenyl)prop-2-en-1-ol (43)



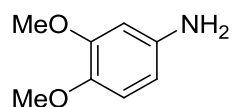
30 mg, 80% isolated yield. $R_f = 0.32$ (hexane/EtOAc = 10/1). Yellow liquid. $^1\text{H NMR}$ (500MHz, CHLOROFORM-d) $\delta = 7.19$ (d, $J = 8.4$ Hz, 2 H), 6.63 (d, $J = 8.4$ Hz, 2 H), 6.47 (s, 1 H), 6.50 (s, 1 H), 6.21 - 6.08 (m, 1 H), 4.26 (d, $J = 6.1$ Hz, 2 H), 3.68 (br. s., 2H). $^{13}\text{C NMR}$ (126MHz, CHLOROFORM-d) $\delta = 146.0, 131.4, 127.6, 127.2, 124.7, 115.1, 63.9$.

2-nitroaniline (44)



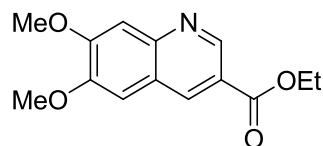
33 mg, 95% isolated yield. $R_f = 0.32$ (hexane/EtOAc = 10/1). Yellow liquid. $^1\text{H NMR}$ (500MHz, CHLOROFORM-d) $\delta = 8.11$ (d, $J = 8.5$ Hz, 1 H), 7.36 (t, $J = 7.6$ Hz, 1 H), 6.82 (d, $J = 8.5$ Hz, 1 H), 6.70 (t, $J = 7.6$ Hz, 1 H), 6.08 (br. s., 2 H). $^{13}\text{C NMR}$ (126MHz, CHLOROFORM-d) $\delta = 144.6, 135.6, 126.1, 118.7, 116.9$.

3,4-dimethoxyaniline (45)



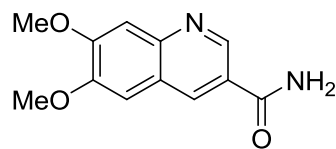
34 mg, 90% isolated yield. $R_f = 0.32$ (hexane/EtOAc = 10/1). Yellow liquid. $^1\text{H NMR}$ (500MHz, CHLOROFORM-d) $\delta = 6.71$ (d, $J = 8.4$ Hz, 1 H), 6.32 (d, $J = 2.7$ Hz, 1 H), 6.24 (dd, $J = 2.7, 8.4$ Hz, 1 H), 3.84 (s, 3 H), 3.81 (s, 3 H), 3.33 (br. s., 2 H). $^{13}\text{C NMR}$ (126MHz, CHLOROFORM-d) $\delta = 149.8, 142.2, 140.5, 113.0, 106.4, 100.7, 56.6, 55.7$.

Ethyl 6,7-dimethoxyquinoline-3-carboxylate (46)



55 mg, 85% isolated yield. $R_f = 0.32$ (hexane/EtOAc = 5/1). Yellow liquid. $^1\text{H NMR}$ (200MHz, CHLOROFORM-d) $\delta = 9.27$ (s, 1H), 8.86 (s, 1H), 7.47 (s, 1H), 7.13 (s, 1H), 4.46 (q, $J = 8.0$ Hz, 2H), 4.07 (s, 3H), 4.03 (s, 3H), 1.46 (t, $J = 8.2$ Hz, 3H). $^{13}\text{C NMR}$ (100.6 MHz, CHLOROFORM-d) $\delta = 165.65, 154.21, 150.25, 148.04, 147.26, 136.32, 122.40, 121.55, 107.82, 105.82, 61.14, 56.20, 56.04, 14.27$. **HRMS (ESI)** calcd. for $\text{C}_{14}\text{H}_{15}\text{NO}_4$ $[\text{M}]^+$: 261.1001, found: 261.0994.

6,7-dimethoxyquinoline-3-carboxamide (47)

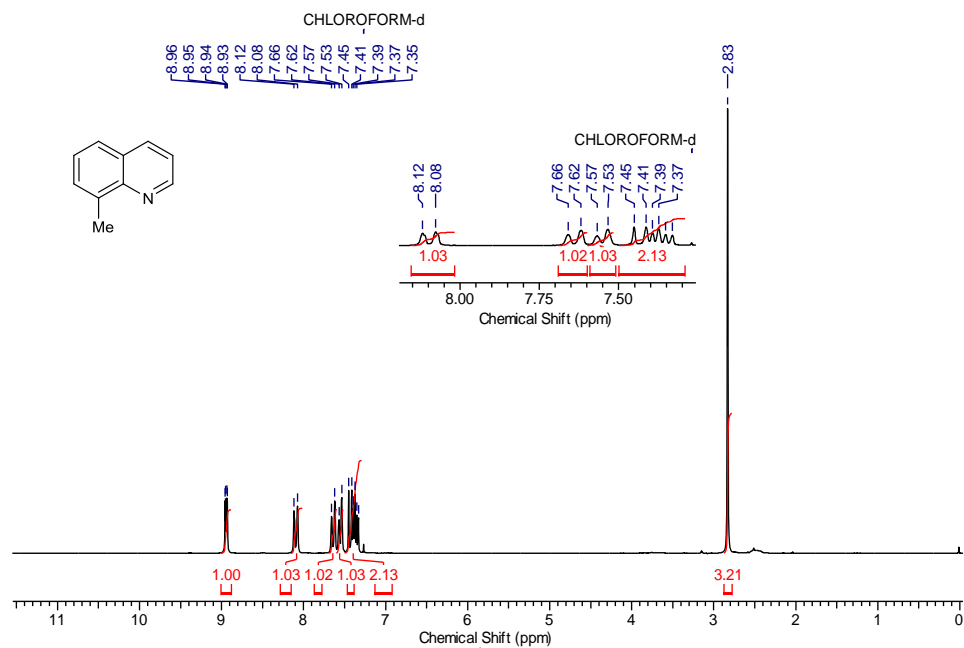
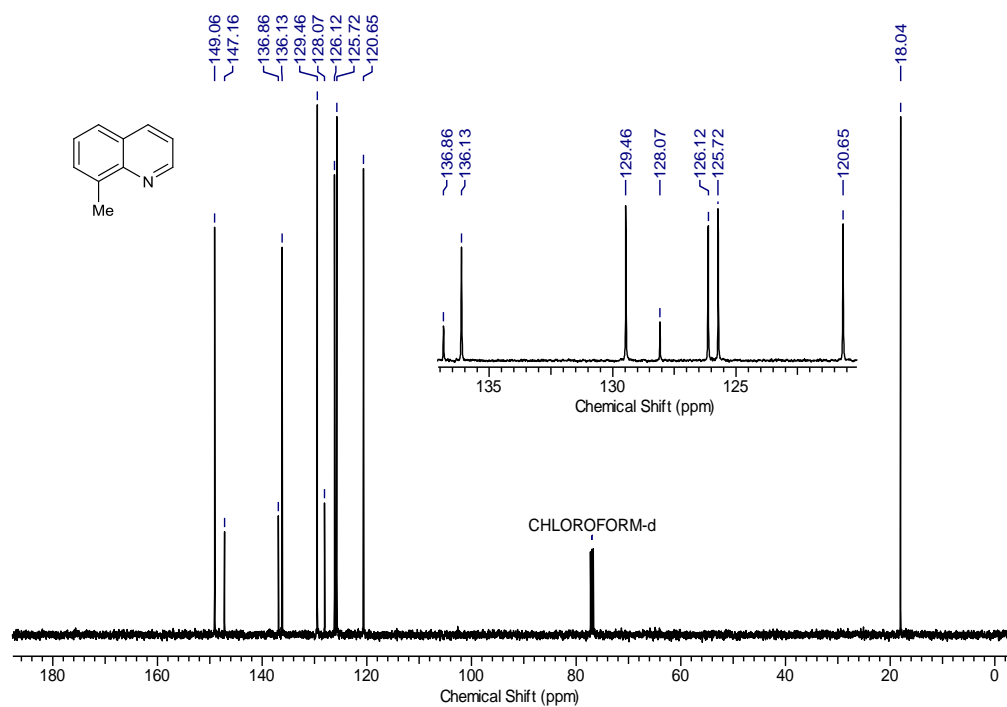


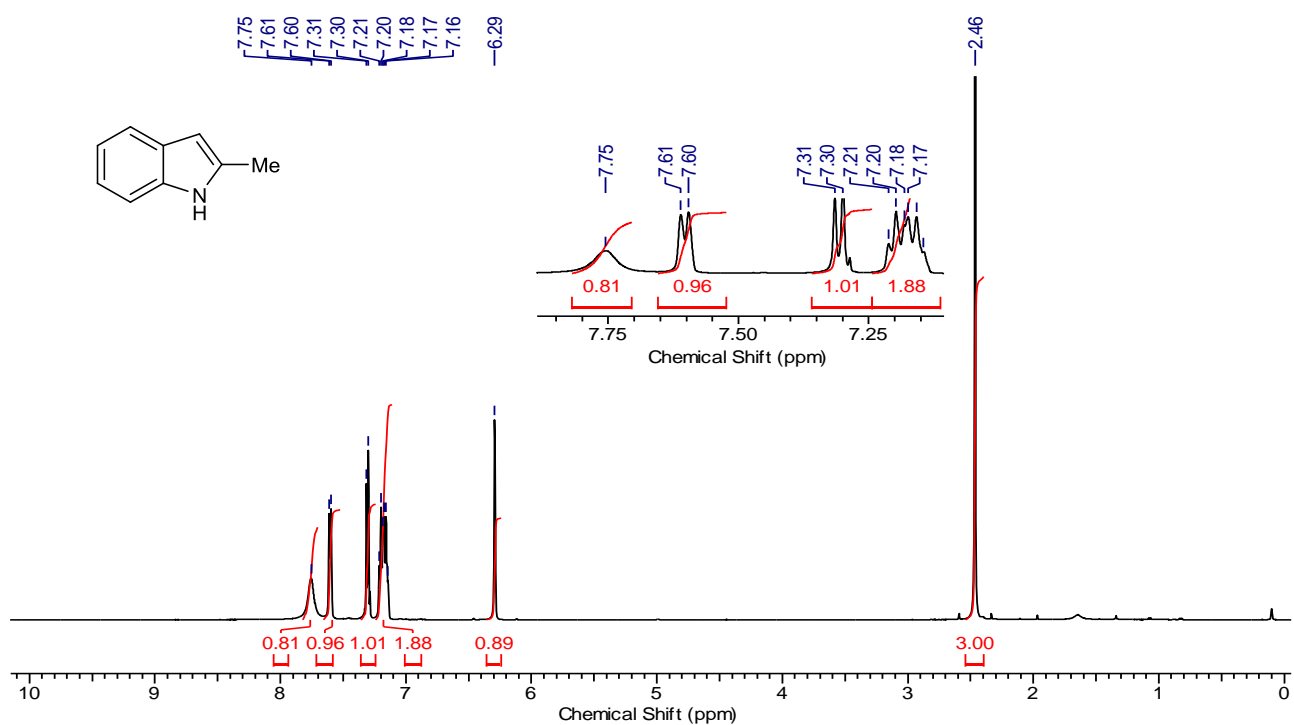
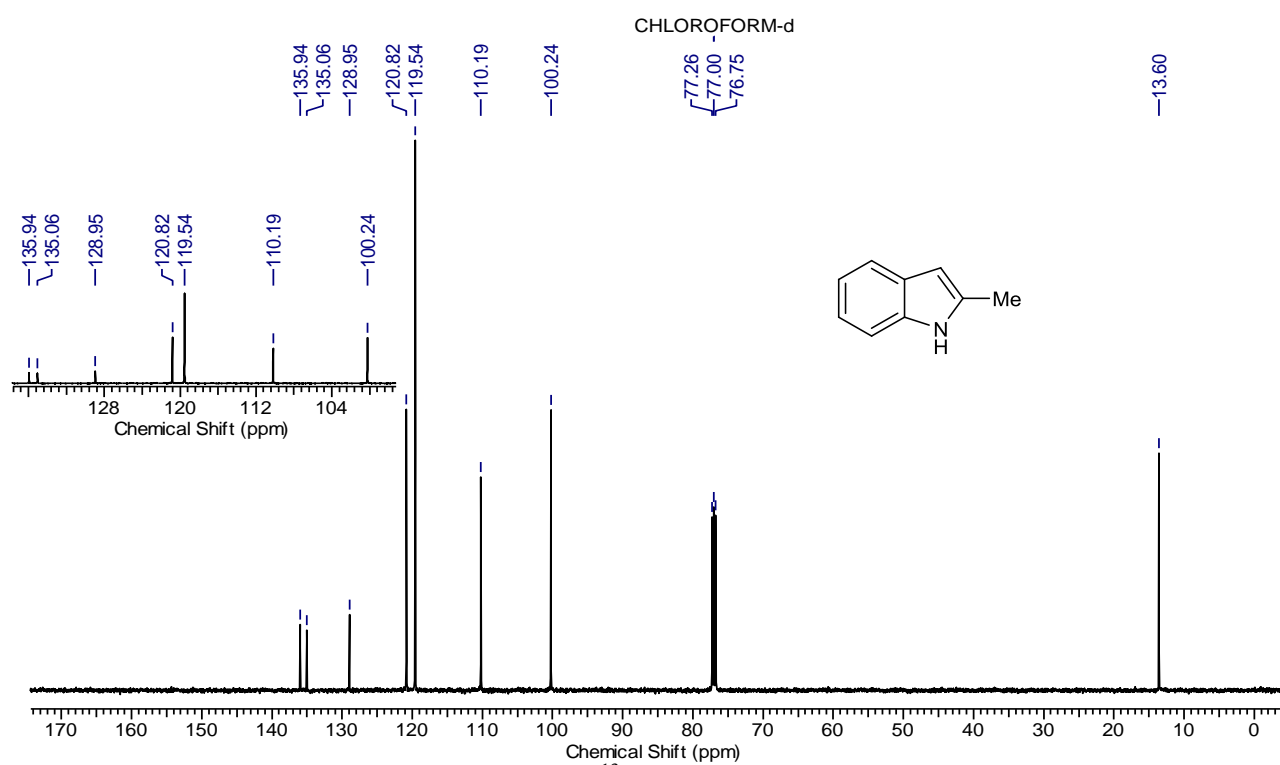
50 mg, 86% isolated yield. $R_f = 0.32$ (hexane/EtOAc = 3/1). Yellow liquid. ^1H NMR (400 MHz, DMSO- d_6) δ 8.19 (s, 1H), 7.75 (s, 1H), 7.29 (s, 1H), 6.63 (s, 1H), 6.52 (s, 1H), 6.50 (s, 1H), 3.06 (s, 3H), 3.03 (s, 3H). ^{13}C NMR (100.6 MHz, DMSO- d_6) δ 166.94, 153.48, 149.95, 146.61, 145.99, 133.94, 125.11, 122.17, 107.43, 106.35, 55.88, 55.80. **HRMS (ESI)** calcd. for $\text{C}_{12}\text{H}_{13}\text{N}_2\text{O}_3$ $[\text{M}+\text{H}]^+$: 233.0918, found: 233.0937.

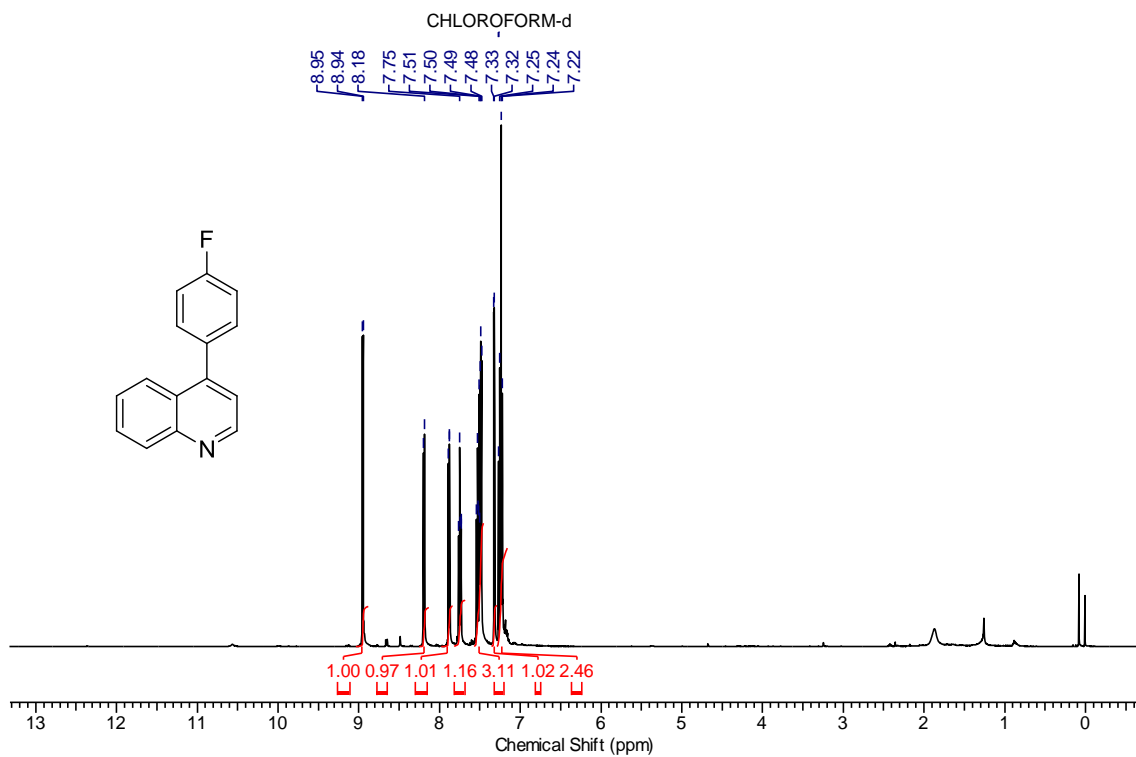
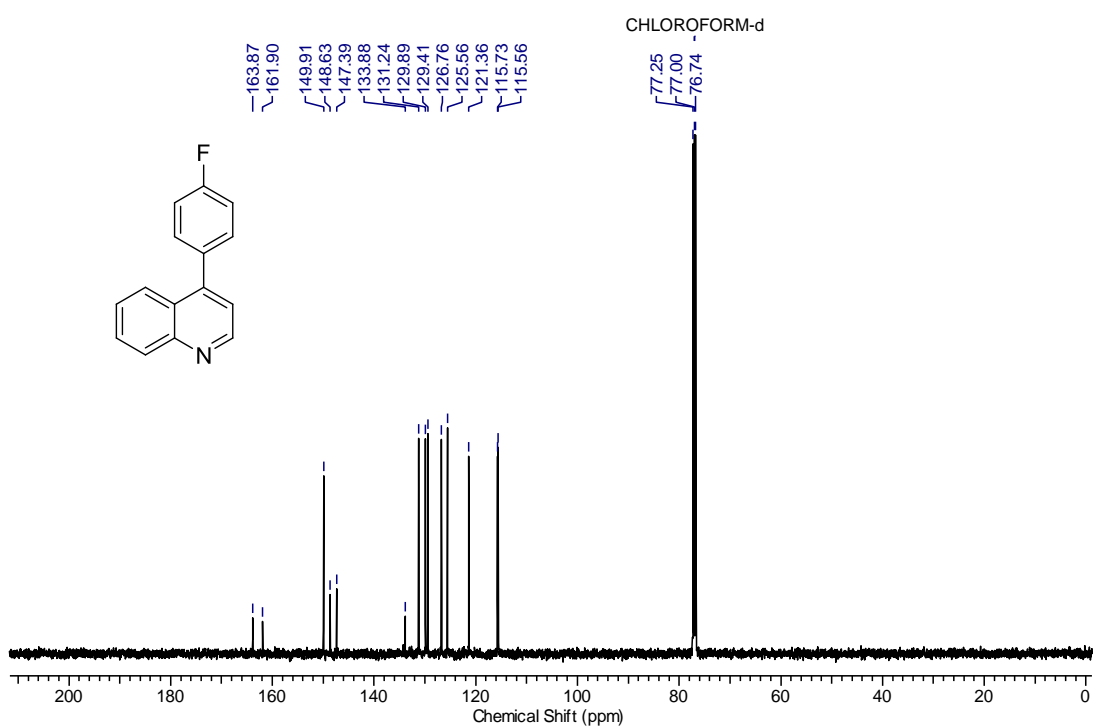
Appendix b

NMR spectra of compounds selected compounds.

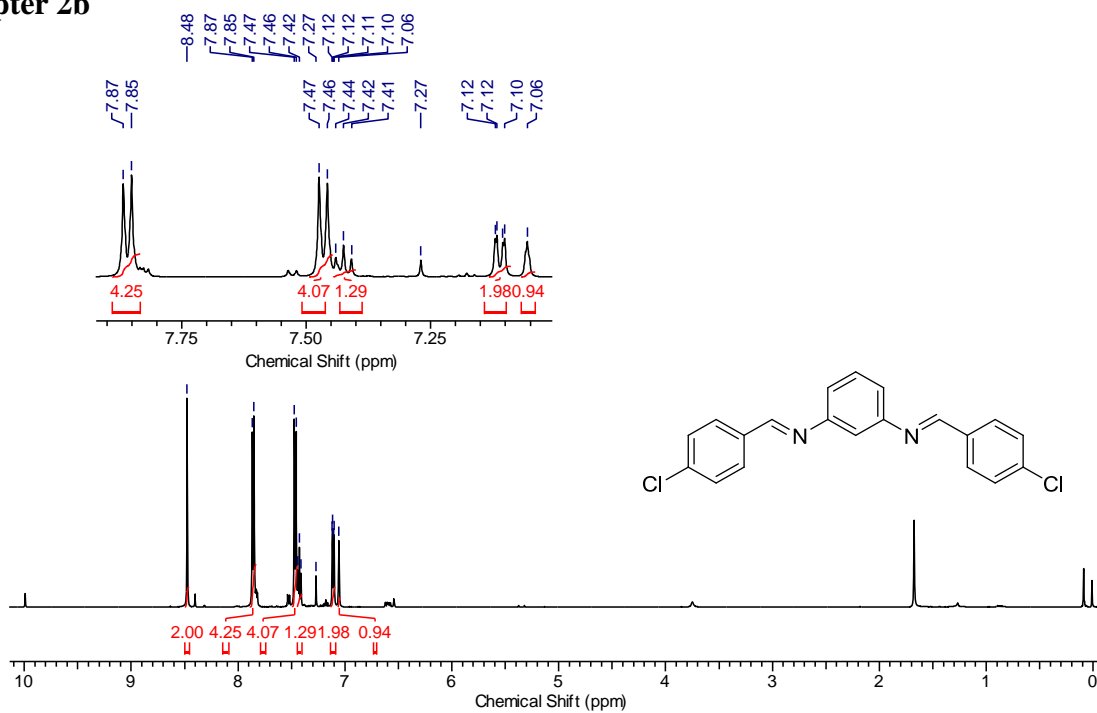
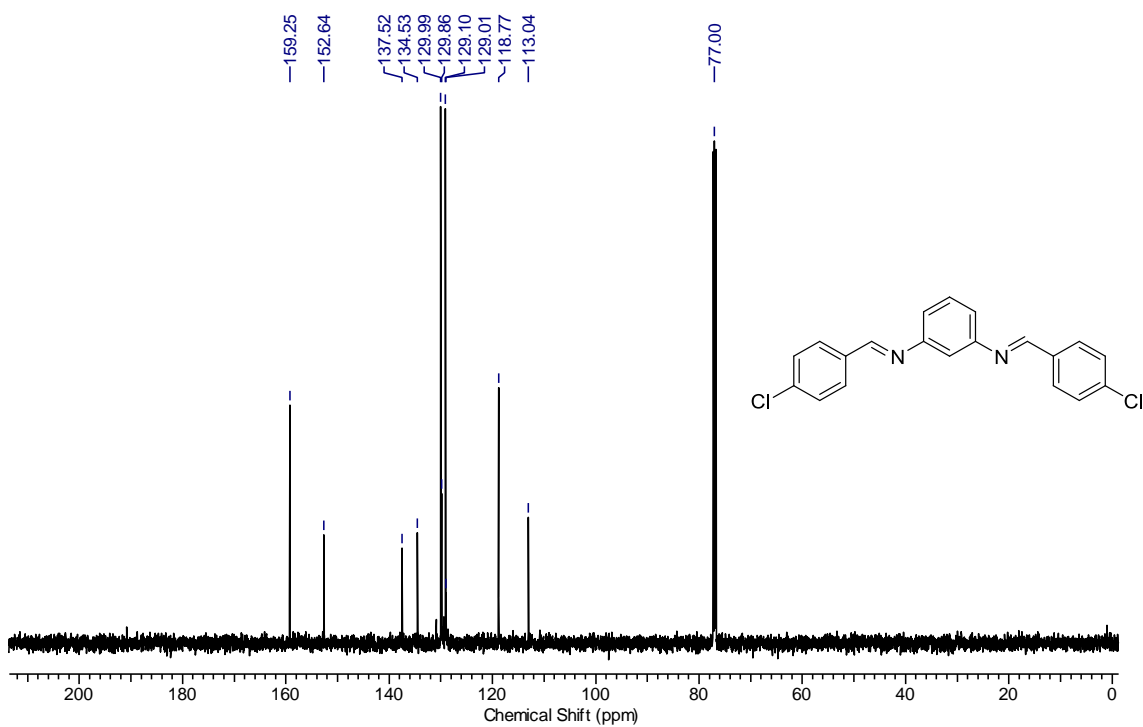
Chapter 2A

Figure 1a. ^1H NMR of **2b**Figure 1b. ^{13}C NMR of **2b**

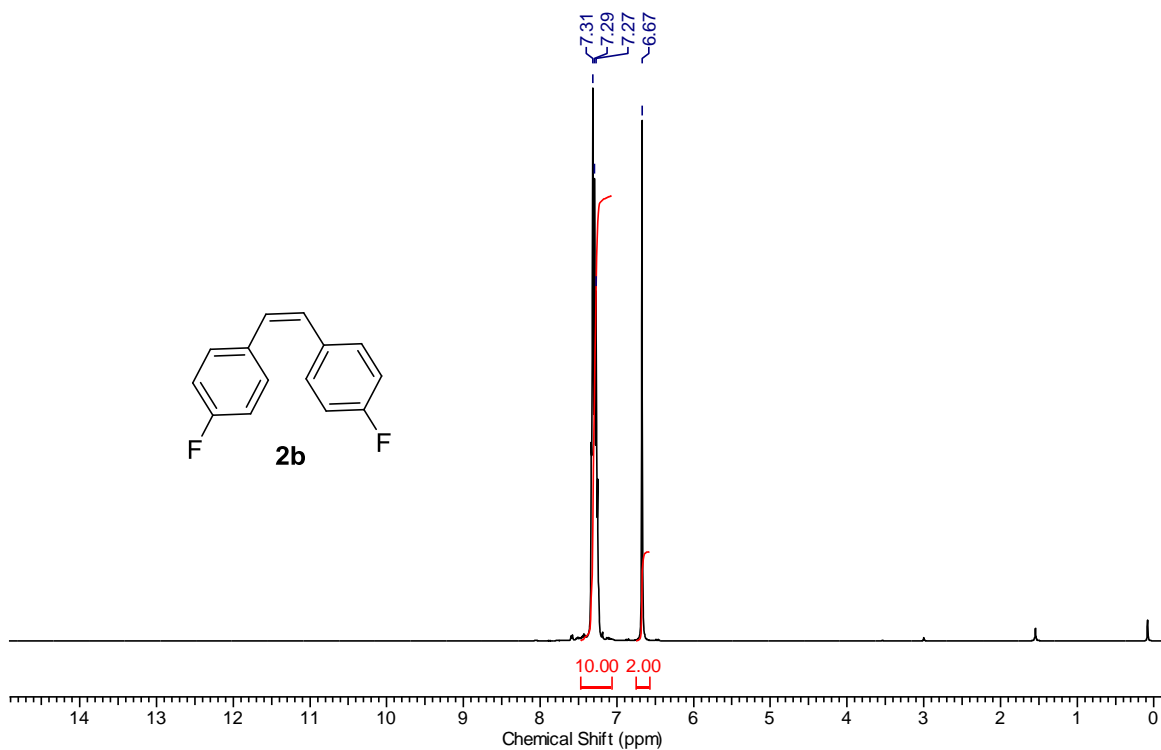
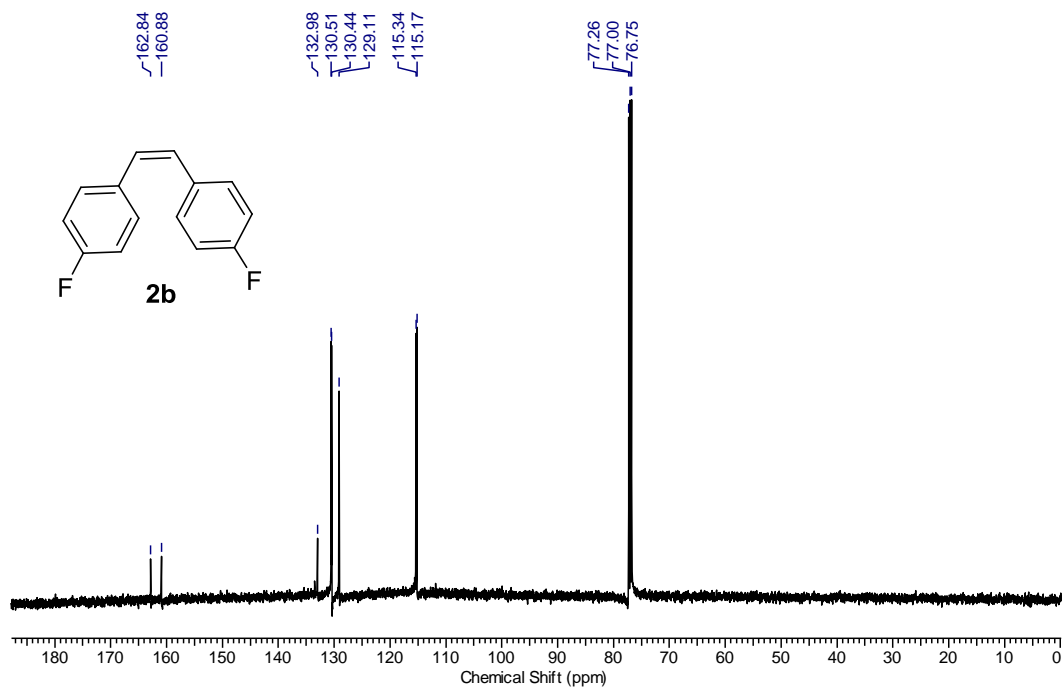
Figure 2a. ^1H NMR of **22b**Figure 2b. ^{13}C NMR of **22b**

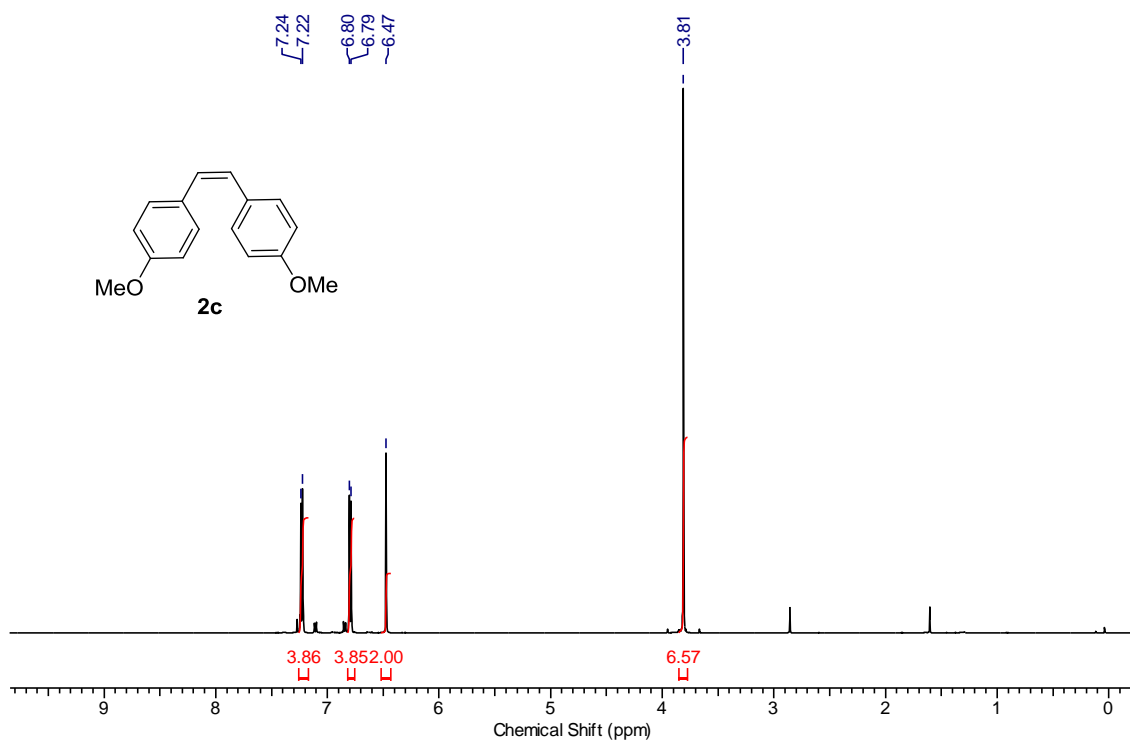
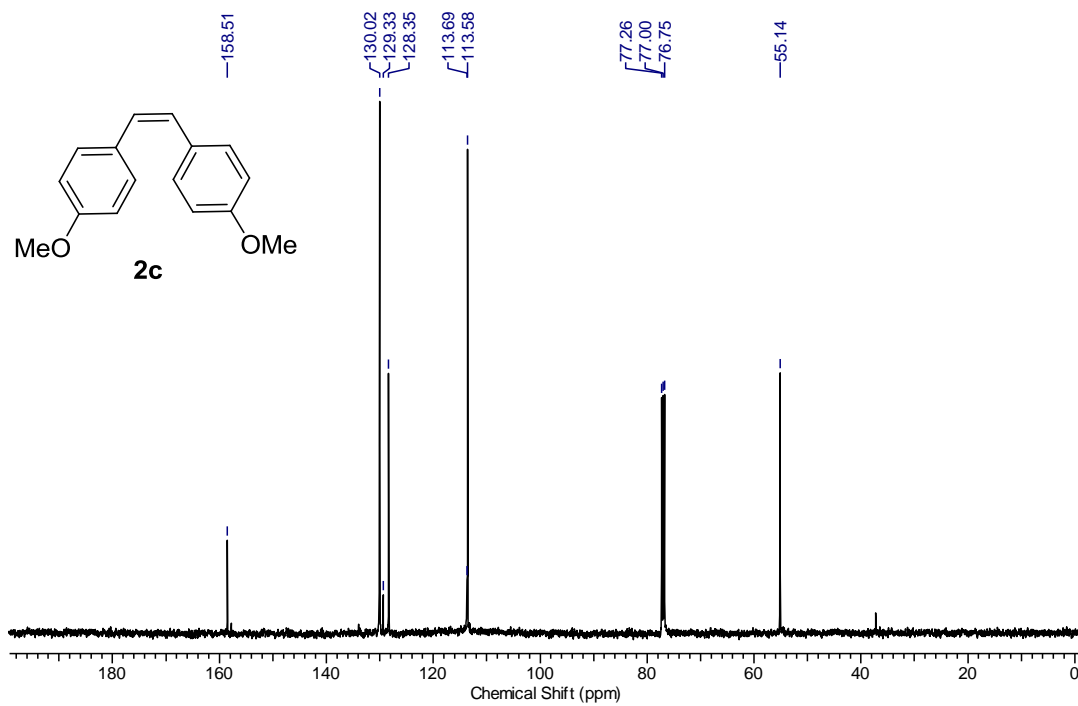
Figure 3a. ^1H NMR of **4**Figure 3b. ^{13}C NMR of **4**

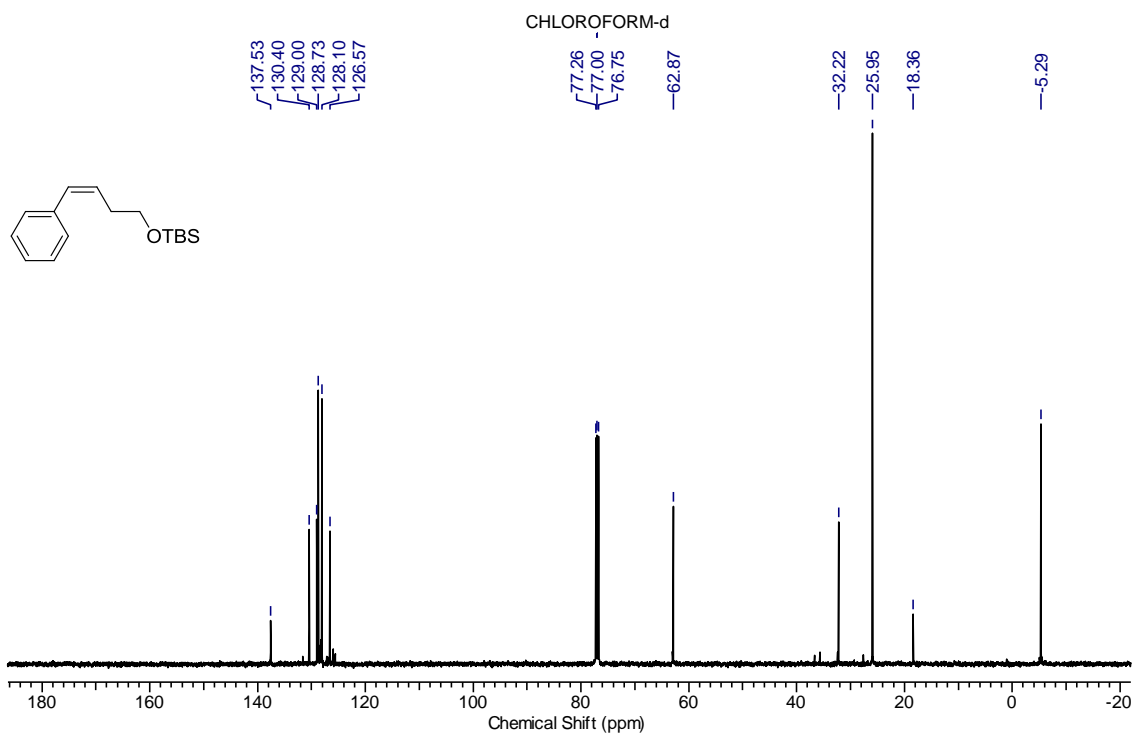
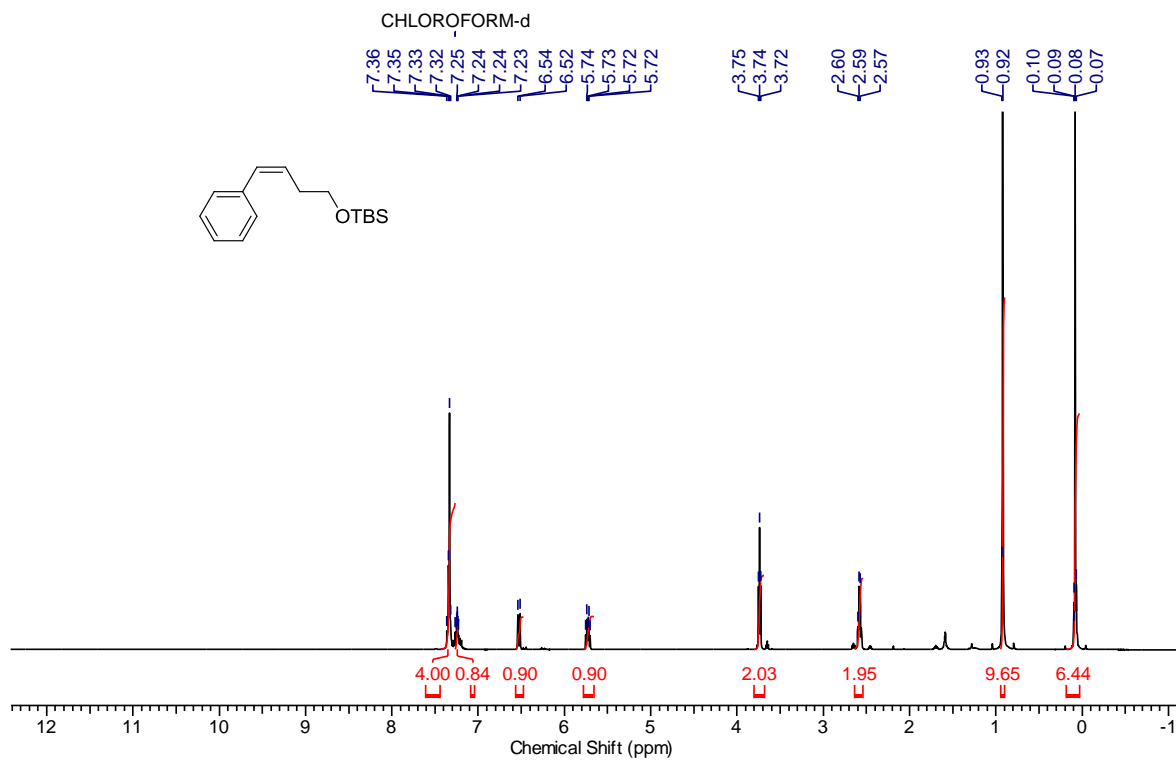
Chapter 2b

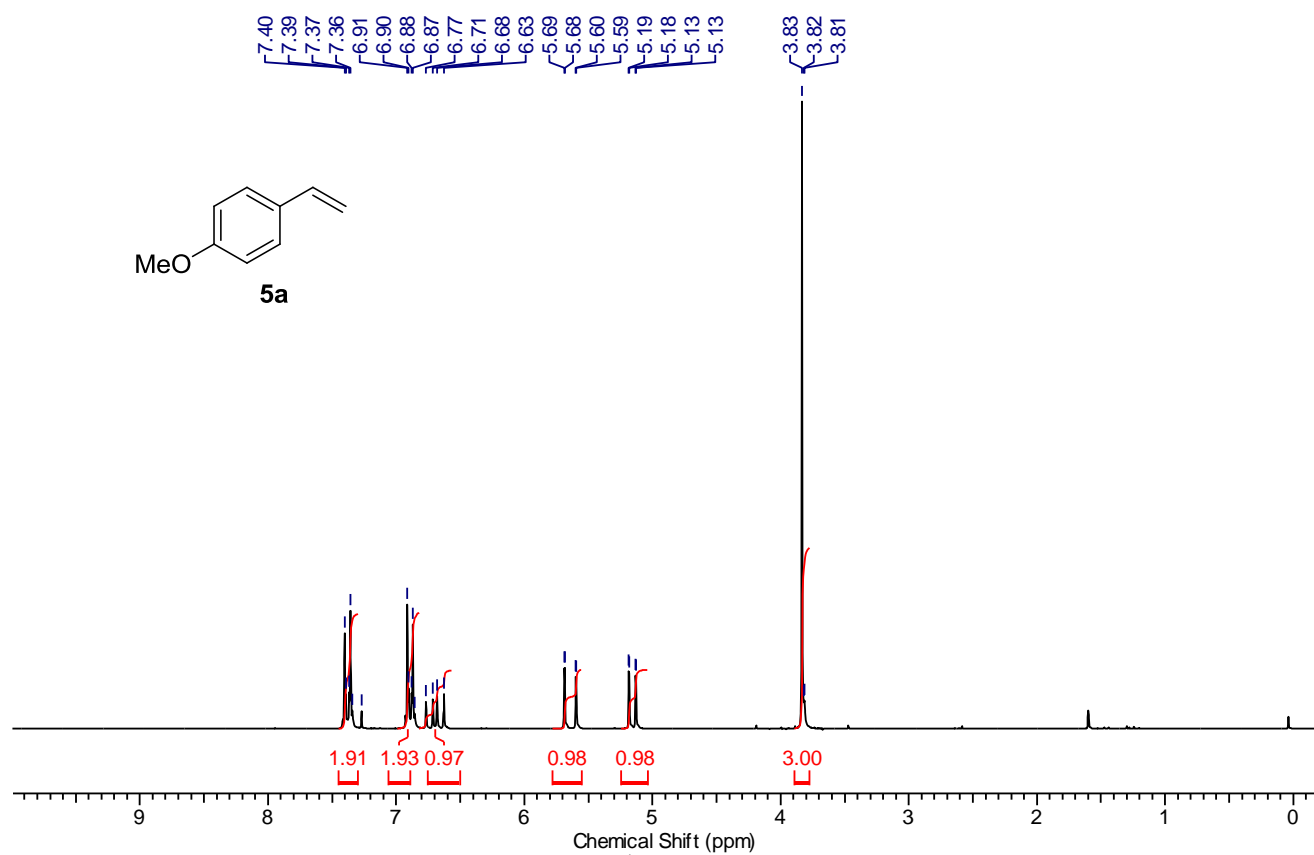
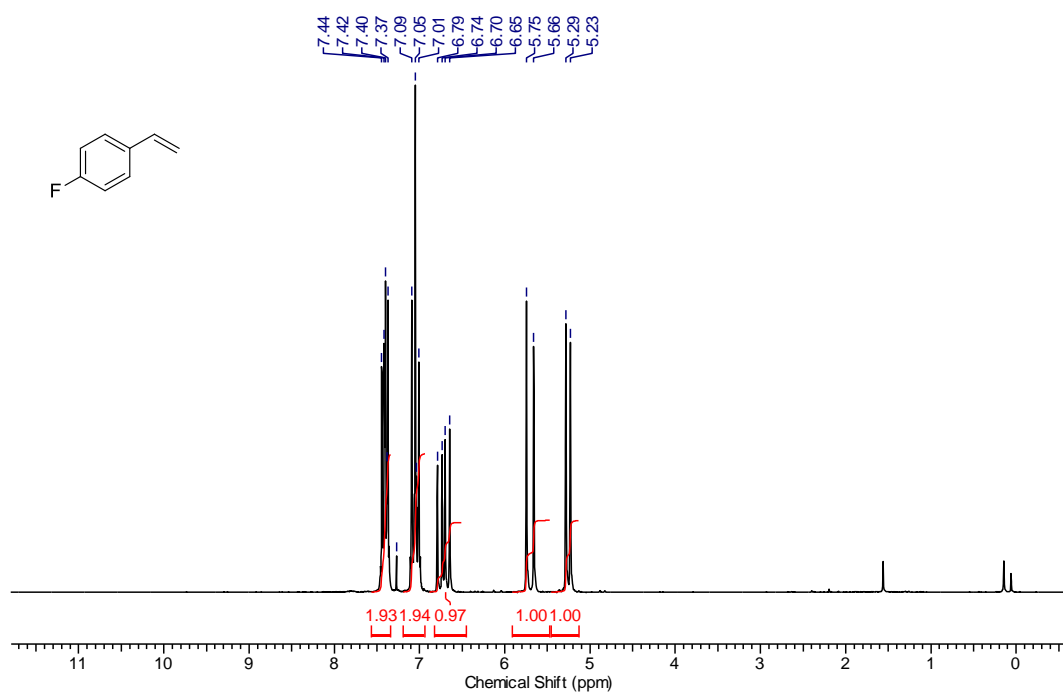
Figure 4a. ^1H NMR of **3as**Figure 4b. ^{13}C NMR of **3as**

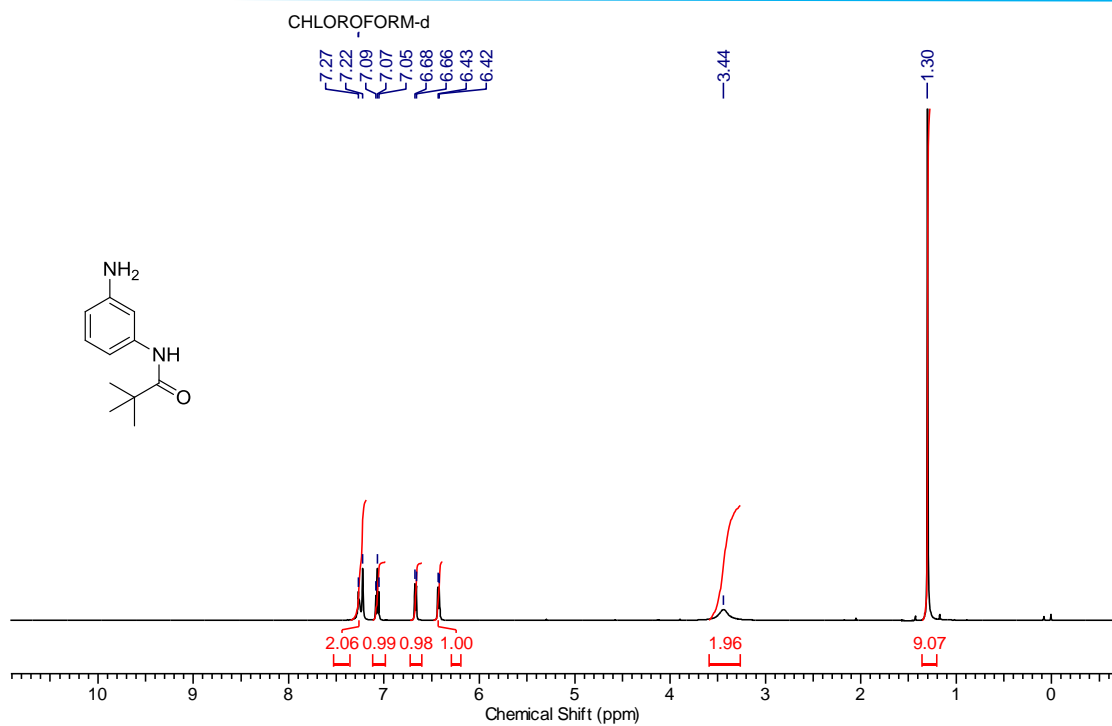
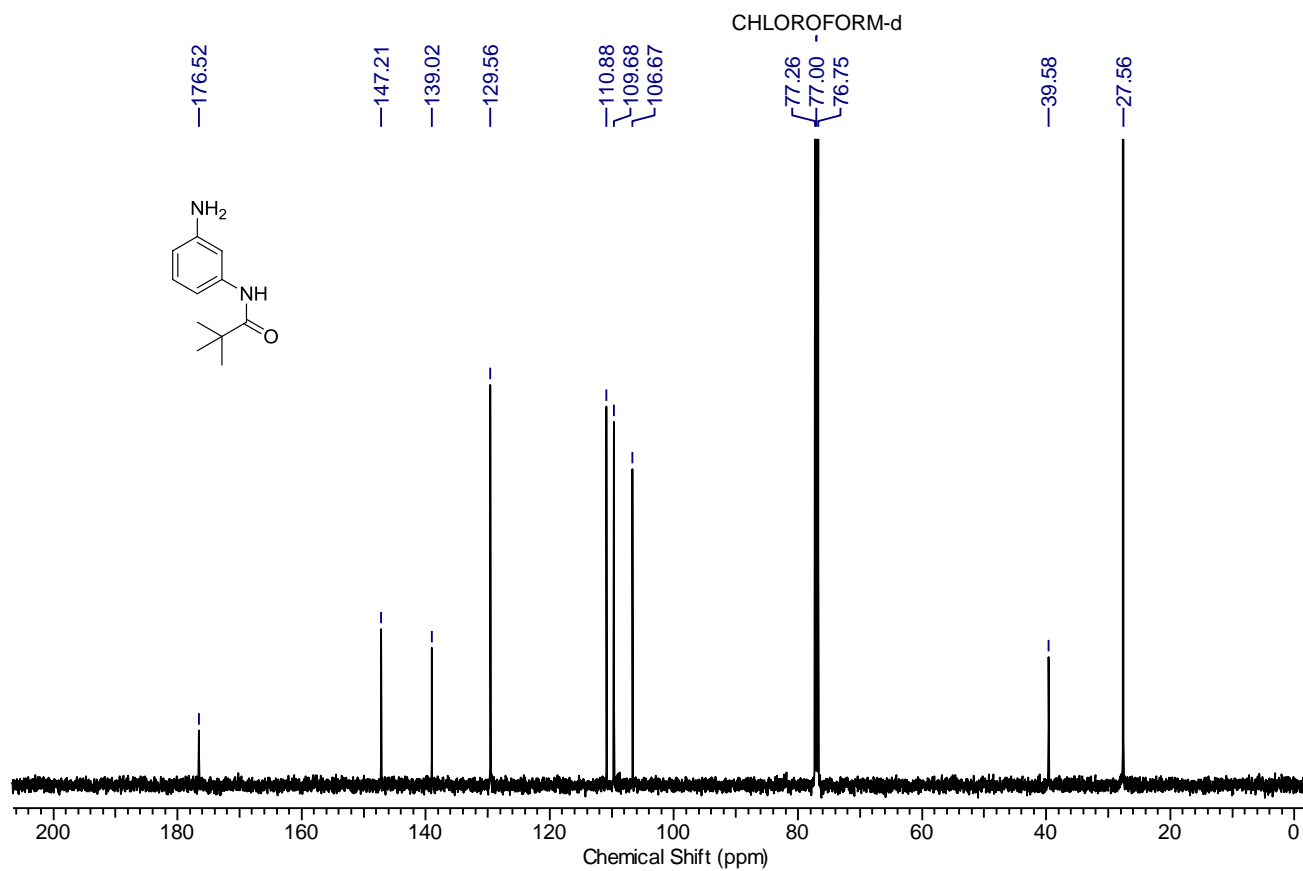
Chapter 3B

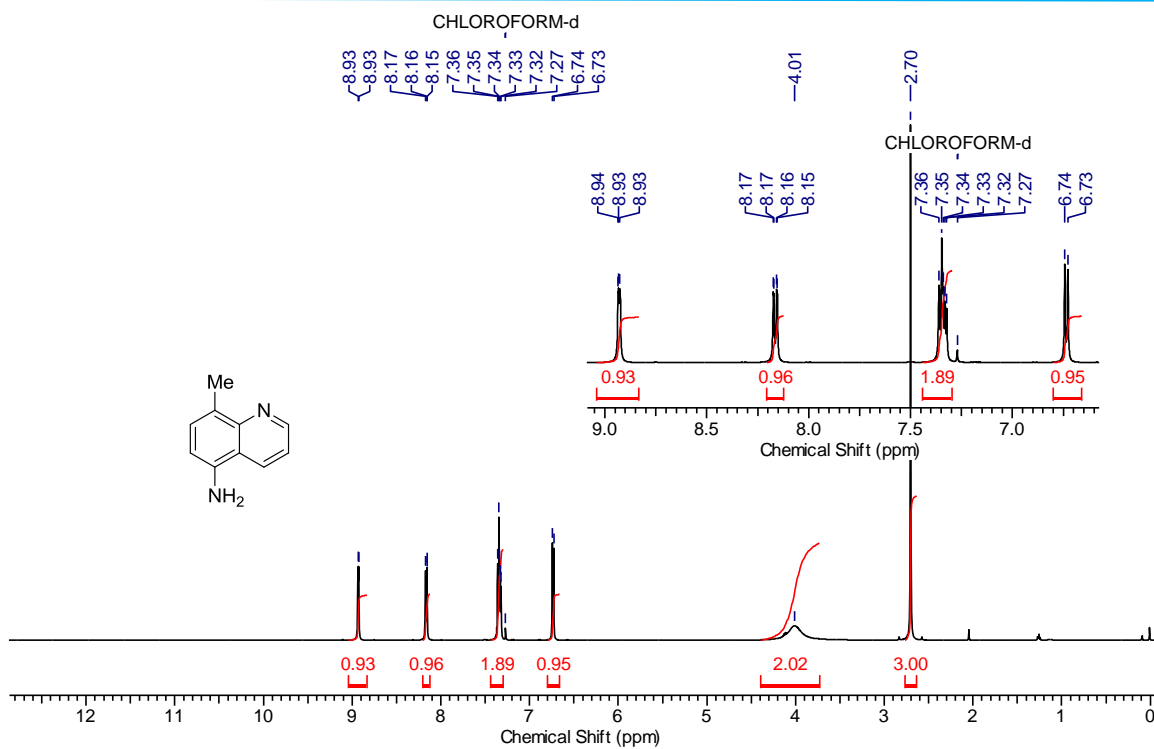
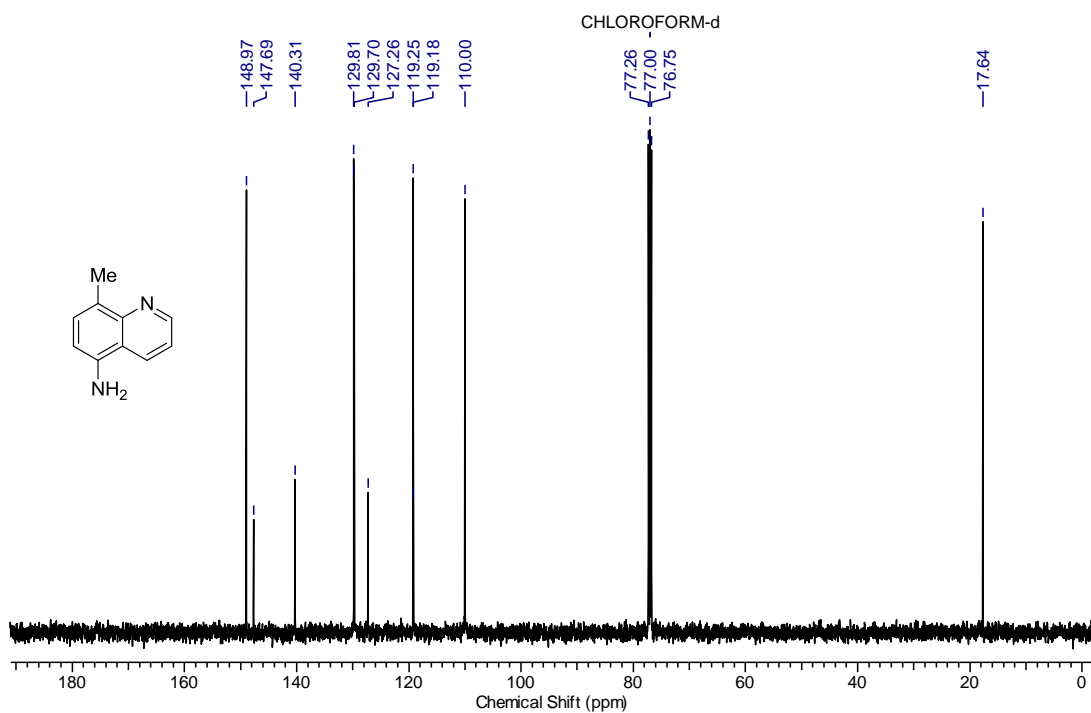
Figure 6a. ^1H NMR of **2b**Figure 6b. ^{13}C NMR of **2b**

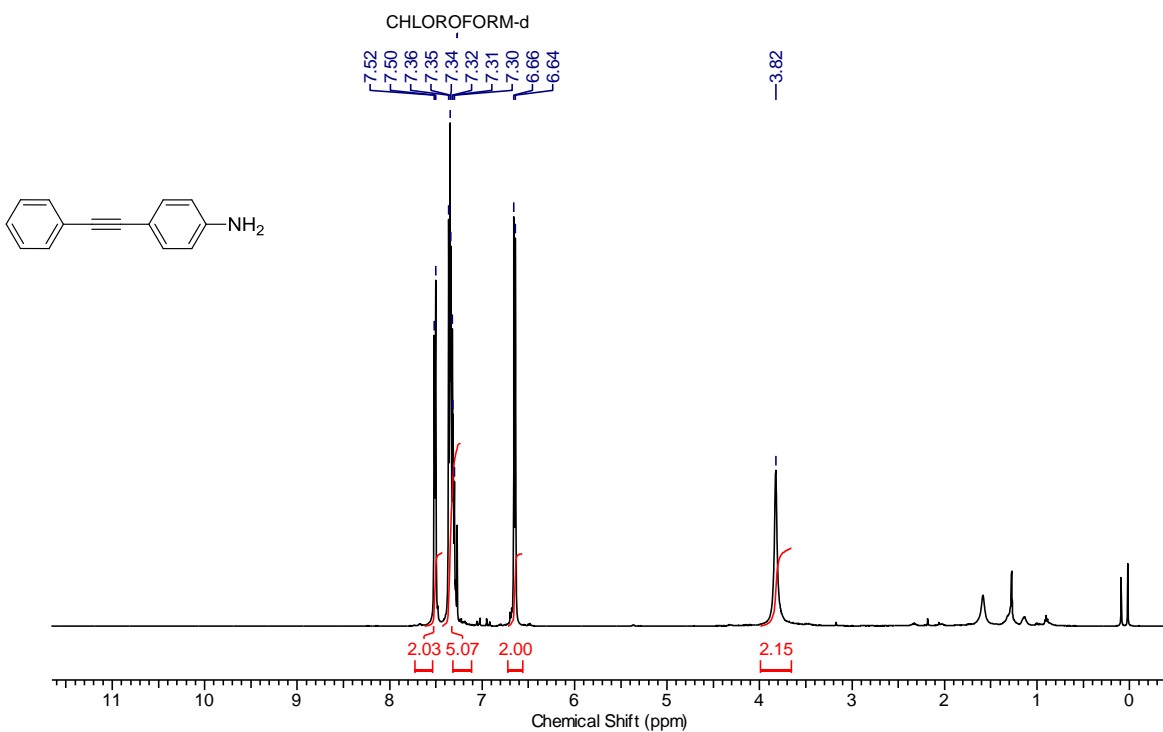
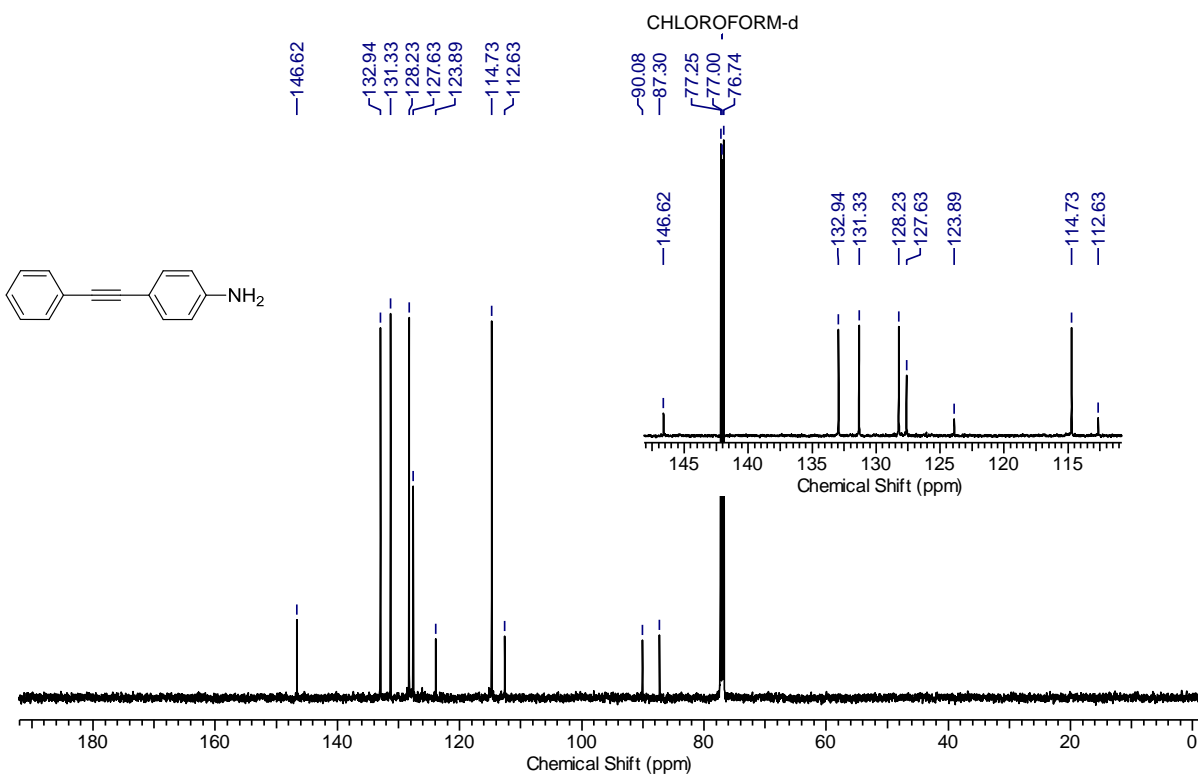
Figure 7a. ¹H NMR of **2c**Figure 7b. ¹³C NMR of **2c**

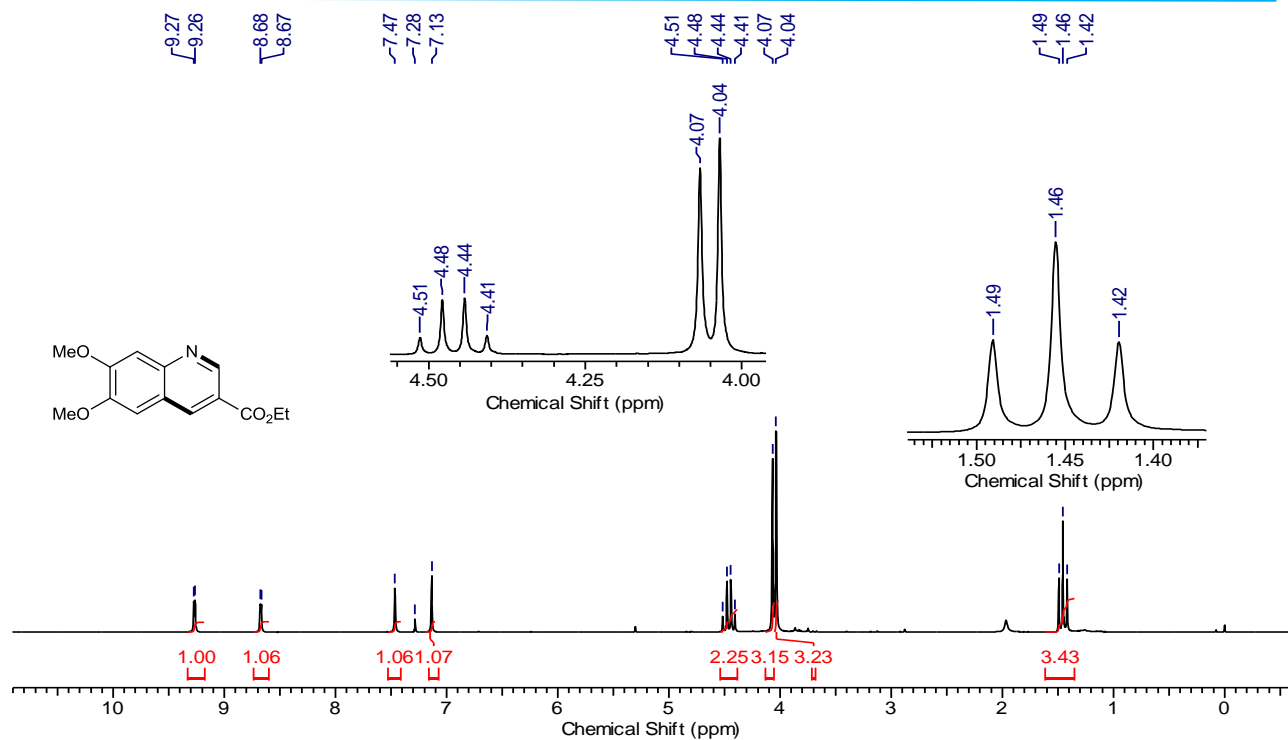
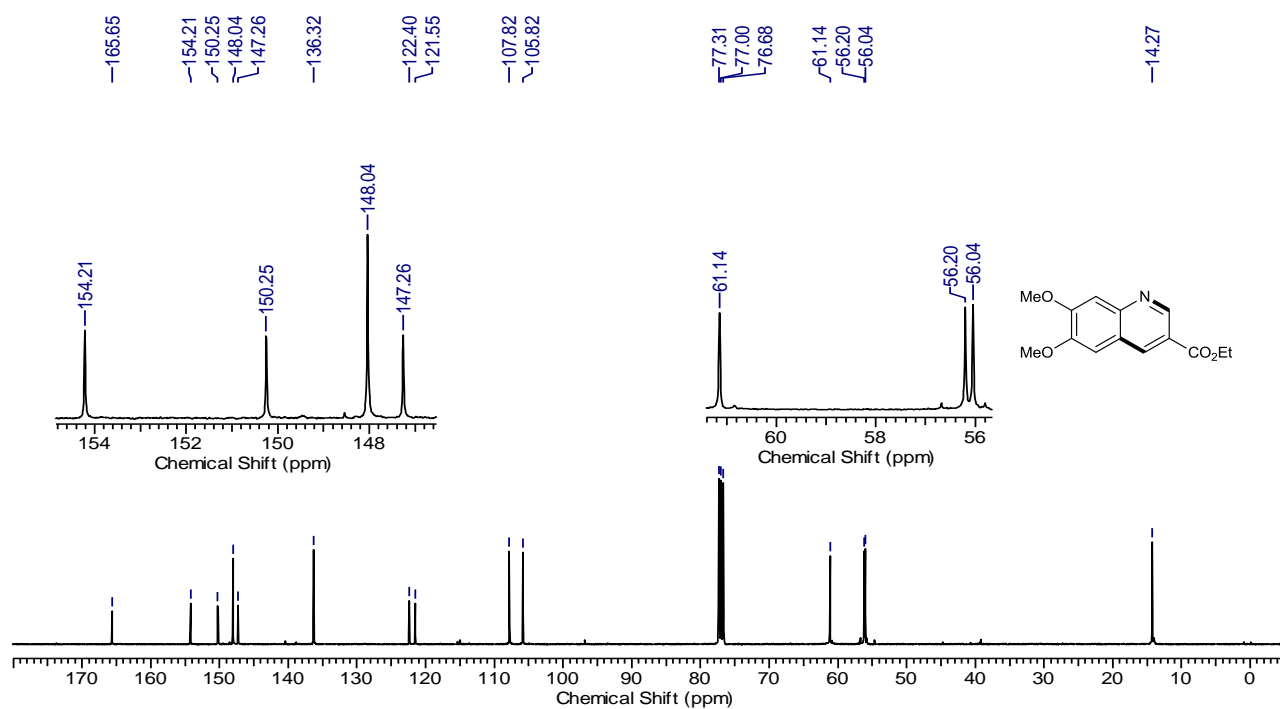


Figure 9. ¹H NMR **5a**Figure 10. ¹H NMR of **5b**

Figure 11a. ^1H NMR of **23**Figure 11b. ^{13}C NMR of **23**

Figure 12a. ¹H NMR of **28**Figure 12b. ¹³C NMR of **28**

Figure 13a. ¹H NMR of **40**Figure 13b. ¹³C NMR of **40**

Figure 14b. ^1H NMR of **46**Figure 14b. ^{13}C NMR of **46**

CURRICULUM VITAE

Garima Jaiswal
CSIR-National Chemical Laboratory (CSIR-NCL)
Dr. Homi Bhabah Road
Doctoral fellow
Pune - 411008, India.



Email: jaiswalgarimal@gmail.com

Academic qualification

Present Status:

Working with Dr. E. Balaraman at CSIR- National Chemical Laboratory (CSIR-NCL) as a doctoral fellow.

Educational Qualification:

PhD in Heterogeneous Catalysis (to be completed by July-2018)

UGC-Senior Research Fellow, registered with AcSIR-New Delhi at CSIR-National Chemical Laboratory (CSIR-NCL), Pune, India.

M.Sc. (Organic Chemistry)

Indian Institute of Technology-Delhi, India (**First Class, (CGPA= 8.2/10)** in June 2013.

B.Sc. (Chemistry)

Banaras Hindu University, Varanasi, India with **First Class, (CGPA= 8.5/10)** in June 2011.

Research Experience

1) M.Sc. Research Project entitled “*Investigations on nanostructured copper, cadmium ternary manganese oxides and cobalt nanoparticles*” with **Dr. Ashok Kumar Ganguli**.

Duration: 1 Year (2011-2012)

2) UGC-Junior Research Fellow for PhD from 12th July 2013 on the topic “Transition metal based nanocatalysts for (de)-hydrogenation reactions” with **Dr. E. Balaraman** at CSIR-National Chemical Laboratory, Pune.

3) UGC-Senior Research Fellow for PhD from 12th July 2015 on the topic “Transition metal based nanocatalysts for (de)-hydrogenation reactions” with **Dr. E. Balaraman** at CSIR-National Chemical Laboratory, Pune.

Symposia Attended

Nation conferences – 2 (Participation)
3 (Poster presentation)
International conferences - 4 (Poster presentation)

- Got best poster award by Journal of Materials Chemistry Poster Presentation Prize at The National Symposium on Convergence of Chemistry and Materials organized Organized by BITS Pilani (Hyderabad Campus)

Details of Publications:

(Published articles)

12. **G. Jaiswal**, V.G. Landge, D. Jagadeesan* and E. Balaraman*.
Iron-based nanocatalyst for the acceptorless dehydrogenation reactions.
Nature Commun. 2017, 8, 2147-2160.

Highlights:

- Vigyanprasar (An autonomous Organization, Under the DST, Govt. of India)
- The Hindu Businessline
- Firstpost

11. E. Balaraman,* A. Nandakumar* **G. Jaiswal** and M. K. Sahoo.
Iron-catalyzed dehydrogenation reactions and its applications in sustainable energy and catalysis.
Catal. Sci. Technol. 2017, 7, 3177-3195 (Minireview).

Highlights:

- Selected as a cover page article.
- Selected as 'HOT' article 2017.

10. M. K. Sahoo, **G. Jaiswal**, J. Rana and E. Balaraman*.
Organo-photoredox catalyzed oxidative dehydrogenation of N-heterocycles.
Chem. Eur. J. 2017, 23, 14167-14172.

9. Sustainable iron-catalyzed direct imine formation by acceptorless dehydrogenative coupling of alcohols with amines.

G. Jaiswal, V. G. Landge, D. Jagadeesan* and E. Balaraman*.
Green Chem. 2016, 18, 3232-3238.

8. Cobalt-Catalyzed Bis-alkynylation of Amides via Double C-H Bond Activation.
V. G. Landge, **G. Jaiswal** and E. Balaraman*.
Org. Lett. 2016, 18, 812-815.

Highlight:

Cited in Organic Chemistry Portal – 2017 (Benzene Derivatives: The Mohr Synthesis of Ilicicolinic Acid)

7. Nickel-catalyzed direct alkynylation of C(sp²)-H bonds of amides: an “inverse Sonogashira strategy” to ortho-alkynylbenzoic acids.

V. G. Landge, C.H. Shewale, **G. Jaiswal**, M. K. Sahoo, S. P. Midya and E. Balaraman*.

Catal. Sci. Technol. 2016, 6, 1946-1951.

6. Earth-abundant iron-rich N-doped graphene based spacer and cavity materials for surface plasmon-coupled emission enhancements.

S. Venkatesh, D. Vernekar[#], G. Jaiswal[#], D. Jagadeesan* and R. Sai Sathish*.

ACS Appl. Mater. Interfaces. 2016, 8, 12324-12329. [#](equal contribution)

5. Well-defined palladium(II) complexes for ligand-enabled C(sp³)-alkynylation.

V. G. Landge, M. K. Sahoo, S. P. Midya, **G. Jaiswal** and E. Balaraman*.

Dalton Trans. 2015, 44, 15382-15386.

Highlight:

• Top 20 Articles (2015) in Dalton Trans.

Unpublished articles:

4. Cobalt-based nanocatalyst for Selective transfer hydrogenation of alkynes.

G. Jaiswal,[‡] V.G. Landge,[‡] M. Subaramanian, R. G. Kadam, R. Zboril, M. B. Gawande and E. Balaraman*

Communicated. [‡](equal contribution).

3. A Reusable Heterogeneous Cobalt-Catalyzed Dehydrogenation of *N*-Heterocycles with the Liberation of H₂.

G. Jaiswal, M. K. Sahoo, M. Subaramanian, and E. Balaraman*

Communicated.

2. Chemo-selective catalytic transfer hydrogenation of nitroarenes by reusable manganese nanocatalyst under base-free conditions.

G. Jaiswal,[‡] V.G. Landge,[‡] M. B. Gawande and E. Balaraman*

Manuscript under preparation. [‡](equal contribution).

1. Photocatalysis Enabling Acceptorless Dehydrogenation of Diaryl hydrazines at Room Temperature.

M. Sahoo, K. Saravanakumar, **G. Jaiswal**, E. Balaraman*

Communicated.

Details of Patents:

5. Phenanthroline based pincer complexes useful as catalysts for the preparation of methanol from carbondioxide.

E. Balaraman, V. G. Landge, S. P. Midya, M. K. Sahoo and **G. Jaiswal**.

International Application No.: PCT/IN2016/050050

- 358/DEL/2015 (IN) and 417/DEL/2015 (IN)
- WO2016128997 (A1)
- US2018021766 (A1)
- EP3256250 (A1)

4. Novel quinoline derivatives and preparation thereof.

E. Balaraman, S. P. Midya and **G. Jaiswal**.

International Application No.: PCT/IN2016/050038

- 304/DEL/2015 (IN)
- WO2016125187 (A1) and WO2016125187 (A4)

3. Magnetically separable iron-based heterogeneous catalysts for dehydrogenation of alcohols and amines.

E. Balaraman, D. Jagadeesan, **G. Jaiswal** and S. P. Borikar.

International Application No.: PCT/IN2016/050157

- 1494/DEL/2015 (IN) and 3688/DEL/2015 (IN)
- WO 2016189553 (A1)

2. *Ortho*-substituted unsymmetrical diarylaniline compounds and a process for preparation thereof.

E. Balaraman, Manoj K. Sahoo, **G. Jaiswal** and S. P. Borikar.

Indian Pat. Appl. (2017), IN 2015DE02331 A 20170203.

1. A one pot process for synthesis of imine by using iron-catalyzed acceptorless dehydrogenative coupling.

E. Balaraman and **G. Jaiswal**.

Indian Pat. Appl. (2018), IN 201611009248 A 20180119.

Media Coverage:

New approach for producing hydrogen gas developed

RATNESHWAR THAKUR INDIA SCIENCE WIRE



Team of researchers at NCL.

New Delhi, January 11 (India Science Wire): Hydrogen is considered one of the best sources of green energy. But economic production and storage remain major challenges in propagating this green fuel. Scientists believe that developing specific catalysts could help produce hydrogen from cheap starting materials.

A research team led by Dr. E. Balaraman at National Chemical Laboratory (NCL), Pune has developed a new strategy to replace expensive noble metal catalysts with an iron catalyst for production of hydrogen gas. The process, they claim, is economical and sustainable. The study was published in journal Nature Communications.

Researchers used abundantly available alcohols such as 20-heterocycles and amines as starting materials. Along with the iron catalyst synthesized in laboratory, Argon gas was then passed through the reaction tube to create inert reaction conditions in place of air. This reaction mixture was refluxed to get maximum conversion of starting material, resulting in generation of hydrogen gas.



A research team led by Dr. E. Balaraman at National Chemical Laboratory (NCL), Pune has developed a new strategy to replace expensive noble metal catalysts with an iron catalyst for production of hydrogen gas. The process, they claim, is economical and sustainable. The study was published in journal Nature Communications.

The research team included Garima Jaiswal, Vinod G. Landge, D. Jagadeesan & E. Balaraman. The study was funded by Science and Engineering Research Board (SERB) of the Department of Science and Technology (DST) under its start-up grant for young scientists.

Published on January 11, 2018

It is known that removal of hydrogen atoms from an organic molecule can be achieved either by the use of strong oxidants or sacrificial hydrogen acceptors, which often produce plentiful waste. In the new study, the catalytic material was obtained by thermally pyrolysing iron complex using a unique core-shell architecture composed of oxide as a shell and carbide as a core iron.

"The economics of hydrogen energy depends on the cost of starting material and the entire process. The use of alcohols could give us a sustainable and economical way to produce hydrogen gas," said Dr. Balaraman.

The research team included Garima Jaiswal, Vinod G. Landge, D. Jagadeesan & E. Balaraman. The study was funded by Science and Engineering Research Board (SERB) of the Department of Science and Technology (DST) under its start-up grant for young scientists.

Published on January 11, 2018

Home Twitter Facebook Author On Twitter

Thursday, 11 January 2018

New Approach For Producing Hydrogen Gas Developed

Researchers at National Chemical Laboratory (NCL), Pune has developed a new strategy to replace the expensive noble metal catalysts with an iron catalyst for the production of hydrogen gas.

By Rataneshwar Thakur Published in India Science Wire
Also appeared in TheHinduBusinessline.com

Dr. E. Balaraman with his research team

Hydrogen is considered one of the best sources of green energy. But economic production and storage remain major challenges in propagating this green fuel. Scientists believe that developing specific catalysts could help produce hydrogen from cheap starting materials.

A research team led by Dr. E. Balaraman at National Chemical Laboratory (NCL), Pune has developed a

Search This Blog

Follow by Email

Latest Post

New Technology May Help Reach 1% Renewable Energy Capacity

Researchers at Indian Institute of Technology (IIT) Bombay have demonstrated the control of nanoscale switching characteristics of Plasmonics

About Author

Rataneshwar Thakur
Working as Research Scientist, Emerging Technologies, Materials, and Electronic Systems in the Department of Energy and Environment, Institute of Energy Studies, Indian Institute of Technology, Bombay

Popular Posts

Home About us Resources Contact us

India Science Wire

Latest S&T News from India

Home > Category > Indian Science News

New approach for producing hydrogen gas developed

Tweet

By Rataneshwar Thakur · New Delhi, Thursday, January 11, 2018

Hydrogen is considered one of the best sources of green energy. But economic production and storage remain major challenges in propagating this green fuel. Scientists believe that developing specific catalysts could help produce hydrogen from cheap starting materials.

A research team led by Dr. E. Balaraman at National Chemical Laboratory (NCL), Pune has developed a new strategy to replace expensive noble metal catalysts with an iron catalyst for production of hydrogen gas. The process, they claim, is economical and sustainable. The study was published in journal Nature Communications.

Researchers used abundantly available alcohols such as, N-heterocycles and amines as starting reaction materials, along with the iron catalyst synthesized in laboratory. Argon gas was then passed through the reaction tube to create inert reaction conditions in place of air. This reaction mixture was refluxed to get maximum conversion of starting material, resulting in generation of hydrogen.

Recent posts

- New approach for producing hydrogen gas developed
- अणुशक्ति का जन्म: विद्युत और सूर्योत्पन्न से उत्पन्न
- No lessons learnt in quake-prone Northeast
- Decoding genome of HIV variant found in India
- एन सीएल में अणुशक्ति का जन्म: विद्युत और सूर्योत्पन्न से उत्पन्न

Synfacts 2018; 14(03): 0322
DOI: 10.1055/s-0037-1609274

Polymer-Supported Synthesis

© Georg Thieme Verlag Stuttgart · New York

Acceptorless Dehydrogenation by Using an Iron-Based Nanocatalyst

Contributor(s): Yasuhiro Uozumi, Anggi Eka Putra

Further Information

Abstract Full Text Figures

Buy Article > Permission



(Highlighted in Indian Science Wire, The Hindu Businessline; Vigyanprasar, Synfacts, NRDC (Invention & Intelligence) and Firstpost)